SKB

TECHNICAL REPORT 95-15

Estimation of effective block conductivities based on discrete network analyses using data from the Äspö site

Paul R La Pointe[1], Peter Wallmann[1], Sven Follin[2]

1 Golder Associates Inc., Seattle, WA, USA
2 Golder Associates AB, Lund, Sweden

September 1995

SVENSK KÄRNBRÄNSLEHANTERING AB
SWEDISH NUCLEAR FUEL AND WASTE MANAGEMENT CO

P.O.BOX 5864 S-102 40 STOCKHOLM SWEDEN
PHONE +46 8 665 28 00 TELEX 13108 SKB
FAX +46 8 661 57 19

ESTIMATION OF EFFECTIVE BLOCK CONDUCTIVITIES BASED ON DISCRETE NETWORK ANALYSES USING DATA FROM THE ÄSPÖ SITE

Paul R La Pointe[1], Peter Wallmann[1], Sven Follin[2]

1 **Golder Associates Inc., Seattle, WA, USA**
2 **Golder Associates AB, Lund, Sweden**

September 1995

ESTIMATION OF EFFECTIVE BLOCK CONDUCTIVITIES BASED ON DISCRETE NETWORK ANALYSES USING DATA FROM THE ÄSPÖ SITE

Paul R. La Pointe
Peter Wallmann

Golder Associates Inc., Seattle, WA USA

Sven Follin

Golder Associates AB, Lund, Sweden

Keywords: fracture flow, DFN, Äspö, block-scale flow, modeling, hydraulic conductivity

September 12, 1995

IC3-1161
0911PRL1.PRE

TABLE OF CONTENTS

LIST OF FIGURES

LIST OF TABLES

LIST OF APPENDICES

ABSTRACT (English)

Numerical continuum codes may be used for assessing the role of regional groundwater flow in far-field safety analyses of a nuclear waste repository at depth. Such codes are sensitive to a number of factors, among them, the values of conductivity or permeability assigned to the grid cells or blocks in the model. The focus of this project is to develop and evaluate one alternative method based on Discrete Fracture Network (DFN) models to estimate block-scale permeability values for continuum codes such as HYDRASTAR, NAMMU and PHOENICS. Data from the Äspö HRL and surrounding area are used.

DFN models consist of discrete fractures in a three-dimensional volume of rock. The models constructed in this study are based upon measurements of fractures in the HRL and from the KAS series of boreholes. The model is stochastic, so it is possible to generate multiple fracture network realizations. A 30-m packer test is simulated in each realization, and the result is compared to the 30-m transient well tests carried out in KAS02 and KAS03. Only those realizations similar to the actual transient tests are retained. These realizations are then partitioned into a series of blocks ranging in size from 10 m to 50 m. The fractures in each block are converted into finite elements, and the effective block permeability between opposing faces is computed using the MAFIC code. These results are analyzed to determine population statistics and spatial correlation models for each block size, and for different DFN model fracture size assumptions. To evaluate this approach further, a 50-m NAMMU model was created out of 125 10-m blocks. The results of a simple flow experiment on this 50-m NAMMU model were compared to the results for the same boundary conditions on the parent 50-m MAFIC DFN model from which the 10-m blocks were derived. The comparison illustrates that there are a number of important factors relating both to the selected continuum code and to the geometry of the fracture network that are important to consider if a stochastic continuum approach is used. The work also demonstrated that revision of the fracture mapping and well test protocols used in the HRL and elsewhere at Äspö could reduce the uncertainty for portions of the DFN models.

ABSTRACT (Swedish)

Datorbaserade kontinuumberäkningar i regional skala är vanligt förekommande vid uppskattning av grundvattnets roll för säkerheten i fjärrzonen kring ett djupförvar. Syftet med denna rapport är att utveckla och utvärdera en alternativ metod för att uppskatta s.k. blockpermeabiliteter i olika skalor för användning vid kontinuumberäkningar. För närvarande används vid SKB tre olika kontinuumkoder, nämligen HYDRASTAR, NAMMU och PHOENICS. Rapporten baserar sig på data från Äspölaboratoriet.

Metoden går ut på att skapa en stokastisk spricknätverksmodell för Äspö som överensstämmer med uppmätta sprickdata i området. De spricknätverksrealiseringar som vid numerisk simulering reproducerar uppmätta pumptestförlopp från kärnborrhål på Äspö diskretiseras i 10-50 m stora block. Blockens permeabilitet bestäms i tre olika riktningar med hjälp av flödeslösaren MAFIC. Blockpermeabiliteterna analyseras geostatistiskt och sambandet mellan blockstorlek, spricklängd och blockpermeabilitet kvantifieras. Avslutningsvis jämförs flödet genom ett 50-m stort spricknätverksblock med flödet genom samma block efter att detta diskretiserats i 125 stycken 10-m block. Jämförelsen visar att det finns många viktiga faktorer att ta hänsyn till som har att göra med såväl sprickornas geometri egenskaper som val av kontinuumkod om man vill beskriva berget som ett stokastiskt kontinuum. Rapporten visar också ett annorlunda förfaringsätt av utförda sprickkarteringar och pumptester på Äspö hade i vissa avseenden reducerat en del av av de osäkerheter som för närvarande föreligger vid konstruktion av spricknätverksmodeller för Äspö.

ACKNOWLEDGMENTS

The author of this report would like to thank the many reviewers for their insightful and useful comments and criticisms, which have greatly improved this report. In particular, we would like to thank Anders Ström, Ingvar Rhén, Sven Norman, Mats Olsson, Thomas Doe and William Dershowitz for their careful review and discussions. We would also like to acknowledge the work of Anders Boghammar of Kemakta AB who performed all of the NAMMU simulations described in this report.

1. INTRODUCTION

1.1 Goals

Performance assessment calculations for the SKB SR-95 project require numerical modeling for fluid flow and mass transport over several cubic kilometers of rock surrounding the Äspö Hard Rock Laboratory (HRL). One modeling approach under consideration will represent the rock as a heterogeneous continuum discretized into three-dimensional cells. Each cell will be given fluid flow properties that are estimated from mappable geological features or from statistical models. The results from these continuum flow simulations will be used to define pathways for radionuclide migration and to determine the flow and mass transport properties of these paths for subsequent use in pipe flow-based performance assessment models. The purpose of the work reported in the present study is to develop and evaluate a methodology based on Discrete Fracture Network (DFN) models to provide more realistic block-scale fluid flow properties for these continuum flow codes. The project consists of three parts: analysis of the geological and hydrological data at Äspö for creation of DFN models; construction and conditioning of the DFN models to match transient well tests; and demonstrating the methodology for creating input data sets.

In performance assessment modeling, mapped fracture zones such as are found at Äspö can be represented explicitly. This was the case for flow modeling at Finnsjön in SKB 91. Fracture zones were deterministically incorporated into the NAMMU model by assigning higher permeability values (up to 35 times greater) to grid cells which contained portions of the zones than the surrounding non-fracture zone grid cells (Lindbom and Boghammar, 1992). Each zone was given individual hydraulic properties based on hydraulic tests or by inference to other measured zones. In general, grid cells which contain mapped fracture zones will be given specific hydraulic properties which are often based upon well tests. The present study is not directed towards computing better values for known fracture zones, for this is a problem in well testing; rather it focuses upon improving the permeability values for non-fracture grid cells, which comprise the majority of the rock volume to be modeled.

As a result, the analysis specifically excludes data from mapped fracture zones for any of its analyses. This makes it possible to more accurately calculate grid cell properties for those cells not containing the zones.

1.2 Previous Attempts to Estimate Block Scale Flow Properties

A stochastic continuum flow model for Äspö will require that the rock volume be discretized according to a finite difference or finite element method. The scale of the discretization is likely to vary and could be on the order of 10 m to 50 m (A. Strom, personal comm., 1994). This implies that it will be necessary to compute hydraulic conductivity values for rock blocks for a range of different scales. Ultimately, the permeability values for these blocks must be estimated from either well tests or hydraulic experiments conducted in underground caverns such as the Äspö HRL.

Previous efforts to compute realistic block-scale conductivity estimates at Äspö and Finnsjön have focused either upon extrapolation and regularization of packer test data (Norman, 1992a; Geier, 1993; La Pointe, 1994) or the estimation of block-scale conductivity distributions from flow experiments on discrete fracture network (DFN) models (Axelsson and others, 1990; Geier and others, 1992).

Regularization of packer test data to larger-scale blocks has thus far proved inadequate at Äspö and Finnsjön. The first problem is that values for interval packer tests in wells reveal very little about what the value of another interval is only a few tens of meters away. Geostatistical analysis of the 3 m and 30 m packer test data at Äspö (La Pointe, 1994) suggests that the degree of spatial correlation in packer test data is weak. Even for very short distances, non-spatially correlated variability overwhelms the spatially correlated component. This weak spatial correlation means that it will be very difficult to extrapolate well data to the majority of the rock mass that is more than a few tens of meters distant from well tests. The weak spatial correlation may be due to three possible causes:

- mixing of packer test subpopulations with different spatial correlation structures.

- differences in well testing conditions or interpretation over the course of the data collection, which would lead to the introduction of noise, or

- actual lack of spatial correlation in the packer test data.

The issue of sub-populations has been addressed by Liedholm (1991) and La Pointe (1994) who considered whether the 3 m packer test data can be divided into sub-populations on the basis of geology or other mappable parameters. They found no reason for subdividing the packer test data into separate populations. However, work by Axelsson and others (1990) indicated that there may be some correlation between *block-scale* conductivity and geology at Äspö. It may be that the 3 m tests are more sensitive to local geometric features of individual fractures, whereas the regional fracture network, which relates more to mappable geology, controls block-scale tests.

Another possible reason for the lack of correlation in the 3 m tests may have to do with the radius of influence of a test. Follin (1992b) showed that the magnitude of the packer test-derived transmissivity may relate to the volume of rock tested, or the test's statistical *support*, in heterogeneous porous media. This same relation may be true for fractured, non-porous rocks such as those at Äspö, though this has not been studied. If so, then the non-spatial variability might be reduced by estimating spatial correlation models for different thresholds of interpreted packer test transmissivity.

The other two possible causes for the observed noise are not so easily overcome. There is little that can be done to improve geostatistical interpolation of 3 m packer tests if the noise derives from differences in testing or from actual lack of spatial correlation.

The second problem is that there is no simple way to relate the block-scale hydraulic conductivity value of a fractured rock block to packer interval values of conductivity, or to calculate the properties of a large block from the properties of an assemblage of small blocks. Axelsson and others (1990), Geier and Doe (1992), and Geier and others (1992) examined whether it was possible to analytically relate packer interval conductivity values to larger-scale blocks that contained the tested intervals. Geier and Doe (1992) created a series of DFN models for studies at Finnsjön in which they simulated packer tests as well as determined properties of the larger blocks. They concluded that interval

packer test conductivity values compare very poorly with block-scale conductivity, "even for block-scales close to the tested length of borehole" (Geier and Doe, 1992; p. 31). In other words, they were not able to construct a calibration curve with the interval permeability value on one axis and the block-scale permeability value on the other. There work showed that it could be quite difficult to use a packer test result to directly infer a meaningful block-scale value in a fractured rock mass.

There have been attempts reported in the literature to determine the block-scale conductivity values from the values of assemblages of sub-blocks making up the larger block. A common approach is to apply different types of harmonic and arithmetic averaging (for example, Le Loc'h, 1989). While these averaging techniques often define a usefully narrow range of block-scale properties for porous media, they have not been demonstrated for fractured rock. Although different types of averaging have not been applied to Äspö small-scale block data, this approach would still require a way to extrapolate and regularize packer test data to small blocks, and would require development and testing of a theory for upscaling small blocks to larger blocks for a fracture-dominated flow system.

Thus, previous work at Äspö and Finnsjön has identified two areas of concern for creating input for large-scale, three-dimensional stochastic continuum models:

1) It is difficult to interpolate or extrapolate packer tests results more than a few meters away from the tested interval, and

2) It has not been possible to relate packer test conductivity values to block-scale conductivity values.

1.3 Alternative Strategy to Estimate Block Scale Flow Properties

Where blocks are close enough to hydraulic tests or experiments, it may be possible to condition the models by means of these tests and avoid the complications described in Sec. 1.2. Conditioning may follow one of two paths: adjusting the block properties until simulated hydraulic tests match actual well tests; or retaining only those simulations

which match tests. The first alternative is a form of *calibration,* in which model parameters are altered so that model simulations match actual data. This procedure is often carried out for continuum reservoir simulation models in the petroleum industry, and is termed *history matching.* The second alternative is a form of *filtering,* in which models or model realizations are retained *only if* they match actual well tests with sufficient accuracy. In this second alternative, model parameters are not altered. Conditioning has the advantage that model parameters, which are based upon carefully considered geological data, are not arbitrarily changed to achieve a match. For this project, well tests have been used to filter models and their realizations as described in Section 4.

The overall goal of this project is to develop and test a methodology to estimate block-scale hydraulic conductivity values for stochastic continuum codes, such as NAMMU or HYDRASTAR. The approach is to create Discrete Fracture Network (DFN) models based upon the fracture geology at Äspö, filter the models using transient well tests, and then carry out a series of numerical calculations on the acceptable models to derive the necessary input for stochastic continuum codes. This strategy differs from that adopted by Geier and Doe (1992) in which they sought to compute block values for DFN models from simulated packer tests. In this project simulated well tests are compared to actual well tests in order to filter out DFN models. The use of well tests as a filter will produce DFN models that:

- are conditioned to known geological, structural and geometrical data
- produce simulated transient well test results similar to actual field tests.

This approach offers the following potential advantages of:

- creating models that can incorporate a large amount of the conductive fracture geology and geometry that relates to fracture network flow,
- calculating the block conductivity values directly at the scale of interest, avoiding entirely any complications having to do with upscaling conductivity from small blocks or interpolated well tests,

- reducing the impact of noisy data or insufficiently strong spatial correlation, since the model for the connective flow geometry is derived from geological data, not just well test variograms, and

- freeing the model from narrow statistical assumptions, since DFN models make no *a priori* assumption that conductivity values are stationary or follow a Gaussian or some other type of statistical distribution.

However, conditioning larger scale DFN models to transient well tests does not resolve all of the problems for calculating block-scale input for stochastic continuum codes. Hydraulic tests have a region of influence that is a function of the type of test and testing parameters, as well as rock properties. In fact, the majority of the rock volume in the model is probably outside the region of influence of any of the well or underground hydraulic tests. This means that the properties for the rock blocks which are outside the influence region of hydraulic tests cannot be conditioned to well tests. Rather, they must be inferred through some combination of interpolation, extrapolation and geological conditioning. In particular, it is necessary to devise statistical models of how block properties change with scale, what types of spatial correlation exists for block-scale values, and how values may change or be correlated with mappable geological features. All of these issues are addressed in this report, as outlined in Section 2.

2. PROJECT OUTLINE AND TASK DESCRIPTIONS

2.1 Overview

The process for calculating block-scale hydraulic conductivity values conditioned to local packer tests follows the three-stage process described in Section 1.1: Data Analysis; DFN Model Creation and Conditioning; Calculation of Block Scale Permeability Values for a Stochastic Continuum Code (Figure 2-1).

The first stage is to *analyze* the fracture and fluid-flow data to:

1) determine the relation, if any, between the fluid flow properties and mappable parameters of individual fractures or fracture networks;

2) calculate the statistical distribution properties of discrete fractures necessary for constructing DFN models of the Äspö site.

The first step is necessary to ascertain *what* fracture parameters need to be modeled for fluid flow calculations, and thus provide a plan for building the DFN models. The second step provides the specific input for the DFN models.

The second stage consists of the DFN model construction and conditioning to well tests. This second stage consists of two steps as well:

1) construction of DFN models, which consists of creating discrete fracture models that have been geometrically conditioned to outcrop and HRL tunnel fracture maps, and

2) the use of transient well tests to idenitify which of the geometrically conditioned large-scale block DFN models and realizations have hydraulic properties similar to Äspö.

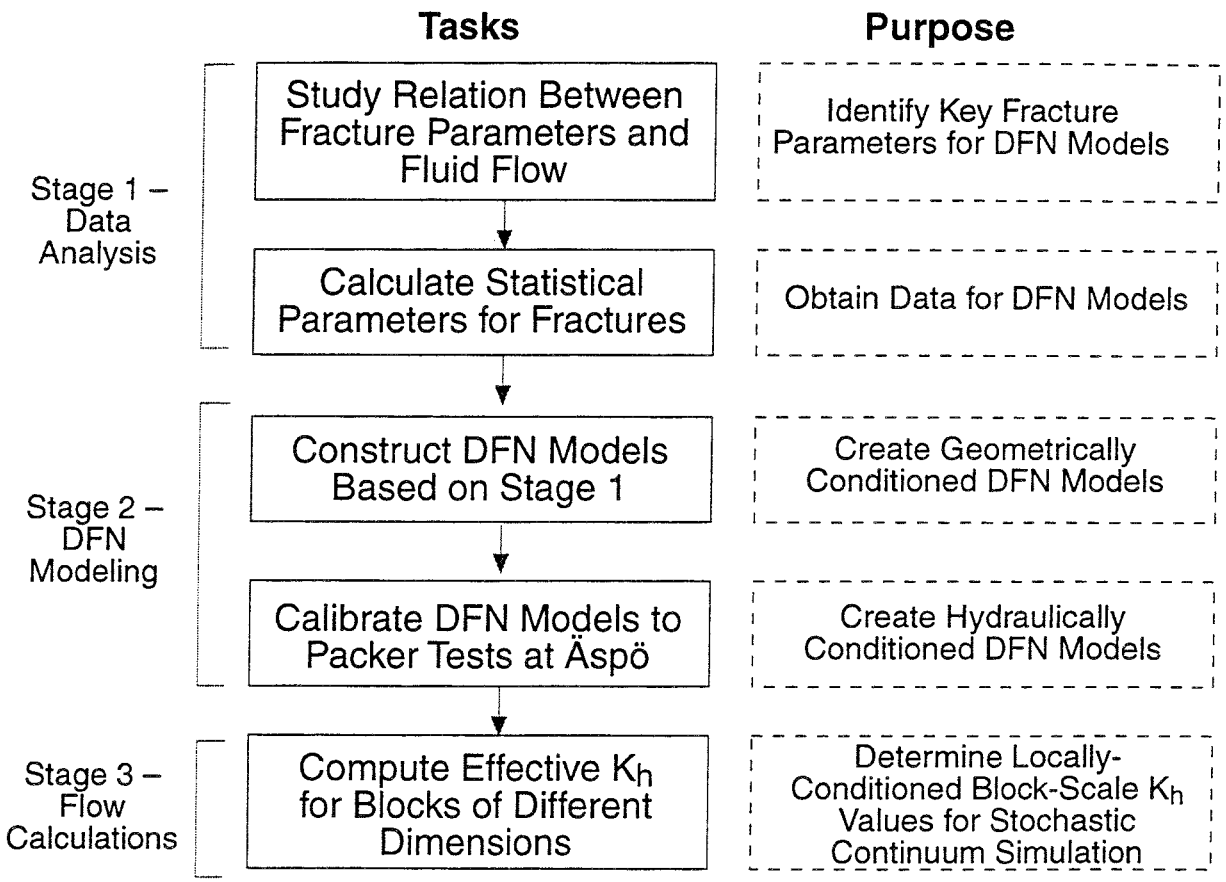

FIGURE **2-1**

PLAN FOR CALCULATING LOCALLY-CONDITIONED, BLOCK SCALE KH VALUES FOR STOCHASTIC CONTINUUM SIMULATION

SKB/BLOCK K/SWEDEN

This stage produces a series of stochastic models that are consistent with available fracture geometry data and well tests carried out at Äspö.

In the third stage, numerical flow simulations are carried out on blocks of varying dimensions that are subregions of the acceptable DFN models. The results are used to determine how block properties change with scale, what type of spatial correlation exists for blocks at each scale, and how the computed values might be used as input to HYDRASTAR or a similar stochastic continuum flow code.

2.2 Task 1 - Data Analysis

The goal of Task 1 is to determine the statistical and geological properties of the fractures important for block-scale DFN models at Äspö. The analysis specifically focuses on fracture that are not part of major identified fracture zones, since these would be determinstically rather than stochastically represented in a continuum model.

The geometry of a DFN model consists of the following primary parameters:

- number of sets or sub-populations,
- orientation model for each set,
- size distribution model for each set,
- spatial location model for each set,
- fracture intensity value for each set.

The source for data to estimate the above parameters typically come from two-dimensional rock exposures, such as outcrops or underground drift maps, or from one-dimensional samples, such as core or well logs. At Äspö, the primary data sources consist of the outcrop mapping performed by Ericsson (1987, 1988), HRL tunnel drift maps (e.g. Stanfors and others, 1994; Rhén and others, 1994), GEOTAB fracture mapping data sets from the HRL, and geological data from the investigation boreholes in Äspö and Laxemar (Nilsson 1989, 1990).

Data from the HRL access tunnel and drifts were not available for previous DFN models. In the present study, over 2 km of fracture data for the access tunnel and the ramps in the HRL were used as well. This new data provides several advantages:

1) it is subsurface rather than surface, thus less affected by surficial stress-relief, weathering and other factors that are unlikely to persist at the depths at which many of the blocks in the stochastic continuum model will be situated,

2) the access tunnel alone is over a kilometer in length, providing a large-scale horizontal sample of the fracturing at Äspö,

3) data on a variety of potentially important geological features and the conductive state of each fracture was recorded, and

4) the amount of data is large enough to provide statistically significant samples for analysis in most cases.

The HRL data has some disadvantages, as well:

1) locations of fractures were not recorded, only the panel in which they were found,

2) blasting and other excavation-related activities probably produced new fractures or altered existing ones. Although an attempt was made in the field data collection process to only include natural fractures (M. Olsson, personal comm.), it is possible that blasting- or excavation-induced or enhanced fractures make up part of the data, since it is often very difficult to distinguish natural and artificial fractures with certainty underground,

3) fracture traces are often larger than the exposed drift, so the standard methods for estimating fracture sizes from two-dimensional exposures is poorly constrained, and

4) fracture termination geometry was not recorded in the data base. This geometric information, which could include the angle of the intersection, whether one fracture "hooked" into another, or terminated as a "T" intersection, could be used to develop a classification of fractures into chronologic sets which might have very different geometric or fluid flow properties.

For these reasons, the geometry of the DFN model was derived from both the previous information and the newer HRL data, as described in Section 3.1.

2.3 Task 2 - Construction of the DFN Models and Conditioning Fluid Flow Properties

The goal of this task is to create several block-scale models that match both fracture geometry and well test results. Previous DFN models for Finnsjön were conditioned to fracture geometry, but their transmissivity was estimated through OxFilet (Osnes and others, 1988). The OxFilet algorithm assumes that the transmissivity measured over an interval is a function of the individual transmissivity values for each fracture intersecting the interval, and corrected for factors such as channeling along fracture. For example, the algorithm computes the transmissivity (T_i) for the **ith** packer interval as:

$$T_i = \sum_{j=1}^{n_i} T_{ij} \qquad \text{Equation 2-1}$$

where T_{ij} is the at-borehole transmissivity of the **jth** fracture intersecting the **ith** interval, and

n_j is the number of fractures intersecting the interval.

If the at-borehole fracture transmissivity is not equal to the cross-fracture transmissivity T_{fj}, then corrections are made. For example, if the at-borehole transmissivity is more a function of network effects, then:

$$T_{ij} = \frac{\overline{m}}{\sum_{i=1}^{\overline{m}} \frac{1}{T_{fj}}} \qquad \text{Equation 2-2}$$

where T_{fj} is the cross-fracture transmissivity of the **jth** fracture, and

m is the mean number of fractures per network affecting the fracture intersecting the borehole interval.

Thus, the values of transmissivity assigned to individual fractures by OxFilet are not computed through a numerical flow solution with appropriate boundary conditions. Rather, the interval transmissivity is computed from the individual fracture transmissivity values and their assumed surface and network geometry alone.

The advantage of OxFilet is that it is a very computationally efficient algorithm. The disadvantage of OxFilet is that it does not derive fracture transmissivity values through numerical flow simulations. Thus, there is no guarantee that well test simulations in the DFN model, whose transmissivity field was estimated using OxFilet, will actually match transient well tests.

There are two alternatives for generating DFN models that match well tests. The first alternative is to adjust the transmissivity field or other properties of the DFN model until an acceptable match is achieved. This is the well-known production-history matching process commonly used in the oil industry to calibrate the flow properties of reservoir simulation models. This approach can become computationally intensive and lead to a DFN model with fracture network geometry or individual fracture transmissivity values that no longer match mapped fracture geometries or reasonable values of individual fracture transmissivities determined from field tests, although they do reproduce the distribution of interval well test transmissivity values.

A second alternative is to generate a large number of realizations of the fracture geometry and fluid-flow properties, retaining only those realizations in which simulated well tests acceptably match the actual well test results. This alternative has the advantages that it is computationally more straightforward, and the closeness of the match between the DFN model geometry and individual fracture flow properties with the measured field data is not changed. The disadvantage lies in the risk that simulated well tests in few or none of the realizations will match the actual well test values. When few realizations match simulated transient well tests, then the geological/statistical models underlying the DFN model may be wrong, or the DFN approach as a modeling approach is inappropriate. This turned out not to be a problem, as described in Section 4.

In summary, the strategy for generating conditioned DFN models consists of:

1) basing the DFN model geometry on the outcrop, borehole and HRL data described (Section 3.1);

2) generating large-scale block realizations of this geometrical and using the fluid flow data previously derived (Uchida and others, 1994) from analysis of the hydraulic investigation boreholes (Section 3.2);

3) simulating packer tests in the large scale block models (Section 4);

4) comparing the results to the actual tests and discarding those realizations that do not match acceptably (Section 4).

2.4 Task 3 - Block Scale Flow Calculations

2.4.1 Task 3.1 - Estimation of Block-Scale Properties

Task 2 will produce several DFN blocks that match fracture geometry *and* match, within statistical and numerical accuracy, the actual transient well tests. These blocks are the basis of all subsequent calculations in Task 3.

In particular, Task 3.1 will calculate the statistical distributions for the principal components of hydraulic conductivity for blocks at five different modeling scales. This work will address the questions as to how conductivity values, anistropy and variaibility change with both block scale and some key model uncertainties such as conductive fracture size. The results are described in Section 5.1.2

2.4.2 Task 3.2 - Estimation of the Spatial Correlation Models for Block Properties

Currently there does not exist a theoretical basis for estimating either the scaling or spatial correlation properties of blocks in a fracture-dominated flow system such as Äspö. However, block-scale correlation models can be estimated empirically from conditioned DFN models. Each acceptable block model will be subdivided into smaller blocks, and effective flow properties computed for them. For example, a 50-meter block

could be divided into 125 10-meter blocks. Numerical flow calculations on these 10-meter blocks will yield principal component values for each of the 125 sub-blocks. The block values can then be analyzed for spatial correlation. The results are described in Section 5.1.3.

2.4.3 Task 3.3 - Generation of Input for HYDRASTAR or Other Stochastic Continuum Models

The purpose of the final task is to develop and evaluate a method for creating and assigning appropriate values for stochastic continuum codes from the block-scale simulations completed in previous tasks. In particular, the goal of this task is to demonstrate that the approach is feasible; that the results are useful; and that the methodology can be applied more generally and is not limited to Äspö.

The first part of the task is to transform the fluid-flow modeling results for block-scale DFN models into the type of fluid-flow input required by the stochastic continuum code. For example, some codes require a single scalar value of permeability for each block, others can incorporate a full permeability tensor, while still others can include non-neighbor connections. The results from the block-scale flow experiments must be converted to this type of information.

The next part of this effort is a preliminary cross-verification of a DFN model and a continuum model constructed through the approach outlined. This is a preliminary test to understand the strengths and weaknesses of the overall modeling approach. The results are discussed in Section 5.2.

The final part of this task is to outline a generalized strategy for creating input for stochastic continuum models from DFN models. These results are described in Section 5.3.

3. CREATION OF CONSTRAINED DFN MODELS

3.1 Data Analysis

Figure 3-1 shows the sources of data for this Task. Fracture zones are of sufficiently large scale and hydraulic importance that they will be represented as deterministic features in flow modeling, or properties modified on a block by block basis. In order to estimate the hydraulic properties of blocks in which no fracture zones occur, it is necessary to examine the relation between water-bearing fractures and mappable geological features. Outcrop fracture data has been analyzed previously by Ericsson (1987, 1988) and Uchida and Geier (1992), and was not re-analyzed for the present study. Analysis of this outcrop data for the purposes of constructing DFN models was reported in Uchida and others (1994).

Fracture data from outside fracture zones in the Äspö HRL was delivered in the file **/skbtmp/sr95/tunneldata_9501/fracture.dbf** in 23 January, 1995 on the SKB CONVEX computer. Subsequent to this project, this data was loaded in the GEOTAB data base and is essentially the same as the data used for this project. A large portion of this file contains data on single fractures rather than zones, and so provides a suitable basis for examining the relation between geology and fracture conductivity. However, this file contains inaccurate entries. Mostly, these consist of codes in fields which do not exist in the tunnel mapping protocols set forth by Christiansson and Stenberg (1991). Occasionally some of the data have clearly incorrect values, such as strikes of 900 degrees. Records in which data under analysis was possibly inaccurate or inconsistent with mapping protocols were deleted from the two-way contingency table analysis described in this section. The data in **fracture.dbf** comes from the main tunnel, side tunnels and the TBM drifts up through sections 3191.3 m, including data measured on the tunnel face for each excavation round prior to excavation of the next round. The entire data set as delivered contains 11,545 entries.

A more serious problem is the assignment of the correct rock type to the code contained in **fracture.dbf**. The codes for rock type are mostly B0 through B9 (with some additional bad

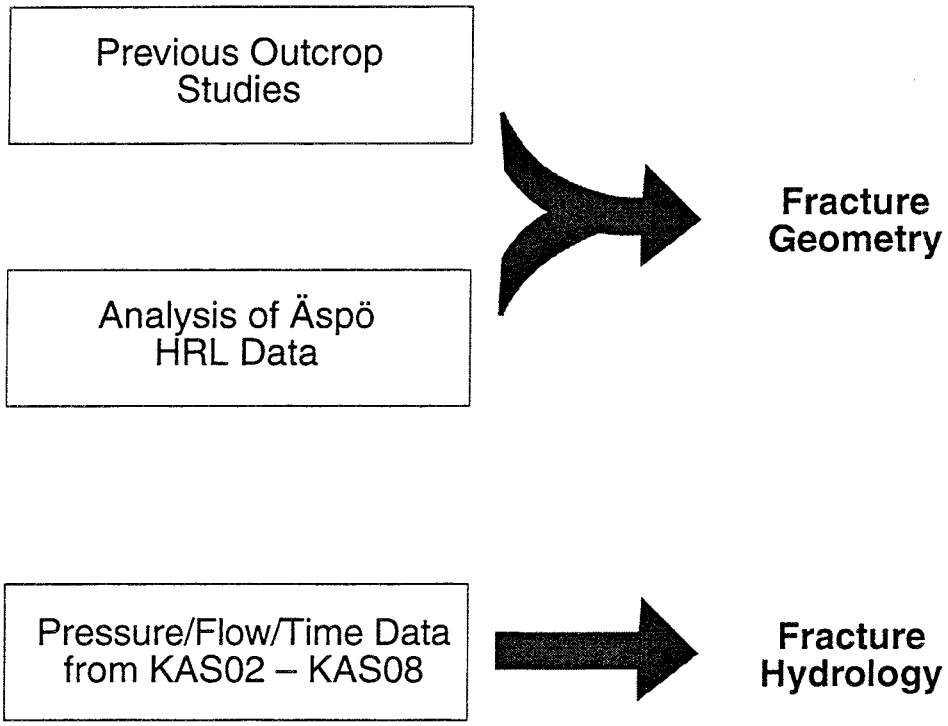

FIGURE **3-1**
DATA SOURCES FOR LOCALLY-CONDITIONED BLOCK FLOW SIMULATIONS
SKB/BLOCK K/SWEDEN

PROJECT NO. IC3 1161.003 DRAWING NO. 60488 DATE 9/7/95 DRAWN BY EA

Golder Associates

entries and typographic errors). However, these codes designate different rock types in different tunnel sections. The file **rock.dbf** was supplied by SKB to provide the correct identification of the codes B0 through B9 for the HRL. However, about one-third of the data in **fracture.dbf** occurs in sections not described in **rock.dbf**, so this data was not included in the analysis of rock type.

Table 3-1 summarizes the data sources for the analyses reported in Sections 3 & 4.

Table 3-1
Summary Of Data Used For Analyses

Analysis	Report Section	Data Used
Definition of Conductive Fracture Sets	3.1, Appendix A	**fracture.dbf** file Incorrect or questionable data not used. See discussion in Sec. 3.1
Fracture Orientations	3.1.2	**fracture.dbf** file using only fractures marked as water-bearing
Fracture Size	3.1.3	**fracture.dbf** file and tunnel maps for straight tunnel sections from Loop 1, Legs E-F, F-G & G-H; also Uchida and Geier (1992)
Fracture Spatial Location Model	3.1.5	Uchida and others (1994)
Fracture Intensity	3.1.4	HRL tunnel Secs. 7.4 m through 1497.7 m; also OxFilet analysis of 3 m packer tests from KAS02 through KAS08
Fracture Transmissivity, Storativity	3..2	Uchida and others (1994)
Well Tests for Calibration	4.1	30-m tests from KAS02 and KAS03

3.1.1 Relation Between Geological Factors and Fracture Sets

The data from the HRL was used to determine whether there are different fracture sub-populations at Äspö, and more importantly, whether the conductive fractures have distinguishing geological characteristics. Several factors were considered: mineral infilling, rock host type, openness, roughness, shape, and orientation. Each fracture has a designation showing if water was found in the fracture (Christiansson and Stenberg,

1991). Throughout the remainder of this report, such fractures are termed "water-bearing", "conductive" or "wet". Note that this designation does not imply how much water may have been flowing or how wet the surface may have been. The manual for documenting field work in the HRL tunnel (Christiansson and Stenberg, 1991) does not define the characteristics of water-bearing fractures.

To evaluate first-order relations among the data, fracture data was sorted and processed to form two-way contingency tables. Two-way contingency table analysis is a particularly good way to investigate first-order effects between class or ordinal variables. Table 3-2 illustrates how a contingency table indicates a correspondence or lack of correspondence between two variables. This table shows the relation between Surface Roughness and Conductive State. The total number of fractures classified as "Dry" is 10532, while the total number of fractures classified as "Wet" or conductive is 1009. In other words, the probability that a randomly-selected fracture will be dry is 0.913 (or 0.087 that it will be wet). If Surface Roughness Type is an indicator of whether a fracture is wet or dry, then we would expect to see a disproportionate number of fractures being wet or dry for one or more roughness types. For example, if "Rough" fractures were preferentially dry, then the marginal probability for "dryness" should exceed 0.913 by a statistically significant amount. In Table 3-2, the probability is actually 0.905, which is insignificantly different from 0.913. Thus, the fact that a fracture is classified as "Rough" does not indicate anything significant about whether it is conductive or not.

Further inspection of Table 3-2 shows no relation between any of the roughness classifications and the conductive state of the fracture.

Table 3-2
Relation Between Surface Roughness And Conductive Fracture Probability.

Surface Roughness Type	Number Dry	Number Wet	Marginal Probability Dry	Marginal Probability Wet
Rough	3720	392	0.905	0.095
Smooth	6790	616	0.917	0.083
Slickensided	13	0	1.000	0.000
Other	9	1	0.900	0.100
Total	10532	1009	0.913	0.087

The analysis of fracture openness is summarized in Table 3-3. This table indicates that open fractures tend to be about three times more likely to be conductive, but the fact that a fracture is not open provides no information about its conductive state. The fractures classified as "Other" in Table 3-3 consist of fractures with numerical codes not described in Christiansson and Stenberg (1991). Unfortunately, the number of open fractures is less than 1% of the total number, and as such, not likely to be a useful predictor of conductive state.

Table 3-3
Relation Between Fracture Openness And Conductive Fracture Probability.

Openness Classification	Number Dry	Number Wet	Marginal Probability Dry	Marginal Probability Wet
Coated	10420	986	0.914	0.086
Open	50	19	0.725	0.275
Other	64	4	0.941	0.059
Total	10534	1009	0.913	0.087

Another geological parameter that conceivably could indicate a fracture's conductive state is its observed mineral fillings. Table 3-4 and Figure 3-2 illustrate the relation between the primary mineral infilling and the conductive state, ranked in order of importance for predicting conductive fractures.

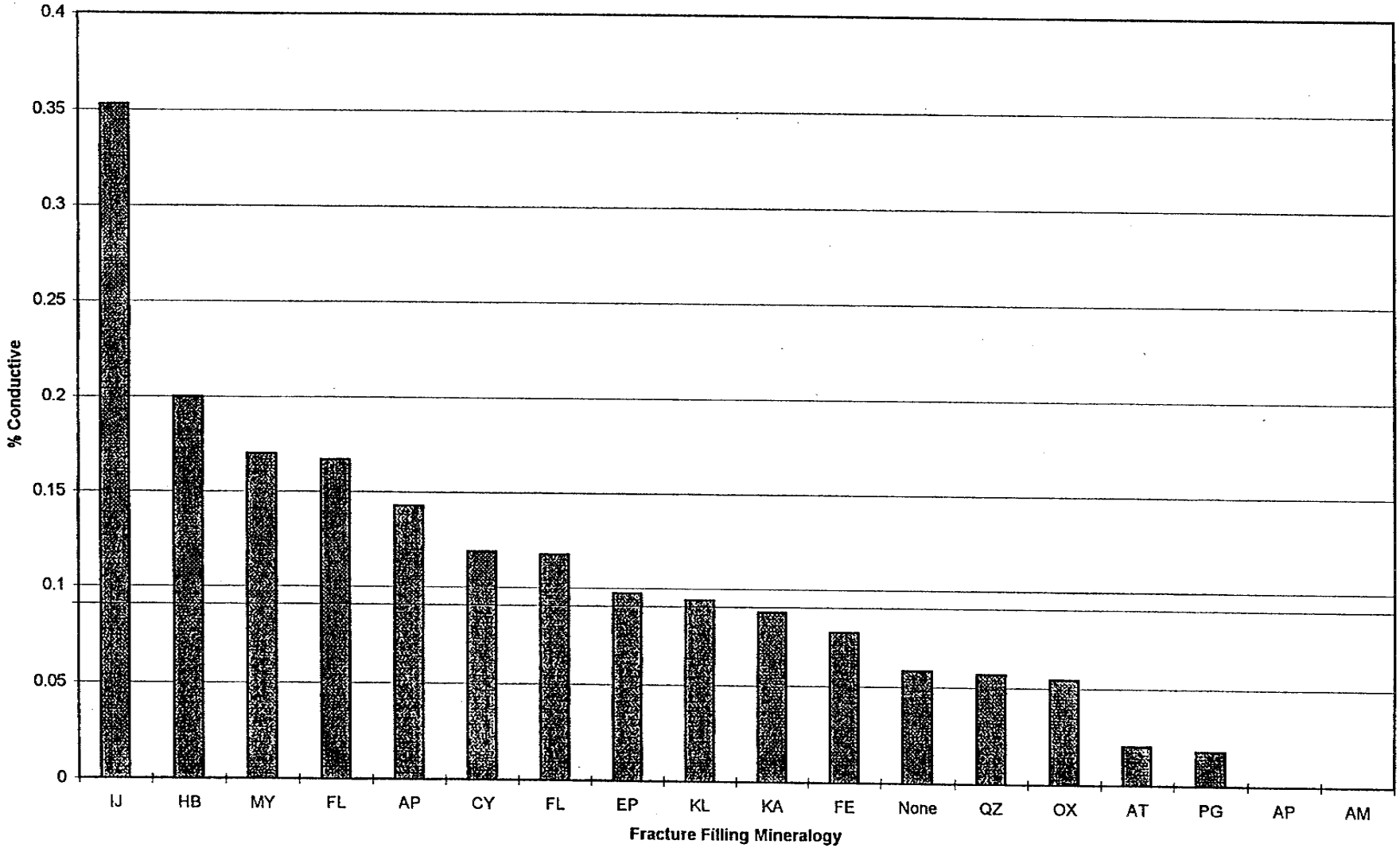

FIGURE **3-2**
RELATION BETWEEN MINERAL FILLING AND CONDUCTIVITY
SKA/ASPO-DFN/SWEDEN

PROJECT NO. IC3-1161.003 DRAWING NO. 60489 DATE 9/7/95 DRAWN BY EA

Golder Associates

In this data set, 9% of the fractures are conductive, while 91% are dry. Statistically significant differences between these percentages and the values for the filling mineralogies indicate a possible predictive relation between the filling and the conductive state. Those fractures with injected grout, hornblende, mylonite, fluorite and apatite have a slightly higher probability for being conductive, while those with no filling, quartz, oxidation rims, aplite or pegmatitic veining or amphibole have a have a lower probability. However, the amount of data for most of these classes is small and possibly statistically insignificant. Approximately 84% of the fractures have filling types that show no correlation with conductive state. Thus, mineral infilling is not a useful predictor of conductive state as only a small proportion of fractures are likely to have a filling that has even a small positive correlation with conductivity.

Table 3-4
Relation Between Fracture Filling Mineralogy And Conductive Fracture Probability.

Filling	Number Dry	Number Wet	Marginal Probability Dry	Marginal Probability Wet
Injected Grout	33	18	0.647	0.353
Horneblende	4	1	0.800	0.200
Mylonite	44	9	0.830	0.170
Fluorite	30	6	0.833	0.167
Apatite	6	1	0.857	0.143
Clay	74	10	0.881	0.119
Epidote	677	73	0.903	0.097
Chlorite	5071	526	0.906	0.094
Calcite	2630	254	0.912	0.088
Iron Oxide	201	17	0.922	0.078
No Filling	773	48	0.942	0.058
Quartz	265	16	0.943	0.057
Oxidation	225	13	0.945	0.055
Aplite	146	3	0.980	0.020
Pegmatite	219	4	0.982	0.018
Amphibole	1	0	1.000	0.000
Totals	10366	999	0.912	0.088

Rock type (Table 3-5) does not appear to play a major role in distinguishing conductive from non-conductive fractures either for fractures outside of fracture zones. Approximately 92% of all the fractures are classified as dry. The probability for dryness for fractures in all rock types for which there are a statistically significant number of

samples is nearly identical to this value. Thus it appears that rock type will be of limited use in conditioning the fracture intensity of a DFN model.

Table 3-5
Relation Between Rock Type And Conductive Fracture Probability.

Rock Type	Number Dry	Number Wet	Marginal Probability Dry	Marginal Probability Wet
Pegmatite	14	0	1.00	0.00
Fine-Grained Granite (Aplite)	678	87	0.89	0.11
Småland Granite	3199	358	0.90	0.10
Äspö Diorite	5849	512	0.92	0.08
Greenstone	387	33	0.92	0.08
Acidic Volcanic	20	1	0.95	0.05
Totals	10147	991	0.91	0.09

Although there appears to be no distinction in the probability of conductive fractures for the three rock types that dominate the Äspö site - Småland granite, Äspö diorite and fine-grained granite, the "permeability" of each rock unit (as calculated in Rhén and others, 1994) suggests that the fine-grained granite has a higher value than the Småland granite, with the Äspö diorite having the lowest value. When these gross rock unit flow rates are apportioned to the mapped fractures, the fractures in the fine-grained granite show the highest flow rates, followed by the Äspö diorite and the Småland granite. Fine-grained granite also has the highest proportion of wet surface area exposed in the HRL.

The lack of correlation between fractures designated as water-bearing in the **fracture.dbf** data base and rock type, as opposed to the finding of Rhén and others (1994) and Mazurek and others (1995) that rock type has some effect may be due to two reasons:

1) Joints vs. faults or fault zones: The analysis in this report focuses on fractures outside of fracture zones, whereas fracture zones were included in the studies conducted by Rhén and others (1994). Mazurek and others (1995) also examined only large faults or fault zones that completely cut the HRL tunnel. Their database consisted of 87 faults from the interval 600 m to 3050 m. They found

the density of fault surfaces and splay cracks is 5 to 10 times greater than for other rock types (op. cit., pg 63). They suggest that since a majority of the water-bearing fractures cut through patches of fine-grained granite, there is a higher conductive probability for faults in fine-grained granites. However, the fact that the number of splays may be greater does not necessarily imply that the P_{32} intensity (fracture area per unit volume rock) is higher, which is important, since P_{32} strongly relates to the percolation properties of the fracture network (Dershowitz and others, 1992).

2) The ratio of water-bearing to dry fractures shown in Table 3-4 describes nothing about the quantity of flow, which is a more useful parameter for modeling and is estimated in different forms by Rhén and others (1994). Unfortunately, it is not possible to calibrate a DFN model from the data presented in Rhén and others (1994) because it is necessary to know the location and orientation of each individual fracture, as described in the next four sections of this chapter.

Analysis of fracture orientations suggests that the orientations of conductive fractures are indistinguishable from the orientations of the non-conductive fractures. The data used in this analysis comes from the main tunnel from section 250.0 m through section 2600.0 m. The analysis was limited to this portion of the tunnel as coordinates (Forsmark and Rhén, 1994; p 6:2) are only given for these sections. It is necessary to have the tunnel coordinates in order to make the appropriate intensity corrections for the relative orientation between the tunnel and the fractures. Figures. 3-3a-i show stereoplot of fracture orientations for different fracture subsets. Figure 3-3a shows the orientations of all fractures, while Figure 3-3b shows orientation of conductive fractures, and Figure 3-3c shows orientations of all non-conductive fractures. While subject to alternative interpretations since some of the fracture concentrations are not well defined, it appears that there are three reasonably

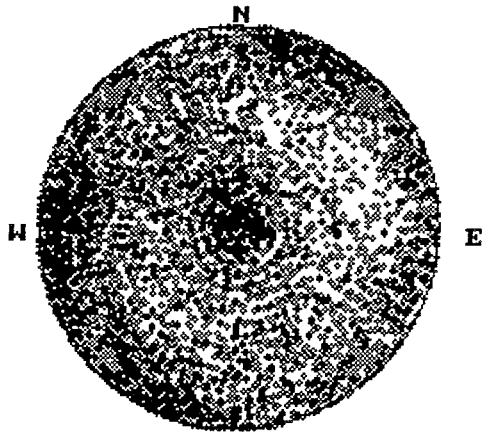

(a) All Fractures

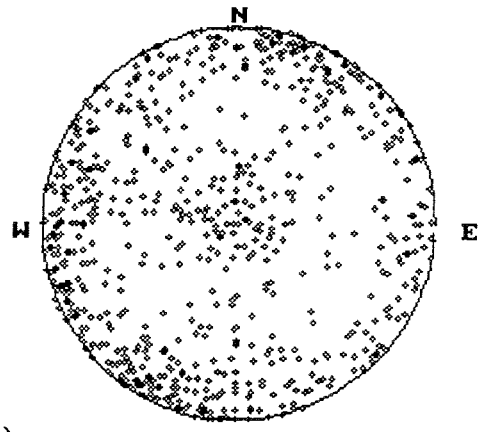

(b) Conductive

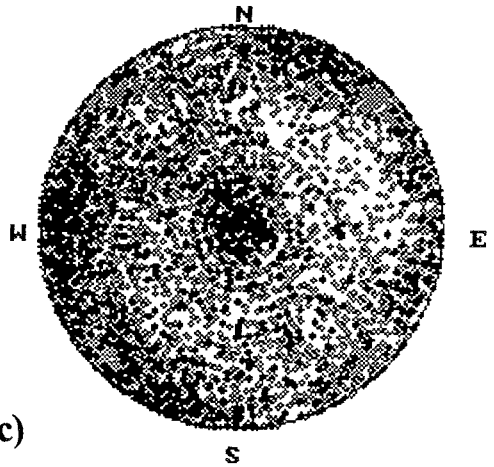

(c) Non-Conductive

FIGURE **3-3**
STEREOPLOT OF POLES FOR DIFFERENT FRACTURE SUBPOPULATIONS
SKB/BLOCK K/SWEDEN

Pegmatite

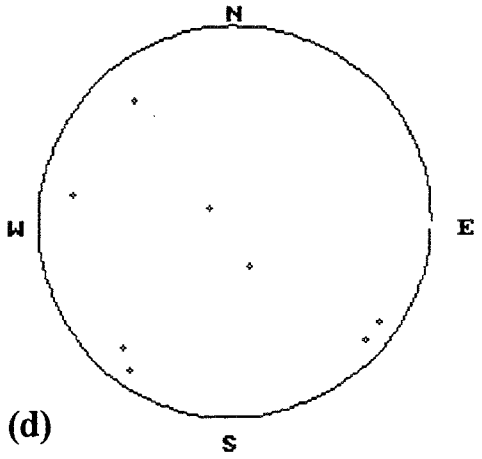

(d)

Fine-Grained Granite

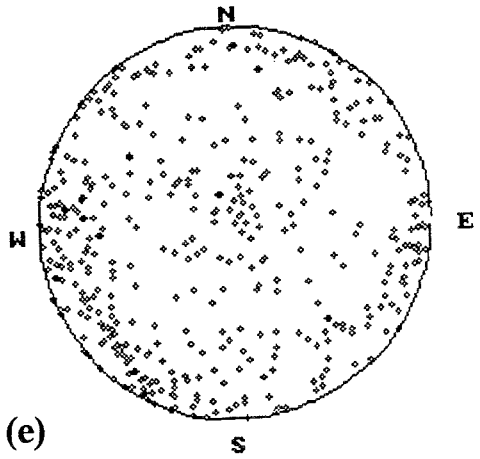

(e)

Småland Granite

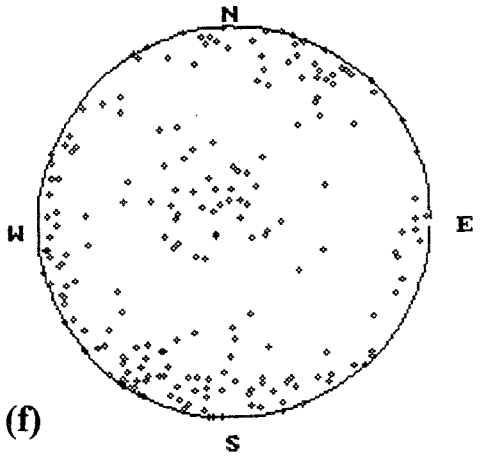

(f)

Äspö Diorite

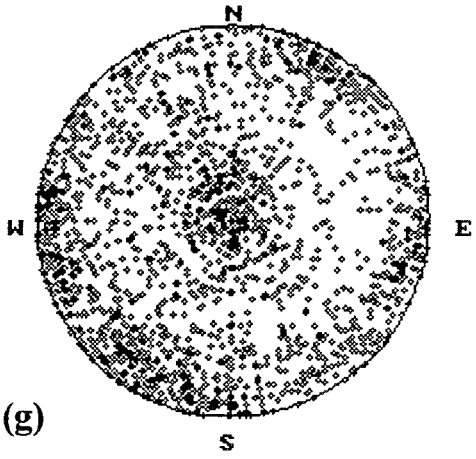

(g)

Greenstone

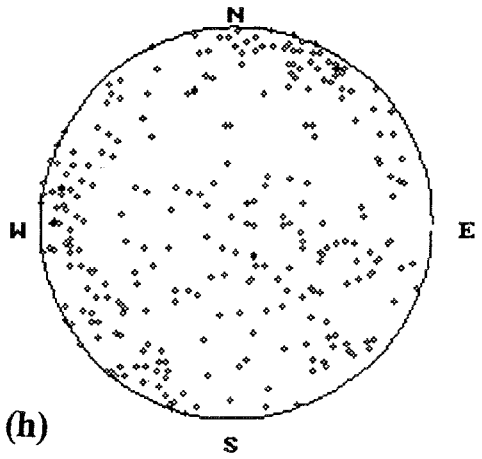

(h)

Acidic Volcanic

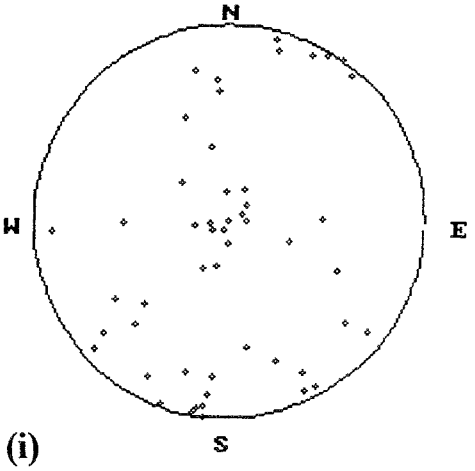

(i)

FIGURE **3-3**
STEREOPLOT OF POLES FOR DIFFERENT FRACTURE SUBPOPULATIONS (CONT.)
SKB/BLOCK K/SWEDEN

well-defined orientation sets. Two of these sets are steeply dipping and the other is subhorizontal. The two subvertical sets are oriented North/South and Northwest/Southeast. Table 3-6 summarizes the mean pole for each cluster, its dispersion, and the approximate percentage of fractures (after Terzaghi correction) belonging to that set. The Kolmogorov-Smirnov (K-S) statistic and its percent significance are shown in Table 3-6. These statistics describe how well a Fisher distribution with the same mean pole trend, plunge and dispersion match the data. In all cases, the K-S statistics indicate a very poor match.

Table 3-6
Relation Between Fracture Orientation And Conductive Fracture Probability.

Set	Mean Pole Trend	Mean Pole Plunge	Dispersion	Percentage of Fractures	K-S Statistic (value, % signif.)	
All Fractures	286.6	6.7	5.78	35.0%	0.037	0.1%
	204.0	4.0	7.11	37.6%	0.033	0.4%
	310.0	82.6	6.22	27.4%	0.090	<0.001 %
Conductive	289.0	6.0	6.04	33.7%	0.068	11.8%
Fractures	202.7	1.7	9.37	46.2%	0.072	3.1%
	292.7	81.1	6.30	20.1%	0.093	9.0%

Table 3-7 shows the relation of conductive fracture by fracture set. Set 1 is a subvertical set striking nearly north-south; Set 2 is also subvertical and strikes west-northwest; Set 3 is subhorizontal. The table indicates that there is a small difference in conductive probability with joint set. The subvertical set that strikes west-northwest has the highest percentage of conductive fractures, followed by the other vertical set, with the subhorizontal set having the lowest probability. The difference in conductive probability among the sets might be due to the differences in dilation/closure effects in the immediate vicinity of the HRL drift. Horizontal fractures will tend to be observed along the tunnel walls, where lithostatic stresses will enhance the compression perpendicular to the horizontal plane. Alternatively, vertical fractures oriented sub-parallel (Set 1) to the HRL access tunnel will experience a similar enhanced compression on the roof.

Table 3-7
Conductive Probability By Fracture Set.

Set Number	Mean Pole Trend	Mean Pole Plunge	Number Dry	Number Wet	Marginal Probability Dry	Marginal Probability Wet
1	286.6	6.7	2419	206	0.92	0.08
2	204.4	4.0	2503	314	0.89	0.11
3	310.0	82.6	1948	109	0.95	0.05
Total			6870	629	0.916	0.084

These findings for joints differ from the results presented by Mazurek and others (1995; p. 43). Their analysis of 87 large faults suggested that almost 60% of these faults had a NW to WNW strike and near-vertical dip. The majority of the other water-bearing faults were also nearly vertical. Horizontal conductive faults are insignificant. However, because the data were not subjected to the Terzaghi correction, faults striking perpendicular to the HRL tunnel would be preferentially represented in the data base at the expense of those sub-parallel to the tunnel. This means that the north to north-northwest vertical and subhorizontal faults would be under-represented relative to the northwest to west-northwest faults. This may explain the difference. Another explanation is that the analysis in this report focuses upon joints and small faults. Joints are extensional features while faults are shear features or joints that have been sheared. Joints form in different orientations than shear features. The increased percentage of water-bearing fractures that are horizontal or sub-vertical and not northwesterly-striking in the **fracture.dbf** file may be due to the inclusion of joints. Finally, that fact that a fracture is designated as water-bearing in the **fracture.dbf** file does not imply anything about the quantity of water. It may be that vertical, northwesterly-striking fractures conduct appreciable quantities of water, while horizontal fractures conduct very little. Both would be marked as water-bearing, however.

A final attempt to determine if there are any mappable geological parameters that could be used to condition a DFN model was made using a neural net. Neural networks are a sophisticated form of non-linear pattern recognition that have found geologic application in groundwater characterization and remediation (Rizzo & Doughery 1994, Rogers & Dowla 1994), well-log and well-test interpretation (Rogers et al. 1992, Al-Kaabl & Lee 1993), seismic and satellite image processing (de Groot 1993, Penn et al. 1993), and

earthquake intensity prediction (Tung et al. 1994). Neural nets have been previously used at Äspö (Stanfors and others, 1994) for predicting groundwater chemistry. Appendix A contains a more detailed description of how a neural net works, and how it was applied to the Äspö fracture data. The goal was to determine if more complex non-linear relations exist between the geological parameters and the conductive state, so that geology could be used to condition the DFN model parameters.

The usefulness of a neural net can be quantified by comparing how well it classifies known data compared to random biased guessing. Consider a test set consisting of 100 fractures, 30 of them conductive, 70 of them non-conductive. Random biased guessing would consist of classifying 70 randomly-chosen fractures as dry and 30 as conductive. Because these fractures have been chosen at random, 70% of the 70 fractures classified as dry should be dry; in other words, 49 of the 70 fractures would be correctly classified as dry, while 21 of the 70 fractures would be incorrectly classified as conductive. Like wise, 30% of the 30 conductive fractures (or 9) would be correctly classified as conductive while 70% of the 30 conductive fractures (or 21) would be misclassified as conductive. The overall correct classification would be 49 + 9 or 58%.

If the geological information relates to fracture conductivity, then the use of this information should improve the correct classification to a value greater than 58%. For example, if the neural net correctly classified 87% of the fractures, the improvement over random guessing is 50%.

These statistics have been compiled (Table 3-8) for the neural net analyses described in Appendix A. Table 3-8 shows results for two different training and testing data sets. A training set is one that is randomly selected from the entire fracture data set that is used to "train" or calibrate the neural net. Ideally it should have an equal number of conductive and non-conductive fractures. A test set is made up of fractures that are not used to calibrate the neural net.

Table 3-8
Neural Network Performance Under Training Sets T1 and T2 Compared with Random Biased Guessing

Testing Set	T1		T2	
Training Epochs (Iterations)	3000		2500	
Data Set	Training	Testing	Training	Testing
Number of Fractures	800	7529	1000	7329
Actually Wet	50.0%	4.1%	40.0%	4.2%
Actually Dry	50.0%	95.9%	60.0%	95.8%
Correctly Predicted as Wet/Dry				
Neural Network	78.0%	49.6%	79.2%	80.6%
Random Biased Guessing	50.0%	50.0%	52.0%	59.2%
Percent Improvement	*56.0%*	*-0.8%*	*52.3%*	*36.1%*

Overall, the neural net did slightly worse than random guessing for the first training set, and improved about 36% for the second training set. The reason for the difference in performance between the two sets is the difference in ratio of dry to wet fractures in the training sets. In the first training set, the probability for wet and dry fractures is equal, while in the second set, the probability for dry fractures is higher. What this means is that the neural net in the second case will tend to classify fractures as dry when the geological information does not strongly indicate that a fracture is wet. Because the testing sets have a much higher ratio of dry to wet fractures, a much higher proportion of the dry fractures will be correctly classified as dry, as shown in Table A-2 in Appendix A.

The variables that the net is using to classify unknown data can be identified by examining the synaptic weights of the trained Äspö net. A common method for viewing the synaptic weights in a network is the Hinton diagram (Figures 3-4, 3-5). In this diagram, input parameters with greater influence over the classification are represented by rows of larger positive or negative weights, which are shown as boxes. Bigger boxes indicate bigger weights. Boldface box outlines indicate that the weight is negative. For the trained Äspö neural network, larger negative weights have a positive correlation to wetness.

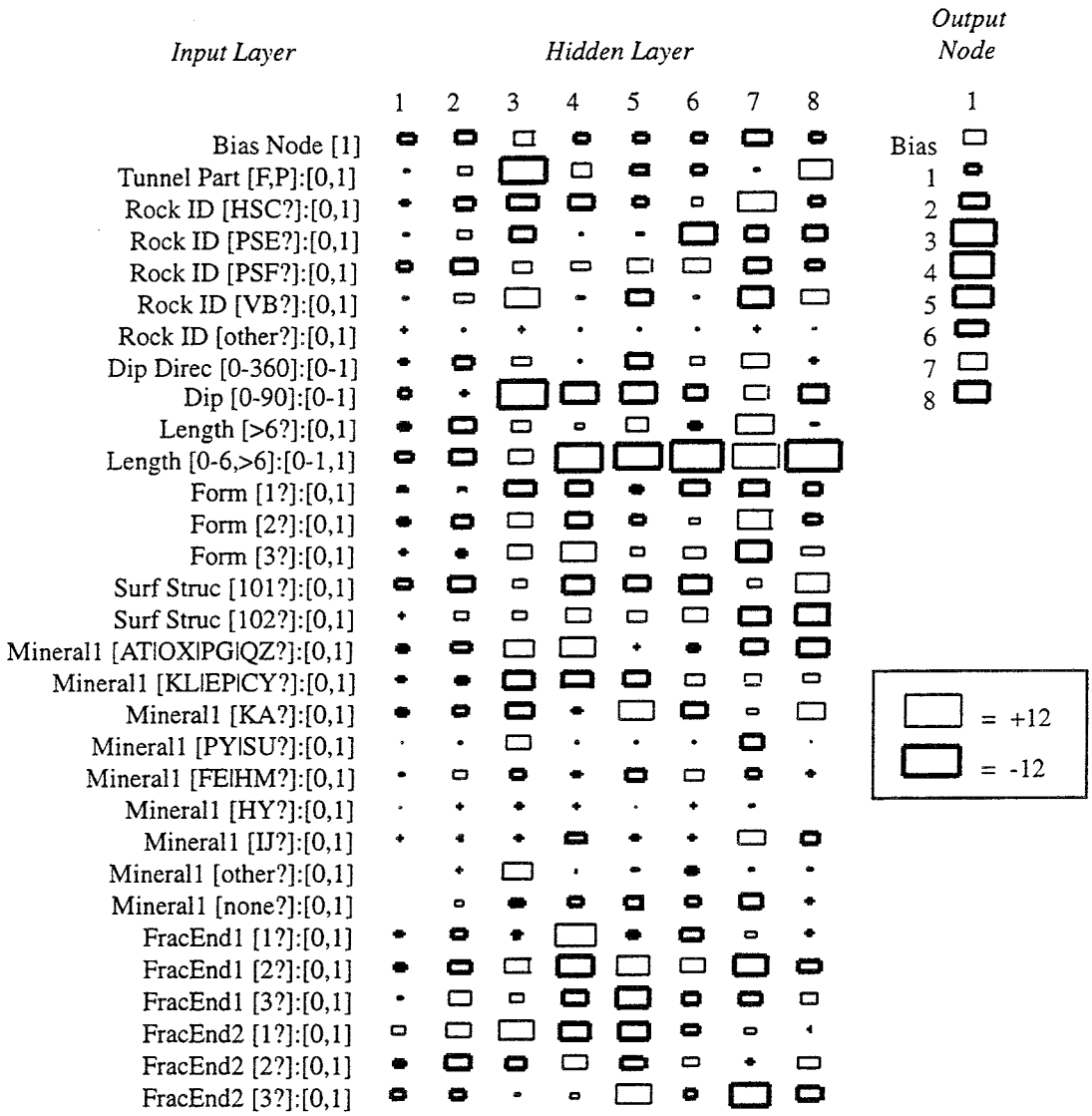

FIGURE **3-4**

SYNAPTIC WEIGHTS – TRAINING SET T1
2000 TRAINING EPOCHS

SKB/ÄSPÖ-DFN/SWEDEN

PROJECT NO. IC3-1161.001 DRAWING NO. 60491 DATE 9/8/95 DRAWN BY EA

Golder Associates

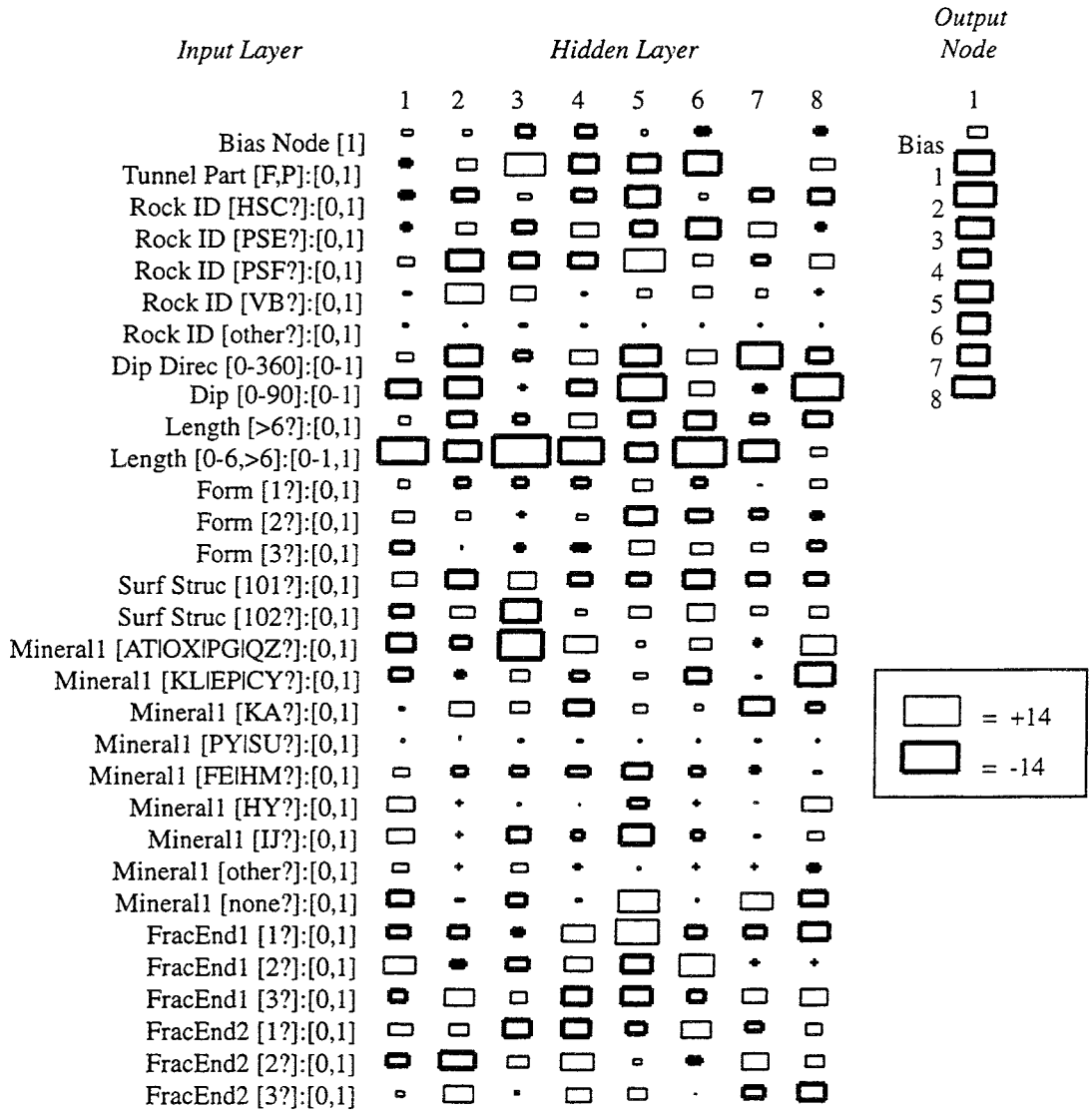

FIGURE **3-5**

SYNAPTIC WEIGHTS – TRAINING SET T2
2000 TRAINING EPOCHS
SKB/ÄSPÖ-DFN/SWEDEN

A more quantitative estimate of input parameter influence is provided by relation factors. Of these, the simplest is *relation factor one*, which is computed by subtracting the output of the network with all input neurons set to zero from the output with a single neuron set to one. For the Äspö network, an input parameter with a positive relation factor promotes fracture wetness. The largest relation factor one for the T2-trained network is 0.06, indicating that no single fracture property is diagnostic of fracture wetness. Instead, a fracture is classified as conductive only if possesses a series of properties in combination.

From the network weights shown in Figures 3-4 and 3-5 and the relation factors shown in Table 3-9, it can be seen that the most important factors for classifying a fracture as wet are length (longer fractures tend to be more conductive), dip (steeply dipping fractures tend to be more conductive), and rock type (fine-grained granite tends to be more conductive; greenstone tends to be dry). Of secondary importance are mineral infillings, surface structure, form, and termination relations.

The relation between certain geological features identified by the neural net and conductivity is sensible. The neural net indicates that conductive fractures are more likely to be long, steeply dipping and have terminations that lie outside of the mapped surfaces. There is a slight positive correlation with increasing roughness, a mineral filling of chlorite, epidote and clay, and a planar shape. Big fractures have a higher probability of intersecting other fractures, and so have a higher probability of forming a regionally interconnected network. Steeply dipping fractures might be more conductive because vertical fractures would tend to be more open with the present-day in situ stress field in the rock. Curved fractures are usually curved because of the existence of a local boundary effect when they were forming, often a pre-existing fracture. In this setting, either the fracture will cease to propagate, or it will terminate at the boundary. Thus, curved fractures tend to be shorter fractures, which have a lower probability of forming or being part of a regional network.

Table 3-9
Relation Factors for the Äspö Neural Network

Input Node	Description	Relation Factor 1	
		Training Set T1	Training Set T2
1	Tunnel Part	0.00020	0.00000
2	HSC	0.32453	0.00159
3	PSE	0.00135	0.00000
4	PSF	0.00000	0.00000
5	VB	0.00000	0.00000
6	Other	0.00003	0.00000
7	Dip Direc	0.00034	0.00001
8	Dip	0.89703	0.00934
9	Length[> 6 m]	0.00003	0.00020
10	Length [0,6 m]	0.19124	0.06451
11	Form = Plane	0.07649	0.00000
12	Form = Undulating	0.00467	0.00000
13	Form = Arched	0.00000	0.00000
14	Surf Struc = Rough	0.00027	0.00003
15	Surf Struc = Smooth	0.00000	0.00000
16	Mineral1 [AT|OX|PG|QZ]	0.00000	0.00000
17	Mineral1 [KL|EP|CY]	0.01940	0.00002
18	Mineral1 [KA]	0.00002	0.00000
19	Mineral1 [PY|SU]	0.00001	0.00000
20	Mineral1 [FE|HM]	0.00007	0.00001
21	Mineral1 [HY]	0.00005	0.00000
22	Mineral1 [IJ]	0.00192	0.00000
23	Mineral1 [OTHER]	0.00002	0.00000
24	Mineral1 [NONE]	0.00044	0.00000
25	FracEnd1 = Outside	0.00001	0.00002
26	FracEnd1 = Free	0.00000	0.00000
27	FracEnd1 = Against	0.00011	0.00000
28	FracEnd2 = Outside	0.00025	0.00000
29	FracEnd2 = Free	0.00001	0.00000
30	FracEnd2 = Against	0.00000	0.00000

However, the most important result of the neural net analysis is that there are no strong relations, linear or non-linear, between mappable geological parameters and the conductive subpopulation of fractures. While it might seem that the net's 80.6% correct prediction for the second testing set is quite high, random guessing is correct 59.2% of the time. Moreover, if one automatically classified all fractures as dry regardless of geological factors, then 95.8% of the fractures would be correctly classified! However, the error for this method is highly biased (all the misclassifications are for the wet

fractures), which implies that it is of no use whatsoever. The error for the neural net predictions are far less biased (for example, see Table A-2 in Appendix A).

The contingency table and neural net analyses imply that:

1) Present data does not suggest that the geometry or hydraulic properties of a DFN model of the rock outside of the fracture zones should vary according to rock type or other mappable geological feature for regional flow modeling. In other words, the geometric and hydraulic properties of the fracturing at Äspö appear to be stationary, and the DFN models should also be stationary.

2) Conductive fractures probably represent the larger size fraction of all of the fracture sets at Äspö. They are otherwise not significantly different than non-conductive fractures in terms of geology and geometry.

3.1.2 Orientation Analysis

Table 3-6 also summarizes the orientation statistics for the three identified conductive sets. The K-S statistic reported in this table is the Kolmogorov-Smirnoff test statistic followed by its percent significance. These statistics represent how well a Fisher orientation distribution model fits each set. As the poor statistics show, a Fisher model is a poor representation for any of the sets. For this reason, the orientations for the fractures in the DFN models created in Sec. 4 were bootstrapped directly from the stereoplots of conductive fracture orientations rather than generated from a statistical model for distributions of points on a sphere, such as the Fisher distribution.

3.1.3 Size Analysis

Fracture size is an important component of any fracture network, since size plays an important role in the scale of fracture network connectivity.

Previous work on determining the size of fractures at Äspö was based upon trace length analysis in outcrop (Ericsson, 1987, 1988; Uchida and Geier, 1992, *see also* Doe and others, 1994), or from the HRL (e.g. Stanfors and others, 1994; Rhén and others, 1994). Outcrop work by Ericsson on fractures with trace lengths greater than 0.5 m indicated that

median fracture trace lengths vary from about 0.6 m to 1.2 m (Ericsson, 1987, p. 12), with some variation by rock type. The greenstones appear to have the shortest traces, while the tonalities and porphyritic granites show the largest. All rock types have similar trace length standard deviations, on the order of 0.37m. In an additional outcrop study, Ericsson (1987) reports that the traces lengths for calcite filled and red-stained fractures have mean lengths varying from 1.2 m to 1.57 m (median 0.85 m to 1.10 m) on Äspö. The calcite filling and staining is thought to be possible evidence of fluid flow and indicative of the fracture having been part of a regional conductive fracture network. Supplemental work reported by Ericsson (1988) examined trace length in terms of other mappable geological and geographic factors, and still found that mean trace lengths were on the order of 1.0 m to 1.5 m. This data was collected from exposures from 30 m^2 to 200 m^2. As a result, the trace length data was severely censored. The trace length data for this types a data becomes more an expression of the dimensions of the cleared outcrop surface shape and area rather than the actual lengths of the fracture traces.

Uchida and Geier (1992) mapped 10 outcrops spread over Äspö Island which were not subject to the same severe censoring problems. The sample used was much smaller, consisting of 200 fracture trace lengths. The mean trace length for this sample was 13.0 m. The standard deviation was 8.12 m, and the median length was 11.0 m. No work on relating mapped trace length to rock type or other geological parameters was attempted.

Uchida and others (1994) used this outcrop data to estimate fracture size from the fracture trace length distribution using the FracSys module in FracMan (Dershowitz and others, 1994). The FracSys algorithm consists of making a guess as to the fracture size distribution, simulating a 3D discrete fracture model with fracture sizes conforming to that guess, placing planes into the simulation of the same orientation as the outcrops, and observing the simulated trace length distribution. If the simulated trace length distribution matches the mapped trace length distribution within acceptable limits, then the "guess" is accepted as being a useful estimate of the actual fracture size distribution. In practice, the "guess" is usually unacceptable; however, FracMan contains non-linear optimization algorithms to change the "guess" until better matches are achieved. Using this algorithm, Uchida and others (1994) found that a distribution of fracture sizes conforming to a lognormal distribution with mean 13.7 m and standard deviation 12.7 m

produced an excellent trace length distribution match. No work concerning fracture size as a function of orientation or any geological parameters was reported in this study.

Mapping of exposures underground in the HRL including measuring the length of fracture traces exposed on the tunnel walls and advancing face during tunnel construction. Fractures with traces greater than 0.3 m were recorded, along with many other types of geological parameters. Examination of the dependence of trace length upon mappable geological features concluded that:

1) fracture trace lengths vary with filling mineralogy

2) trace lengths do not vary with rock type

3) fracture traces in fracture zones appear to be shorter

4) conductive fractures tend to have longer traces than non-conductive fractures

5) steeply-dipping fractures striking in the interval 60° to 130° tend to have shorter trace lengths.

There exists a problem with relating trace length in the tunnels to the actual size of the fracture, once again because of severe censoring caused by the insufficient size of the tunnel relative to the fracture areas. La Pointe and others (1993b) showed how when fractures are larger than the tunnel cross section, the distribution of trace lengths that would be observed on tunnel walls can be statistically the same for very different fracture size distributions. They are highly non-unique. Thus, trace length distributions where many of the fracture traces are censored are not very useful for inferring fracture size. However, the censoring effect itself can be used to estimate fracture size.

Consider the fact that the larger the fracture, the more likely it is to completely intersect a tunnel, given that it intersects the tunnel at all. For example, a fracture 1 m in diameter might intersect the Äspö HRL tunnel. Its trace would be at most 1 m in length. This trace would generally be exposed on a single tunnel surface, such as the left wall or the roof. In the rarest of occasions, it might intersect a corner of the tunnel. In no cases

would its trace be exposed on both wall or both wall and the roof. On the other hand, a very large fault with a diameter of 1 km would typically have a trace that extends all the way around the tunnel opening. It turns out that for a particular fracture orientation, tunnel orientation and tunnel cross-section, the probability that the trace could be mapped all the way around the tunnel surfaces is a function of the fracture size. Virtually 100% of 2 km-diameter fractures would have traces mappable around the entire tunnel, given that they intersected the tunnel. 0% of the 1 m diameter fractures would have traces mappable around the entire tunnel. A very high percentage (the exception being the fractures which intersected tunnel corners) of the 1 m fractures would have traces confined to a single tunnel wall or surface. A very low, nearly 0% of the 2 km fractures would have traces only on a single surface. By computing the statistics for the *amount* of the tunnel surface that traces for a particular fracture set occur on, it is possible to estimate the fracture size distribution. To simply the quantification of the *amount* of tunnel surface for fractures in the HRL, it was determined whether each trace was mapped on one wall, the roof, or the other wall. Statistics were compiled to determine the probability that a trace intersected one, two or three tunnel surfaces. Simulations were then carried out with different fracture size assumptions, a series of simulated tunnel surfaces then emplaced into the DFN, and the trace length one-, two- and three-surface statistics computed (Figure 3-6). This method was applied to the Äspö data in order to estimate the fracture size distribution.

Since the DFN model is based upon the conductive fractures, it is the size of these fractures which should be estimated. Indications from mapping in the HRL (Stanfors and others, 1994) suggest that the conductive fractures might be larger than the general population of fractures. This is consistent with previous experience in other crystalline rock sites (La Pointe and others, 1993b). This is logical, since larger fractures will have a higher probability of intersecting other fractures and forming a regional flow network. Smaller fractures are less likely to intersect other fractures and be attached to the regional flow network.

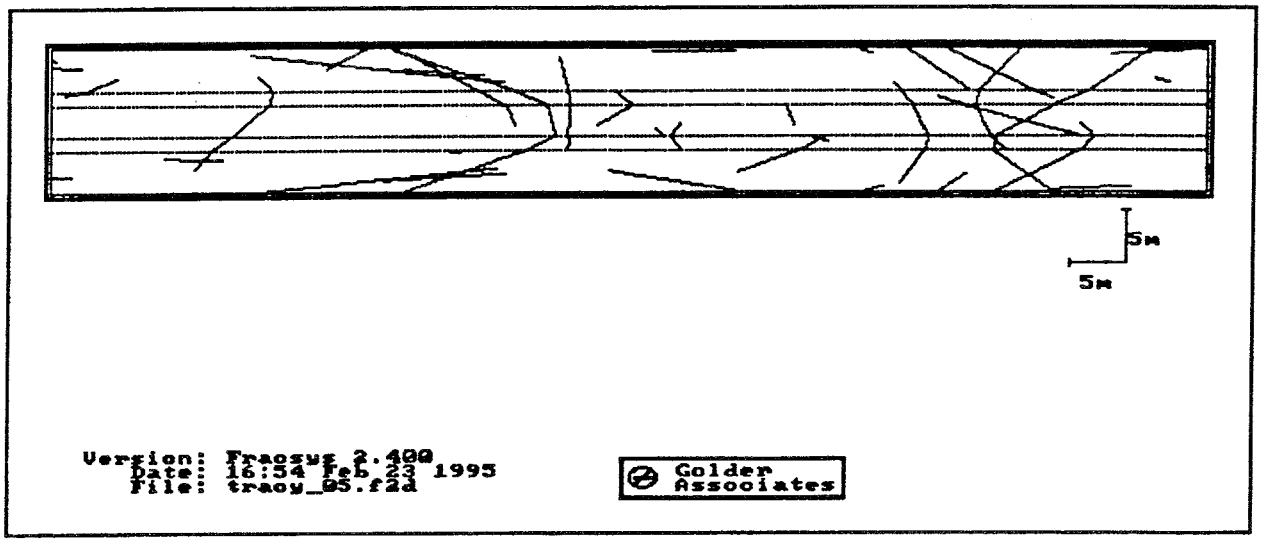

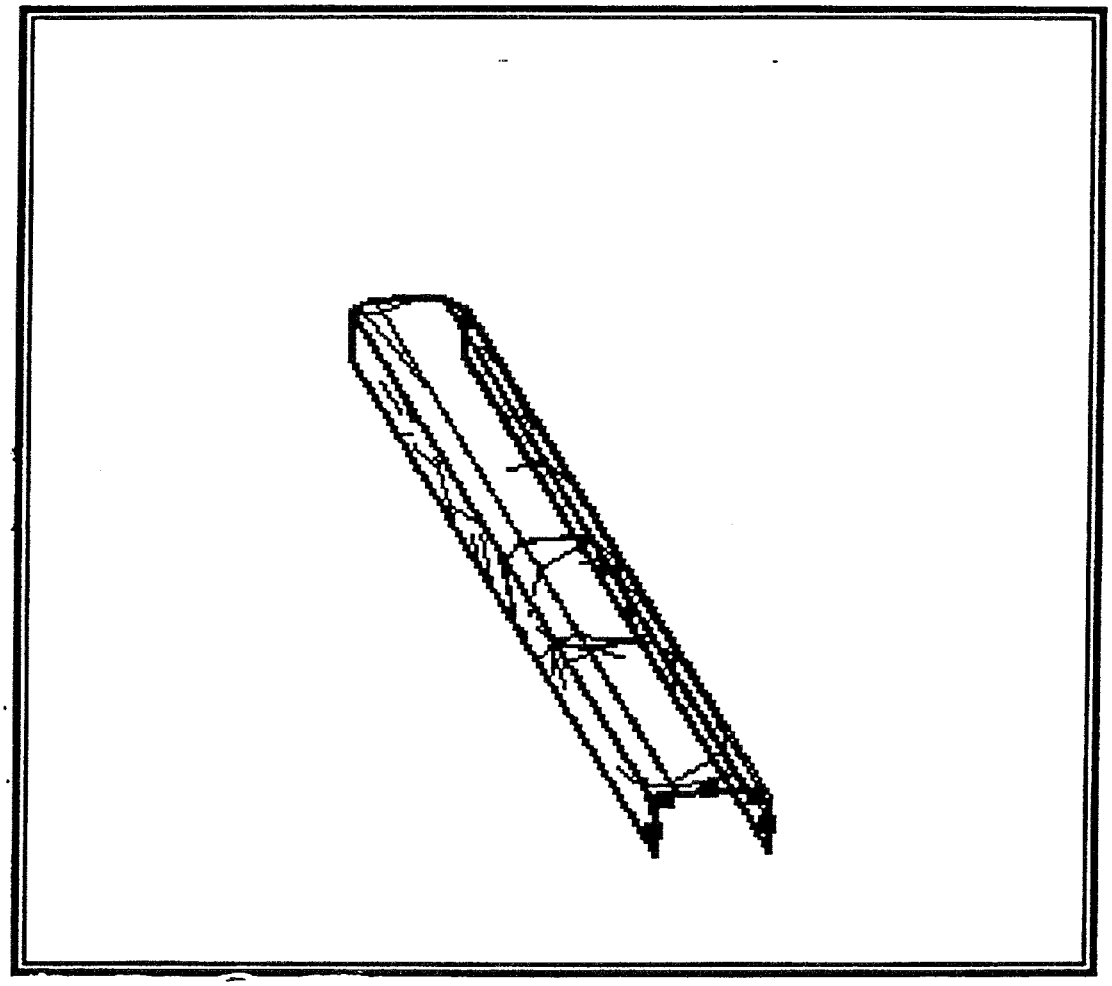

FIGURE **3-6**
METHOD FOR ESTIMATING FRACTURE SIZE
SKB/ASPO-DFN/SWEDEN

The tunnel maps in Stanfors and others (1994; Figures 3-2, 3-3, 3-4 and 3-5) that show the fracture trace data were used to calculate how many fractures were observed on 1, 2 or 3 tunnel surfaces. There were two problems encountered in using this data:

1) blasting/excavation creation or extension of fractures, and

2) integration of tunnel maps with the fracture data base.

When a tunnel is excavated through blasting, it is likely that new fractures are created and existing fractures are enlarged. These effects will distort the size distribution. The newly-created fractures may be difficult to distinguish from existing fractures. There are a few features which can help distinguish natural fractures from artificial fractures (Kulander and others, 1990). Natural fractures often have mineral coatings while artificial ones do not. Also, blasting-induced fractures tend to be small. However, there are naturally occurring, small, uncoated fractures as well, so these criteria will not correctly separate all natural fractures from the artificial fractures.

No specific guidelines are prescribed in the HRL tunnel mapping protocol (Christiansson and Stenberg, 1991) for discriminating between natural and artificial fractures. The guidelines specifically state that all fractures greater than 1.0 m (PR 25-91-19, p. 6) should be recorded on the tunnel maps. This may have led to the inclusion of artificial fractures.

Since fractures created through blasting and excavation should tend to be small, in general they should only intersect one tunnel surface rather than span two or three surfaces. An enhancement of an existing fracture that already spans two surfaces will unlikely be sufficient to make it span three surfaces. Thus, if the size estimate is based upon only the intersection statistics for 2 and 3 panel intersections, the effects of blasting should be reduced. The disadvantage is that an additional constraint, the 1-panel intersection probability, is removed. This is a problem in that most size distributions have two degrees of freedom - the mean and standard deviation - but the ratio of 2 panel intersections to 3 panel intersection provides only a single constraint. Thus it is possible to have a much wider range mean and standard deviation combinations that produce acceptable intersection probabilities. Because the 1 panel intersection

probabilities are unreliable without additional attempt to distinguish natural fractures from artificial ones, the size estimates were based only on the 2 panel and 3 panel intersection probabilities.

The second problem relates to the way in which fracture locations were recorded in the HRL drifts. In **fracture.dbf**, fracture locations are described by the tunnel section in which they occur. These sections can be many meters in length, so there is no easy way to relate a fracture in the database to a specific fracture shown in the tunnel maps. If they could be related, then it would be possible to calculate the panel intersection probabilities for only the fractures identified as being conductive in the database. Unfortunately for this study, the amount of work and time required to integrate the map and electronic data made this not feasible. As a result, the size estimates from the Äspö tunnel data are for all fractures, both conductive and non-conductive. Since the conductive fractures are likely to be the same size or larger than the non-conductive, these size estimates provide a lower bound on the conductive fracture size.

Table 3-10 summarizes the results from the analyses of the three drift maps published by Stanfors and others (1994). Only data from the straight portions of each drift map were analyzed, since this portion could be most easily simulated for the DFN calculations. The net length of the drift map analyzed was converted to a normalized weight. The relative 2- and 3-panel intersection percentages were determined by counting the number of fracture traces that appeared on two adjacent or three tunnel surfaces, and dividing by the total number of 2- and 3-panel intersections. The absolute 1-panel percentage was not measured directly from the map, but was calculated by subtracting the total 2- and 3-panel intersections from the total number of fractures recorded over the same interval in the electronic fracture data base. Mismapping or mis-classifying one or two fracture traces will lead to an error of 1 or 2% for the 2- and 3-panel intersection percentages reported in Table 3-10.

Table 3-10
Panel Intersection Statistics Derived From Underground Mapping
In The HRL Access Tunnel

Tunnel Section Map Figure Reference (PR 25-94-19)	Absolute 1-Panel %	Relative 2-Panel%	Relative 3-Panel%	Normative Weight Based on Section Length Analyzed
Loop 1, Leg E-F	82.1	77.4	22.6	0.348
Loop 1, Leg F-G	82.2	76.6	23.4	0.294
Loop 1, Leg G-H	89.4	82.5	17.5	0.358
Weighted Averages	84.7	79.0	21.0	1.0

The data in Table 3-10 show that the relative number of 3-panel intersections is in the neighborhood of 21% (21% of all mapped fracture traces are seen on portions of all three mapped tunnel surfaces). The number of fractures found only on one panel is approximately 85%. Since the number of 1-panel fractures induced by blasting and excavation is likely to be higher than for the 2- and 3-panel intersections, 85% probably represents a maximum upper bound. Previous work at other crystalline rock sites (La Pointe and others, 1993b) indicates that the absolute 1-panel percentage of conductive fractures can be as low as 20% while the 1-panel percentages for all of the fractures can reach 60%. Thus it is not unreasonable to expect that the number of 1-panel intersections with blasting effects removed might half or less of the measured 85%. Relative 3-panel intersections might range between 15% to 25%.

Figures 3-7 through 3-10 summarize the results from the size analysis. Two types of distributions were tested: lognormal and exponential. Virtually all published studies on fracture size indicate that fracture sizes correspond to one of these distributions. While there are several combinations of mean and standard deviation that produce the same percentage of 2 panel vs. 3 panel intersections, distributions with a very small standard deviation are geologically improbable. A small standard deviation implies that fracture size is nearly constant. Constant fracture sizes are not predicted by any current theory of rock breakage, nor is there any published field study that suggests that rock fractures

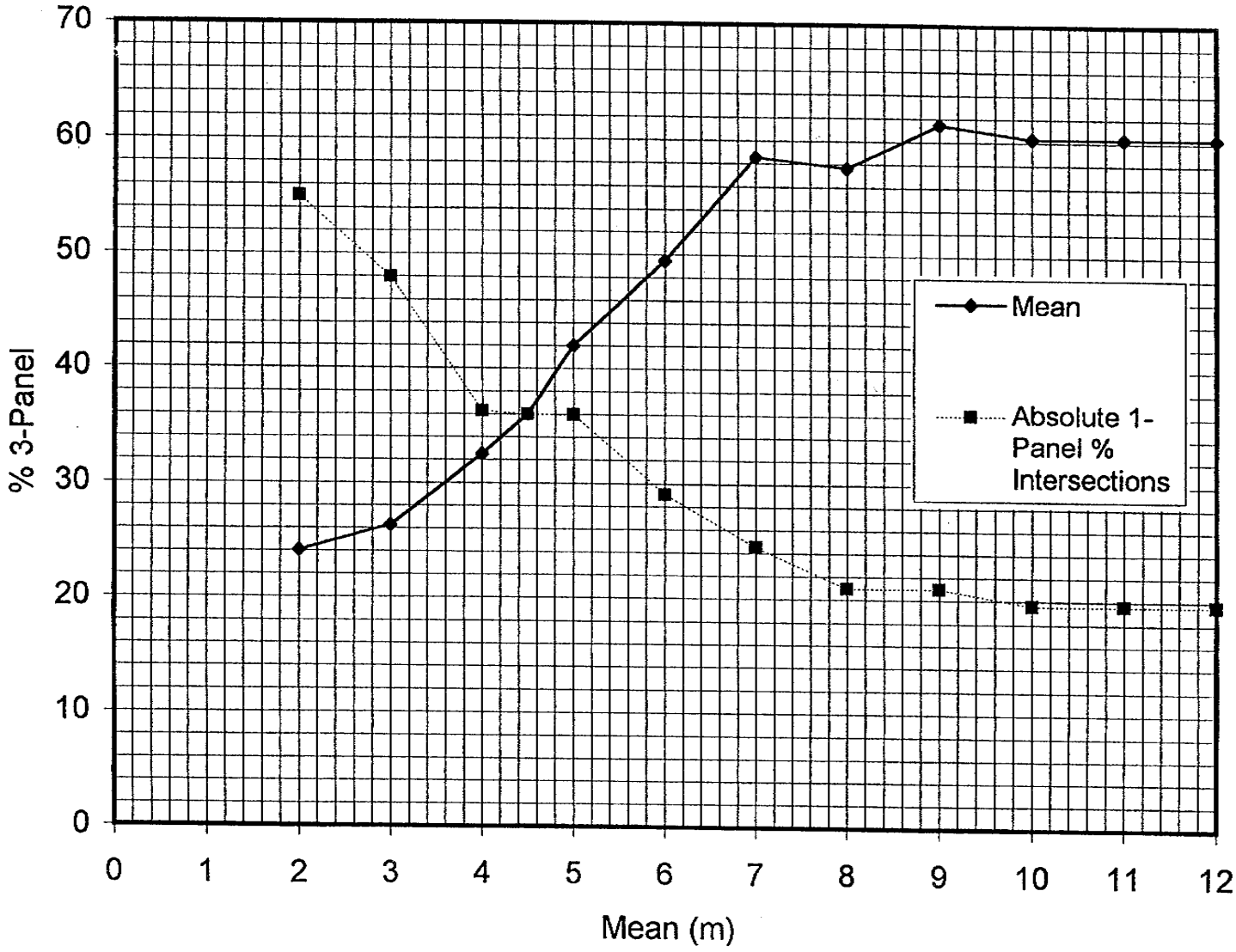

FIGURE **3-7**
PERCENTAGE 3-PANEL INTERSECTIONS FOR ALTERNATIVE EXPONENTIAL SIZES
SKB/ASPO-DFN/SWEDEN

PROJECT NO. IC3-1161.003 DRAWING NO. 60494 DATE 9/8/95 DRAWN BY EA

Golder Associates

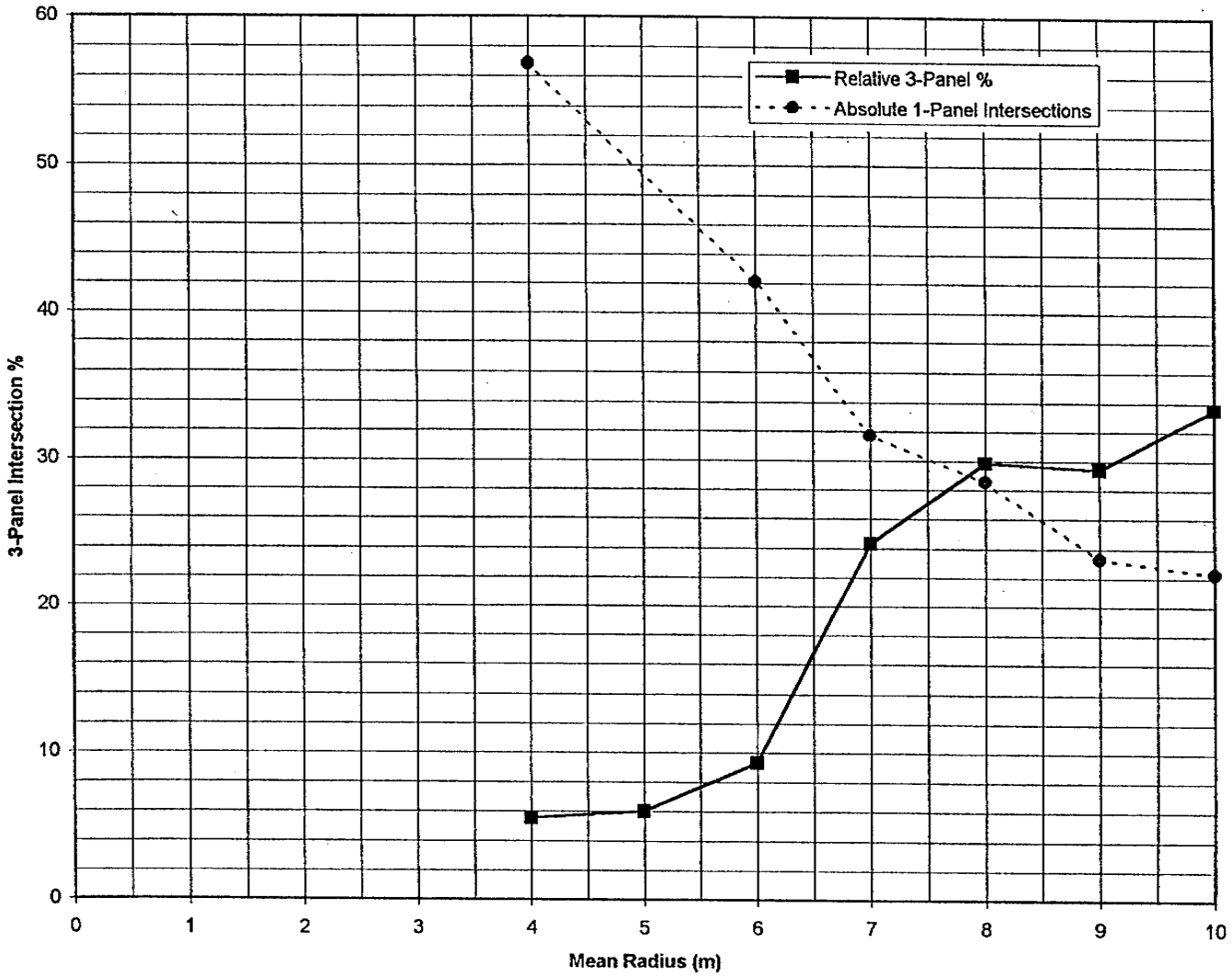

FIGURE **3-8**
3-PANEL INTERSECTION PERCENTAGES FOR DIFFERENT MEAN RADII
SKB/ASPO-DFN/SWEDEN

PROJECT NO. IC3-1161.003 DRAWING NO. 60495 DATE 9/8/95 DRAWN BY EA

Golder Associates

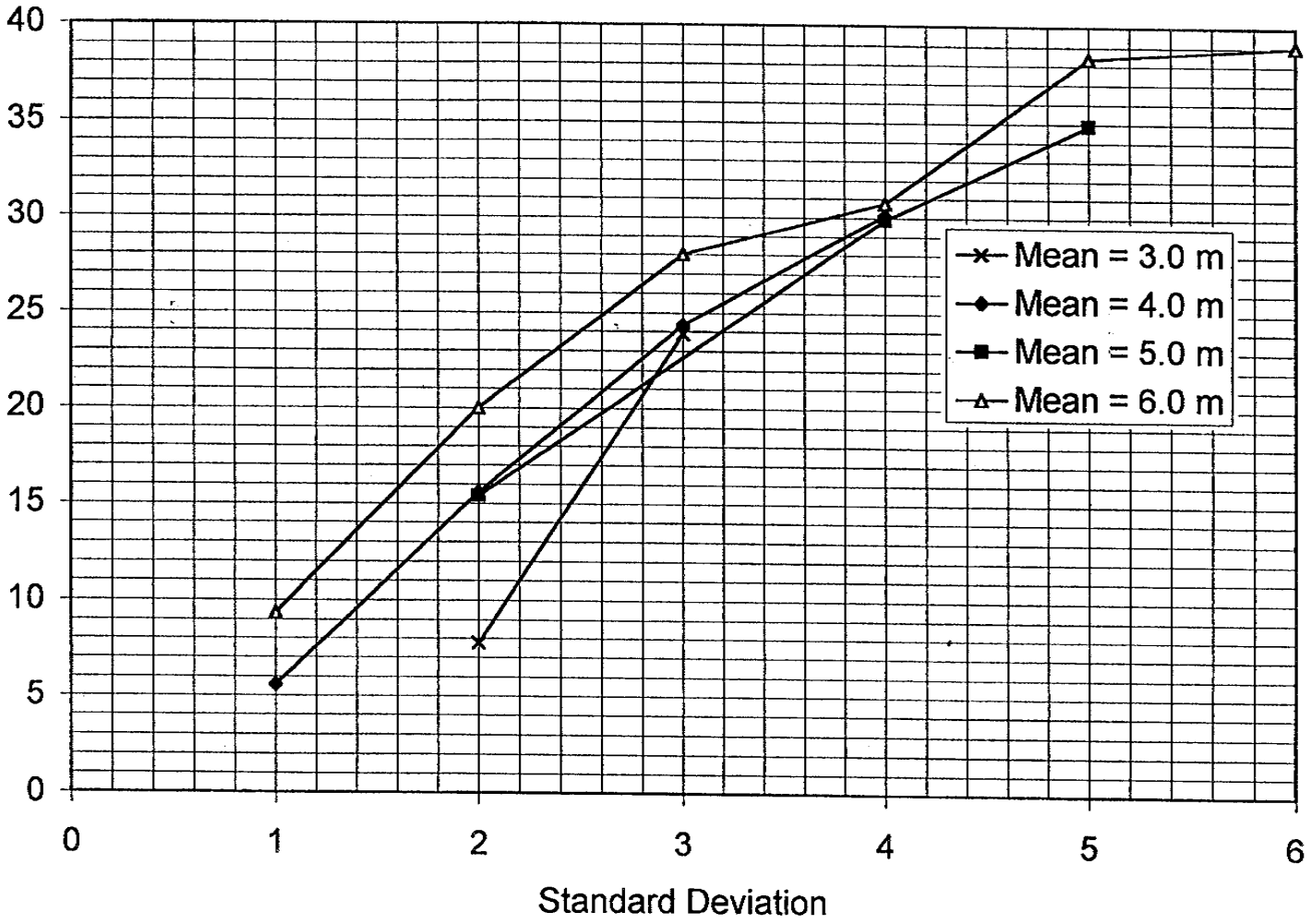

FIGURE **3-9**
PERCENTAGE OF 3-PANEL INTERSECTIONS FOR ALTERNATIVE LOGNORMAL SIZES
SKB/ASPO-DFN/SWEDEN

PROJECT NO. IC3-1161.003 DRAWING NO. 60496 DATE 9/8/95 DRAWN BY EA

Golder Associates

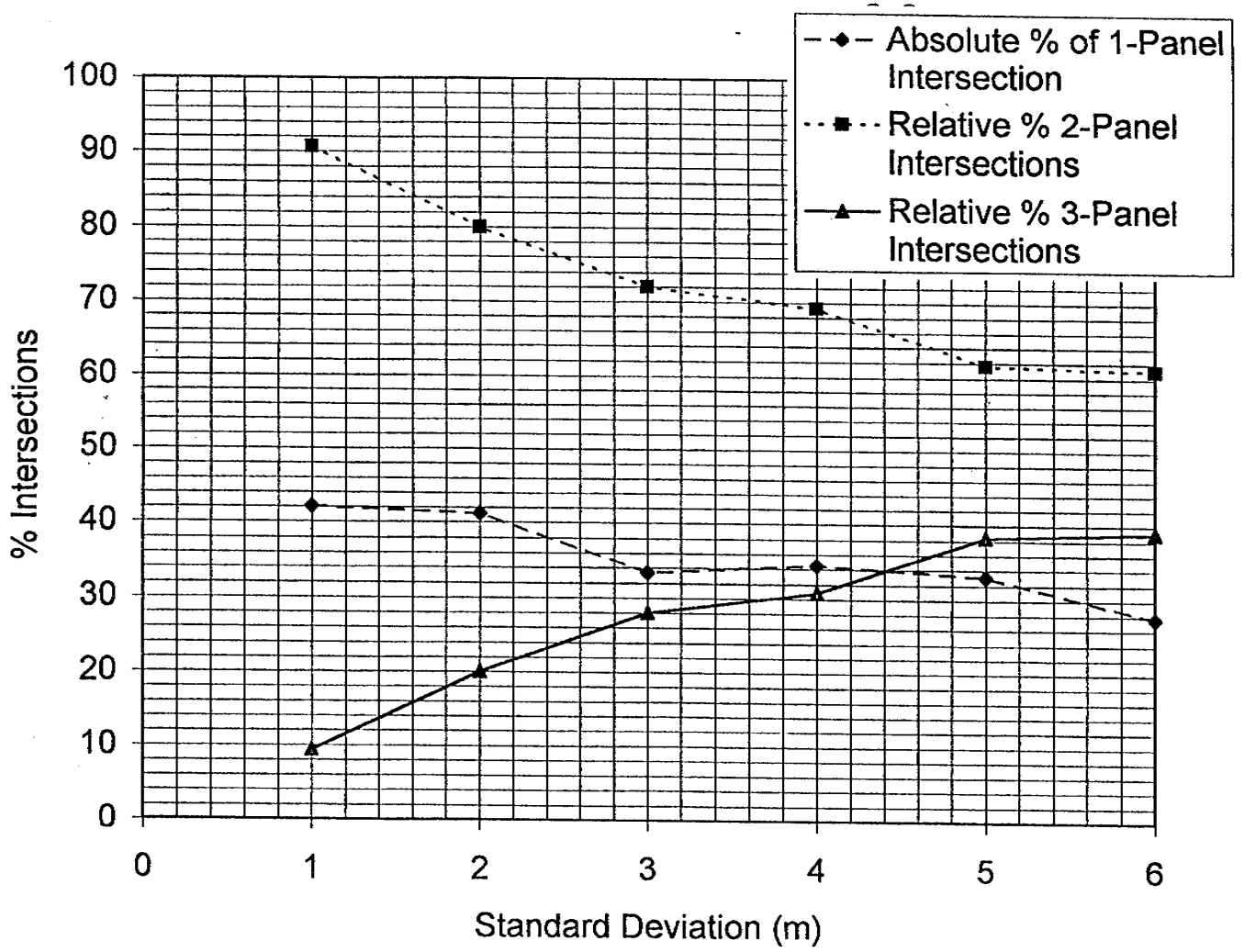

FIGURE **3-10**
DETAILED STATICS FOR LOGARITHMIC SIZE DISTRIBUTION WITH MEAN RADIUS = 6.0 m
SKB/ASPO-DFN/SWEDEN

PROJECT NO. IC3-1161.003 DRAWING NO. 60497 DATE 9/8/95 DRAWN BY EA

Golder Associates

are of nearly constant size. On the contrary, published maps of fracture traces show a wide range of fracture trace lengths, suggesting that fracture sizes for each fracture set may vary widely. For these reasons, the criteria adopted for picking the "best" match was to:

1) Compare the simulated 3-panel percentages to the mapped percentages. They should be approximately 21%;

2) Compare the simulated absolute 1-panel percentages to the mapped percentages. The should be no more than 85%. Values half this value may be reasonable;

3) Favor size distribution parameters that maximize mean and standard deviation.

Criterion 3 served two purposes: to reject size distributions with a very low standard deviation, which are geologically unrealistic, as described previously; and to try to partially account for the statistical analysis that indicates that conductive fractures tend to be larger than the general population.

Figure 3-7 shows the results for the exponential distribution. The solid line shows the results for mean fracture radius varying from 2.0 m to 12.0 m. Values of 2.0 m or less would match the 3-panel and 1-panel intersection criteria within the error of the study, but such sizes are unrealistically small.

Figures 3-8 and 3-9 show the results for alternative combinations of mean and standard deviation for a lognormal radius assumption. Figure 3-8 shows how the percentages vary for a constant standard deviation of 1.0 m and alternative values of mean radius. Mean radii greater than 6.0 m produce 3-panel percentages that are too high without having unrealistically low (<1.0 m) standard deviations. Figure 3-9 shows matches for means ranging from 3.0 m to 6.0 m and different values of standard deviation. A very good match is shown for a mean of 6.0 m and a standard deviation of 2.0 m (Figure 3-10). The 3-panel intersection percentage is about 20%, while the absolute 1-panel percentage is about 40%. This appears to be a reasonable match with statistics calculated from the trace maps. For this reason, a lognormal radius distribution with

mean equal to 6.0 m and a standard deviation of 2.0 m was chosen as a lower size bound for the modeling carried out in Section 4 of this report.

A lognormal distribution with mean equal to 13.7 m and standard deviation equal to 12.7 m as determined by Uchida and others (1994) was chosen to be an upper size bound. The resulting difference in block-scale flow properties is discussed in Section 4.4.

3.1.4 Fracture Intensity Analysis

For a DFN model, fracture intensity is defined as the amount of fracture area divided by the volume rock in which the fractures are located. It has units of m^{-1} and the symbol P_{32}. This measure of fracture intensity has desirable mathematical properties which other measures, such as the number of fractures per volume of rock, do not. One property that is very useful for constructing a DFN fracture model is that there is a linear relation between P_{32} and the number of fractures intersected along a borehole (P_{10}) or the trace length per unit area on a planar surface (P_{21}). These two constants depend only upon the orientation distribution of the fractures, their size distribution, their shape, and the size and shape of the borehole or plane. The constants do not depend upon how many fractures there are.

The fracture intensity measure, P_{32}, cannot be measured directly in the field. However, because P_{32} has a constant relation to the fracture intensity measured in a borehole or along tunnel walls, it can be calculated from borehole or tunnel intensity values. The procedure consists of guessing a value of P_{32} and using this value to create a DFN with appropriate fracture sizes and orientations. Then synthetic boreholes or underground drifts are inserted into the DFN model, and the amount of fractures per unit length of wellbore or trace length per unit area of tunnel surface is calculated. The ratio between the guess of P_{32} and the number of fractures per meter of wellbore in the simulation is the desired constant. To estimate the true P_{32}, this constant is multiplied by the actual wellbore or trace plane fracture intensity.

The goal of this portion of the project is to estimate values of P_{32} for conductive fractures only using each of the two size assumptions. There are two available datasets for

estimating the conductive P_{32}. One data set consists of the borehole packer tests from wells KAS02 through KAS08. The other data set consists of the conductive fracture intensity measured in the HRL access tunnel.

The first data set has previously been analyzed by Uchida and others (1994) using the OxFilet algorithm. Analysis of the 30 m tests yielded an estimate of 0.033 conductive fractures/m, while analysis of the 3 m packer tests produced an estimate of 0.038 conductive fractures/m. The value of 0.033 was selected since this corresponds to the larger scale tests.

Figures 3-11 and 3-12 show the relation between P_{32} and the average conductive fracture intensity in wells KAS02 through KAS08 based upon DFN simulations. Twenty-five realizations were carried out for each value of P_{32}. For the small fracture size assumption, the value of P_{32} corresponding to a fracture intensity of 0.033 is 0.0664. For the large fracture size assumption, the fracture intensity is insignificantly less, so a single value of 0.0664 was chosen from these analyses.

The analyses of the tunnel data (Figures 3-13 and 3-14) produced higher estimates of P_{32}. The conductive fracture intensity for the HRL access tunnel was based on the data from the main tunnel entrance through the end of Section 1497.7. Since this portion of the drift is approximately linear, it makes calculations within the DFN model much simpler. Over this section of the HRL, 499 fractures were marked as conductive in the database, leading to an intensity of 0.333 fractures/m. Simulations for the two different fracture sizes yielded the graphs shown in Figures 3-13 and 3-14. For the large assumption, the analysis estimates a conductive P_{32} of 0.33, while for the small size assumption, the estimate is 0.207.

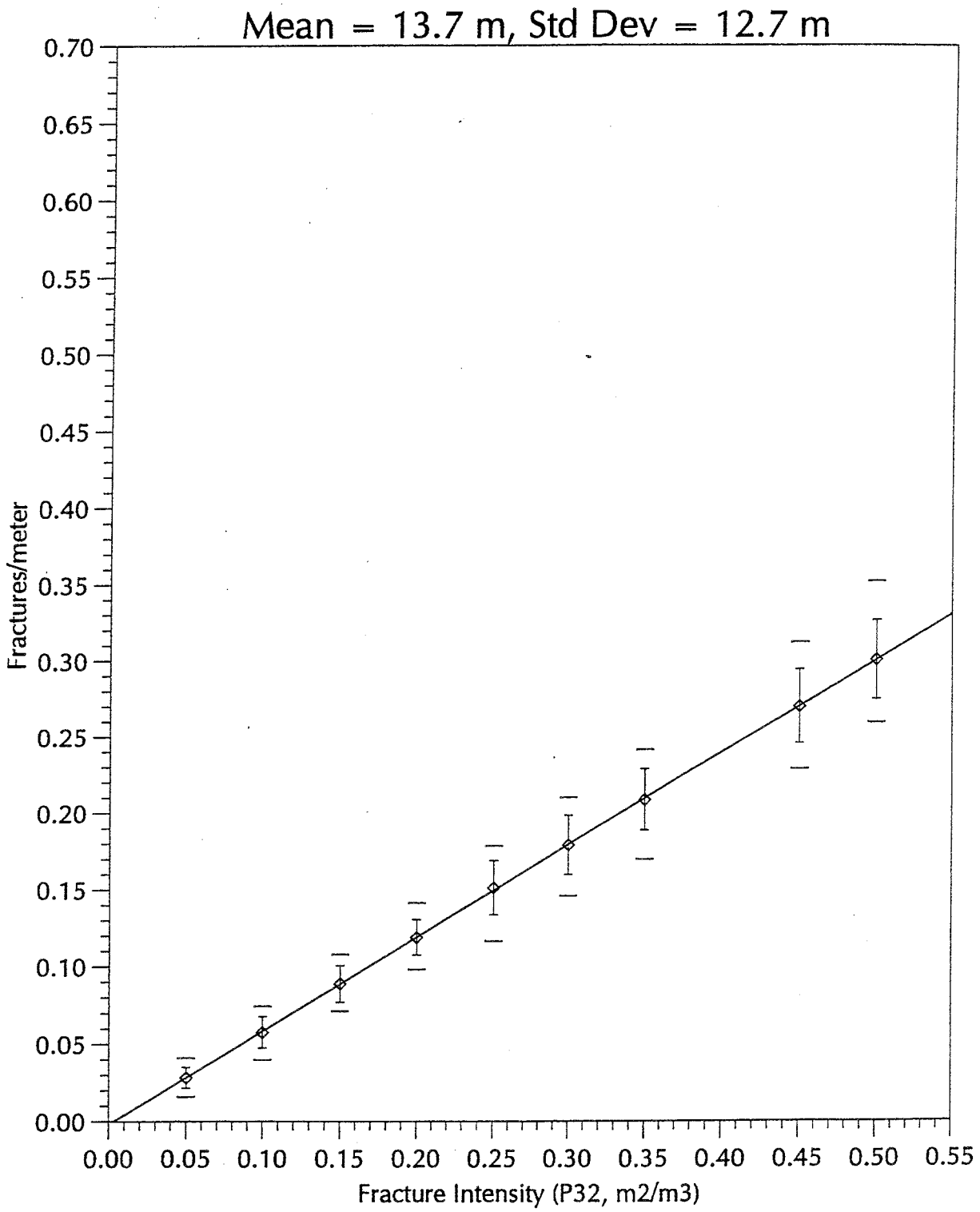

Bar on symbol shows ± one standard deviation
Horizontal brackets indicate maximum
and minimum results

FIGURE **3-11**
BOREHOLE FRACTURES/METER VS P_{32}
SKB/ASPO-DFN/SWEDEN

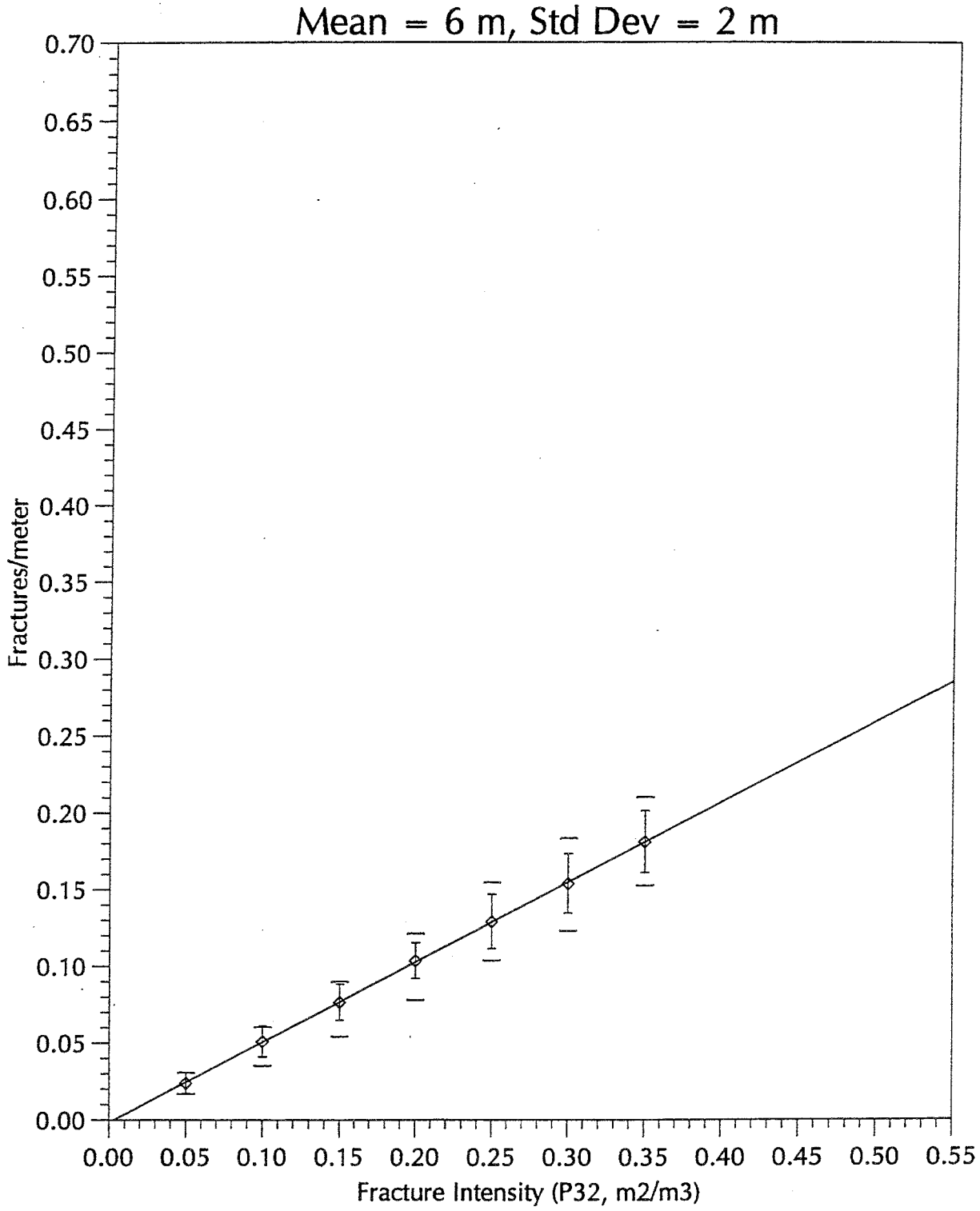

Bar on symbol shows ± one standard deviation
Horizontal brackets indicate maximum
and minimum results

FIGURE **3-12**
BOREHOLE FRACTURES/METER VS P_{32}
SKB/ASPO-DFN/SWEDEN

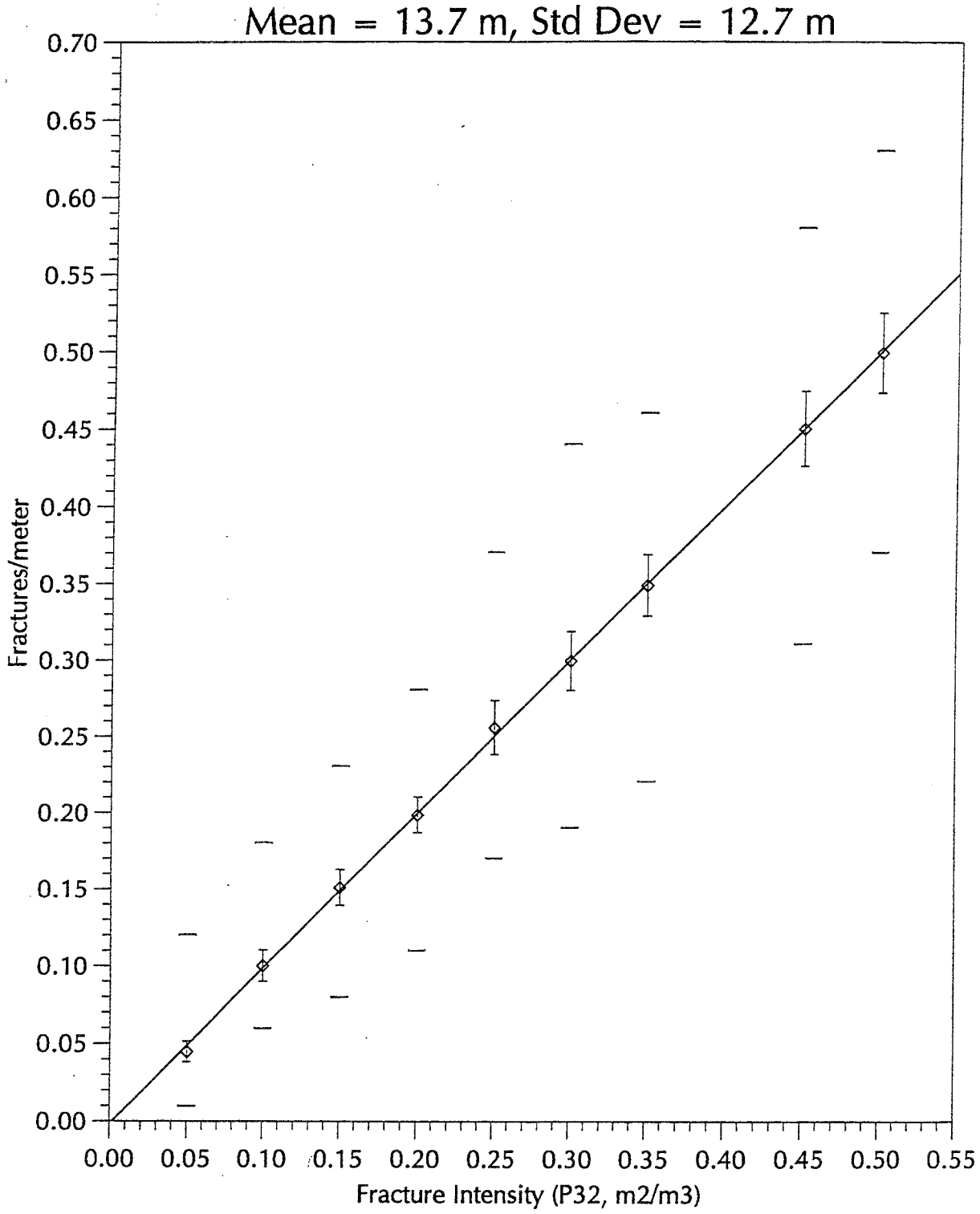

Bar on symbol shows ± one standard deviation
Horizontal brackets indicate maximum
and minimum results

FIGURE **3-13**
TUNNEL FRACTURES/METER VS P_{32}
SKB/ASPO-DFN/SWEDEN

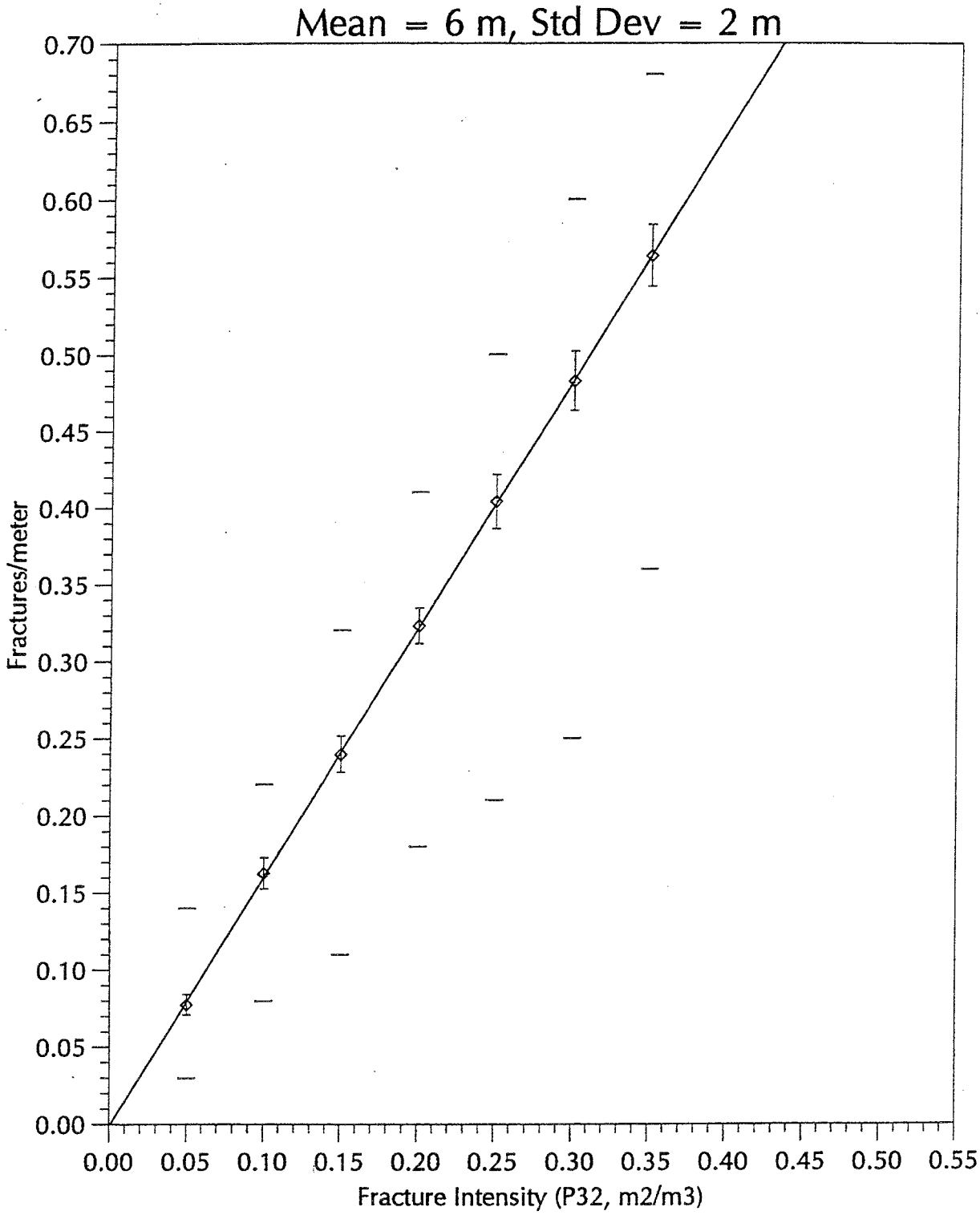

Bar on symbol shows ± one standard deviation
Horizontal brackets indicate maximum
and minimum results

FIGURE **3-14**
TUNNEL FRACTURES/METER VS P_{32}
SKB/ASPO-DFN/SWEDEN

There may be several reasons for the difference between the estimates of P_{32} based on the boreholes and the drift:

1) Blasting and excavation effects in the drift,

2) Higher probability of recognizing a conductive fracture in the drift,

3) Stress effects to enhance or reduce fracture permeability near the drift,

4) Gas exsolution, and

5) Calibrating the P_{32} for the tunnel from the number of conductive fractures/m rather than their trace length/area.

It is likely that blasting and excavation created additional fractures and enlarged existing ones in the vicinity of the drift. Many of the newly-created or enlarged fractures which were previously non-conductive could have intersected existing conductive fractures become part of the conductive network.

Likewise, it is easier to recognize a conductive fracture when more of it is exposed. Flow along a fracture surface may be uneven. Flow channels may be interspersed with very low permeability or dry portions. A borehole has a lower probability of intersecting a conductive portion than does a drift of much larger cross-sectional area. More importantly, the test equipment resolution threshold for well tests may significantly affect the interpretation of conductive fracture intensity. As the minimum value of interval transmissivity that can be measured increases, the inferred conductive fracture intensity decreases. When conductive fractures are identified along a drift or tunnel face, the minimum threshold is nearly 0.0.

Local stress effects on fractures surrounding the drift and gas exsolution may also play a role, but the magnitude of their effects at Äspö are unknown.

The estimate of conductive P_{32} from the tunnel data assumes that the tunnel has a small cross-sectional area relative to the fracture sizes. This is not the case for many of the

fractures. A true line through the center of the HRL access drift would have intersected fewer conductive features, so the impact of the tunnel having a finite cross-section is to increase the number of conductive fractures per unit length of tunnel.

However, both estimates of P_{32} were retained at this stage of the modeling to evaluate how different simulated 30 m transient well tests would be, and which might actually better approximate them. These results are described in Sec. 4.3 of this report.

3.1.5 Spatial Model

As discussed in the previous section, the fracture data measured in the HRL drifts has not been registered spatially. This makes it impossible to determine a spatial model from this additional data. Previous studies (Dershowitz and others, 1994) have utilized stationary Poisson models based upon analysis of boreholes and outcrops. The lack of spatial correlation found in geostatistical analysis of packer tests (La Pointe, 1994) and the lack of significant relation between fracture conductivity and mappable geological features provides additional support for using a stationary, non-correlated model. For these reasons, the DFN models for this project are stationary Poisson spatial fields.

3.2 DFN Model Summary

Table 3-11 summarizes the values for DFN models determined from the analyses in this section.

As described in the preceding sections, some of these parameters are less uncertain than others. The least well-constrained aspects of the DFN model are the fracture size distribution and the spatial model. Fracture sizes determined from all of the fractures in the HRL are probably the minimum bound on the conductive fracture size distribution. The size distribution determined from previous outcrop studies may be more realistic, but whether it represents an upper bound on the size distribution is unknown. Observations of fracturing in the HRL where drifts intersect or other large exposures of the rock occur underground reveal fractures that are at the scale or larger than many seen in outcrop. Thus the large fracture size distribution with mean 13.7 m is probably a better estimate of the conductive fracture size distribution than is the 6.0 m assumption. Size is important because it relates to both the fracture intensity and the network

connectivity. As Sections 4 and 5 show, the results of the block-scale hydraulic conductivity calculations are sensitive to the assumed size distribution of the fractures.

The spatial model used was not determined from analysis of the conductive fractures intersecting the HRL, since the spatial position of the conductive fractures was not available at the time of this project. Previous work indicated that a Poisson model in which fractures are located at random fit other Äspö fracture data from wells and outcrop. From a fracture mechanics perspective, it is less satisfying to use a spatial model that is spatially random, since fragmentation theories do not predict random locations. If the conductive fractures had a fractal pattern of locations (Barton, 1995), for example, then the fracture network connectivity could be very different (La Pointe and others, 1993a). This would also affect the block-scale calculations, depending on the value of the fractal dimension. However, the size and intensity parameters of a fractal system become less important (La Pointe and others, 1993a).

Overall, the DFN models used are reasonable given the current data for Äspö. The size is uncertain, but observational evidence in the HRL suggests that the larger size assumption is probably closer to the true size distribution. The fact that the well tests simulated in the DFN model realizations match actual transient well tests, as described in Section 4 of this report, suggests that the model uncertainties have not led to significant errors and are useful for estimating block-scale properties.

Table 3-11
Summary of DFN Model Parameters

Spatial Location Model	Enhanced Baecher, 0% Termination
Orientations	Bootstrapped from conductive fracture orientations as measured in the HRL access drift
Fracture Size (radius distribution)	Lognormal Large Size: mean=13.7 m , std. dev.=12.7 m Small Size: mean=6.0 m, std. dev. = 2.0 m
P_{32} Intensity	0.0664 m^{-1}
Transmissivity	Lognormal, mean=9.0×10^{-7} m^2/sec, std. dev.=5.0×10^{-6} m^2/sec
Storativity	Constant, 1.0×10^{-6}

4. OVERVIEW OF DFN SIMULATIONS

4.1 Well Test Analysis

Well test analysis constitutes the basis for estimating block-scale properties for continuum models for fluid flow and mass transport through porous media. However, well tests in fractured rock are still often interpreted within the framework of porous media. Follin and Thunvik (1994) have concluded that the body of the present perception of the heterogeneity observed in Swedish crystalline rocks is based on classical porous-media interpretation models, notwithstanding the debatable assumption of a space filling radial flow regime around the borehole associated with these models.

Although there exist more elaborate and flexible porous-media models for double-packer test analysis, for example, the generalized radial flow model of Barker (1988), this still does not solve a major problem with the stochastic continuum approach. This problem is how can well tests be used to calculate representative flow properties of model blocks, in particular at locations where there exist no neighboring well test data? The transmissivity of a well test interval may be very different than the larger-scale transmissivity of the volume of rock surrounding the well, and attempts to develop calibration curves for relating a packer test result to a block-scale flow property have not been very successful in fractured media.

A common approach to circumvent this problem has been to consider the heterogeneous equivalent hydraulic conductivity, determined by classical porous-media interpretation models, as a spatially varying parameter for which spatial continuity is defined in geostatistical terms (Neuman, 1987, 1988; Rubin and Gómez-Hernández, 1990; Follin, 1992a; Norman, 1992; Geier, 1993; La Pointe, 1994). The application of the geostatistical approach to fractured rocks is not without problems, however. For instance, Follin and Thunvik (1994) have demonstrated two problems with this form of geostatistical interpolation. First, it is incorrect to assume that the characteristic length of support (support scale) of interpreted hydraulic conductivity values is constant-valued and equal to the length of the test section (Follin, 1992b). Secondly, the statistical techniques used for interpolation, extrapolation and regularization treat the heterogeneous equivalent hydraulic conductivity as a scalar property, which is not

physically correct in the general case, and particularly for flow systems dominated by fractures (e.g. La Pointe and Hudson, 1985).

Rather than following the classical route of computing block-scale properties by means of well test analyses, this project is based on an entirely different approach. The purpose of well tests is to filter out those DFN models that are geologically and geometrically acceptable but lead to unrealistic test responses as compared to real well test responses. The filtering procedure itself is described in detail in Sec. 4.3.

Not all well tests are of equal value as filters. Some are of a type that provides information that is hard to compare with results from a flow simulation. Other tests were not run for sufficient lengths of time, or took place under less than ideal testing conditions, so that the results are not robust or are very noisy and consequently are too broad to serve as useful filters. Thus, the selection of well test data for use as a filter must be done so that the resulting well test data set provides a narrow enough constraint on the DFN well simulated well tests.

4.2 Data Quality

The best well test data available for Äspö consists of packer tests carried out over two different interval scales: 3 m and 30 m. The 3 m tests were conducted in wells KAS02 through KAS08. 30 m tests were carried out in only two of these wells: KAS02 and KAS03.

The 3 m tests were carried out over a period of 10 minutes, while the 30 m tests lasted 120 minutes. The 30 m tests are preferred for two reasons:

1) The radius of investigation for the 30 m tests is more than three times greater than that of the 3 m tests, based upon Jacob's approximation. This suggests that the 30 m results reflect more of the fracture network fluid flow properties rather than that of individual fracture properties. While Jacob's formula is for porous media, the size and spacing of conductive fractures (see Sec. 3) is such that no more than one to two conductive fractures are likely to intersect a single 3 m interval. The high number of non-conductive intervals found in Äspö 3m well tests (La Pointe, 1994) shows that the scale of the conductive network is greater

than the 3 m scale. However, in the three wells in which 30 m packer tests have been carried out (KAS02, KAS03, KLX01), a much higher percentage of the intervals were conductive. This suggests that 30 m interval tests are probably testing a greater component of fracture network response, and are less influenced by flow properties of single fractures.

2) The constraint afforded by the 30 m tests is a more restrictive one. Figure 4-1b, c show how a number of simulated well tests that are rejected based on the 30 m tests would still be retained based only upon the 3 m tests due to the small time interval for the 3 m tests. The upward turn of the simulation results (shown as solid lines on Figures 4-1b and c) suggest that the fractures or fracture networks connected to the borehole are of finite extent and only allow flow to the limit of compressibility. These limits are not always reached by ten minutes for either fracture size assumption. In fact, a number of tests that clearly are poorly connected do not show the limits until after ten minutes of testing. However, they do show the limits for the longer test duration used in the 30-m tests.

For these two reasons, the 30 m packer tests have been used to filter out unacceptable block-scale DFN model realizations.

A drawback with using 30 m tests is that there are only two wells which have been tested at this scale, KAS02 and KAS03 (Nilsson, 1989). The quality of the tests was found to be quite poor, which unfortunately has limited the amount of data useful for this project. Out of a total of 41 well tests conducted in KAS02 and KAS03, only 12 well test were found to be acceptable for the filtering process. However, a comparison of the porous-media hydraulic conductivity values reported by Nilsson (1987) suggest that the properties of the acceptable well tests are well distributed about the median. Thus, there is no obvious reason to expect a bias due to the small sample size. The 20 well tests conducted in KLX01 were not available for this project.

Thus the use of twelve 30 m tests from only two wells probably provides a sufficiently robust filter for the realizations. Another possible concern is that the KAS02 and KAS03 wells do not represent the diversity of response that might be found elsewhere at Äspö.

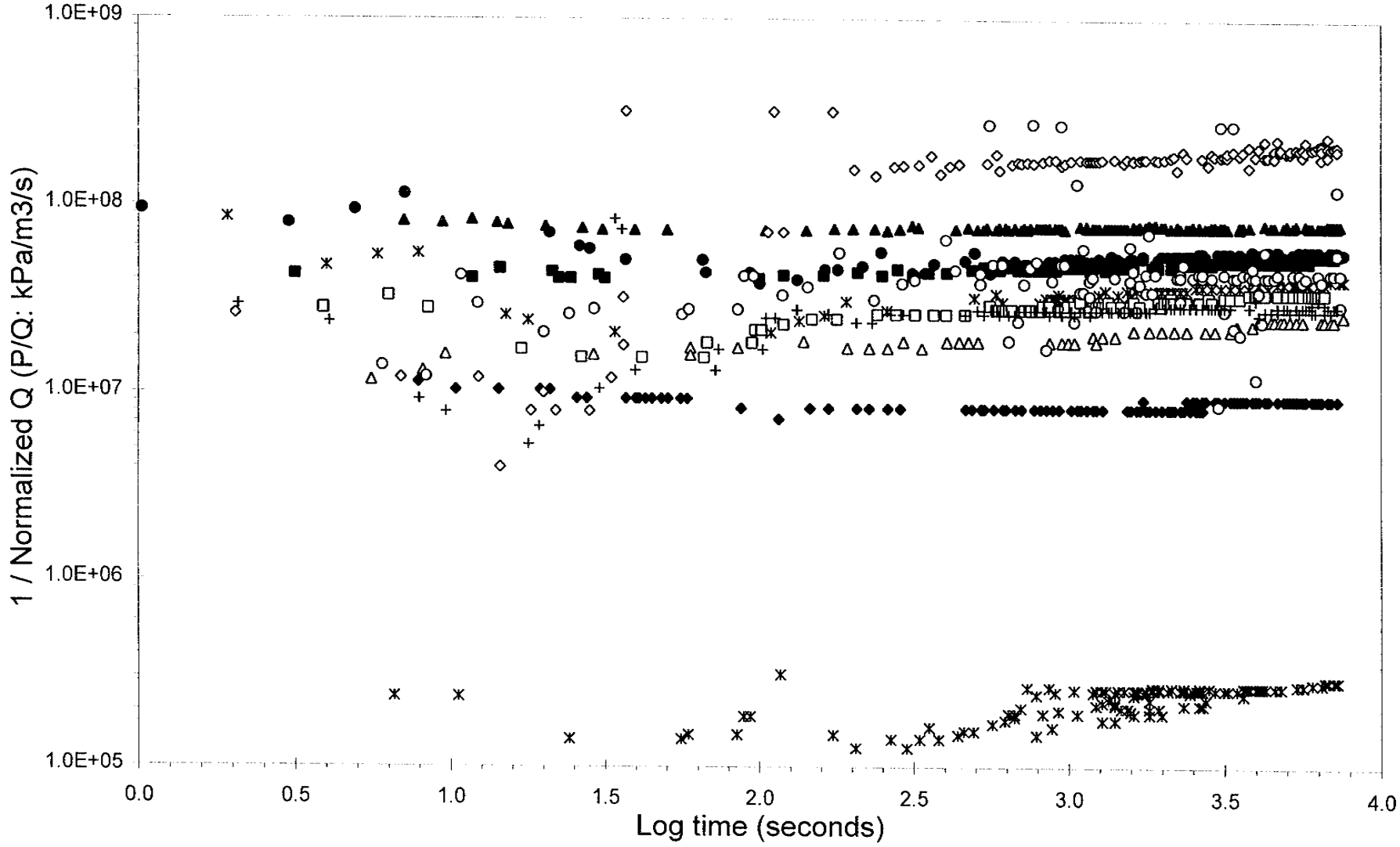

FIGURE **4-1a**

PLOT OF 30 m WELL TEST DATA FROM ÄSPÖ

SKB/BLOCK K/SWEDEN

PROJECT NO. IC3 1194 DRAWING NO. 55600 DATE 6/2/95 DRAWN BY EA

Golder Associates

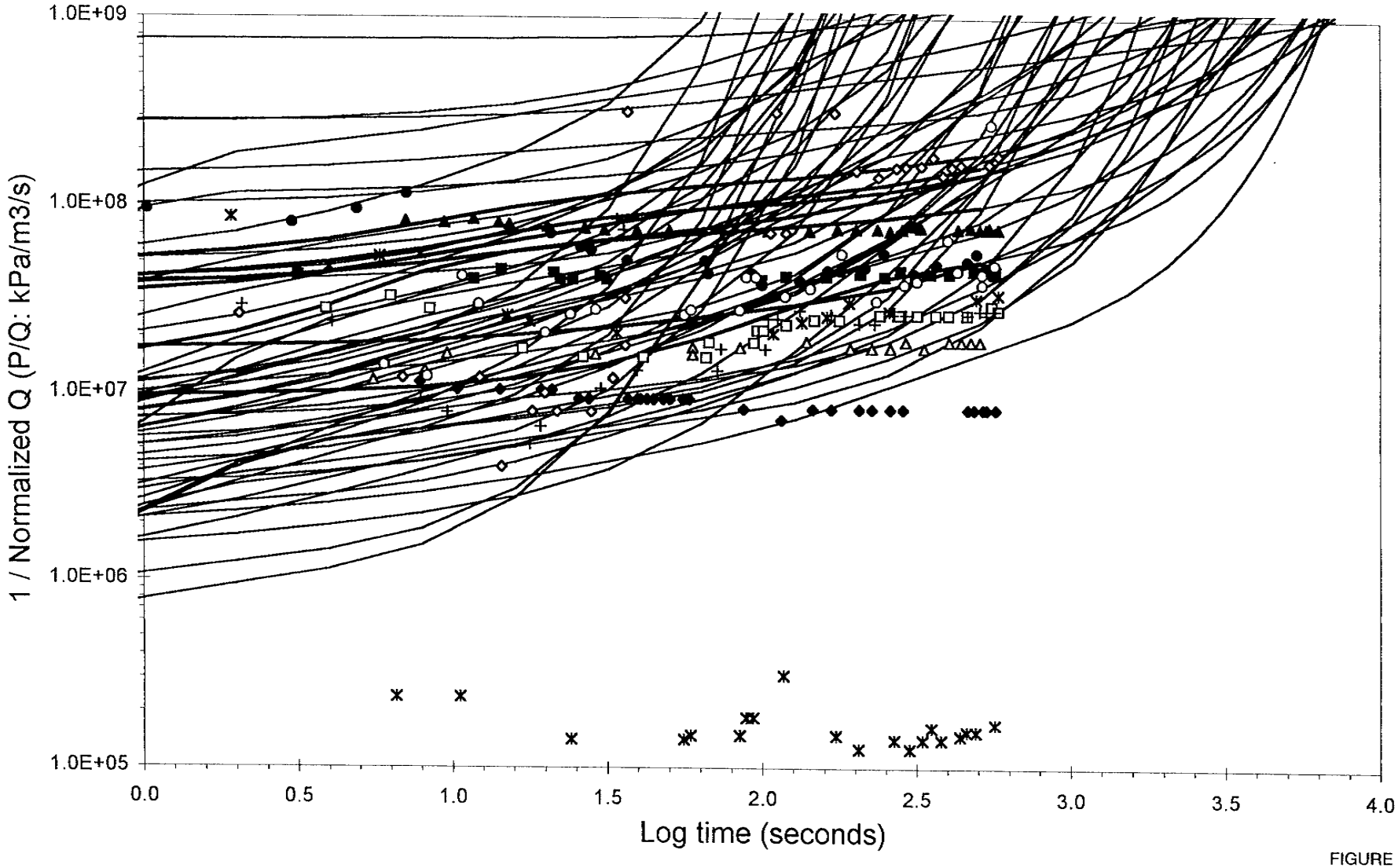

FIGURE **4-1b**

PLOT OF WELL TEST SIMULATIONS REJECTED ON THE BASIS OF THE 30 m WELL TESTS SUPERIMPOSED ON THE SHORTER TIME PERIOD OF THE 3 m TESTS, SMALL FRACTURE SIZE MODEL

SKB/BLOCK K/SWEDEN

PROJECT NO. IC3 1194 DRAWING NO. 55601 DATE 6/2/95 DRAWN BY EA

Golder Associates

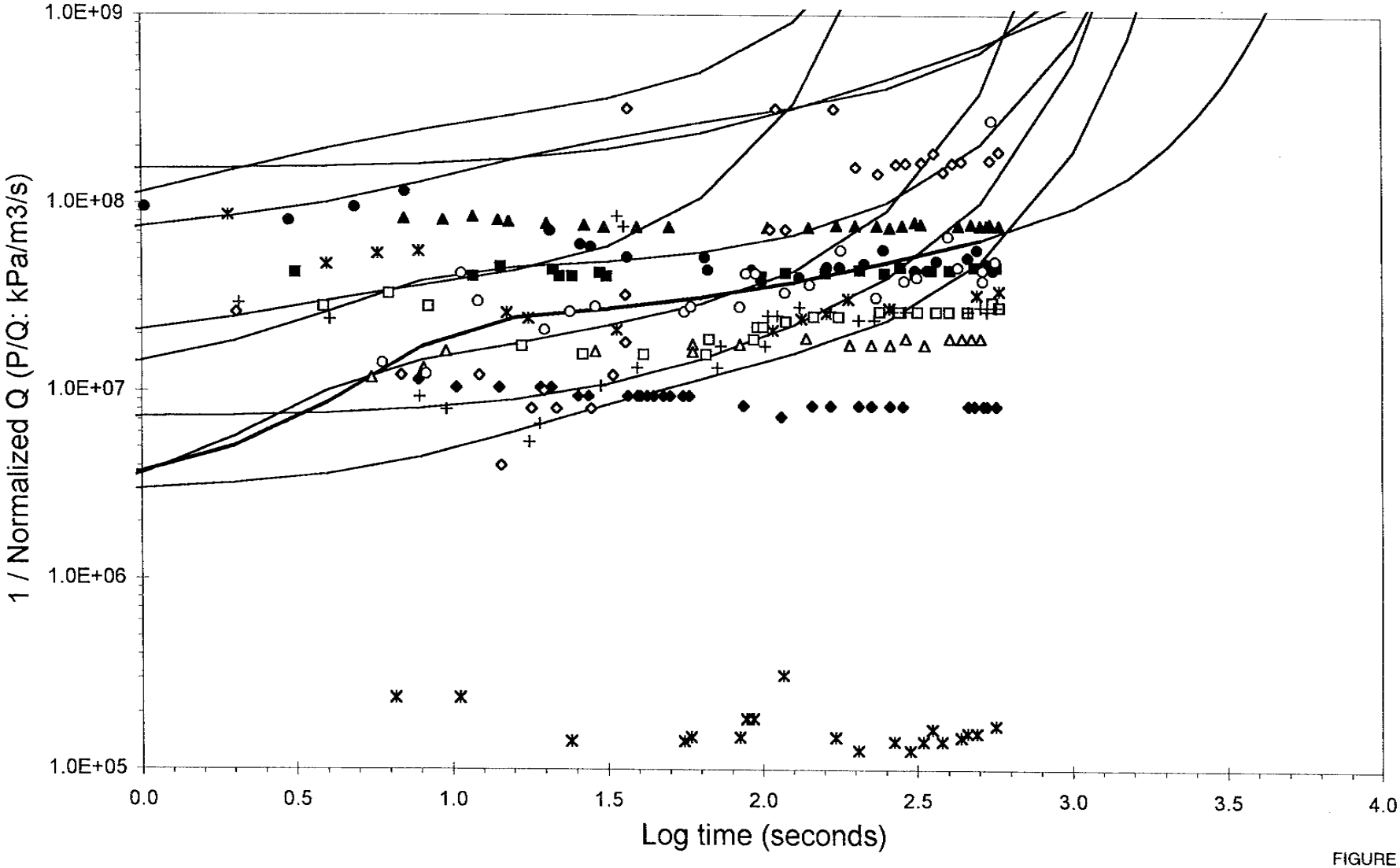

FIGURE **4-1c**

PLOT OF WELL TEST SIMULATIONS REJECTED ON THE BASIS OF THE 30 m WELL TESTS SUPERIMPOSED ON THE SHORTER TIME PERIOD OF THE 3 m TESTS, LARGE FRACTURE SIZE MODEL

SKB/BLOCK K/SWEDEN

PROJECT NO. IC3 1194 DRAWING NO. 55602 DATE 6/2/95 DRAWN BY EA

Golder Associates

However, the 3 m tests are more geographically widespread and numerous, and their values have been analyzed to determine whether or not there are systematically different values in different areas either due to mappable geological factors or other causes. Neither Liedholm (1991) nor La Pointe (1994) have found such variations in the 3 m tests. This suggests that results of 30 m tests from KAS02 and KAS03 may be representative of a much larger portion of Äspö than the rock in the immediate vicinity of KAS02 and KAS03.

The 30 m tests used in this project for filtering out DFN models that produce unrealistic test responses are shown in Figure 4-1. Unfortunately, the test recordings were not available in a digital form. Figure 4-1 is based on digitizing available paper copies of the tests.

4.3 Well-Test and Block-Scale Simulations

4.3.1 Overview

One of the key aspects of this current work is that not all of the discrete fracture networks created in the stochastic generation process will be used to calculate block permeabilities. Only those networks which have a transient 30 m packer test response which falls within the range observed in KAS02 and KAS03, the data discussed in the previous section, will be accepted for block permeability calculations.

4.3.2 Methodology

The general approach in the block simulations is to construct fracture networks based on the geometric and hydrologic analyses of field data and testing. A simulated transient well test is then run for each network realization, and the results are compared to actual Äspö well test measurements. Networks which meet the qualification criteria are then used in block permeability simulations. This process is described in more detail in the following sections.

4.3.3 Boundaries and boundary conditions

The boundary geometries for the generation region and the well test simulation region are shown in Figure 4-2. Fractures for this project were generated within a 95 m x 95 m

x 95 m region. These fracture sets are then meshed to produce a cubic external boundary 90 m on a side with a 30 m long, four-sided well bore centered within this 90 m cube. The external boundaries of this meshed region are aligned so that they are parallel to the Äspö coordinate system (15.45 degrees counter-clockwise from N). All external faces have a constant head, both spatial and temporal, of 0 m applied to each boundary node. The internal boundary, the wellbore, has a 20 m head, again both spatially and temporally invariant (Figure 4-3). This 20 m head boundary condition is approximately equal to the 200 kPa overpressure which was the target for the Äspö 30 m packer tests. A total of 28 time steps from 0.125 to 7168 seconds are used to calculate the transient response to this pressure applied at the wellbore.

The normalized inverse flow (P/Q) from a transient flow simulation of a fracture realization is compared to the actual data from packer testing at Äspö and the fracture network is either accepted or rejected for block permeability calculations. If it is accepted, it will be used in two different sets of simulations. The first simulation partitions the inner 50 m cube of the 90 m well test cube into 125 discrete 10 m blocks, and overlapping 20, 30, and 40 m blocks (Figure 4-2). The 20, 30, and 40 m blocks are situated such that they exactly overlap or could be constructed of the 10 m subblocks. These simulations can provide information on spatial correlation as well as constraints on the distribution of block permeabilities.

Implicit in this approach is an assumption that a matching well test "qualifies" the entire block and not just the immediate region around the well test.

The second type of simulation assumes that only the blocks centered on the well test region are "qualified" by successful well test match. In these models only the 10, 20, 30, 40, or 50 m cube centered on the well test is tested. This second set of models can examine the effect of scaling on bulk properties in addition to providing permeability values. Both types of simulation were run in this modeling effort.

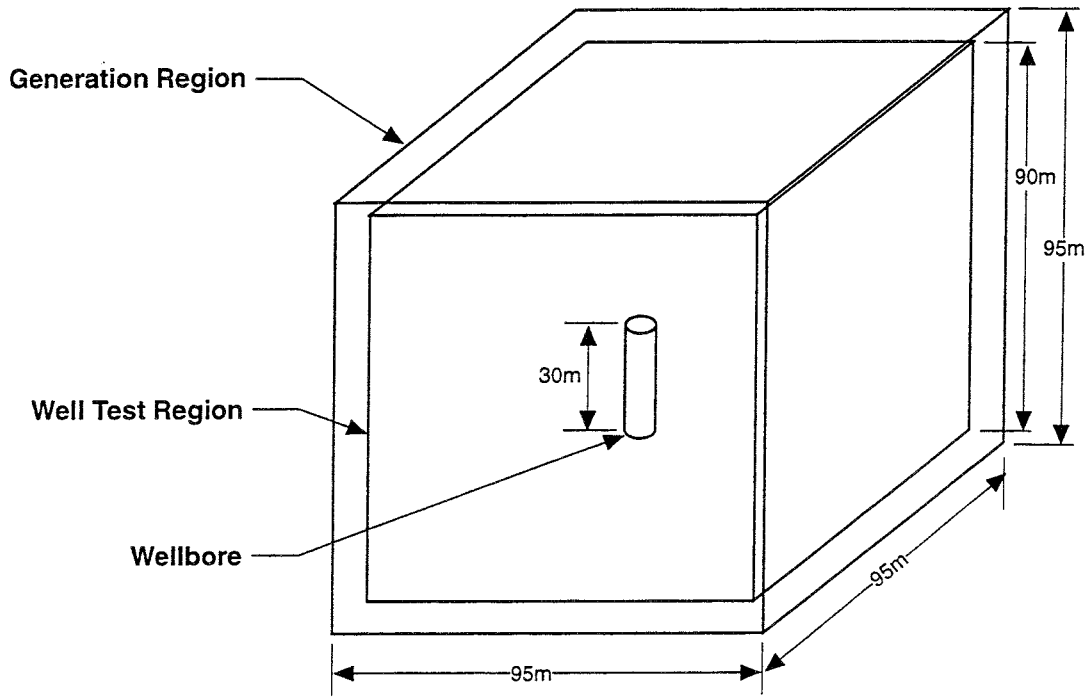

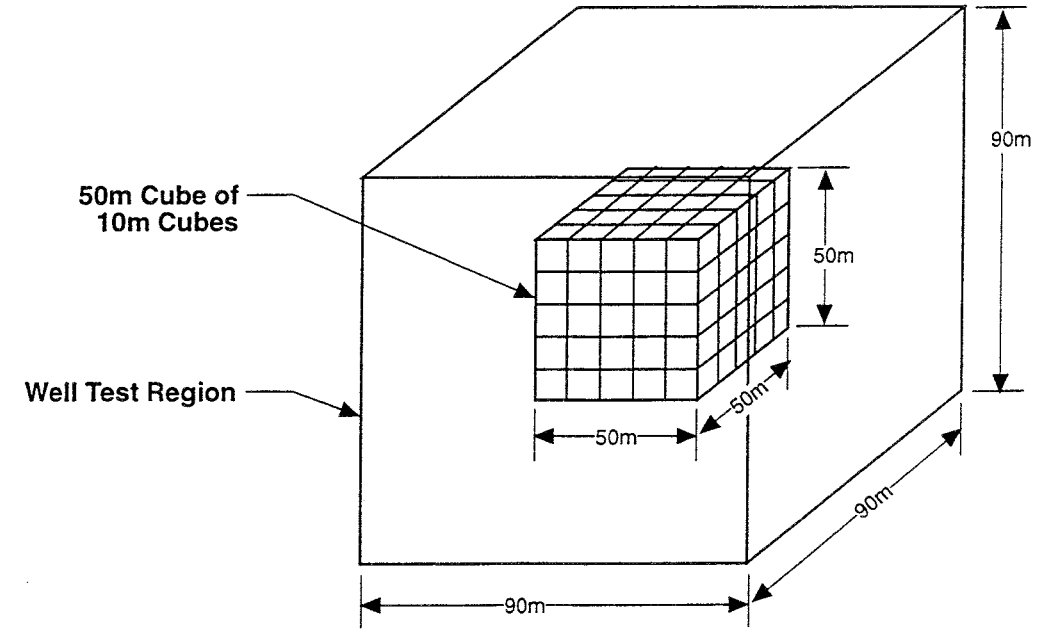

FIGURE **4-2**
GENERATION REGION, WELL TEST REGION WITH WELLBORE, AND 50m BLOCK COMPOSED OF 10m BLOCKS
SKB/BLOCK K/SWEDEN

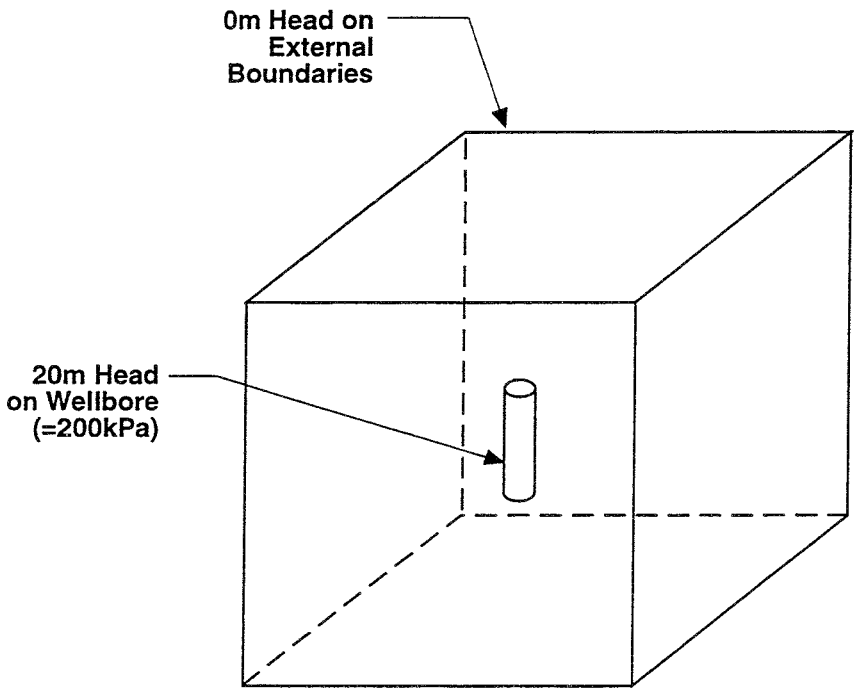

FIGURE **4-3**
WELL TEST BOUNDARY CONDITIONS
SKB/BLOCK K/SWEDEN

Table 4-1

Number Of Computer Models Run For Block Permeability Simulations

	P_{32} = 0.06644		P_{32} = 0.224	
	Large Radius	Small Radius	Large Radius	Small Radius
Well Tests	200	200	25	25
Accepted/Qualified	24	20	0	0
50 m Whole Block				
10 m blocks	9000	7500	-	-
20 m blocks	4608	3840	-	-
30 m blocks	1944	1620	-	-
40 m blocks	576	480	-	-
100 m Whole Block				
10 m sub-blocks	3000	3000	-	-
Centered Blocks				
10 m block	72	60	-	-
20 m block	72	60	-	-
30 m block	72	60	-	-
40 m block	72	60	-	-
50 m block	72	60	-	-
Sub Total	19688	16940	25	25
TOTAL	**36678**			

In all cases of block permeability tests the boundary conditions were fundamentally the same. Figure 4-4 displays the boundary conditions for South to North flow in a block. A constant head of X m, where X is equal to the scale of the test (10, 20, 30, 40, or 50 m) is applied to the South face and a constant head of 0 m is imposed on the North Face establishing a unit gradient across the numerical test block. All other faces in the model are given a no-flow (Q = 0 m^3/s) boundary condition. The flow calculation is always steady-state. Table 4-1 lists the types and numbers of simulations which were run as part of this project. The boundaries for these block flow simulations, like the well test cube, are rotated so that all of sides are perpendicular (depending on the face) to principal axes of the Äspö coordinate system.

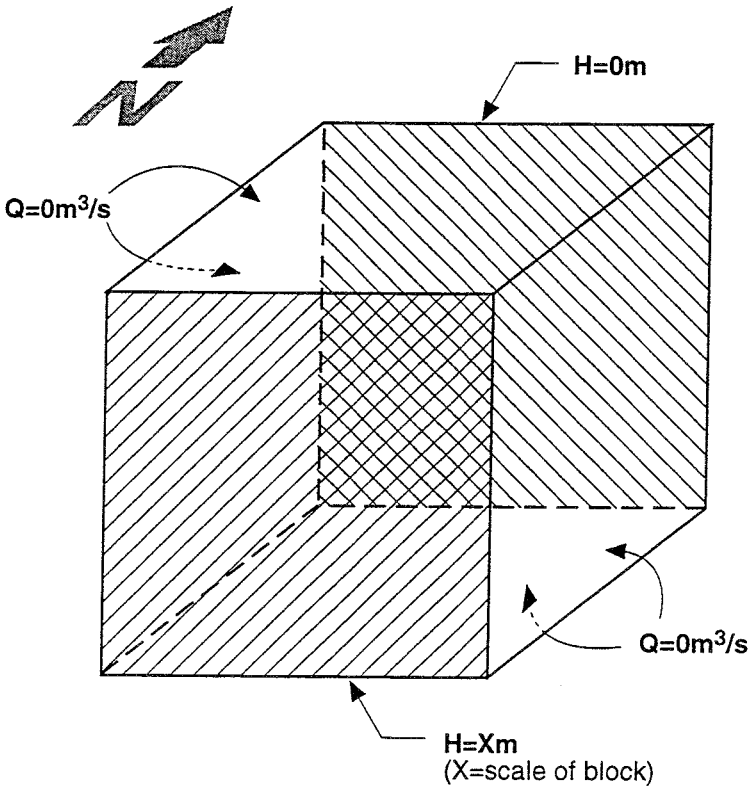

FIGURE **4-4**
SOUTH TO NORTH FLOW BOUNDARY CONDITIONS
SKB/BLOCK K/SWEDEN

4.3.4 Comparison of simulated with actual well tests

The conductivity of a block is calculated from

$$Q = -KiA \qquad \text{Equation 4-1}$$

where Q = volumetric flow rate (m^3/s), K = hydraulic conductivity (m/s) , i = head gradient (m/m), and A = cross-sectional area of flow (m^2). For the given boundary conditions, with a head gradient of 1 m/m, this equation rearranges to give

$$K = -Q/A. \qquad \text{Equation 4-2}$$

Thus, the hydraulic conductivity is obtained by dividing the volumetric inflow (m^3/s) at the injection face by the area of the block.

Permeability is calculated according the following relationship

$$k = K\mu/\rho g \qquad \text{Equation 4-3}$$

where k = permeability (m^2), K = hydraulic conductivity (m/s), μ = viscosity (Pa·s) = 1.0×10^{-3} Pa·s, and ρ = density (kg/m^3) = 1000 kg/m^3. Combining the last two equations provides the permeability for a block with a unit hydraulic gradient

$$k = Q\mu/\rho gA. \qquad \text{Equation 4-4}$$

Not all of the sections reported in Section 4-1 and Figure 4-1 are used in the comparison process. KAS 03 section 613 has normalized inverse flow rates approximately two orders of magnitude less than all of the other test sections which were appropriate for use. Because this test appeared to be an outlier with respect to the others it was not used in the comparison. Allowing tests which fall between this test section and the others which cluster around 1.0×10^7 kPa/(m^3/s) (Figure 4-1), would not lead to a selective acceptance criteria as the majority of tests fall within this range.

It is important to note that the comparison made is between the flow measurements in the actual well tests and the simulations. This avoids the problems which may arise in calculating the interval conductivities due to the use of the space-filling and homogeneity assumptions commonly used in these calculations. Both assumptions - space-filling and homogeneity - are probably violated in the sparse networks used in this study. Use of uninterpreted flow measurements and simulation results avoids complications and errors which may arise from comparing conductivities.

After the initial selection comparison is completed, the tests which met the acceptance criteria are plotted along with the results from the actual Äspö tests. At this point tests which fall between the upper and lower bounds of the Äspö results and which do not have steep slopes on the t vs. P/Q plot, indicating rapid drops in flow rate in the test interval, are chosen. These plots are those which will be used in the block permeability simulations.

There are three possible states for fracture realizations after well test simulation: (1) acceptance, (2) rejection, and (3) no fractures connected to the borehole. Statistics for these three categories are shown in Figure 4-5. Given the data from Äspö well tests which was available for comparison, no use could be made of the percentage of no fracture connections. If a lower threshold for measurement could be assigned to these "non-conductive" tests, then a comparison could be made between the OxFilet analysis, which estimates the percentage of non-conductive intervals for the specified lower threshold, and the actual percentage of "non-conductive" intervals in the actual testing. This would be another method to verify the parameters (such as transmissivity distribution and fracture intensity) used in the model.

Figures 4-6 and 4-7 show the normalized inverse flow (P/Q) plots for the large (μ = 13.7 m, σ = 12.7 m) and small (μ = 6 m, σ = 2 m) fracture radius distributions respectively. In general the model results from the large fracture radius simulations do a better job of fitting the observed results from Äspö than do those of the small fracture radius simulations.

Rejected simulations are shown in a series of plots in Figures 4-8 (large radius) and 4-9 (small radius). The rejected simulations fall into three broad categories: (1) flow rate too high (inverse flow rate, P/Q, $< 1.0 \times 10^7$); (2) flow rate tends to 0.0 m^3/s (inverse flow rate, P/Q, tends to infinity, (3) rapid changes in flow rate (from low to high P/Q). The first category suggests wellbore connection which is more conductive than observed in most well tests in non-fracture zone rock. Category two are probably fractures and/or networks of limited extent and connection which only allow flow to the limit of compressibility. Networks in the last category suggest that flow is becoming more one-dimensional or channelized than is observed in the actual well tests. Therefore, these

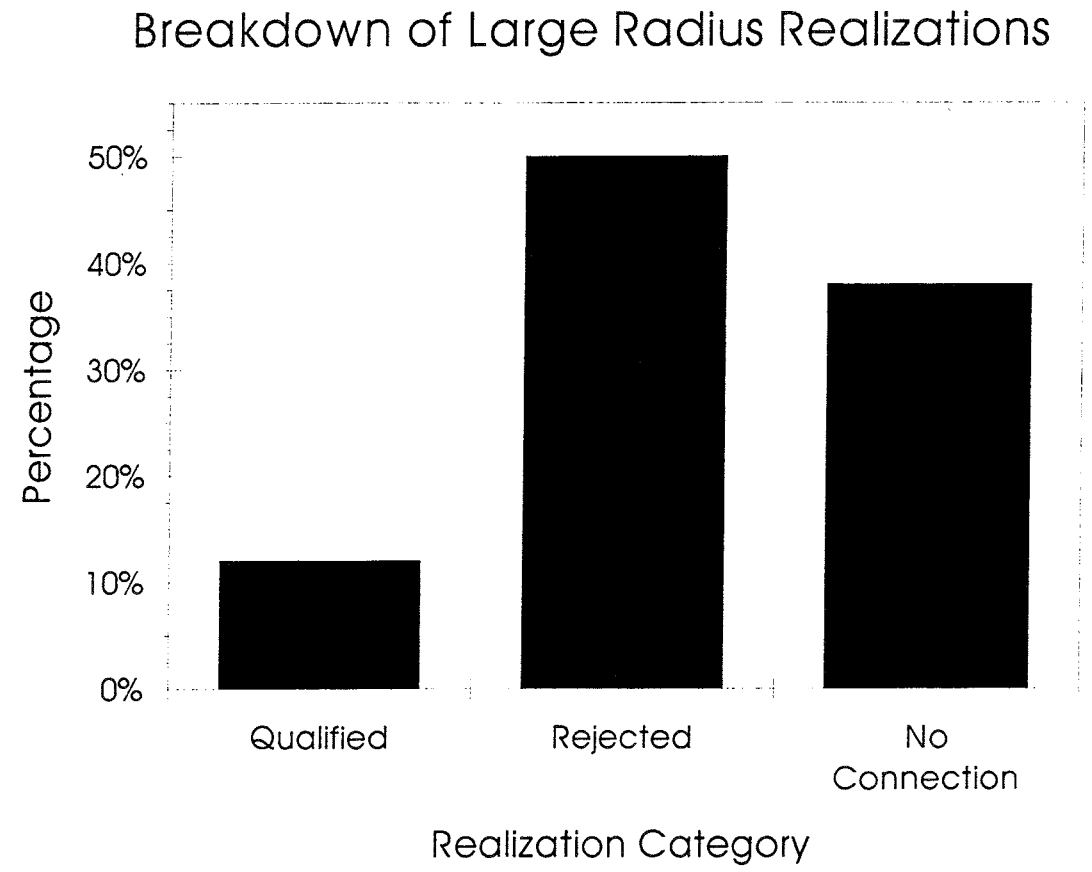

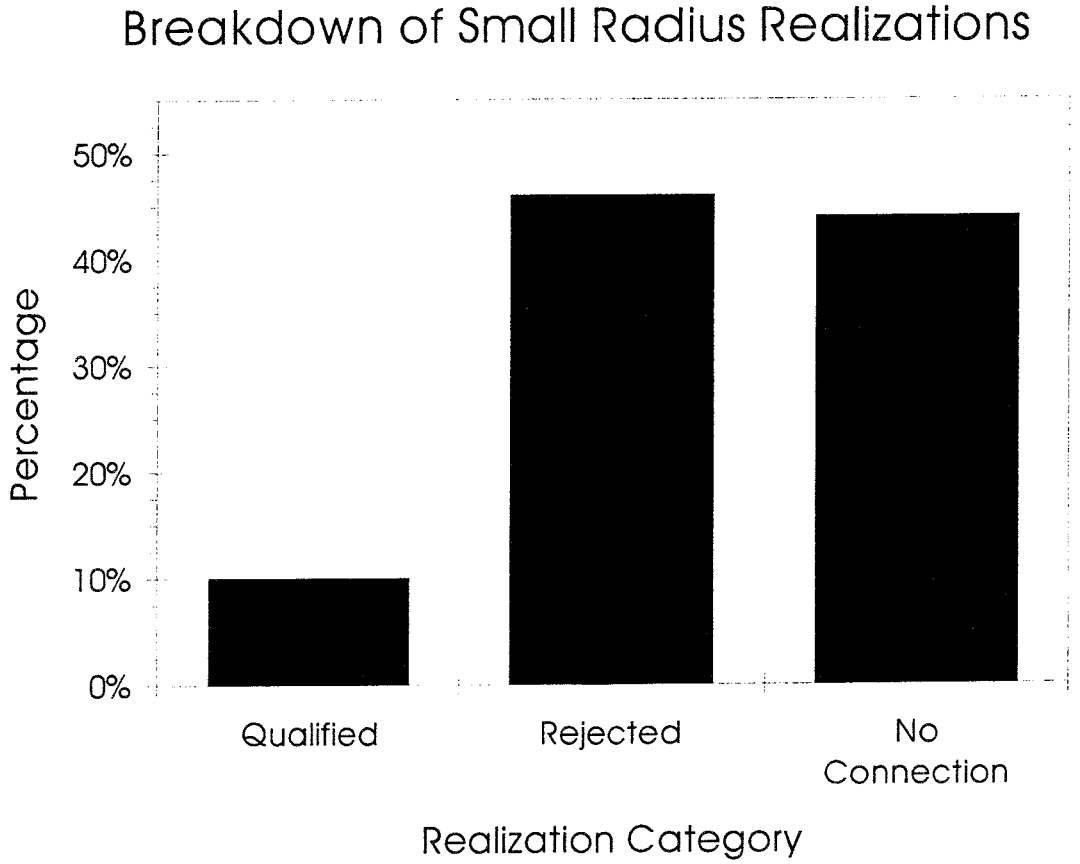

FIGURE **4-5**
STATISTICS
(MEAN = 13.7M & MEAN = 6.0M)
SKB/BLOCK K/SWEDEN

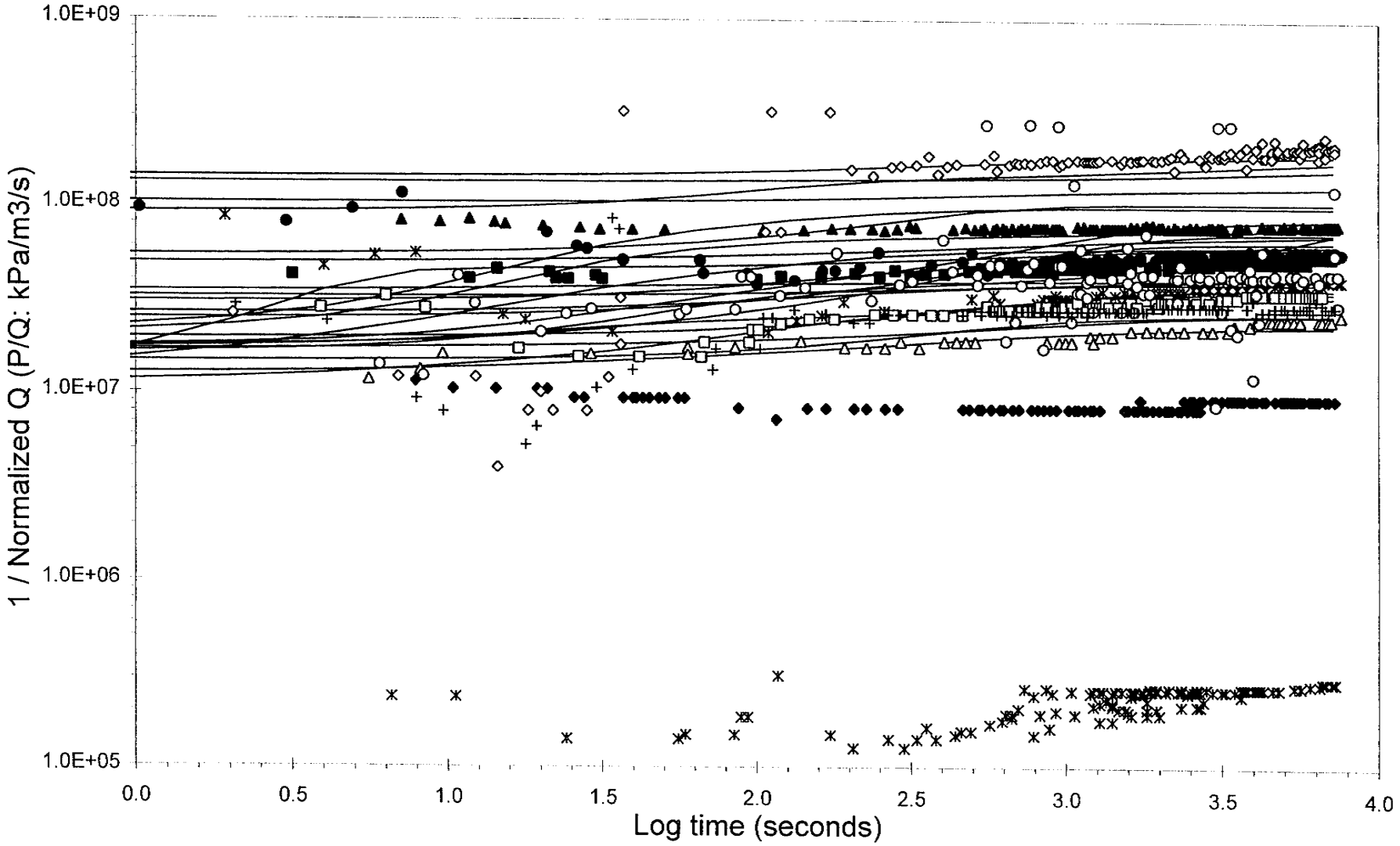

FIGURE **4-6**
ACCEPTABLE RESULTS (MEAN = 13.7M)
SKB/BLOCK K/SWEDEN

PROJECT NO. IC3 1161.003 DRAWING NO. 60038 DATE 4/17/94 DRAWN BY EA

Golder Associates

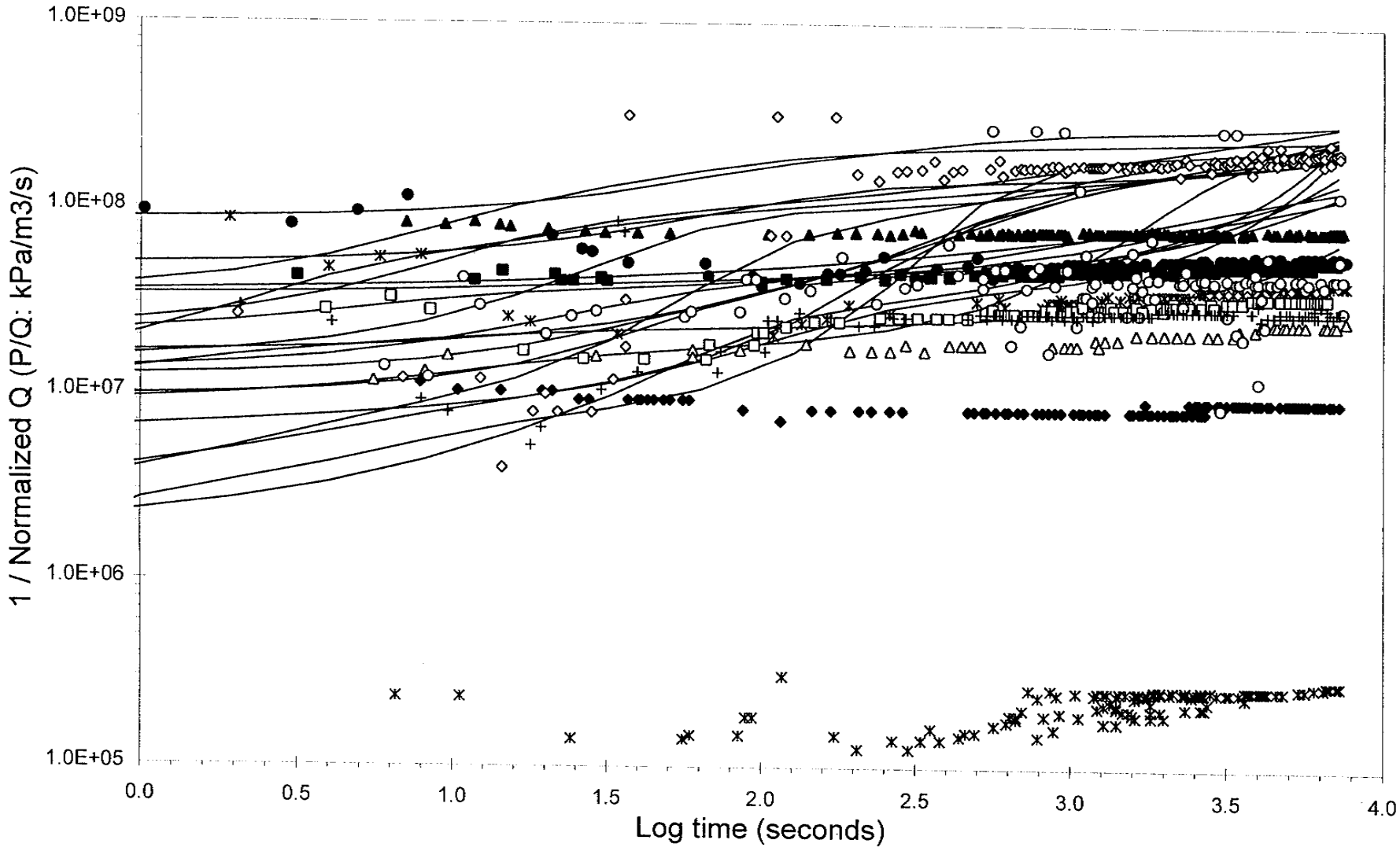

FIGURE **4-7**
ACCEPTABLE RESULTS (MEAN = 6.0M)
SKB/BLOCK K/SWEDEN

PROJECT NO. IC3 1161.003 DRAWING NO. 60039 DATE 4/17/94 DRAWN BY EA

Golder Associates

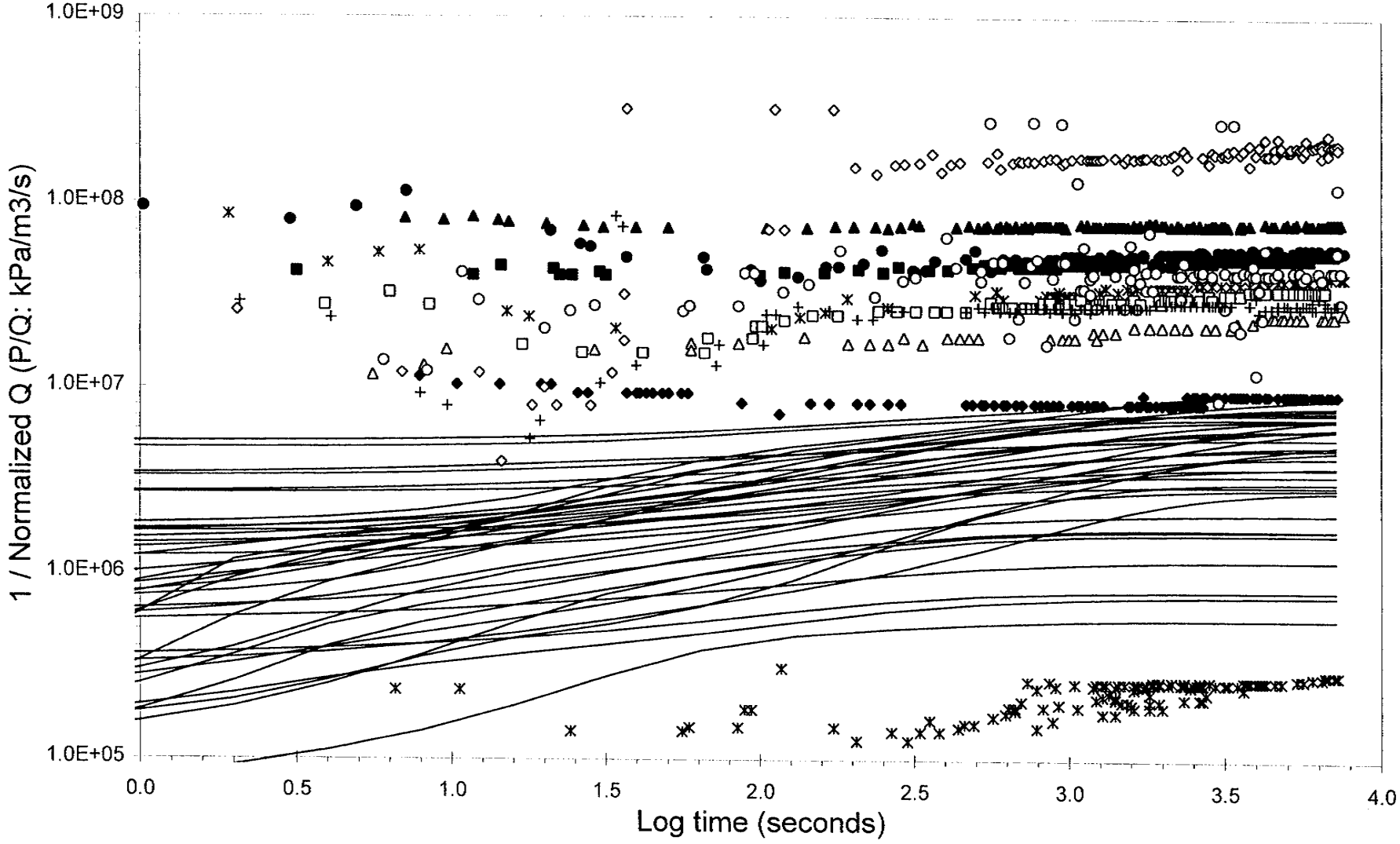

FIGURE **4-8a**
UNACCEPTABLE RESULTS
(MEAN = 13.7M; BOREHOLE P32)
CATEGORY 1
SKB/BLOCK K/SWEDEN

PROJECT NO. IC3 1194 DRAWING NO. 60040 DATE 6/1/95 DRAWN BY EA

Golder Associates

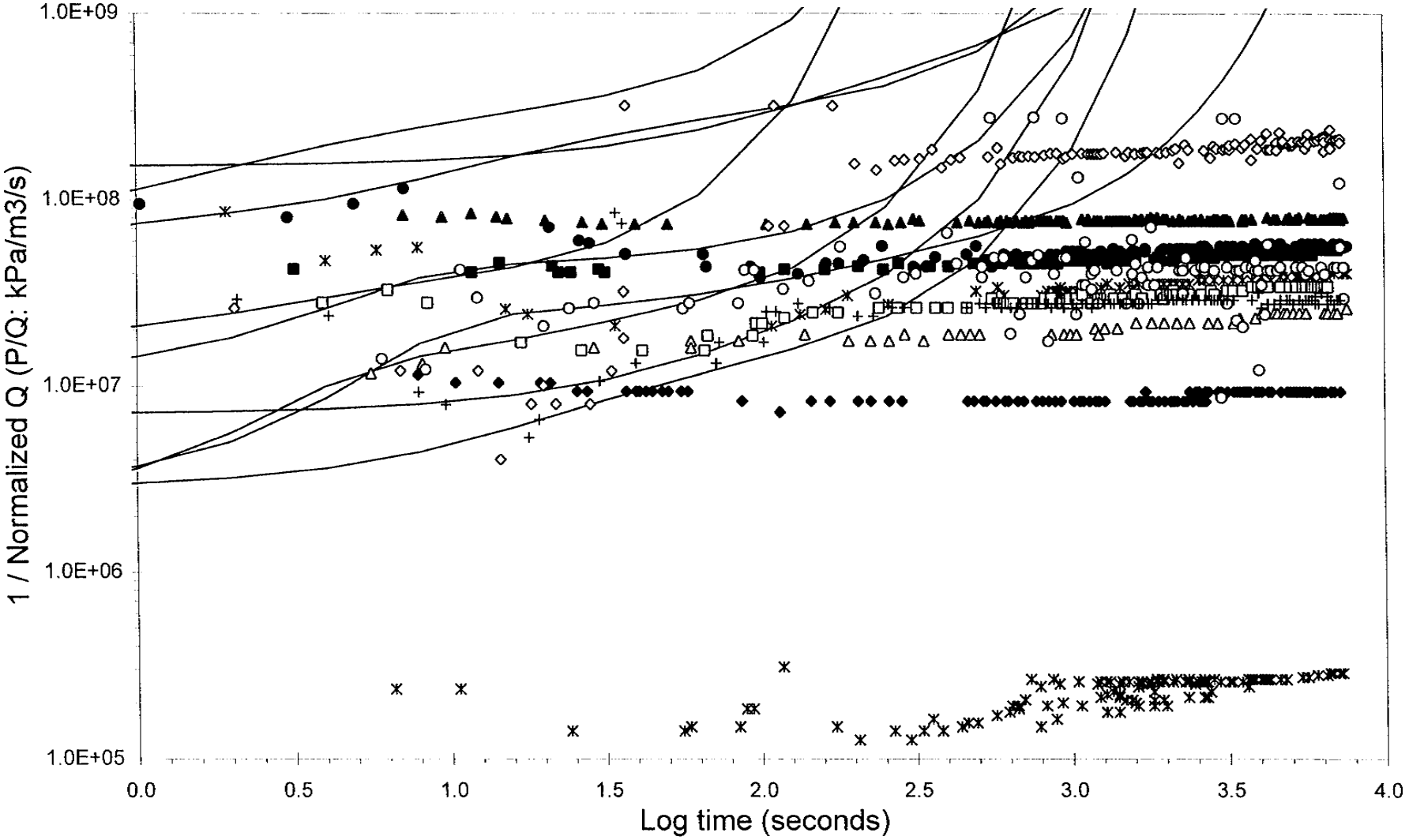

FIGURE **4-8b**
UNACCEPTABLE RESULTS
(MEAN = 13.7M; BOREHOLE P32)
CATEGORY 2
SKB/BLOCK K/SWEDEN

PROJECT NO. IC3 1194 DRAWING NO. 60041 DATE 6/1/95 DRAWN BY EA

Golder Associates

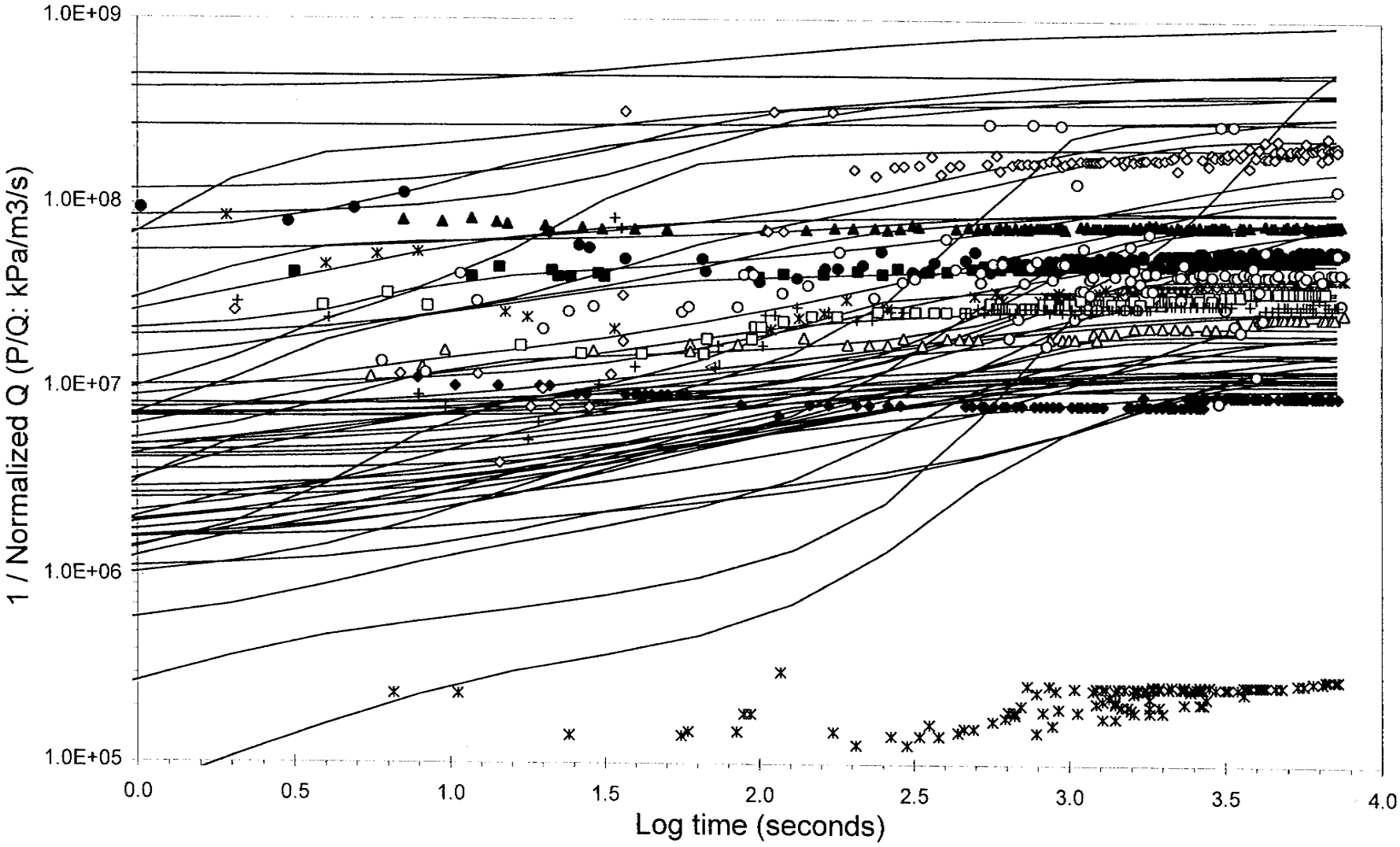

FIGURE **4-8c**
UNACCEPTABLE RESULTS
(MEAN = 13.7M; BOREHOLE P32)
CATEGORY 3
SKB/BLOCK K/SWEDEN

PROJECT NO. IC3 1194 DRAWING NO. 60042 DATE 6/1/95 DRAWN BY EA

Golder Associates

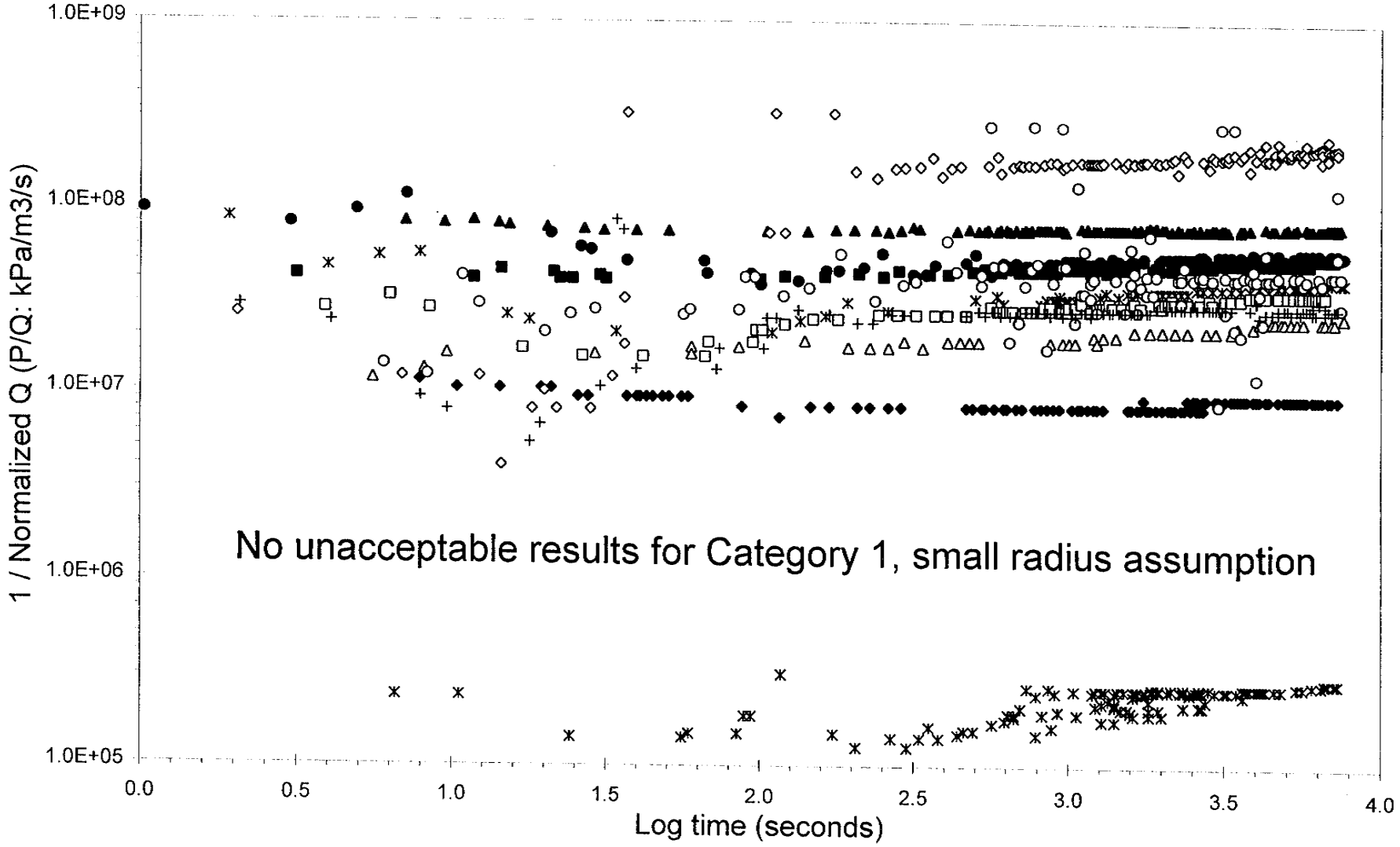

FIGURE **4-9a**
UNACCEPTABLE RESULTS
(MEAN = 6.0M; BOREHOLE P32)
CATEGORY 1
SKB/BLOCK K/SWEDEN

PROJECT NO. IC3 1194 DRAWING NO. 60043 DATE 6/1/95 DRAWN BY EA

Golder Associates

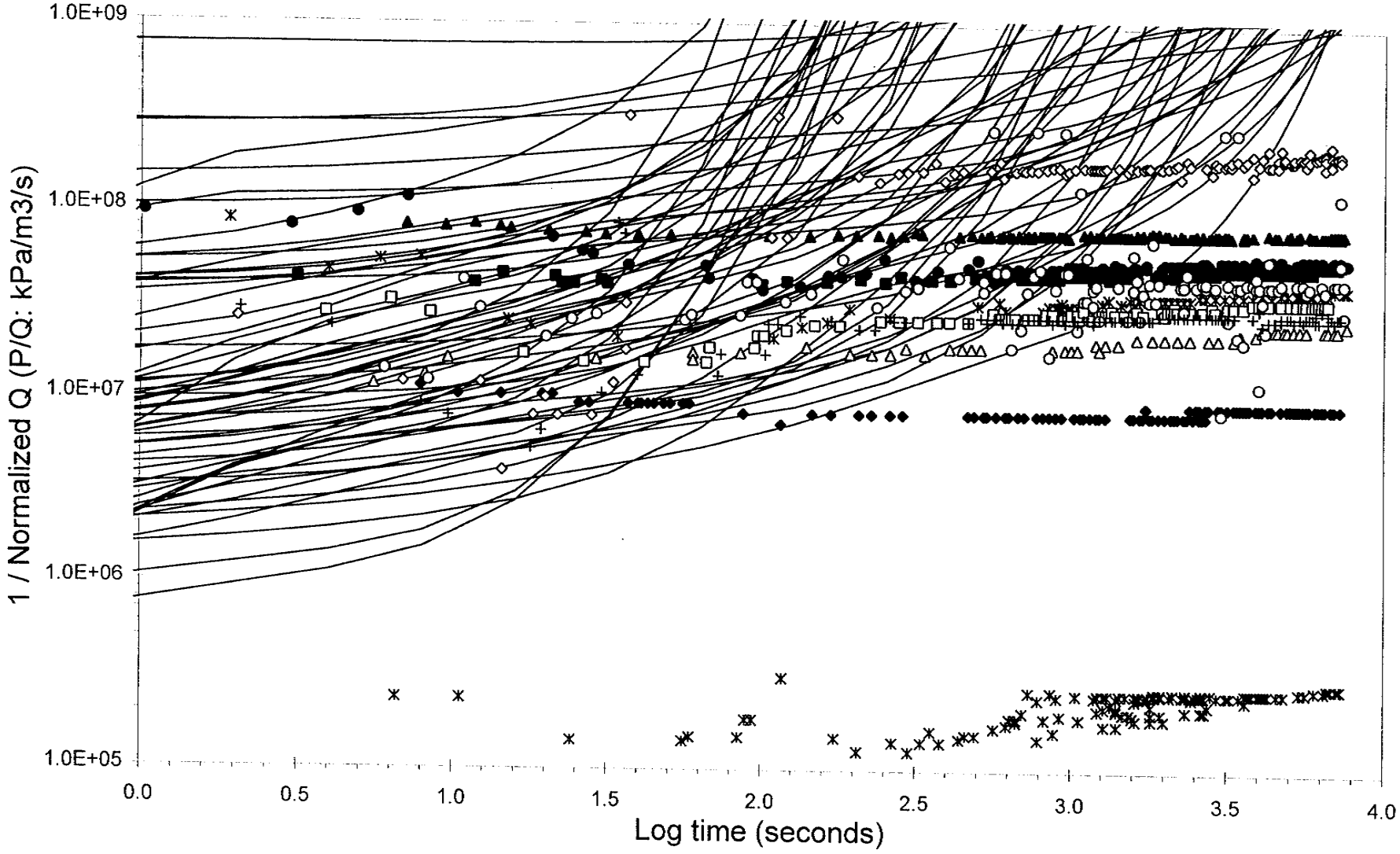

FIGURE **4-9b**
UNACCEPTABLE RESULTS
(MEAN = 6.0M; BOREHOLE P32)
CATEGORY 2
SKB/BLOCK K/SWEDEN

PROJECT NO. IC3 1194 DRAWING NO. 60044 DATE 6/1/95 DRAWN BY EA

Golder Associates

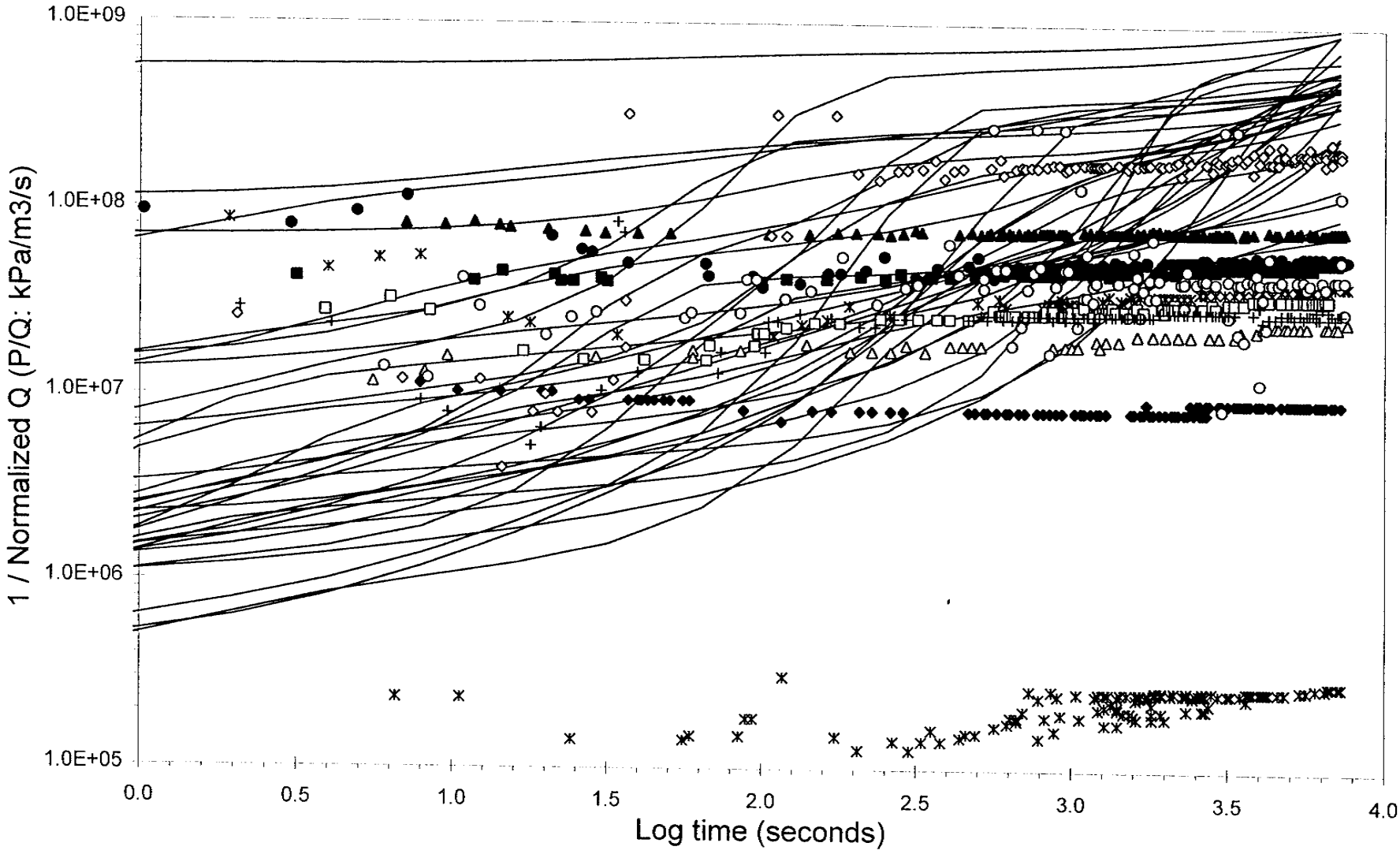

FIGURE **4-9c**
UNACCEPTABLE RESULTS
(MEAN = 6.0M; BOREHOLE P32)
CATEGORY 3
SKB/BLOCK K/SWEDEN

PROJECT NO. IC3 1194 DRAWING NO. 60045 DATE 6/1/95 DRAWN BY EA

Golder Associates

networks do not have a similar spatial structure to the non-fracture zone networks in the Äspö rock mass.

Figures 4-10 and 4-11 show the results of well test simulations with P_{32} set at the tunnel conductive frequency value (0.224 m^2/m^3 vs. 0.06644 m^2/m^3 for the borehole conductive frequency). For the large radius fracture realizations, the normalized inverse flow rates tend to be too small, although a couple of the realizations could qualify for permeability calculations. Small radius fracture sets with the tunnel intensity have more matches to the Äspö well tests than the large radius sets. Indeed some of the simulations match the actual well tests better than the borehole intensity realizations. However, as previously discussed, there are good reasons for using borehole intensity measurements instead of conductive fracture frequencies measure in the tunnel. As with the large radius realizations, these small radius sets are more generally conductive than their borehole intensity counterparts.

The tendency of the transient well test simulations for both fracture size distributions to have a greater upward slope on the t vs. P/Q plot than is observed in the Äspö measurements suggests that the sets may be a bit too sparse since flow is moving into a more linear or channelized mode than is observed. However, the results in Figures 4-10 and 4-11 indicate that the increase in intensity can not be great because then the total conductivity of the system will be too great. This topic was not pursued in this project since the object was not a complete reanalysis of the Äspö data set. Therefore, previous analyses of the data sets were used.

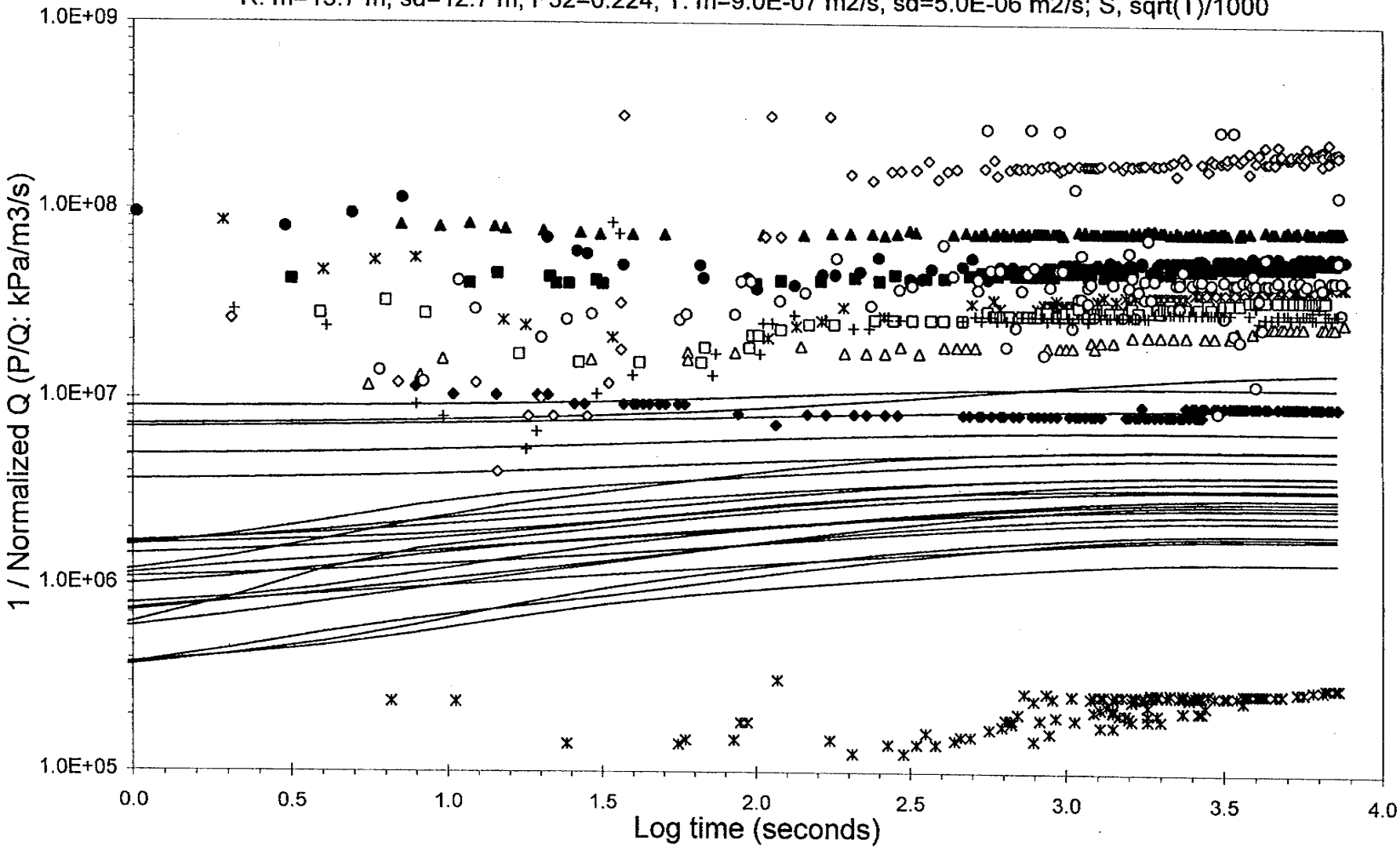

FIGURE **4-10**
WELL TEST RESULTS
(MEAN = 13.7M; TUNNEL P32)
SKB/BLOCK K/SWEDEN

PROJECT NO. IC3 1161.003 DRAWING NO. 60046 DATE 6/5/95 DRAWN BY EA

Golder Associates

Small Radius, Higher P_{32} Well Test Results

R: m=6 m, sd=2 m; P32=0.224; T: m=9.0E-07 m2/s, sd=5.0E-06 m2/s; S, sqrt(T)/1000

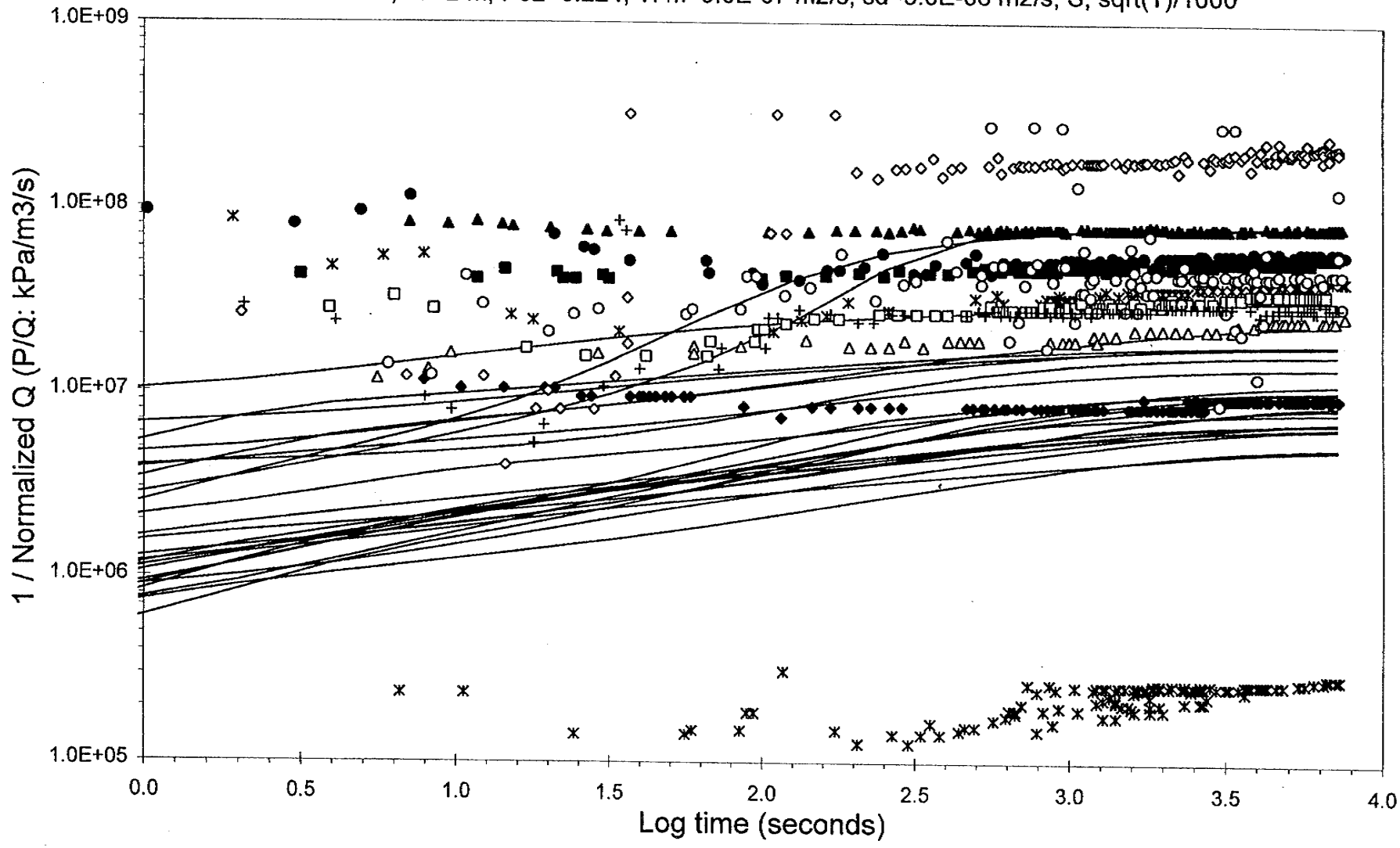

FIGURE **4-11**
WELL TEST RESULTS
(MEAN = 6.0M; TUNNEL P32)
SKB/BLOCK K/SWEDEN

PROJECT NO. IC3 1161.003 DRAWING NO. 60047 DATE 6/5/95 DRAWN BY EA

Golder Associates

5. BLOCK SCALE FLOW RESULTS

5.1 Scaling and Spatial Analysis of Block Simulations

5.1.1 Overview

In order to create a regional scale stochastic continuum model, it is necessary to assign flow properties to a large number of simulation blocks of different sizes that cover a large rock volume. If well tests were abundant, then every block could be conditioned to a well test within it. However, many if not most of these blocks are far enough away from any existing well tests that they cannot be directly conditioned. Their properties must be inferred from statistical models derived from the conditioned blocks or adjusted according derived relations with mappable geological features.

The latter alternative does not appear to be useful for Äspö. The work reported in Section 3 and by Stanfors and others (1994) indicates that block-scale fluid flow properties have at best a weak correlation with mappable geological features. Therefore, the block properties for the stochastic continuum models need to be assigned according to statistical from the conditioned blocks. This assumes that the DFN models described in Section 4.3 are representative of Äspö. Since available analysis to date indicates that the fracturing and fluid flow properties at Äspö are stationary, it is reasonable to assume that the conditioned DFN models are unbiased, representative blocks.

Standard statistical analysis of the block values for a particular scale produces estimates of the mean, standard deviation, minimum and maximum values of the flow properties. The spatial correlation for blocks of a given scale can be estimated by dividing each larger block into many smaller blocks, performing flow calculations on these sub-blocks, and then calculating the semivariogram (Figure 5-1).

Thus the spatial and non-spatial statistical analysis for each block size provides all of the necessary input for a procedure, such as the ones described in Sec. 5.3, to create a conditioned input data set for a regional stochastic continuum model.

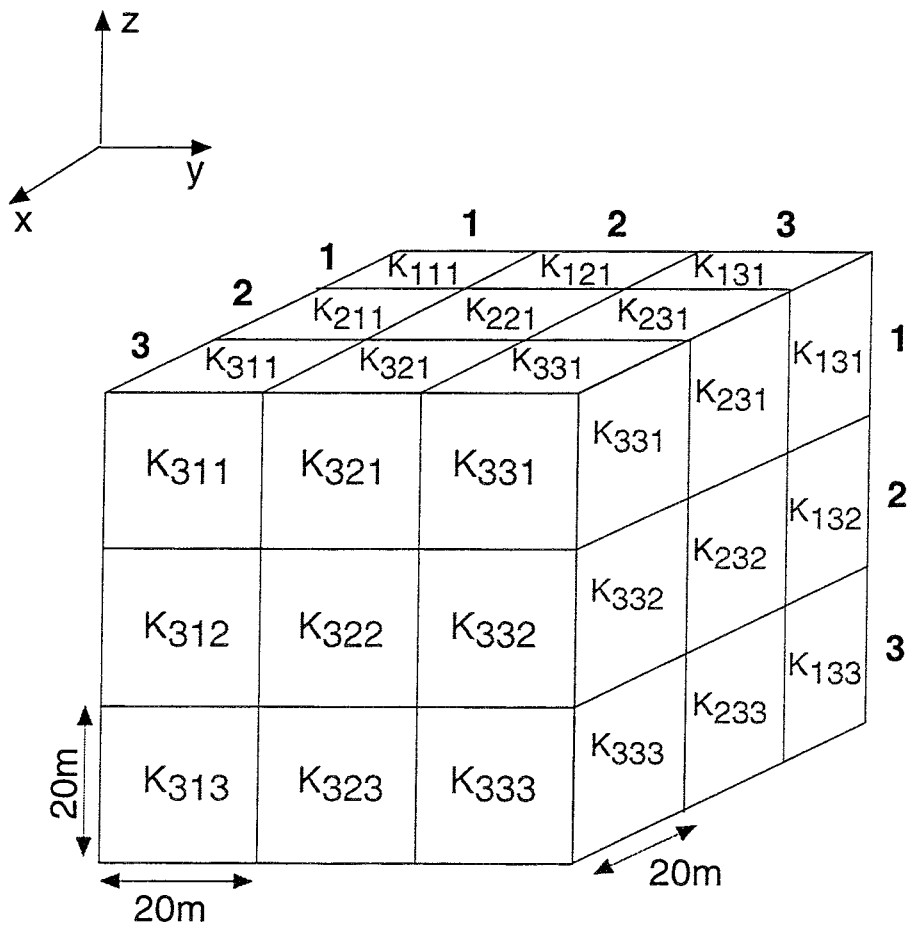

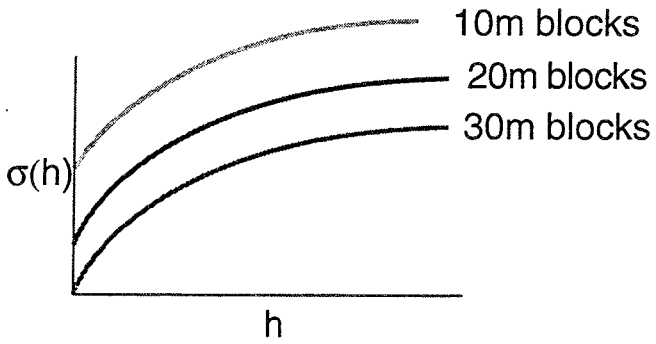

Calculate K_h for smaller blocks

FIGURE **5-1**
SCALING CALCULATIONS
SKB/BLOCK K/SWEDEN

5.1.2 Scaling Analysis

Blocks with edge lengths on the order of 10 m to 50 m were used for numerical flow simulation. In order to obtain data appropriate at these scales, each large DFN block that acceptably matched well tests as described in Sec. 4.2 was subdivided into smaller cubical blocks with edge lengths of 10 m, 20 m, 30 m, 40m and 50m (Figure 4-1). Determination of the block-scale permeability expressed in m^2 was calculated for each of the three principal block coordinate axes - north/south, east/west and up/down. Directions reflect the Äspö coordinate system.

The results from these simulations are described in two ways: population statistics for a particular block scale; and changes in average block properties as a function of scale. Figures A-1 through A-4 and Figure 5-2 describe an important feature of these simulations. Each of these figures summarizes results for the 24 acceptable realizations for the large fracture size, and the 20 acceptable realizations for the small fracture size (Table 4-1). The vertical axis represents the cumulative percentage of these acceptable realizations which had a certain percentage of conductive blocks in the realization. For example, Figure A-1a shows that 90% (18 out of 20) of the acceptable realizations for the small fracture size assumption had 26% percent or fewer blocks with non-zero conductivity in the X-direction. Fewer than 10% of the realizations had more than 26% of the sub-blocks within the realization that were conductive in the X-direction. With the data that is currently available, the DFN models predict that a significant number of blocks will have *no flow* between opposite faces of the cube. The number of conductive blocks varies between 10% and 40%, and it varies by direction. It is significant from a modeling perspective in that this implies that many blocks should have very low values of permeability, and that non-neighbor connections are important to be able to model Äspö. In many ways, the number and spatial pattern of non-conductive blocks may be as important as the properties of the blocks that are conductive.

The figures indicate that the percentage of non-conductive blocks is a function of both the block size and the fracture size assumption. The way in which the conductivity changes is Figure 5-2 somewhat complex, as shown in Figure 5-2. This figure summarizes the percentage conductive blocks as a function of block size, fracture size

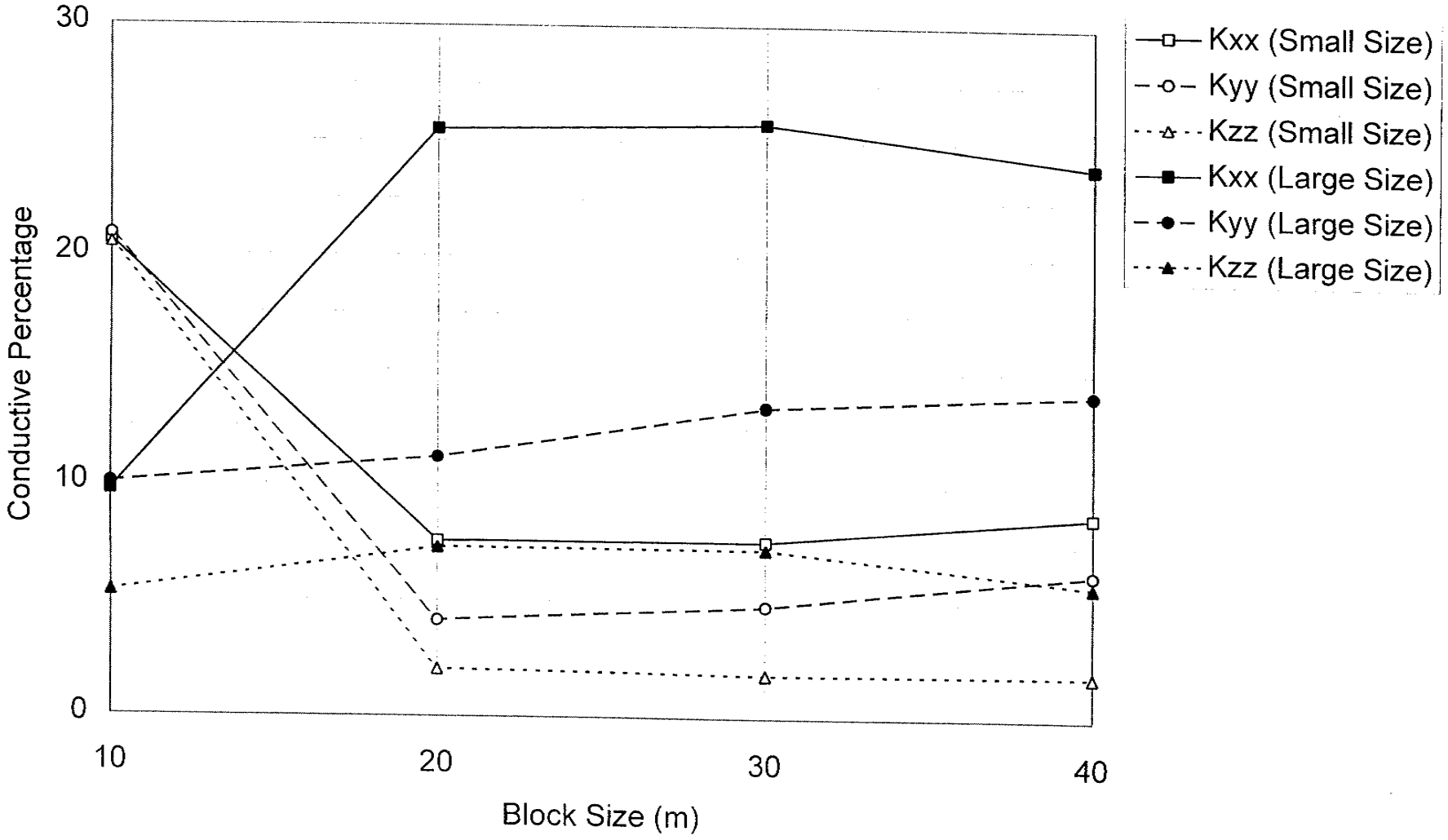

FIGURE **5-2**
CONDUCTIVE BLOCK PERCENTAGE, 50M BLOCKS, MEAN FRACTURE RADIUS = 6.0M
SKB/BLOCK K/SWEDEN

PROJECT NO. IC3 1161.003 DRAWING NO. 63011 DATE 9/8/94 DRAWN BY EA

Golder Associates

and flow direction. The solid symbols show the variation for the large fracture size, while the open are for the small fracture size assumption. For 10 m blocks, the small fracture model has the highest percent of conductive blocks. But as the block size increases, the conductive percentage for the small fracture size decreases rapidly so that it is less than for the large fracture size. The large fracture size percentage initially increases with increasing block size, and then decreases, but still remains higher than for the small fracture size assumption. For blocks greater than 20 m, Figure 5-2 suggests that there is an anisotropy such that the X-direction is most often conductive, followed by the Y-direction and then the Z-direction. This anisotropy persists regardless of fracture size. This difference in connectivity suggests that the X-direction should be the most conductive of the three directions.

The decrease in connectivity for increasing block size is analogous to percolation in a porous medium. The probability of connection over a particular distance relates to the density of connections between pores. The probability decreases as the distance increases (Feder, 1988, Chap. 7) for systems below the critical percolation threshold such as the DFN models in this report. If a fracture plays the role of the connection, and the intersection points between fractures plays the role of the pores in a porous medium, then it is easy to see that the probability of fracture connection over a particular distance decreases with distance. According to percolation theory, the mass of clusters, analogous to the number of fractures making up a cluster, increases weakly with increasing lattice size (Feder, 1988, pg. 109). As a result, the probability that a fracture pathway will exist across a block of a particular scale decreases with increasing block size. The reason for the higher conductivity for the small fractures for the 10 m block scale may be that the mean fracture size (radius = 6.0 m) is on the order of the block itself, so it is possible that a single fracture could connect opposite block faces. This would also be true for the large (radius = 13.7 m) fractures, but there are many more small fractures than large fractures, so the percent conductivity is higher for the small fractures at this scale. As the scale increases, networks of small fractures are required to connect opposite block faces, and because of the decreased percolation probability, connectivity continues to decreases. For the large fractures, there is an increase for blocks up to the scale of the large fractures. At this point, the connectivity begins to decrease.

If a network is very sparse, then most blocks that have connections from one face to the opposite face will have one or two pathways connecting them. As previously described, the number of pathways should be greater for the small fracture mean size assumption than the large fracture size mean assumption. It will be a common occurrence that these paths are independent, and composed of fractures connected end to end in series. For the large fracture size, the series may consist of only one or two fractures. For the smaller size assumption, these paths should consist of more fractures. Since fracture transmissivity is not correlated to fracture length in these models, the situation is like an electrical network with resistors in series: the more resistors added, the higher the overall resisitivity of the circuit.

In other words, the smaller the fracture size, the greater number of fractures in each conductive pathway, and the lower the over all path conductivity. This implies that the block scale conductivity should decrease for smaller mean fracture sizes.

Alternatively, if the network is dense, not sparse, then the increased number of fractures in the small size DFN model will lead to a greater number of pathways that are interconnected. This situation behaves like a circuit with many resistors in parallel. The overall resistance of the circuit decreases as the number of pathways increases. This type of system should exhibit *increasing* conductivity as fracture size decreases.

When the population statistics are calculated from the simulations, they show a behavior characteristic of the sparse network. Figures A-6 through A-15 show the population statistics for conductive blocks as a function of block size. The histograms (Figures A-6 through A-10) suggest that the distribution of the log permeability is approximately normal. Figures A-11 through A-15 show the cumulative frequency distributions as a function of block size, fracture size and flow direction. Comparison of populations as a function of flow direction for any one particular graph may show anisotropy, in other words, that the permeability is greater in one direction than the others. However, additional calculations show that this relation is not consistent for all block sizes.

Figure 5-3 and 5-4 summarize trends in mean directional permeability as a function of

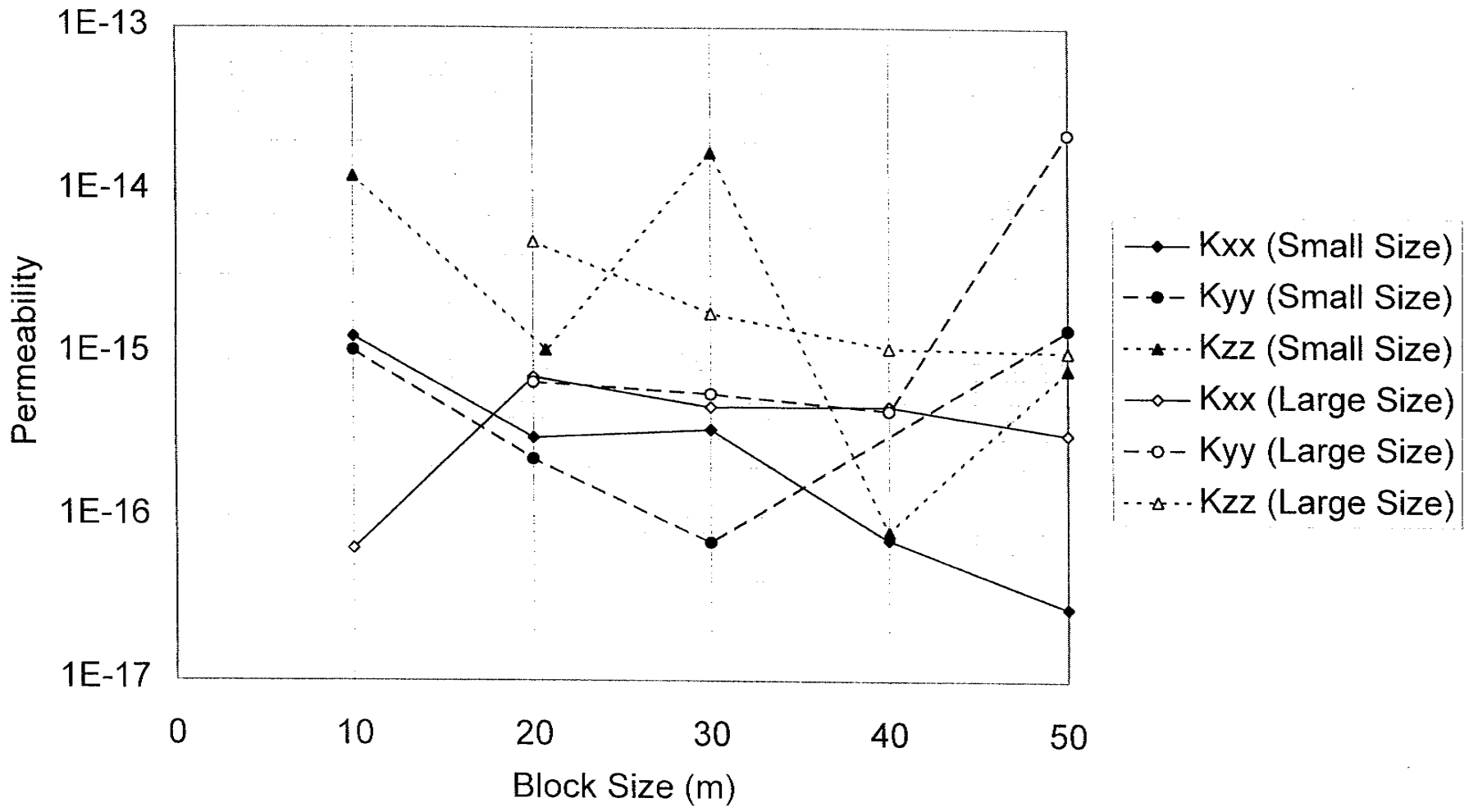

FIGURE **5-3**
SCALING OF PERMEABILITY AS A FUNCTION OF BLOCK SIZE - NESTED SIMULATIONS
SKB/BLOCK K/SWEDEN

PROJECT NO. IC3 1161.003 DRAWING NO. 60836 DATE 9/8/95 DRAWN BY EA

Golder Associates

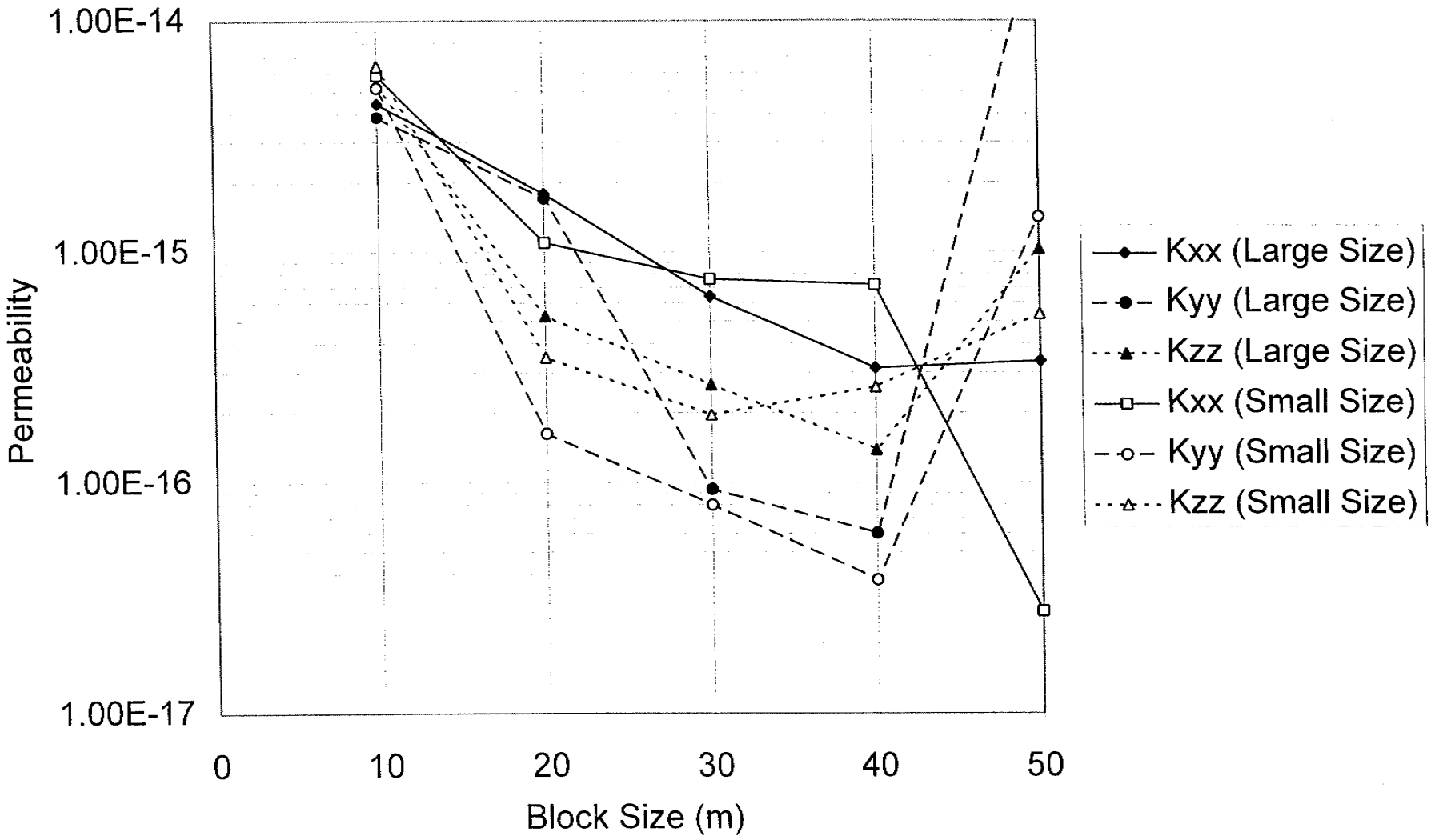

FIGURE **5-4**
SCALING OF PERMEABILITY AS A FUNCTION OF BLOCK SIZE - ENSEMBLE AVERAGING
SKB/BLOCK K/SWEDEN

PROJECT NO. IC3 1161.003 DRAWING NO. 60837 DATE 9/8/95 DRAWN BY EA

Golder Associates

both block size and fracture size. Figure 5-3 represents a series of block experiments carried out in blocks that matched the well test criteria. As described in Sec. 4.3, simulations were carried out on blocks of 10 m through 50 m scale nested or centered at a common point, the center of each large qualified block. The points on the graph represent the mean value for all nested simulations that had non-zero values. Figure 5-4 was calculated from the mean values of from *all* the non-nested simulations. There lower scatter and more consistent trends may reflect the greater number of samples used to calculate each point. The apparent change in behavior in Figure 5-4 for 50 m block sizes could be due to the very small (< 10) number of simulations that were conductive at that scale.

These two figures suggest that:

1) block-scale permeability decreases with increasing block size,

2) some anisotropy may exist, but apparent differences may be artifacts of the small number of points used to calculate statistics for large block sizes. If the results are not artifacts, then the data suggests that the east/west-direction is the least conductive while the north/south-direction is the most conductive. This does not imply that these are principal directions of permeability, but does imply that the principal horizontal direction is probably in a northerly direction.

3) Conductive blocks with smaller fractures are less permeable than conductive blocks traversed by big fractures, supporting the hypothesis that the fracture system behaves as a sparsely connected network in which fluids move primarily through independent conduits.

The decrease in block-scale permeability with scale is significant, about one to two orders of magnitude. It is the type of behavior that would be forecast for a sparsely-connected network.

The sparse connectivity of the networks is a function of several network parameters. One that is important and is open to further investigation is the conductive P_{32} used. Analysis of well tests at Äspö (T. Doe, pers. comm., 1995) suggests that the late time

behaviors of the actual transient well tests indicate less sparse networks than the simulated well tests. It is not known whether increases in the value of P_{32} to values that would better match the well tests would lead to flow behavior characteristic of a dense network, such that the conclusions drawn from the simulations would change significantly.

5.1.3 Spatial Analysis

Analysis of block-scale permeability variation is based on calculating conditional semivariograms from the 10-m block values. The semivariograms are termed *conditional* in the sense that block permeability must be non-zero in order for it to be used in the semivariogram calculation. In other words, the conditional semivariogram for K_{xx} is estimated from only non-zero block-scale K_{xx} values.

The results reported in Sec. 5.1.2 are not very useful, since they are taken from 50-m blocks. These 50-m blocks do not provide a large enough sample of block-scale correlation properties. The maximum number of blocks in any X, Y or Z direction is 5. This means that it is only possible to compute the directional semivariograms for four distance scales - 10 m, 20 m 30m and 40 m. Moreover, the number of pairs for the two longer distances is small, so that these values of the semivariogram would be poorly estimated (Journel and Huijbregts, 1978, p 194). This would leave only two points (the 10 m and 20 m lags), or possibly three, to define each directional semivariogram, which is not sufficiently unique nor does it span a large enough distance to be useful.

In order to improve this situation while still maintaining reasonable computer simulation run times, the spatial correlation analysis was performed instead on 10 m blocks taken from a larger cube, 100 m on a side. This larger cube contains 1000 10-m cubes, whose block-scale permeability values were calculated as described in Sec. 5.1.1. With this larger 100 m simulation region, it is possible to robustly estimate the spatial correlation properties of 10-m blocks over much larger distances.

Since the semivariogram calculations only include conductive 10-m blocks for the particular permeability component analyzed, the data set does not consist of a large number of pairs. This means that the resulting semivariograms have a high fluctuation

variance. An approximate rule for determining over what lag distances the fluctuation variance is acceptably small is to include only lag values that are less than 1/2 the maximum possible lag (Journel and Huijbregts, 1978, p. 194). For directional semivariograms, the maximum lag is 90 m, so the directional semivariograms are only meaningful up to lag values near 40 or 50 m. For the isotropic variograms, in which direction is ignored, the maximum lag distance is the distance ($\approx$ 156 m) between the centers of 10-m blocks lying in opposite corners of the 100-m cube. Thus, the isotropic semivariograms are not meaningful for lags much greater than 80 m. The various semivariograms for the different permeability components, fracture size assumptions and directions are shown in Figures 5-5 through 5-11. Spatial properties for both the small and large fracture size assumption were calculated.

Figure 5-5 shows the directional semivariograms for the small fracture size assumption. The semivariograms are quite noisy due to the small number of pairs, but show no obvious spatial correlation. The horizontal semivariograms are approximately the same, while the vertical semivariograms have a smaller sill value. The reason for this difference has not been investigated. However, there is no increase in semivariance with lag distance for these directional semivariograms for any of the three directions.

The lack of obvious spatial correlation and the high variance may be caused by the fact that only 10 to 20 pairs were used to calculate each point on Figure 5-5 due to the scarcity of blocks having non-zero permeability values. As Journel and Huijbregts (1978, p. 194) note, 30 to 50 pairs may be the minimum required for robust semivariogram estimation. If this is the case, then none of the directional variogram for the small fracture size assumption meet this criterion.

The isotropic semivariogram (Figure 5-6) overcomes the problem with the small number of pairs. Each point on the variogram is estimated from anywhere between 100 to 1000 data pairs. However, there does not appear to be any spatial correlation shown by the semivariograms for any of the three permeability components, with the possible exception of K_{zz}. The first two lags are the only lags that hint at spatial correlation, and these are based on the fewest number of pairs.

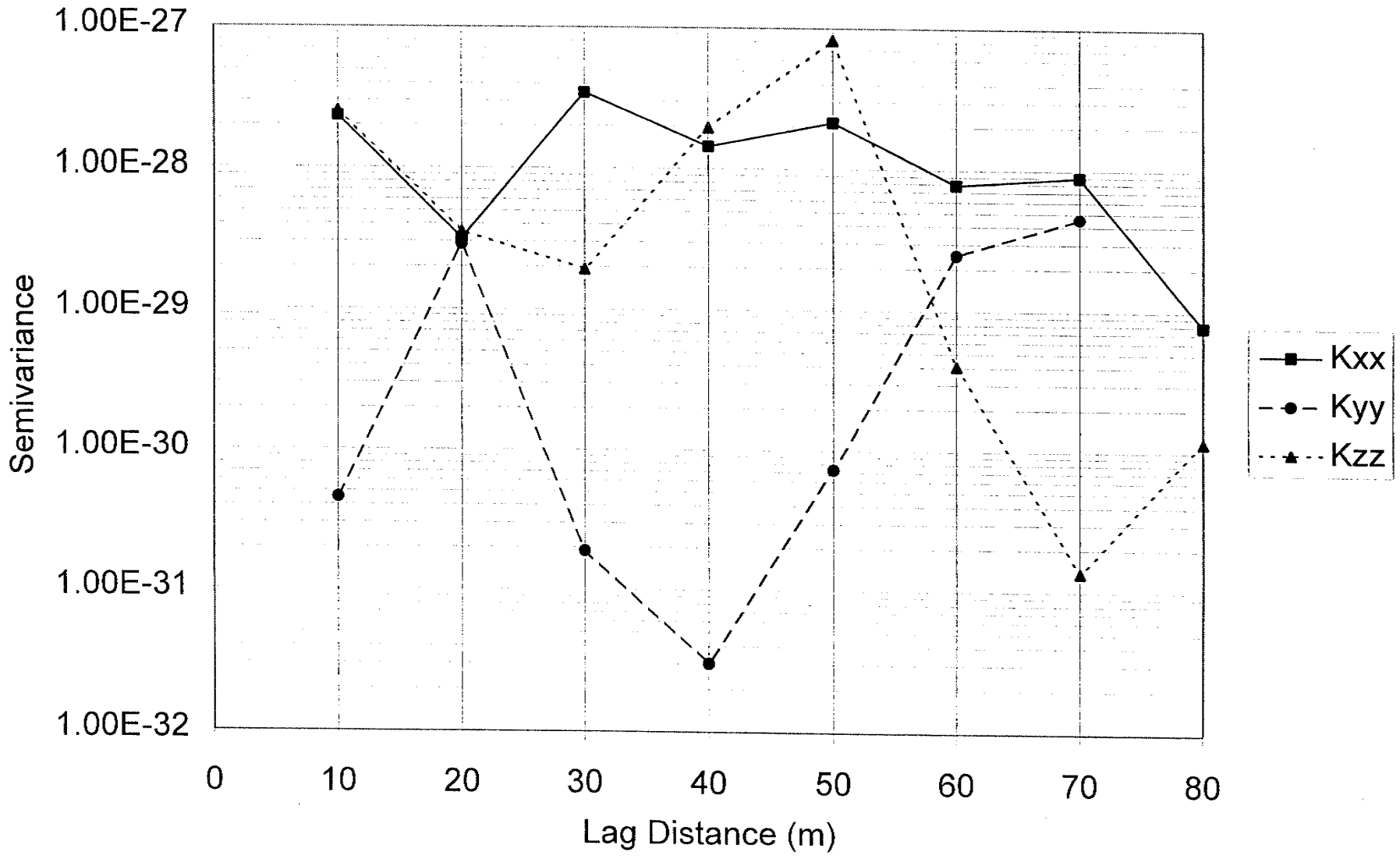

FIGURE **5-5**
DIRECTIONAL SEMIVARIOGRAMS FOR 10 m BLOCKS, SMALL FRACTURE SIZE
SKB/BLOCK K/SWEDEN

PROJECT NO. IC3 1161.003 DRAWING NO. 60838 DATE 9/8/95 DRAWN BY EA

Golder Associates

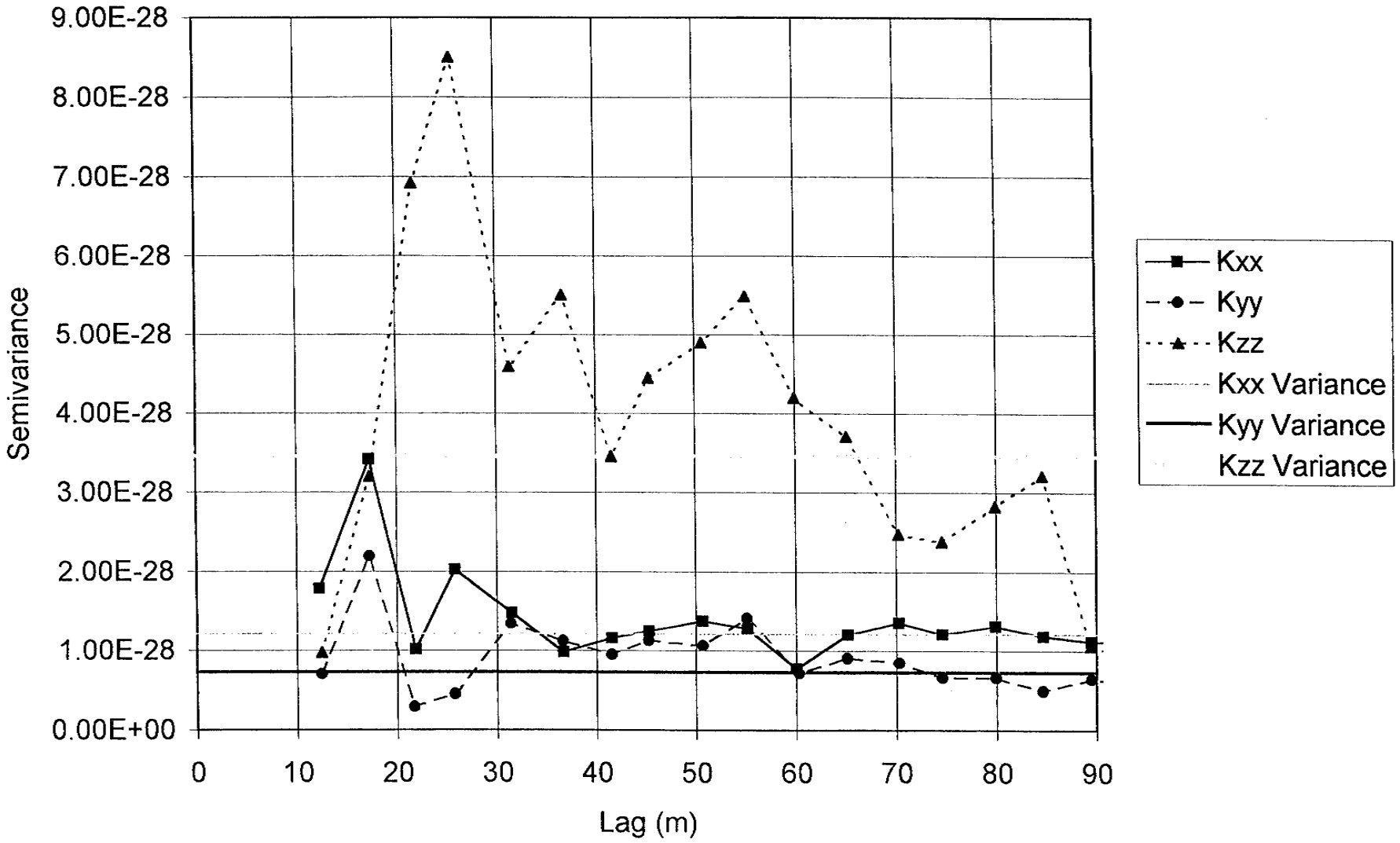

FIGURE **5-6**
ISOTROPIC SEMIVARIOGRAM FOR 10 m BLOCKS, SMALL FRACTURE SIZE
SKB/BLOCK K/SWEDEN

PROJECT NO. IC3 1161.003 DRAWING NO. 60839 DATE 9/8/95 DRAWN BY EA

Golder Associates

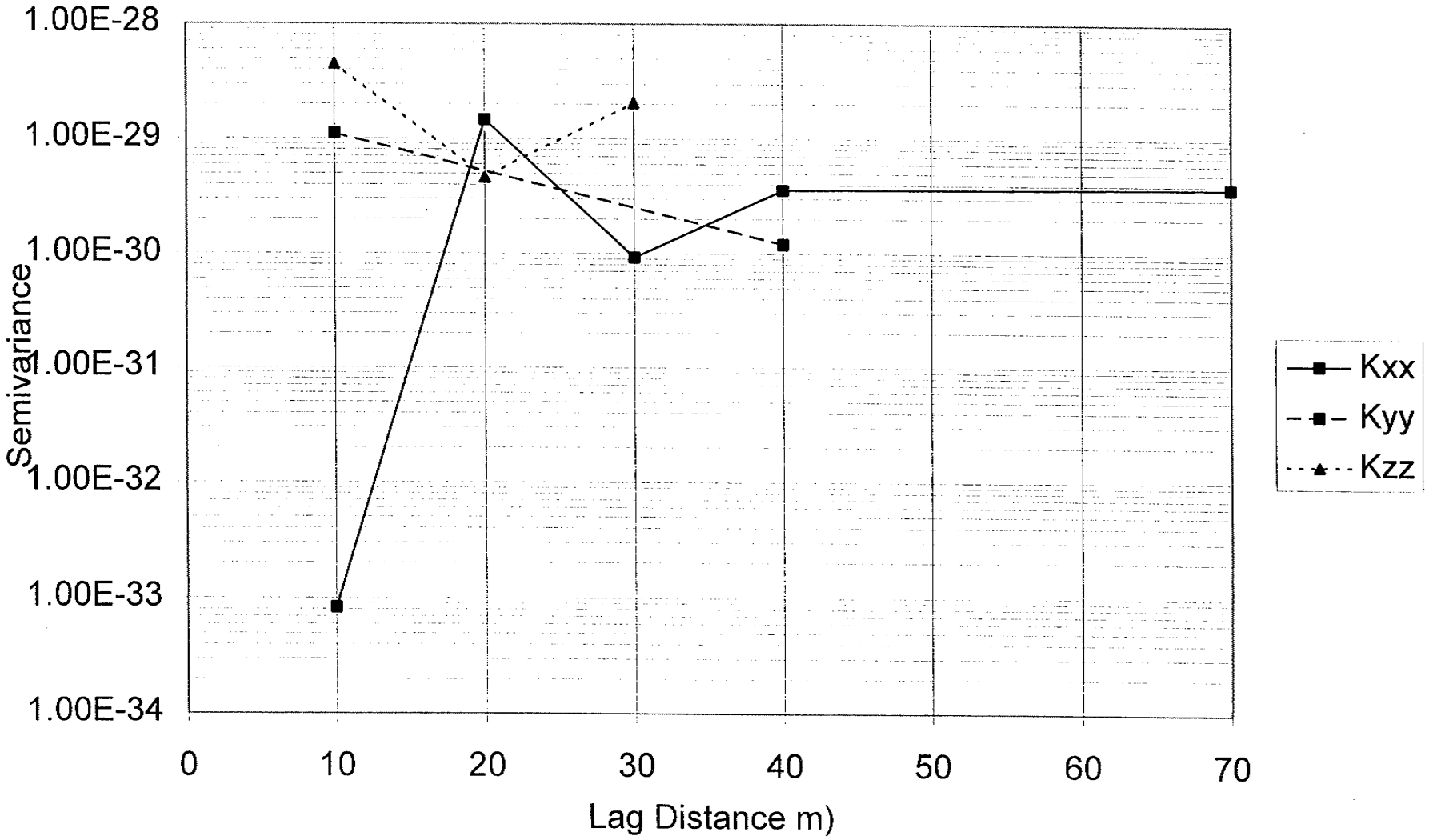

FIGURE **5-7**
DIRECTIONAL SEMIVARIOGRAMS FOR 10 m BLOCKS, LARGE FRACTURE SIZE
SKB/BLOCK K/SWEDEN

PROJECT NO. IC3 1161.003 DRAWING NO. 60840 DATE 9/8/95 DRAWN BY EA

Golder Associates

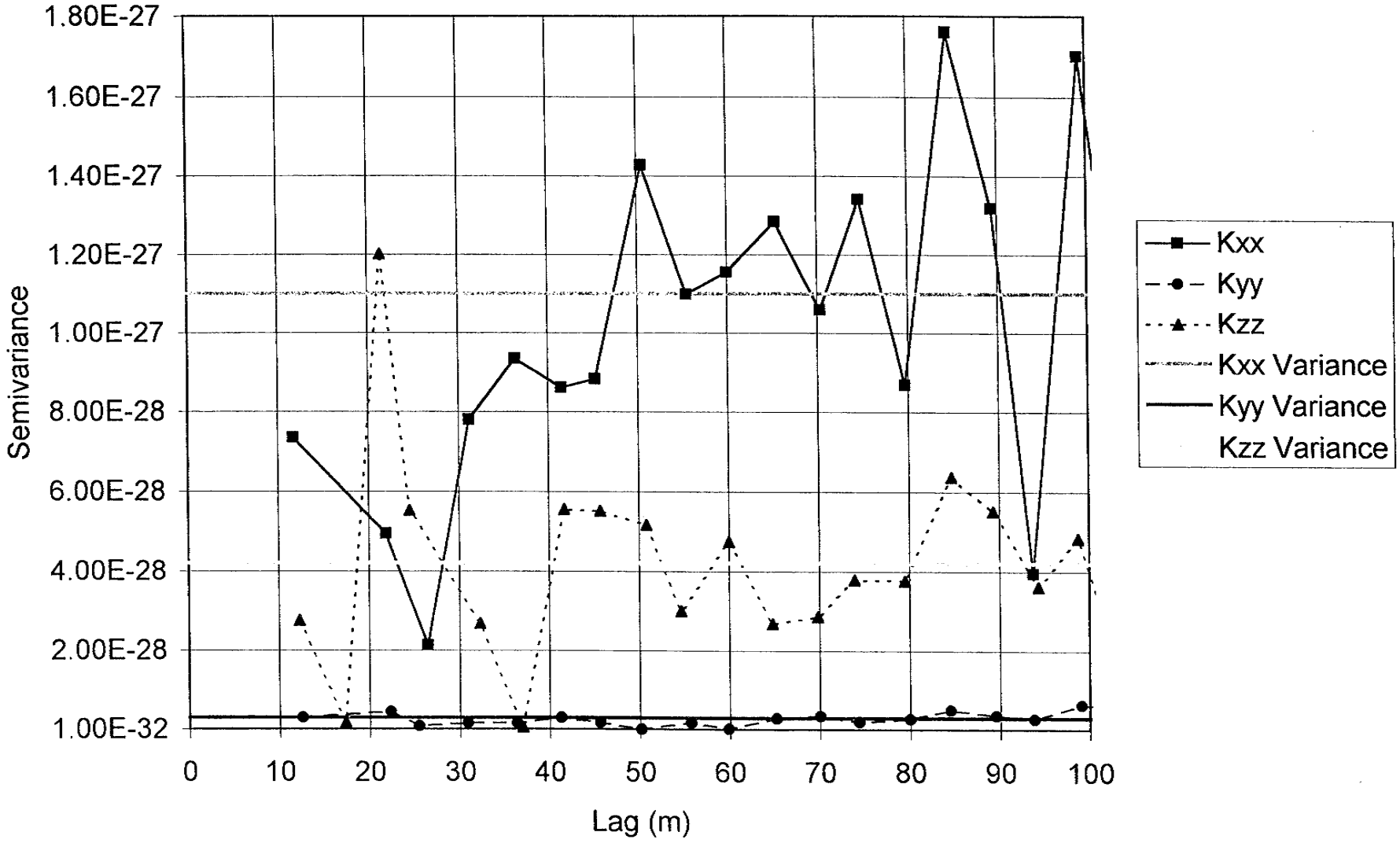

FIGURE **5-8**
ISOTROPIC SEMIVARIOGRAM FOR 10 m BLOCKS, LARGE FRACTURE SIZE
SKB/BLOCK K/SWEDEN

PROJECT NO. IC3 1161.003 DRAWING NO. 60841 DATE 9/8/95 DRAWN BY EA

Golder Associates

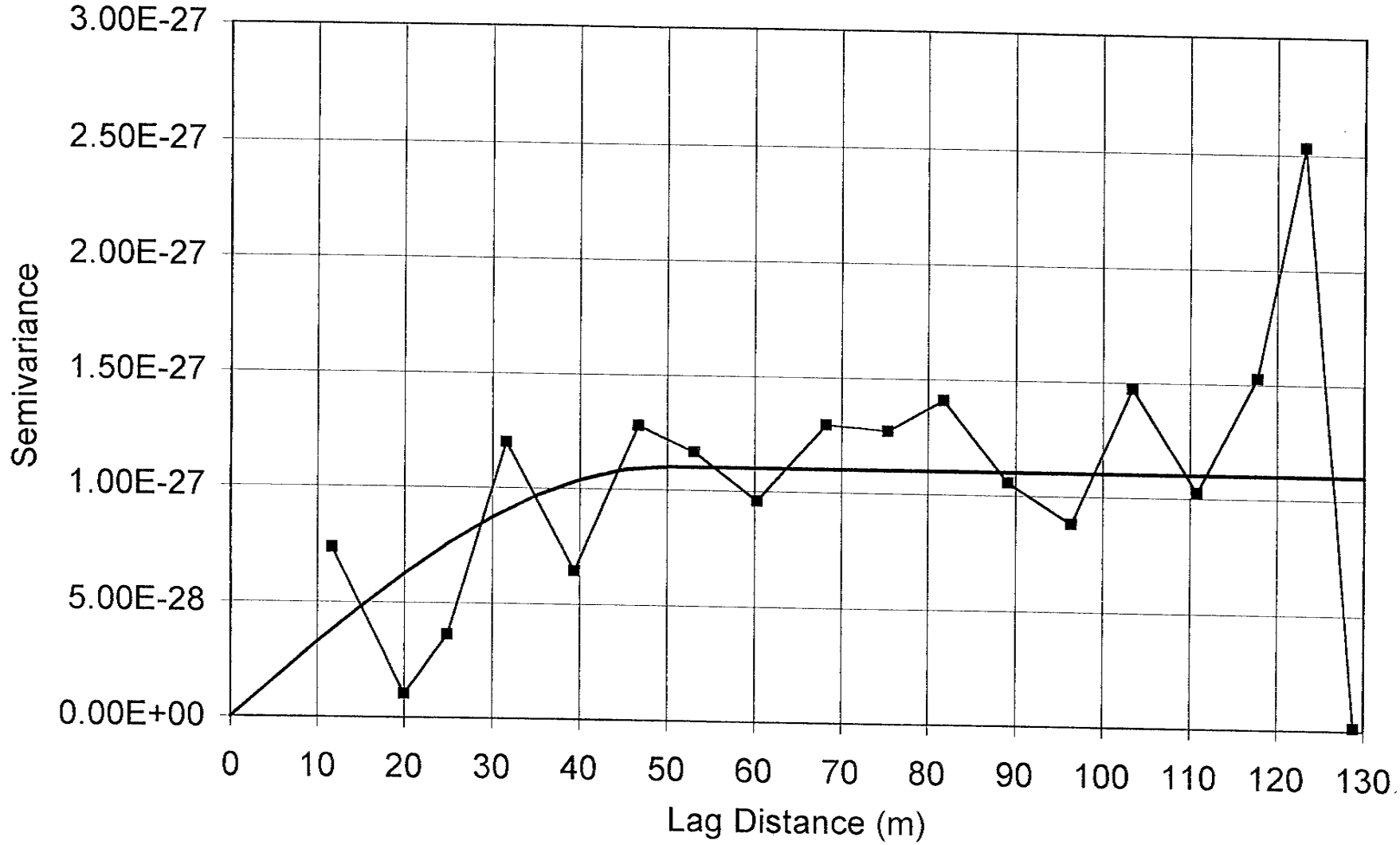

FIGURE **5-9**
ISOTROPIC SEMIVARIOGRAM FOR 10 m BLOCKS, K_{xx} COMPONENT, LARGE FRACTURE SIZE
SKB/BLOCK K/SWEDEN

PROJECT NO. IC3 1161.003 DRAWING NO. 60842 DATE 9/8/95 DRAWN BY EA

Golder Associates

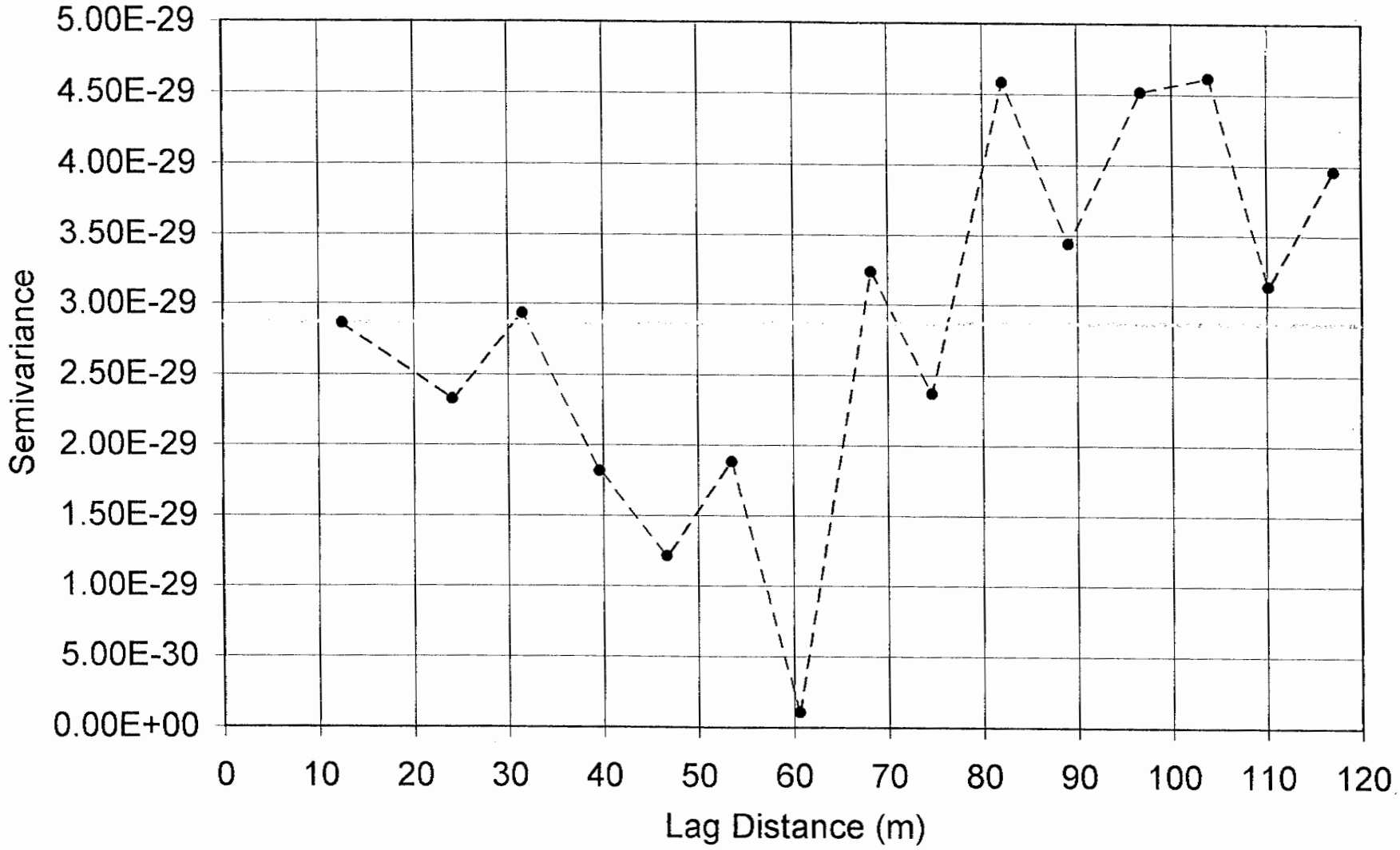

FIGURE **5-10**
ISOTROPIC SEMIVARIOGRAM FOR 10 m BLOCKS, K_{yy} COMPONENT, LARGE FRACTURE SIZE
SKB/BLOCK K/SWEDEN

PROJECT NO. IC3 1161.003 DRAWING NO. 60843 DATE 9/8/95 DRAWN BY EA

Golder Associates

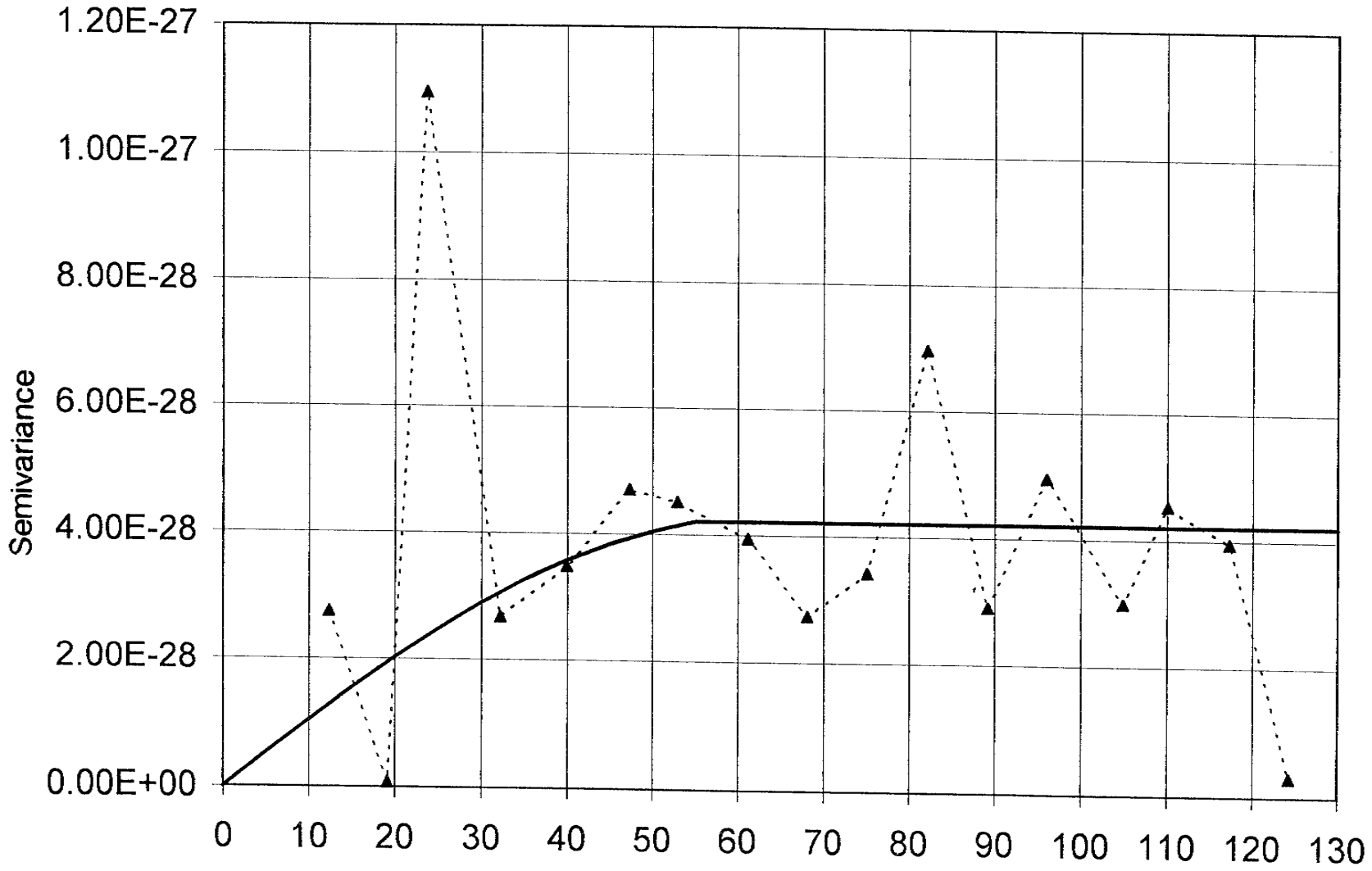

FIGURE **5-11**
ISOTROPIC SEMIVARIOGRAM FOR 10 m BLOCKS, K_{zz} COMPONENT, LARGE FRACTURE SIZE
SKB/BLOCK K/SWEDEN

PROJECT NO. IC3 1161.003 DRAWING NO. 60844 DATE 9/8/95 DRAWN BY EA

Golder Associates

Figure 5-7 shows the directional semivariograms for the large fracture size assumption. Unfortunately, these semivariograms are estimated from an even fewer number of pairs than the corresponding semivariograms for the small fracture size models. It may not be possible to compute robust semivariograms for the large size assumption without generating huge DFN models with tens of thousands of blocks in order to get enough data pairs.

Contrary to the directional variograms and the small fracture size isotropic semivariograms, the isotropic semivariograms (Figures 5-8 through 5-11) show evidence of spatial correlation. This is somewhat surprising in that:

1) this result appears to be inconsistent with the other semivariograms, yet it is based upon a sufficiently large number of data pairs, and
2) none of the parameters describing the fractures in the blocks were given any spatially correlated properties.

Figure 5-8 shows the three raw semivariograms for the three permeability components. It is clear that the variance of the K_{xx} values is the greatest, the variance for the K_{yy} values the lowest, and the vertical component somewhere in between. Because of the difference in variance, it is useful to examine each semivariogram plotted at their own characteristic scales.

Figure 5-9 shows the semivariogram for the K_{xx} component, and a theoretical spherical model with range = 50 m superimposed on the experimental semivariogram. Unlike the K_{zz} semivariogram in Figure 5-7, the part of the semivariogram that suggests spatial correlation is based upon at least 5 plotted points, which strengthens the possibility that there is spatial correlation in the block values. A similar plot for K_{zz} also suggests spatial correlation. Whether the spherical model shown superimposed with a range of 55 m is the best model would require much more additional simulation and cross-validation. The semivariogram for K_{yy} shows no spatial correlation. This may be due to the much greater percentage of blocks that are non-conductive in the Y-direction than in either the X or Z directions (FigureB-1b).

The explanation for the existence of spatial correlation for the large fracture size isotropic semivariogram and the lack of spatial correlation in the other semivariograms is important for deriving block-scale input properties for stochastic continuum models in fracture-dominated systems, *whether they be based upon DFN models or not.*

For a set of fractures with a lognormal radius distribution with mean radius equal to 13.7 m mean and standard deviation equal to 12.7 m, as many as 50% of the fractures have diameters greater than 20 m, and 30% of the fractures have diameters greater than 30 m. For the small size assumption, over 95% of the fractures have diameters smaller than 20 m, and 99% have diameters smaller than 30 m. Thus, if there are three or four 10-m blocks connected in a row for the large fracture size, most of the time it will be the same fracture pathway consisting of one or two fractures crossing all four blocks. Since each fracture has constant fluid flow properties, the chances that the 10-m block scale permeability will be the same for the three or four blocks in a row is high. This is similar to the problem of computing a variogram from overlapping regularized windows (La Pointe, 1994). Even though the 10-m blocks are disjoint (non-overlapping), they sample more or less the same feature or features, since the block scale is much less than the fracture path scale. For the large fractures, only about 10% have a diameter greater than 54 m. This suggests that somewhere around the scale of 50 m to 60 m, paths are more likely to be made up of multiple fractures, so there is no longer much spatial correlation among the blocks at these and greater lag distances.

For the small fracture size, all paths are more or less made up of features that are at a scale smaller than the 10 m block size and lag. Only 1% of the fractures for the small fracture size assumption have diameters greater than 24 m. Thus, since there is no spatial correlation whatsoever in the transmissivity field or the fracture location field, there is virtually no spatial correlation in the block-scale properties.

This is an important consideration for stochastic continuum modeling of fracture or fault-dominated flow. If it is necessary in the near-field to have grid cells smaller than the scale of the conductive features, and if flow networks are sparse rather than dense, then block scale permeability values should show spatial correlation, *even though there is no spatial correlation in the underlying faults or joints.* This suggests that a spatially uncorrelated Monte Carlo assignment of block scale properties is *never* correct for a

stochastic continuum flow model if the fractures are about the same size or larger than any of the blocks. A spatially uncorrelated assignment of block properties in this situation would lead to a flow model with less potential for larger scale flow conduits. Since block sizes are often smallest in the regions of greatest interest, such as the canister drifts, assigning block scale properties with no spatial correlation would lead to a more optimistic performance assessment since large scale channelized flow would be reduced.

Another implication for continuum modeling is that it is necessary to determine the size of the significant flow features for the scale of the flow simulation, *even if a DFN approach is not used to compute block-scale properties*. Without knowing the size of the important flow features, it is not possible to determine if the blocks are small with respect to the flow features.

5.1.4 Conclusions

The modeling results for blocks of different sizes have shown that, for the given models based upon available data, the flow system behaves as a sparsely connected network. In particular,

1) It is possible to condition DFN simulations to match transient well tests,

2) Block scale permeability decreases with block size once the scale of the blocks begins to exceed the scale of the individual fractures,

3) Block scale permeability decreases with the assumed mean fracture size,

4) Permeability anisotropy may exist, such that the Äspö-north direction permeability is the largest, followed by the vertical direction, with the Äspö-east direction permeability the least.

5) Block scale permeability is approximately lognormally distributed, with means ranging from 10^{-14} to 10^{-16} m^2.

6) Blocks show a low degree of inter-block spatial correlation for the small fracture size assumption. For the large fracture size assumption, the blocks show correlation up to 50 or 60 m. This may be very important for correctly modeling the more finely-meshed region around canister drifts or other near-field features.

5.2 Application of Approach to NAMMU, HYDRASTAR and PHOENICS

5.2.1 Cross Verification

Section 5.1 showed that it is possible to derive block-scale permeability values from DFN models. To evaluate how well a stochastic continuum model whose permeability values are generated in this way predicts flow, results from a stochastic continuum code were compared to a DFN finite element code for a simple test case.

The numerical codes currently considered by SKB for regional continuum modeling of fluid flow and mass transport through fractured crystalline rocks are HYDRASTAR (Norman, 1992b), PHOENICS (Spalding, 1981) and NAMMU (Hartley and others, 1994). Both HYDRASTAR and PHOENICS are finite difference models, whereas NAMMU is a finite element model. SKB has focused mainly on using HYDRASTAR and PHOENICS as potential stochastic continuum codes, although NAMMU also has the necessary capabilities.

The approach outlined in this report assumes that a continuum model consisting of an assemblage of smaller sub-blocks whose permeability properties are derived from a DFN model reproduces the flow behavior of the DFN model. This assumption can be evaluated by conducting some stochastic continuum simulations. The strategy is compute the effective hydraulic conductivity tensors for 10-m blocks by conducting flow simulations on these smaller blocks. This produces values of K_{xx}, K_{yy}, and K_{zz} for each 10-m block. The flow simulations are essentially numerical Darcy experiments, in which opposing block faces are given specified constant head boundary conditions, and the remaining four faces are given no-flow boundary conditions, as in Figure 4-4. The flux across each boundary is computed, which is then used to calculate the effective permeability across the block in the flow direction. These values of K_{xx}, K_{yy}, and K_{zz} are then used as input to a 50-m NAMMU simulation consisting of 125 10-m cells. Ideally, the permeability for the 50-m NAMMU simulation should be the same as the 50-m DFN

simulation. Some errors between the NAMMU and the DFN models are to be expected as the numerical Darcy experiment used in this study does not allow the computation of the off-diagonal components of the permeability tensor. Furthermore, because matrix singularity problems, NAMMU does not allow a 0.0 value for one or all of the permeability components. The following simulations were used to test whether the assemblage of 10-m continuum blocks behaves the same as the 50-m DFN model.

Figure 5-12 compares the effective 50-m block scale permeability for the NAMMU and DFN simulations. Many of the 50-m scale simulations were not conductive from one face to the opposing face. NAMMU has a threshold of 1.0e-22 m^2 in order to avoid singularities in the global conductance matrix; values below this indicate that there is no connection between opposing faces. The same threshold was applied to the MAFIC DFN flow simulations. Only those simulations in which both the NAMMU and MAFIC results were above the threshold are plotted in Figure 5-12. There are significantly more NAMMU simulations that fall below the threshold than the corresponding MAFIC DFN simulations. The line shown on the graph represents where the results should plot if there were a perfect correlation between the NAMMU and DFN results. The results for both the large and small fracture size assumptions are shown.

Figure 5-12 shows that the correspondence between the stochastic continuum and DFN simulations is not straightforward. The behavior appears to depend upon the relation between fracture size and block size. For the small fracture size assumption, two of the eight conductive realizations are within 1.5 orders of magnitude. NAMMU overestimates in three other realizations, while underestimating in three others. Overall, the correspondence is not good, but the error is unbiased. For the large fracture size assumption, NAMMU significantly underestimates the DFN result.

The underestimate is probably due to the fundamental problem of the numerical Darcy experiment used in this study, which cannot be used to calculate the off-diagonal components of the permeability tensor. Consider the situation where a conductive fracture cuts across the bottom right-hand corner of a 10-m block and intersects another fracture in a neighboring block. Further assume that this intersected fracture cuts back

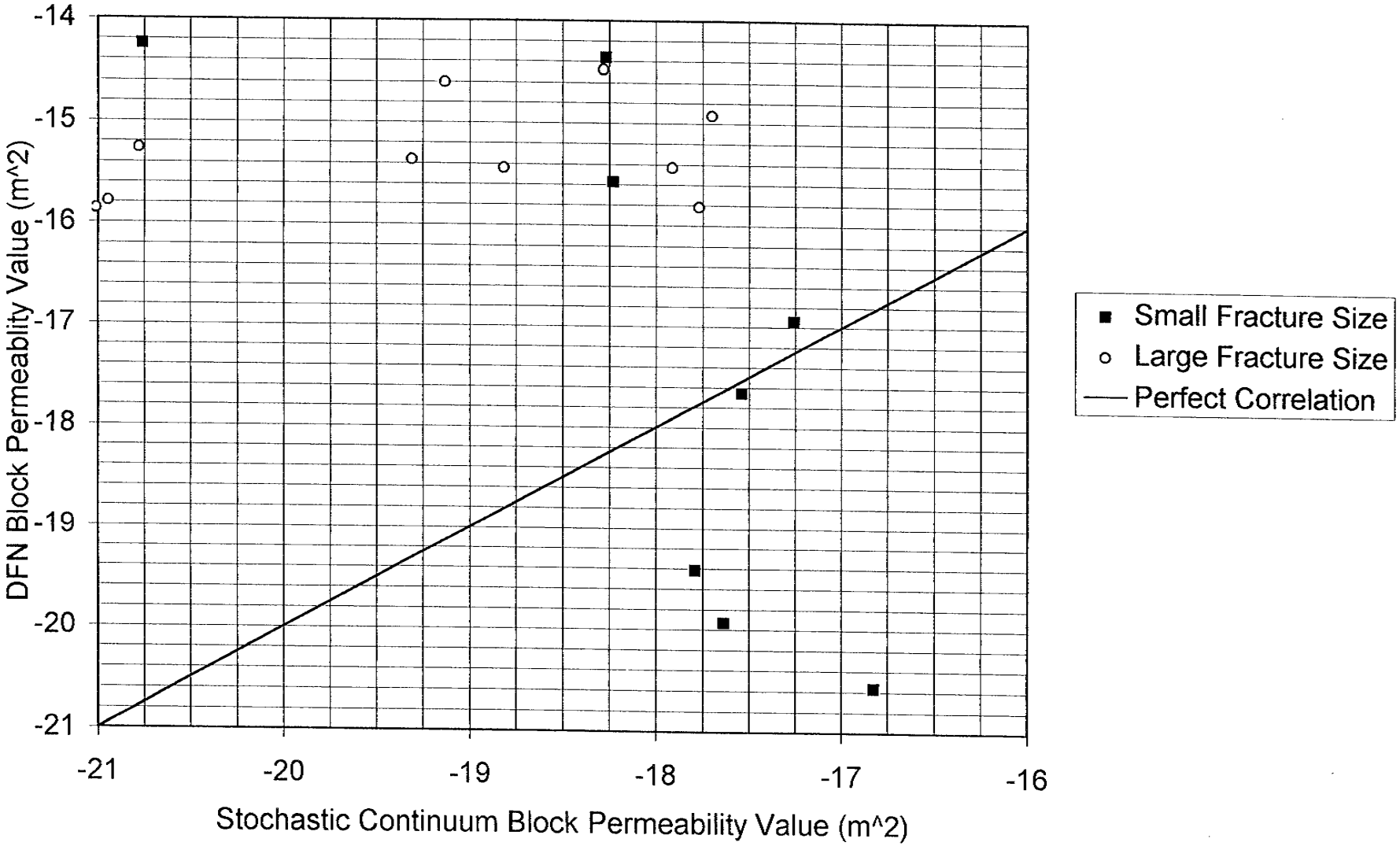

FIGURE **5-12**
COMPARISON OF NAMMU AND MAFIC RESULTS FOR 50 m BLOCK PERMEABILITY CALCULATIONS
SKB/BLOCK K/SWEDEN

PROJECT NO. IC3 1161.003 DRAWING NO. 60845 DATE 9/8/95 DRAWN BY EA

Golder Associates

through the top right corner of the original block and intersects the top face. In the DFN, there is a highly conductive path from the bottom face to the top face. This path, however, leaves the original block and then re-enters it. In many numerical codes, this sort of connection is referred to as a *non-neighbor connection*.

This portion of the DFN model actually has a significant value of permeability. However, if a numerical Darcy simulation were run on the same block, there would be no connection between the top and bottom faces, so the resulting block-scale permeability would be 0.0. The probability that this sort of edge-cutting fracture would occur is related to the ratio of fracture size to block size. As this ratio increases, the probability that such non-neighbor connections exist also increases, since the network becomes increasingly sparse with respect to the block size. Thus this underestimation should be greater for a particular block size as the mean fracture size increases. This behavior is shown very clearly in Figure 5-12.

As the ratio of fracture size to block size decreases, there are still some underestimates. However, they become less probable, and other types of errors become important when the effective DFN permeability is low. When a DFN 10-m block simulation indicates that the permeability is 0.0, a problem arises for some stochastic continuum codes. Because of matrix singularity problems, they do not allow a 0.0 value for one or all of the principal permeability components. Instead, they numerically represent zero values as some minimum value. For NAMMU, this value was 1.0e-22 m^2. As a result, blocks that had a true 0.0 m^2 permeability component in the MAFIC DFN simulations were given a value of 1.0e-22 in the NAMMU simulations. This leads to an over-estimation of the block-scale permeability values.

Figure 5-12 shows this effect. When the DFN simulation results have low values, the NAMMU results tend to have higher values. This occurs mainly with the small fracture size assumption simulations. This could be due to a reduction in the overestimation related to the probability of fractures cutting block corners for the small fractures size assumption, combined with the underestimation brought about by non-zero NAMMU threshold.

The implications of the discrepancy between the NAMMU stochastic continuum results and the MAFIC DFN results are important.

First, the flowpaths may be very different as compared to a discrete solution of flow through the fracture network. Indeed, a uniform flow solution may be obtained using NAMMU for a 50 m block that is non-conducting in a discrete sense. Secondly, the permeability of flow paths and their porosity, which is positively correlated to permeability, will not be the same for the two approaches. Both these implications are likely to affect any travel time calculation.

These simulations also show that the stochastic continuum block sizes cannot be chosen arbitrarily. It is important to pick a block size that is large enough to minimize non-neighbor pathways. Yet, blocks should not be so large that pathways rarely exist. It remains an open question as to how to determine appropriate block sizes for a stochastic continuum model.

5.2.2 A Note on the Numerical Codes Used for Regional Continuum Modeling

From a conceptual point of view, the linkage of conditioned DFN models to regional stochastic continuum models should be independent of the continuum model used. For example, for a given fixed grid spacing between the pressure nodes, the volumetric support and the geostatistical structure of the assigned flow properties should be the same. In this respect, PHOENICS and NAMMU may take on the same volumetric support scale and geostatistical structure which is not the case for HYDRASTAR (Fig. 5-13). HYDRASTAR requires a different support scale and geostatistical structure.

Of particular importance for the linkage of conditioned DFN models to regional stochastic continuum models is the question of hydraulic anisotropy. At present, only PHOENICS and NAMMU can represent hydraulic anisotropy (Fig. 5-13). Follin (1992) and Follin and Thunvik (1994) demonstrated that hydraulic anisotropy may be of great value for accurately scaling stochastic continuum flow properties. They showed that rock volumes modeled by an assemblage of smaller, *scalar* blocks behave as if they are

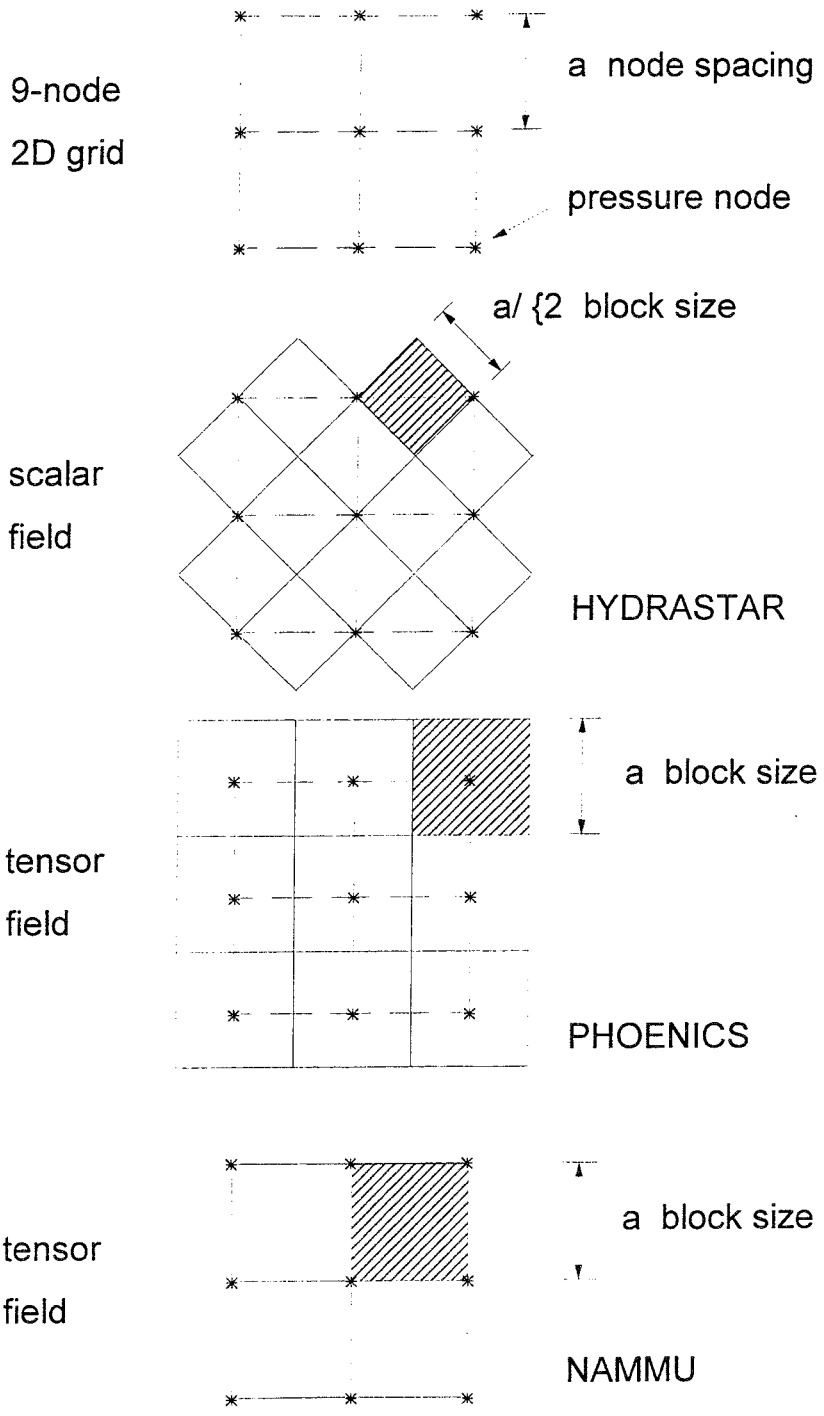

FIGURE 5-13

DIFFERENCES IN VOLUMETRIC SUPPORT FOR A GIVEN PRESSURE NODE SPACING

SKB/BLOCK K/SWEDEN

hydraulically anisotropic if the rock volumes are not of a sufficiently large size. In effect, the incomplete homogenization produces hydraulic anistropy.

The three principal components K_{xx}, K_{yy} and K_{zz}. computed by MAFIC for the 10 m blocks cannot be used by the current version of HYDRASTAR because HYDRASTAR assumes a scalar permeability field. PHOENICS can correctly represent zero-valued principal components provided that the mass balance equation for the individual cells is formulated for an appropriate mean, e. g. the harmonic mean. However, just as for NAMMU, PHOENICS cannot correctly represent all those cases where a fracture cuts through a 10 m block at two sides that are perpendicular to each other. Unfortunately, there is no simple way of computing the off-diagonal components of a stochastic continuum model block. This is probably one of the major problems of relating a discrete description of flow through fractured rocks to a continuous permeability field.

5.3 Methodology for Assigning Permeability Values to Stochastic Continuum Models

5.3.1 Overview of Alternative Strategies

There are two promising strategies for assigning permeability values to stochastic continuum models based upon the results described in this report. The first method exploits the lack of strong spatial correlation in order to efficiently generate input for the models. This method would be appropriate for the results of the small fracture size models.

The second method is proposed for sites in which spatial correlation is important. It would be appropriate for the large fracture size model.

5.3.2 Methodology for Assigning Properties for Weakly Spatially Correlated Models

This method is an efficient method to generate input for a stochastic continuum model for the weakly correlated data found in this study for the small fracture size assumption. It is also appropriate for the present situation in which the population statistics vary with block scale. The procedure is based upon a series of Monte Carlo simulations using the results described in Sec. 5.1 of this report.

The procedure is to generate the input for each group of block sizes. For example, the generation of the values for 30 m blocks would consist of two stages:

Stage 1: Make a random draw from the population represented by Figure B-3a for the fracture size selected. This would yield a value for the percentage of 30 m blocks that would be conductive in the X, Y and Z directions. Assume that the results were that 25 % of the blocks would be conductive in the X-direction, 20 % in the Y-direction, and 18% in the Z-direction.

Stage 2: Select at random 25% of the 30 m blocks and mark them as conductive in the X-direction. Repeat this process for the remaining two directions. Note that different blocks are selected for the different directions - they need not be the same blocks.

Stage 3: For the blocks in the X-direction selected as conductive, make a Monte Carlo realization of the population shown in Figure B-7a and B-12a. This is a value of 30 m block permeability in the X-direction. Repeat this for all of the remaining conductive blocks in all of the directions.

At this point, values will have been assigned to all of the 30 m blocks in the model. To complete the assignment of properties, assign values to blocks of other sizes using the population statistics appropriate for that block size. These values are shown in Figures B-1 through B-14.

This approach has several advantages:

1) Properties are assigned separately for each direction and for each block size accordingly to distributions derived from discrete fracture models that match well test results.

2) It is numerically straightforward and efficient, since spatial correlation is not significant.

5.3.3 Assignment of Block Values for Spatially Correlated Models

The present data analysis indicates that there is significant spatial correlation in block-scale permeability values for the large fracture size assumption. Moreover, the analyses of future sites might indicate that spatial correlation is important. In this case, the procedure outlined in Sec. 5.3.2 will not be adequate. A promising method for assigning spatially correlated data is a technique known as Projection Onto Convex Sets (POCS). This method is an algorithm to produce stochastic data sets conditioned to a useful variety of local and global constraints. Many geological features can be easily expressed as such constraints. These include having:

- specific values at known points,
- minimum and maximum bounds on values,
- discontinuities, such as faults,
- monotonically increasing values along a path, such as a river or a linear drift function,
- known mean,
- anisotropic spatial correlation, including fractal and geostatistical models, and
- known entropy, energy or variance.

The mathematical basis for POCS was first elaborated by Gubin and others (1967). The first applications were to problems in optics and in reconstructing medical imagery (Gerchberg and Saxton, 1972; Youla and Webb, 1982). Menke (1991) and more recently, Malinverno and Rossi (1993) have adapted POCS to reconstruct bathymetric profiles and petroleum reservoir models. La Pointe and others (1995) have used POCS to simulate transmissivity fields for input to finite element models.

Well-known stochastic inversion methods, such as Geostatistics, are based on minimizing estimation error or model length. POCS uses a different approach. It re-

casts various geological constraints as *convex sets*, and then applies a procedure known as a *contraction mapping* or a *non-expansive projection* to find a realization that lies in the intersection of all of the constraint sets. The contraction mapping is an iterative procedure.

A convex set {S} is defined as a set for which any two elements s_a and s_b belonging to the {S}, when linearly interpolated according to the equation:

$$(1-\alpha)s_a + \alpha s_b \quad 0 \le \alpha \le 1 \qquad \text{Equation 5-1}$$

also belong to the set. In a pictorial sense, this means that there are no holes or embayments .

If {S} is a convex set, then P_i is called a *non-expansive projection operator* onto the set {S} if

- P_i leaves unaltered any set member already within {S}, and
- P_i maps any member outside of {S} to the closest element of {S} such that

$$\left|P_i s - s\right| \le \left|s_o - s\right| \text{ for all } s_o \in \{S\} \qquad \text{Equation 5-2}$$

While it may not seem obvious how to convert geological observations into such mathematical constructs, it turns out to be relatively straightforward. For example, it makes no sense to have negative transmissivities in a flow model. This constitutes a lower bound or non-negativity constraint. A non-expansive projection onto the set {S} such that every point (member) is greater than 0.0 is to set members of the set less than 0.0 to 0.0.

The POCS algorithm makes use of these projections in an iterative scheme, to exploit the following theorem (Youla and Webb, 1982): Let S be the intersection of m convex sets $S_1, S_2,...,S_m$. Then the iteration

$$s^{i+1} = (P_1 P_2 \ldots P_m)s^i \qquad \text{Equation 5-3}$$

will converge to {S} from an arbitrary starting point in function space as i goes to ∞.

Several of the POCS constraints can be used to condition the input for the stochastic simulation models like those for Äspö. These include:

- ensuring that blocks within the influence of a well test have values within the range of values calculated in Sec. 5,
- producing a simulation that has the same mean as the blocks conditioned to the wells tests,
- producing a simulation in which the blocks have the properly scaled variance and energy from the variance and energy in the blocks conditioned to the well tests, and
- ensuring that the spatial correlation between the blocks is the same as that determined in Sec. 5.1.3.

Thus, POCS provides a method for taking the results that could arise from the type of analysis carried out in this present project, should the results indicate that spatial correlation among blocks is important to reproduce in the stochastic continuum model.

6. CONCLUSIONS & RECOMMENDATIONS

This study has resulted in a number conclusions and recommendations regarding the conductive fractures at Äspö, improved methods for characterizing fracture hydrology, and for linking DFN models with stochastic continuum flow and transport models. While the study is based upon Äspö site data, most of the conclusions and recommendations pertain to other fracture-dominated rock masses.

6.1 Conductive Fracture Geology and Geometry

1) Conductive fractures are not geologically different from non-conductive fractures. Rather, they appear to consist of the larger fractures from each set which have had a higher probability of connecting with other fractures to form a regional flow network.

2) Conductive fractures do not show any strong correlation to geological parameters that could be used to systematically condition their size, orientation, conductivity or intensity. The few correlations that do exist are weak, and pertain to geological parameters that are widely found at Äspö. For example, there is a slightly higher probability for fractures in fine-grained granite to be conductive. Also, open fractures tend to have a higher chance for being conductive, but open fractures represent less than 1% of all fractures, and there exists no way to map the probability that a fracture is open on a regional basis.

3) There are three fracture sets that are the same for both conductive and non-conductive fractures. Two of these sets are subvertical and strike north/south and west-northwest/east-southeast, respectively. The third set is subhorizontal. Each set roughly represents about a third of the fractures.

4) Fracture geometry and conductivity are stationary at least to the scale of the HRL access tunnel ($\approx$ 1.5 km).

6.2 Fluid Flow Properties Of Blocks At Different Scales For Äspö

1) It is possible to condition DFN simulations to match transient well tests, producing discrete fracture models that match observed fracture geometry and transient flow behavior in packer tests. The models created in this manner suggest that the fracture flow system at Äspö is sparsely connected, in which flow is through independent pathways rather than well integrated networks.

2) The number of non-conductive blocks is high. This implies that the ability to have non-neighbor connections in the stochastic continuum model is important. Also, the spatial pattern of these non-conductive blocks is not known, but may be random, since the conductive blocks seem to have little spatial correlation. Moreover, the percent of non-conductive blocks is a function of block size.

3) Block scale permeability decreases with block size once the scale of the block begins to exceed the scale of the well-connected fracture networks. This occurs because the fracture pathway connection across the block begins to resemble a serial connection as there become fewer and fewer pathways connecting opposite block faces. For smaller block scales, the block-scale permeability may increase, due to the increasing numbers of parallel fracture pathways. This means that different distributions should be used for assigning values for different blocksizes. This occurs for both fracture size models examined and for the range of blocks sizes (10 m to 50 m) examined.

4) Block scale permeability decreases with the assumed mean fracture size,

5) Permeability anisotropy may exist, such that the north-south direction permeability is the largest, followed by the vertical direction, with the east-west direction permeability the least.

6) Block scale permeability is approximately lognormally distributed, with means ranging from 10^{-14} to 10^{-16} m^2.

7) Blocks show a low degree of inter-block spatial correlation for the small fracture size assumption. However, for the larger fracture size model, 10-m blocks

exhibit spatial correlation up to distances of 50 m. This is most likely due to the fact that the size of individual fractures is large with respect to the 10-m blocks and the networks they form are sparse. This leads to the situation in which adjacent conductive blocks may be conductive because only one or two large fractures cross the blocks, making the block-scale permeability very similar for the blocks.

8) If the grid scale used in the stochastic continuum flow modeling is less than the scale of individual conductive fractures, as would be the case for 10 m blocks and the large fracture size model, then the grid cell values should be assigned in a spatially correlated manner, regardless of whether the underlying fracture pattern has spatial correlation. As discussed in Sec. 5.2, this is due to the fact that neighboring grid cells will have more or less the same fractures crossing them, and as a result, will have similar block-scale permeability values.

6.3 Evaluation Of DFN Models For Computing Block-Scale Input For Stochastic Continuum Models

1) A continuum code that does not have the off-diagonal or cross-flow permeability terms cannot represent one aspect of flow in sparsely fractured rock blocks. This situation occurs when fractures may connect adjacent faces of the block, but not opposing faces. In this situation, the permeability value for the flow direction parallel to a line joining the opposite faces (the diagonal term) will be 0.0, as will all other diagonal terms. However, flow will take place in the fractured medium. The consequence will be that the stochastic continuum code may significantly underpredict the larger scale flow in the rock mass. The probability of this happening depends upon the sparsity of fracturing in the system, and the relative scale of the fracturing and the rock block. The smaller the block relative to the fractures, the more likely this situation is to occur. For example,the NAMMU-MAFIC comparison showed that this effect occured for 10-m blocks with the large fracture size assumption. Alternatively, some codes (for example, NAMMU), require non-zero permeability values for the principal components. Even if a very small value is given for the principal components to approximate a zero value, flow will now take place from one face to the opposite face, with the result that the flow properties may be overpredicted. From the perspective of

mass transport, either option for treating the lack of connection between opposing faces leads to a different flow path geometry and transport rate than in the fractured rock mass. How significant these differences are for large scale flow models has not been evaluated, and will vary with model geometry and the underlying fracture network geometry.

2) The size of blocks chosen for contructing flow models should take into account the ratio of fracture size to block size. If the blocks are too small, then the effects described in the previous conclusion may become common and lead to significant over- or under-predictions of flow and mass transport. On the other hand, if the blocks become too large relative to the fracture network clusters, then many blocks will have an effective permeability component of 0.0 in one or more directions. The ways in which each code handles 0.0 components may lead to over- or under-predictions. Moreover, small blocks may need to have their properties assigned in a spatially correlated manner, while the larger blocks have properties assigned in a spatially uncorrelated manner in order to accurately predict flow.

3) Even for the simplest of fractured rock masses, the permeability of blocks depends upon the block size and the fracture size. Thus, it is not sufficient to assign properties to a stochastic continuum model composed of blocks of many sizes from a single distribution. Moreover, the permeability for blocks of the same size and fracture intensity are sensitive to the sizes of the fractures within the block. The numerical simulations reported in this study show that the difference in block-scale permeability due to fracture size alone can produce differences up to an order of magnitude.

4) General Advice for Stochastic Continuum Modeling at Äspö:

- determine the range of grid cell sizes needed to balance the opposing numerical trade-offs of resolution (favors small cells) versus model size/numerical effort (favors big cells). If some of these cell sizes are bigger than 50 m or smaller than 10 m, then block scale flow calculations will be needed for these cell sizes. Consider the problems and complications

introduced when the cells are too big, or are so small that the cell size relative to the fracture size is small and decide whether to modify the cell sizes.

- assuming that the large fracture size model is more likely to be correct than the small size model at Äspö, assign properties using a Monte Carlo procedure *if* the grid cell size is larger than 50 m. For cells of smaller size, assign properties based upon a spherical semivariogram with the appropriate range and sill parameters presented in Fig. 5-11 using a Turning Bands or other simulation technique. The assignment should be based upon the cumulative probability distributions shown in Appendix B for the block size closest to the grid cell size.

- re-assign a proportion of the permeablity components for the blocks to 0.0 using a Monte Carlo procedure to choose blocks. The proportion of 0.0 components is block size dependent, and is given by Figs. B1 through B-4. The way in which the particular code treats 0.0 components may be important and should be well-understood so that the resulting model does not over- or under-predict flow.

6.4 Recommendations For Improving Data Collection for Flow Modeling Using DFN and Stochastic Continuum Models

1) This study has demonstrated the importance of correctly estimating fracture size and intensity because of the dependence of block permeability scaling on fracture size and intensity. However, this study has also shown how difficult it is to obtain reliable values from conventional tunnel mapping or borehole logging. Tunnels are affected by blasting and excavation, while borehole imagery is often unable to precisely resolve fractures, their termination modes and their traces. A new borehole logging tool employing high-resolution imaging, resolves fracturing in borehole walls with far greater accuracy such that better estimates of size and intensity are possible. It is recommended that these logs be routinely obtained in boreholes used for hydrologic characterization.

2) Trace length measurements in tunnels where most hydraulically significant fractures are greater than the tunnel cross-section are of limited value for

estimating fracture size. In this situation, it is more important to estimate what proportion of the tunnel each fracture intersects. This may be done by recording nothing more complex than whether the fracture intersects one or both walls, the roof or the floor of the tunnel. Likewise, data on what percentage of a borehole a fracture intersects can be used to estimate fracture sizes from borehole data.

3) The actual coordinates of each conductive fracture should be recorded rather as well as the tunnel section in which the fracture occurs. If this is not possible due to time constraints during tunnel excavation, then photographs of the tunnels should be obtained and processed to calculate fracture locations. Without this information, it is not possible to calculate a spatial location model for fractures in a DFN model.

4) Fracture storativity influences the transient behavior of pressures during interference tests and single-hole tests. In order to estimate the storativity of fractures for blocks on the scale of a few tens of meters, it is necessary to conduct interference tests between wells at a similar distance. Future well testing programs should consider siting wells at much closer spacings than are currently done.

6.5 Recommendations For Future DFN Modeling Studies

1) Well tests are currently used to estimate transmissivity and storativity values for fractures. Preliminary modeling studies (Doe and Wallmann, 1995) suggest that well tests might also be used to better interpret the conductive fracture network geometry and hydraulic properties. A systematic modeling study to examine the influence of fracture network geometry and properties on simulated well test responses may lead to new ways to incorporate well test information into DFN models.
2) There may be other ways to link DFN models to performance assessment models than by deriving better block-scale properties for continuum flow calculations. One possible way is to apply algorithms from graph theory to identify pathways

through the fracture networks, and then to calculate effective flow and transport properties for these identified paths.

7. REFERENCES

Al-Kaabl, A. and W.J. Lee. (1993). Using artificial neural nets to identify the well-test interpretation model. *SPE Formation Evaluation.* 8:233-240.

Axelsson, C-L. and others. (1990). "Äspö Hard Rock Laboratory Discrete Fracture Modelling," *SKB HRL Progress Report 25-89-21*, SKB, Stockholm.

Barker, J. A. (1988). A generalized radial flow model for hydraulic tests in fractured rock, *Water Resour. Res.*, 24(10), 1796-1804.

Barton, C. C. (1995). *Fractal Analysis of Scaling and Spatial Clustering of Fractures in Fractals in Earth Sciences.* Barton, C. C. and La Pointe, P. R., eds. Plenum Press, New York. 141-178.

Christiansson, R., and L.Stenberg. (1991). Manual for field work in the tunnel. *SKB Progress Report 25-91-10.*

de Groot, P.F.M. (1993). Reservoir characterization form 3-D seismic data using artificial neural networks and stochastic modeling techniques. AAPG Bull. 77:1617-1618.

Dershowitz, W. S. and others, (1992). The implication of fractal dimension in hydrogeology and rock mechanics, Version 1.1. *SKB Technical Report 92-17*, February, 1992.

Dershowitz, W. and others. (1994) FRACMAN interactive discrete feature data analysis, geometric modeling and exploration simulation. User documentation, version 2.4. Golder Associated Inc., Seattle, WA.

Doe, T. W. and P. C. Wallmann. (1995). Proceedings, International Society for Rock Mechanics Symposium, Tokyo, Japan. September, 1995 *submitted manuscript.*

Eberhart, R.C. and R.W. Dobbins. (1990). Neural network PC tools. Academic Press, London, 414p.

Ericsson, L.O. (1987). Fracture mapping on outcrops. *SKB Progress Report 25-87-05.*

Ericsson, L.O. (1988). Fracture Mapping Study on Äspö Island, Findings of directional data. *SKB Progress Report 25-88-10.*

Feder, J. (1988). Fractals. Plenum Press, New York. 283.

Follin, S. (1992a) Numerical calculations on heterogeneity of groundwater flow, *SKB Technical Report 92-14.*

Follin, S. (1992b). On the interpretation of double-packer tests in heterogeneous porous media: Numerical simulations using the stochastic continuum analogue, *SKB Technical Report 92-36.*

Follin, S. and R. Thunvik (1994). On the use of continuum approximations for regional modeling of groundwater flow through crystalline rocks. *Submitted to Advances in Water Resources.*

Forsmark, T. and I. Rhén (1994). Information for numerical modelling 1994: General information and calibration cases for the Äspö HRL, tunnel section 700-2545 metres, *SKB Progress Report 25-94-16,* June, 1994.

Geier, J. (1993). Verification of the geostatistical inference code INFERENS, Version 1.1, and documentation using data from Finnsjön. *SKB Technical Report 93-09.*

Geier, J.E., and others. (1992). Discrete fracture modeling of the Finnsjön rock mass: Phase 2, *SKB Technical Report 92-07.*

Geier, J.E., and T.W. Doe. (1992). Discrete fracture modeling of the Finnsjön rock mass, Supplementary interpretations of actual and simulated well test data. *SKB Arbetsrapport 92-45.*

Gerchberg, R.W. and W.O. Saxton. (1972). *Optik,* 35, 237-246.

Gubin, L.G., B.T. Polyak and E.V. Raik. (1967). The method of projections for finding a common point of convex sets: *USSR Comp. Math. and Math. Physics* (Eng. Trans.), 7(6), 1-24.

Hartley, L. J., C.P. Jackson & S.P. Watson. (1994). NAMMU User Guide, Release 6.2, AEA -ESO-0138.

Journel, A. G. and CH. J. Huijbregts (1978). Mining Geostatistics. Academic Press Inc., New York. 600p.

Kulander, B.R., S.L. Dean, and B.J. Ward, Jr. (1990). Fractured core analysis: interpretation, logging, and use of natural in induced fractures in core. The American Association of Petroleum Geologists, Tulsa, Oklahoma, U.S.A.

La Pointe, P.R. (1994). Evaluation of stationary and non-stationary geostatistical models for inferring hydraulic conductivity values at Äspö. *SKB Technical Report 94-22.*

La Pointe, P. R. and J. A. Hudson (1985). Characterization and interpretation of rock mass joint patterns. *Special Paper 199, Geological Society of America.* 37p.

La Pointe, P. R., W. S. Dershowitz and P. C. Wallmann. (1993a). Flow and connectivity properties of fracture networks as a function of the fractal dimension [abstr.]. *Geological Society of America Annual Meeting,* Oct. 25-28, Boston.

La Pointe, P.R., P.C. Wallmann, and W.S. Dershowitz. (1993b). Stochastic estimation of fracture size through simulated sampling. *Int. J. Rock Mech. Min Sci & Geomech. Abstr.,* Vol. 30, No. 7 pp. 1611-1617.

La Pointe, P.R., A.L. Thomas, and G. Lee. (1995). Projection onto convex sets (POCS): A new method for constrained stochastic simulation of rock properties for geotechnical design and fluid flow modeling, in 35th U.S. Symposium on Rock Mechanics.

Le Loc'h, G. (1989). An efficient strategy for combining permeabilities: practical application on a simulated reservoir. *in* Geostatistics, Kluwer Academic Publishers, Dordrecht. 557-568.

Liedholm, M. (1991). Conceptual modeling of Äspö, Technical notes 18-32, General geological, hydrogeological and hydrochemical information. *SKB Progress Report 25-90-16b.*

Lindbom, B. and A. Boghammar (1992). Numerical groundwater flow calculations at the Finnsjön study site - extended regional area, *SKB Technical Report 92-03,* March, 1992.

Malinverno, A.D. and J. Rossi. (1993). Applications of projection onto convex sets to stochastic inversion: SPE Middle East Oil Tech. Conf., Bahrain, 3-6 April 1993, SPE 25659, 55-522.

Mazurek, M., P. Bossart and T. Eliasson (1995). Classification and characterization of water-conducting features at Äspö: results of phase 1 investigations. *SKB Progress Report 25-95-03.*

Menke, W. (1991). Application of the POCS inversion method to interpolating topography and other geophysical fields: *Geophys. Res. Lett.* 18, 435-438.

Neuman, S.P. (1987). Stochastic continuum representation of fractured rock permeability as an alternative to the REV and fracture network concepts, In: Farmer, I.W. *et al (eds.) Proc. 28th U.S. Symp. Rock. Mech.,* 533-561, Balkema, Rotterdam.

Neuman, S.P. (1988) A proposed conceptual framework and methodology for investigating flow and transport in Swedish crystalline rocks, *SKB AR 88-37,* Stockholm.

Nilsson, L. (1987) Hydraulic test, pumping tests at Ävrö and Äspö, *SKB Progress Report 25-87-11.*

Nilsson, L. (1989). Hydraulic tests at Äspö and Laxemar, Evaluation, *SKB Progress Report 25-88-14,* Stockholm.

Nilsson, L. (1990). Hydraulic tests at Äspö KAS05-KAS08, HAS13-HAS17, Evaluation. *SKB Progress Report 25-89-20.*

Norman, S. (1992a). Statistical inference and comparison of stochastic models for the hydraulic conductivity at the Finnsjön-site. *SKB Technical Report 92-08.* 113 p.

Norman, S. (1992b). Hydrastar - a code for stochastic simulation of groundwater flow, *SKB Technical Report 92-12,* May 1992.

Osnes, J.D., A. Winberg, and J. Andersson. (1988). "Analysis of Well Test Data -- Application of Probabilistic Models to Infer Hydraulic Properties of Fractures," *Topical Report RSI-0338,* RE/SPEC Inc., Rapid City, South Dakota.

Penn, B.S., A.J. Gordon, and R.F. Wendlandt. (1993). Using neural networks to locate edges and linear features in satellite images. *Computers & Geosciences.* 19:1545-1565.

Rhén, I., and others. (1994). Geohydrological evaluation of the data from section 2265-2874 m. *SKB Progress Report 25-94-20.*

Rizzo, D.M. and D.E. Doughery. (1994). Characterization of aquifer properties using artificial neural networks; neural kriging. *Water Resources Res.* 30:483-497.

Rogers, L.L., and F.U. Dowla. (1994). Optimization of groundwater remediation using artificial neural networks with parallel solute transport modeling. *Water Resources Res.* 30:457-481.

Rogers, S.J. and others. (1992). Determination of lithology from well logs using a neural network. *AAPG Bull.* 76:731-739.

Rubin, Y. & J.J. Gómez-Hermández. (1990). A stochastic approach to the problem of upscaling of conductivity in disordered media: Theory and unconditional numerical simulations, *Water Resour. Res.,* 26(4), 691-701.

Spalding, D.B., (1981). A general purpose computer program for multidimensional one- and two-phase flow, *Math. Comput. Sim.* 8, 267-276, 1981.

Stanfors, R., and others. (1994). Geological-structural and rock mechanical evaluation of data from tunnel section 2265-2874 m. *SKB Progress Report 25-94-19.*

Thomas, A.L., and P.R. La Pointe. (1995). Conductive fracture identification using neural networks, in 35th U.S. Symposium on Rock Mechanics.

Tung, A.T. Y., F.S. Wong, and W. Dong. (1994). Prediction of the spatial distribution of the modified Mercalli intensity using neural networks. *Earthquake Eng. & Structural Dynamics.* 23:49-62.

Uchida, M. and J. Geier, 1992, Fracture Mapping on Surface. Personal Communication.

Uchida, M., T. Doe, W. Dershowitz, A. Thomas, P. Wallmann and A. Sawada (1994). Discrete-fracture modelling of the Äspö LPT-2, large-scale pumping and tracer test. *SKB International Cooperation Report ICR 94-09.*

Wikbert, P., and others. (1991). Äspö Hard Rock Laboratory. Evaluation and conceptual modeling based on the pre-investigations 1986-1990. *SKB Technical Report 91-22.*

Youla, D. C. and H. Webb (1982). Image restoration by the method of convex projections: Part 1 - Theory: *IEEE Trans. Med. Imag. MI-1,* 81-94.

APPENDIX A

NEURAL NET ANALYSIS

Neural networks are a sophisticated form of non-linear pattern recognition that have found geologic application in groundwater characterization and remediation (Rizzo & Doughery 1994, Rogers & Dowla 1994), well-log and well-test interpretation (Rogers et al. 1992, Al-Kaabl & Lee 1993), seismic and satellite image processing (de Groot 1993, Penn et al. 1993), and earthquake intensity prediction (Tung et al. 1994).

There are many types of neural networks, but all share a common architecture consisting of *neurons* and *synapses* (Figure A-1). A neuron is simply a node in the network which uses a non-linear transfer function to convert an input signal (value) to an output signal. Neurons are connected by synapses. A synapse takes the output signal from one neuron, multiplies it by a *synaptic weight*, and passes the modified signal to an adjacent neuron as input. Depending on the number of incoming and outgoing synapses connected to it, a neuron can be classified into one of three categories:

1) *Input neurons* have zero incoming synapses and one or more outgoing synapses. They are used to represent input variables, and take the variable value as their output.

2) *Output neurons* have one or more incoming synapses and zero outgoing synapses. They are used to represent output variables, and produce an output signal which equals the predicted variable value.

3) *Hidden neurons* have one or more incoming synapses and one or more outgoing synapses. They sit between the input and output neurons and pass signals through the network.

A distinct advantage of neural networks over other classification methods is their ability to learn the relative importance and complex interrelations among input and output variables.

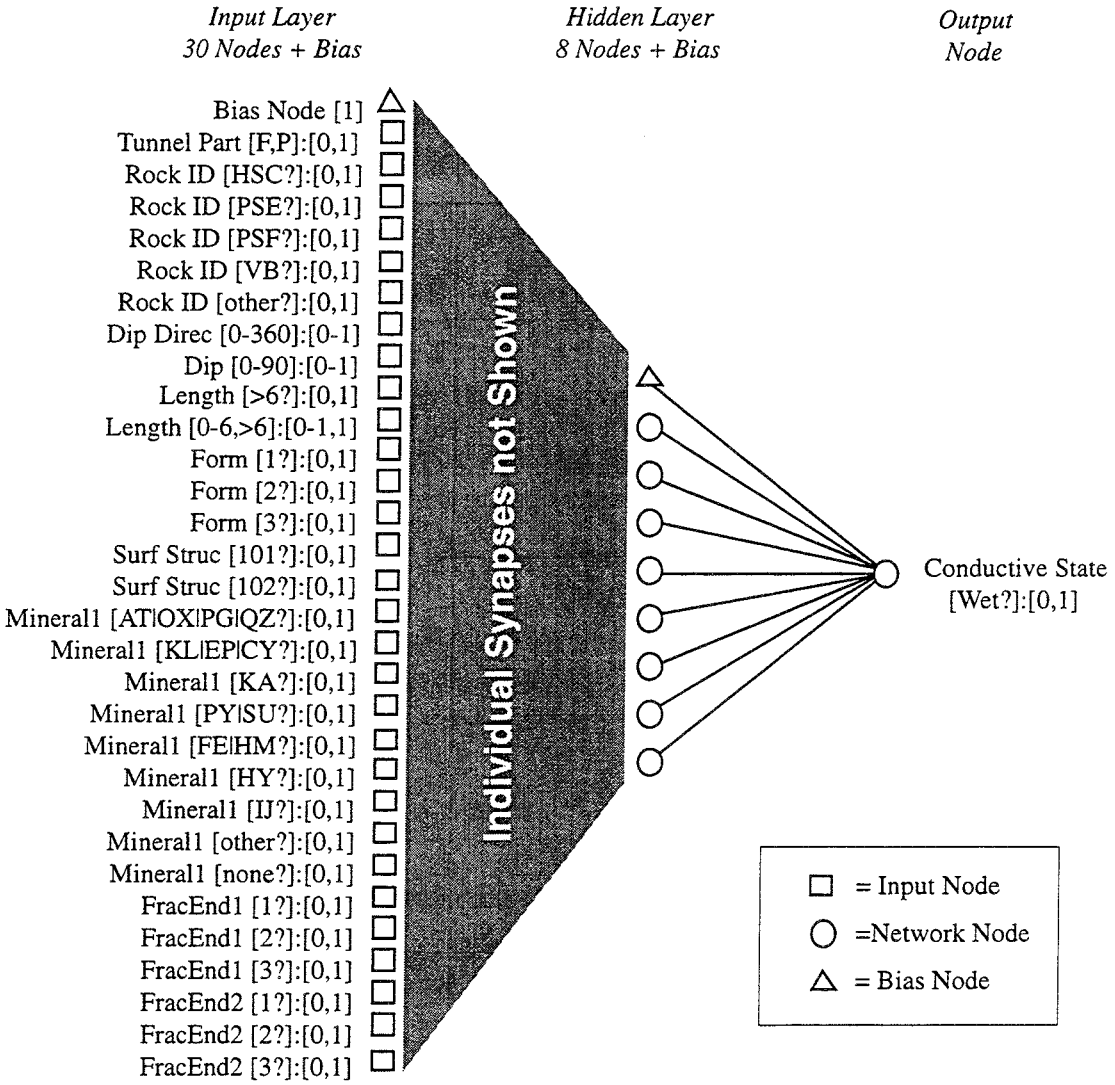

FIGURE **A-1**
TOPOLOGY OF THE ÄSPÖ NEURAL NETWORK
SKB/ASPO-DFN/SWEDEN

PROJECT NO. IC3 1194 DRAWING NO. 55588 DATE 6/1/95 DRAWN BY DAR

Golder Associates

By changing the neuron transfer functions, the synaptic weights, or the network connectivity, a neural network can be conditioned to provide the expected response for a given input pattern. Once trained, a neural network can then be used to make predictions for input patterns whose correct classification is unknown.

This study of Äspö fracture data is an exercise in discriminant analysis: given the measured geological parameters, is a particular fracture likely to be significant conductor or not? Backpropagation neural networks are well-suited for this purpose. In a backpropagation neural network, the input, hidden, and output nodes are arranged in layers. A single *input layer*, consisting only of input neurons, is connected to an *output layer*, consisting only of output neurons, through one or more *hidden layers*, consisting only of hidden neurons (Figure A-1). Each neuron in a given layer is connected to all neurons in the preceding and following layers by synapses, which are characterized by their *synaptic weight*.

In a backpropagation network, the network connectivity and the neuron transfer function are held constant, and network behavior is modified by adjusting synaptic weights. Initial synaptic weights are assigned from a random distribution. The neural network is then presented with a series of training patterns, and an error signal is computed from the difference between the network's output signal and the desired output signal. In an iterative procedure known as back propagation of errors, the synaptic weights connecting each layer are modified so as to reduce the output error. In this way, the network is trained to successfully classify the training data. Any backpropagation network with one or more hidden layers using a non-linear neuron transfer function is capable of learning complex non-linear mappings. For a more complete description of training by back propagation of errors, see Eberhart and Dobbins (1990).

The dataset used to construct, train and test the backpropagation neural network for Äspö consists of 8329 fractures mapped in the primary access tunnel. Several neural network configurations were tried, but the best performance was obtained from a network consisting of an input layer of 30 input neurons, a single hidden layer of 8 neurons, and a single output neuron representing the conductive state of the fracture (Figure A-1). Each input neuron corresponds to a mapped fracture parameter. The

normalization techniques used for various fracture parameters are summarized in Table A-1. In this table, each network node is described as follows:

```
Variable Name  |  Actual Range  |  Normalized Range ,
```

where `Variable Name` is the fracture property name (e.g. Length, Dip, etc.), `Actual Range` is the continuous or discrete actual range of the variable, and `Normalized Range` is the range after normalization. For example, the input node

```
Rock ID  |  HSC?  |  0,1
```

is a Boolean node whose value, 1 or 0, indicates whether the mapped fracture is or is not found in rock type HSC, respectively. The input node

```
Length  |  0-6,>6  |  0-1,1
```

on the other hand, takes on continuous normalized values between 0 and 1 for fracture lengths between 0 and 6 meters and a value of 1 for fracture traces longer than 6 meters.

A single output neuron is used to represent the conductive state of the fractures. For training set fractures, this node is assigned Boolean value of either 1 or 0 to indicate whether the mapped fracture is or is not conductive, respectively. However, because all neural network nodes produce continuous output in the range [0-1], some convention must be chosen to convert the continuous output to Boolean form. For purposes of prediction, input patterns producing output neuron values greater than 0.5 are considered to be wet fractures, while input patterns producing output values less than 0.5 are considered to be dry fractures.

Of the 8329 mapped fractures used for neural network training and testing, 705 (8.5%) were wet while 7624 (91.5%) were dry. From this population, 400 wet fractures were selected at random to form a base training set. Two training sets, T1 and T2, were then created from this base set by adding 400 and 600 randomly selected dry fractures, respectively (Table 3-8). The remaining wet and dry fractures were placed into testing sets which were used to evaluate the predictive accuracy of the trained neural network.

In each training iteration or *epoch*, every input pattern in the training set was presented to the network. The cumulative output error for all training patterns was then back-propagated to adjust synaptic weights and reduce output error.

Table A- 1
Normalization Ranges And Relation Factor One For The Äspö Neural Network

Input Node	Description	Actual Range	Normalized Range	Relation Factor 1	
				Training Set T1	Training Set T2
1	Tunnel Part	[F,P]	[0,1]	0.00020	0.00000
2	Rock ID	[HSC?]	[0,1]	0.32453	0.00159
3	Rock ID	[PSE?]	[0,1]	0.00135	0.00000
4	Rock ID	[PSF?]	[0,1]	0.00000	0.00000
5	Rock ID	[VB?]	[0,1]	0.00000	0.00000
6	Rock ID	[other?]	[0,1]	0.00003	0.00000
7	Dip Direc	[0-360]	[0-1]	0.00034	0.00001
8	Dip	[0-90]	[0-1]	0.89703	0.00934
9	Length	[>6?]	[0,1]	0.00003	0.00020
10	Length	[0-6,>6]	[0-1,1]	0.19124	0.06451
11	Form	[1?]	[0,1]	0.07649	0.00000
12	Form	[2?]	[0,1]	0.00467	0.00000
13	Form	[3?]	[0,1]	0.00000	0.00000
14	Surf Struc	[101?]	[0,1]	0.00027	0.00003
15	Surf Struc	[102?]	[0,1]	0.00000	0.00000
16	Mineral1	[AT|OX|PG|QZ?]	[0,1]	0.00000	0.00000
17	Mineral1	[KL|EP|CY?]	[0,1]	0.01940	0.00002
18	Mineral1	[KA?]	[0,1]	0.00002	0.00000
19	Mineral1	[PY|SU?]	[0,1]	0.00001	0.00000
20	Mineral1	[FE|HM?]	[0,1]	0.00007	0.00001
21	Mineral1	[HY?]	[0,1]	0.00005	0.00000
22	Mineral1	[IJ?]	[0,1]	0.00192	0.00000
23	Mineral1	[other?]	[0,1]	0.00002	0.00000
24	Mineral1	[none?]	[0,1]	0.00044	0.00000
25	FracEnd1	[1?]	[0,1]	0.00001	0.00002
26	FracEnd1	[2?]	[0,1]	0.00000	0.00000
27	FracEnd1	[3?]	[0,1]	0.00011	0.00000
28	FracEnd2	[1?]	[0,1]	0.00025	0.00000
29	FracEnd2	[2?]	[0,1]	0.00001	0.00000
30	FracEnd2	[3?]	[0,1]	0.00000	0.00000

For this application, the predictive power of the trained neural network can be evaluated by comparing its predictions against those of random biased guessing.

Random biased guessing is the process of predicting conductive state based solely on the known relative frequency of wet and dry fractures. The Äspö training dataset T2 contained 40.0% wet fractures and 60.0% dry fractures. In the absence of additional data, a random biased coin designed to come up wet 40.0% of the time and dry 60.0% of the time would correctly predict the conductive state of 52.0% of the fractures (Table A-2). However, because this method selects fractures at random, only 40.0% of those fractures predicted as wet would actually be wet, while 60.0% of those fracture predicted as dry would actually be dry. Likewise, 40% of wet fractures would be correctly predicted as wet, while 60% of dry fractures would correctly be predicted as dry.

The relative abundance of wet and dry fractures in the T2 testing set is markedly different: only 4.2% of the fractures are wet while 95.8% are dry. A random biased coin calibrated using the T2 training set would correctly predict the conductive state of 59.2% of the fractures. The apparent increase in performance occurs because the coin is biased toward dry fractures, and the proportion of dry fractures in the testing set is much higher than in the training set. Other performance measures are also affected by the change in relative fracture abundance. For example, the percentage of fractures predicted as wet that are actually wet drops from 40.0% to 4.2%, while the percentage of fractures predicted as dry that are actually dry increases from 60.0% to 95.8%.

The behavior of the Äspö neural network under training sets T1 and T2 is markedly different. Table 3-8 summarizes the results obtained from the neural network under training sets T1 and T2 after 3000 and 2500 training epochs, respectively. Under training set T1, with equal numbers of wet and dry fractures, the network is quick to assume that a fracture is wet and only reclassifies it as dry if a number of criteria are satisfied (Figure A-2). However, under training set T2, with 50% more dry than wet fractures, the network does just the opposite. Fractures are initially assumed dry and are only classified as wet if several criteria are satisfied (Figure A-3).

For the *training set data*, the two cases result in nearly identical overall network performance, measured as the percentage of fractures correctly predicted as wet or dry (Table A-2). However, for the *testing set data*, training set T2 results in far better overall

Training Set

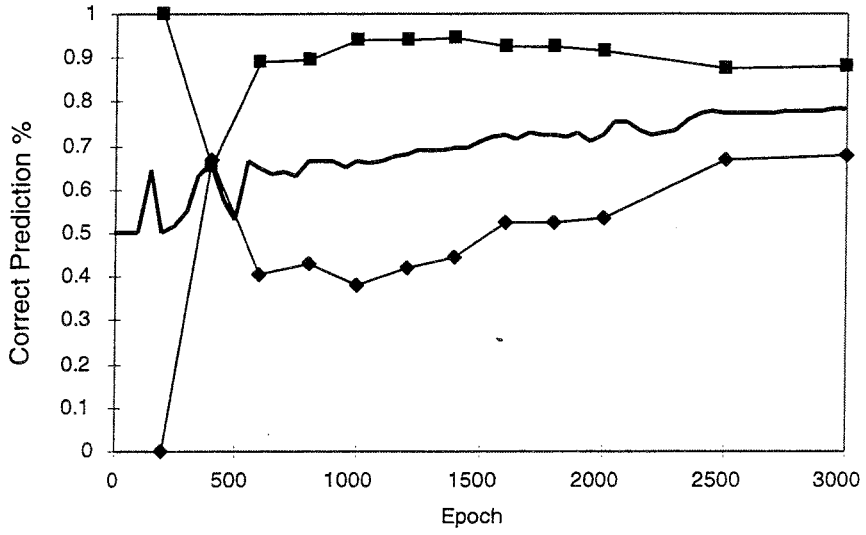

Testing Set

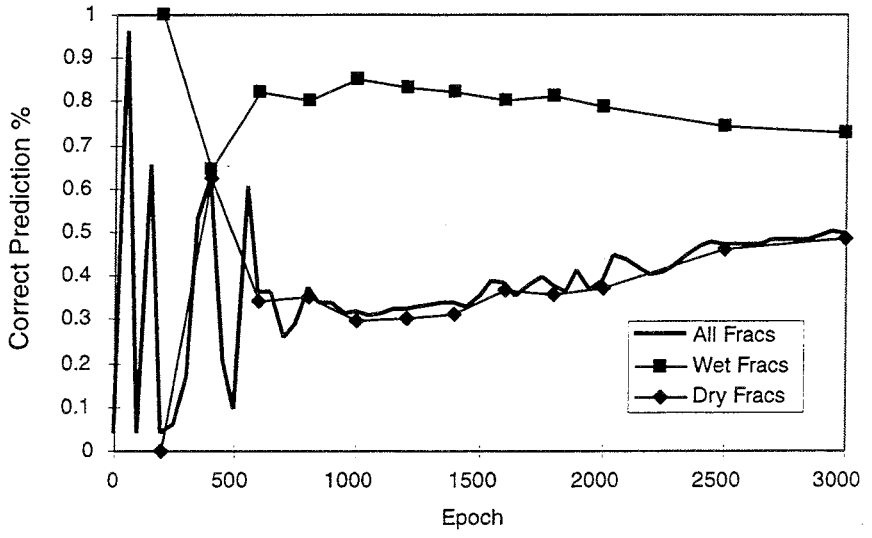

FIGURE **A-2**
CORRECT PREDICTION PERCENTAGES – TRAINING SET T1
SKB/ÄSPÖ-DFN/SWEDEN

Training Set

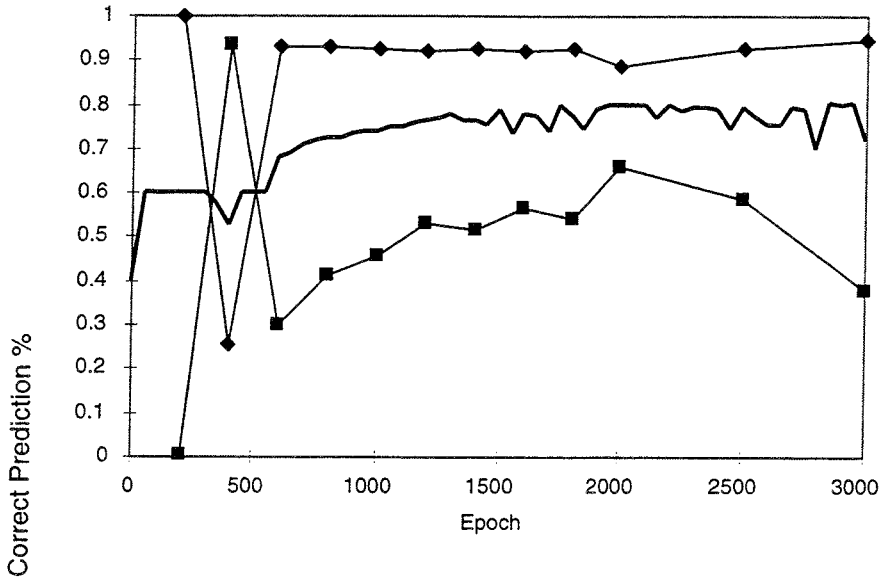

Testing Set

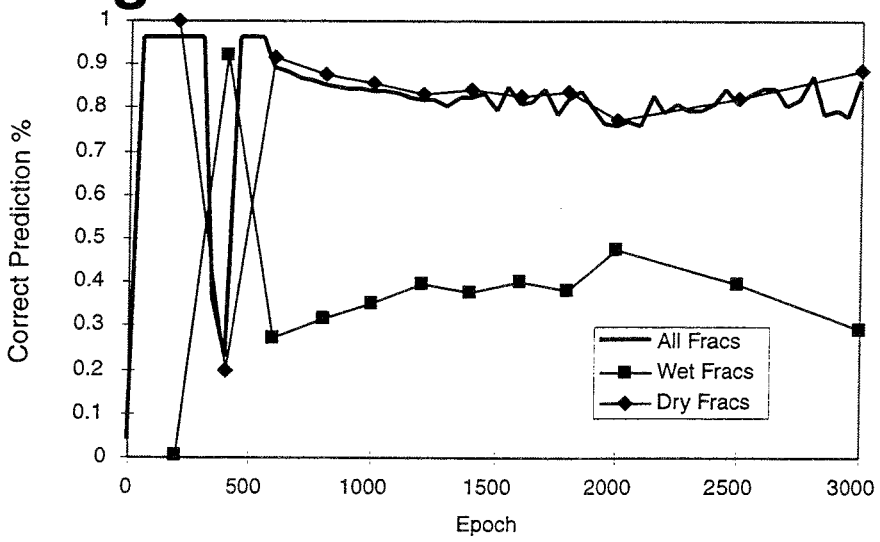

FIGURE **A-3**
CORRECT PREDICTION PERCENTAGES–TRAINING SET T2
SKB/ÄSPÖ-DFN/SWEDEN

network performance. This is because the testing sets are dominantly composed of dry fractures and training set T2 biases the network toward predicting fractures as dry. Despite this bias, the network is still much better than random biased guessing at picking wet fractures from the testing set. By way of illustration, 8.9% of fractures predicted as wet by the neural network are actually wet as compared with 4.2% for random biased guessing; an improvement of 119.9%. Because the T2 training set produces significantly better wetness predictions, the T2-trained network will be used as the reference case in the network analysis and discussion that follows.

Table A- 2
Neural Network Performance Under Training Sets T1
And T2 Compared With Random Biased Guessing

Testing Set	T1		T2	
Training Epochs	3000		2500	
Data Set	Training	Testing	Training	Testing
Number of Fractures	800	7529	1000	7329
Actually Wet	50.0%	4.1%	40.0%	4.2%
Actually Dry	50.0%	95.9%	60.0%	95.8%
Correctly Predicted as Wet/Dry				
Neural Network	78.0%	49.6%	79.2%	80.6%
Random Biased Guessing	50.0%	50.0%	52.0%	59.2%
Percent Improvement	*56.0%*	*-0.8%*	*52.3%*	*36.1%*
Actually Wet, Predicted Wet				
Neural Network	88.0%	72.8%	58.8%	39.5%
Random Biased Guessing	50.0%	50.0%	40.0%	40.0%
Percent Improvement	*76.0%*	*45.6%*	*47.0%*	*-1.3%*
Actually Dry, Predicted Dry				
Neural Network	68.0%	48.6%	92.8%	82.3%
Random Biased Guessing	50.0%	50.0%	60.0%	60.0%
Percent Improvement	*36.0%*	*-2.8%*	*54.7%*	*37.2%*
Predicted Wet, Actually Wet				
Neural Network	73.4%	5.7%	84.5%	8.9%
Random Biased Guessing	50.0%	4.1%	40.0%	4.2%
Percent Improvement	*46.8%*	*39.0%*	*111.3%*	*111.9%*
Predicted Dry, Actually Dry				
Neural Network	85.0%	97.7%	77.1%	96.9%
Random Biased Guessing	50.0%	95.9%	60.0%	95.8%
Percent Improvement	*70.0%*	*1.9%*	*28.5%*	*1.1%*

By examining the synaptic weights of the trained Äspö network, we can gain insight into its classification strategy and the geological parameters most important for classification. A common method for viewing the synaptic weights in a network is the Hinton diagram (Figures A-4, A-5). In this diagram, input parameters with greater

influence over the classification are represented by rows of larger positive or negative weights. For the trained Äspö neural network, larger negative weights have a positive correlation to wetness.

A more quantitative estimate of input parameter influence is provided by relation factors. Of these, the simplest is *relation factor one*, which is computed by subtracting the output of the network with all input neurons set to zero from the output with a single neuron set to one. For the Äspö network, an input parameter with a positive relation factor promotes fracture wetness. The largest relation factor one for the T2-trained network is 0.06, indicating that no single fracture property is diagnostic of fracture wetness. Instead, a fracture is classified as conductive only if possesses a series of properties in combination.

From the network weights shown in Figures A-4 and A-5 and the relation factors shown in Table A-2, it can be seen that the most important factors for classifying a fracture as wet are length, dip, and rock type. Of secondary importance are mineral infillings, surface structure, form, and termination relations (FracEnd). However, the correlations are not strong, and the analysis also points out some other factors in the relation between geology and fracture conductivity:

- *Parameter Interaction:* For the T2 trained network, no single fracture property can cause a fracture to be classified as wet. Fractures are initially assumed dry and are only classified as wet when several conditions are met at once.

- *Non-Uniqueness of Predictions:* While the network was able to establish the fracture properties most strongly correlated with fracture wetness, the correlations are by no means unique. A significant proportion of fracture predicted as dry were actually wet and vice versa. This indicates that the mapped fracture data by itself is insufficient to uniquely predict fracture conductive state.

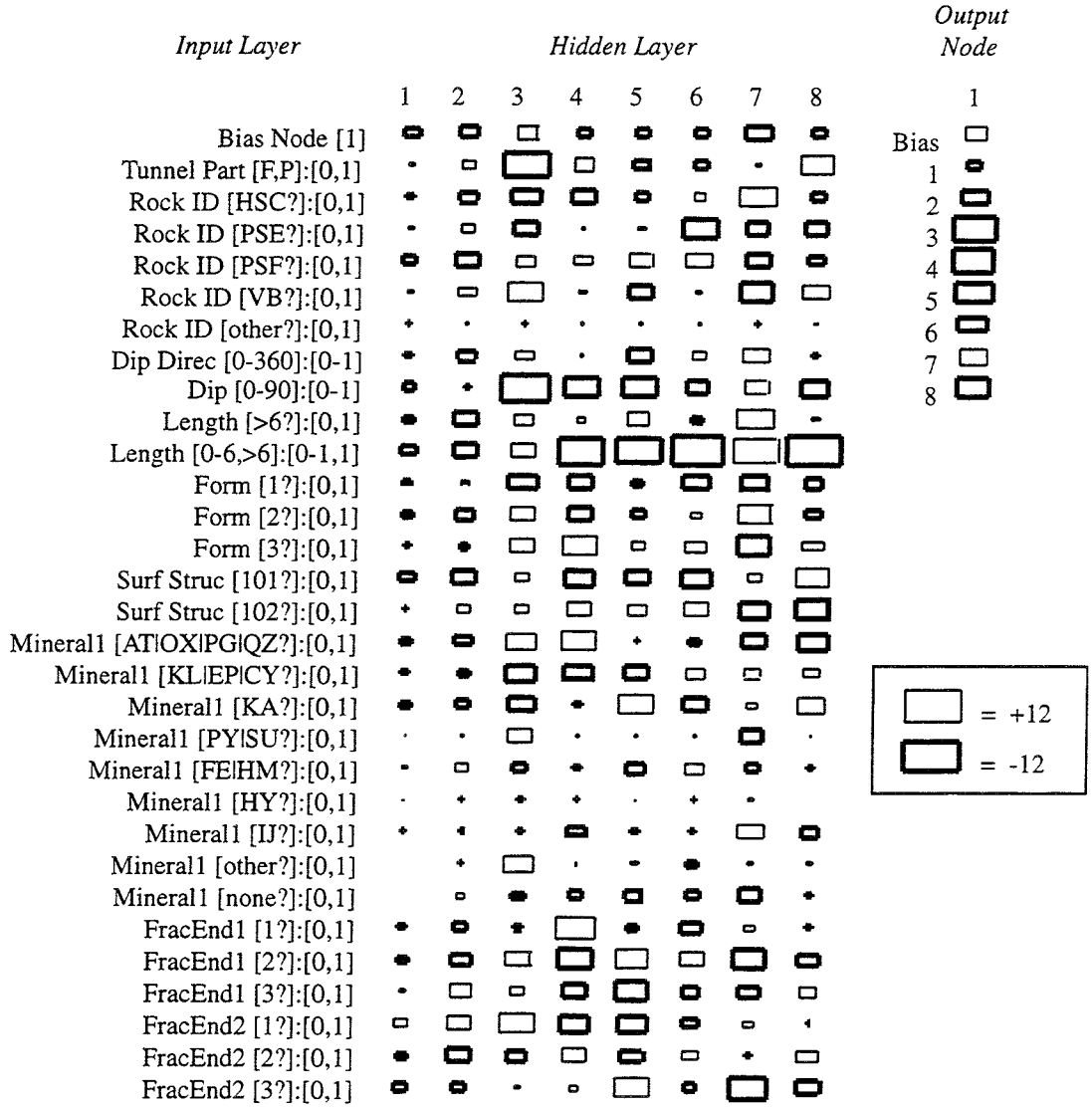

FIGURE **A-4**

SYNAPTIC WEIGHTS – TRAINING SET T1
2000 TRAINING EPOCHS
SKB/ÄSPÖ-DFN/SWEDEN

PROJECT NO. IC3-1194 DRAWING NO. 55586 DATE 6/1/95 DRAWN BY DAR

Golder Associates

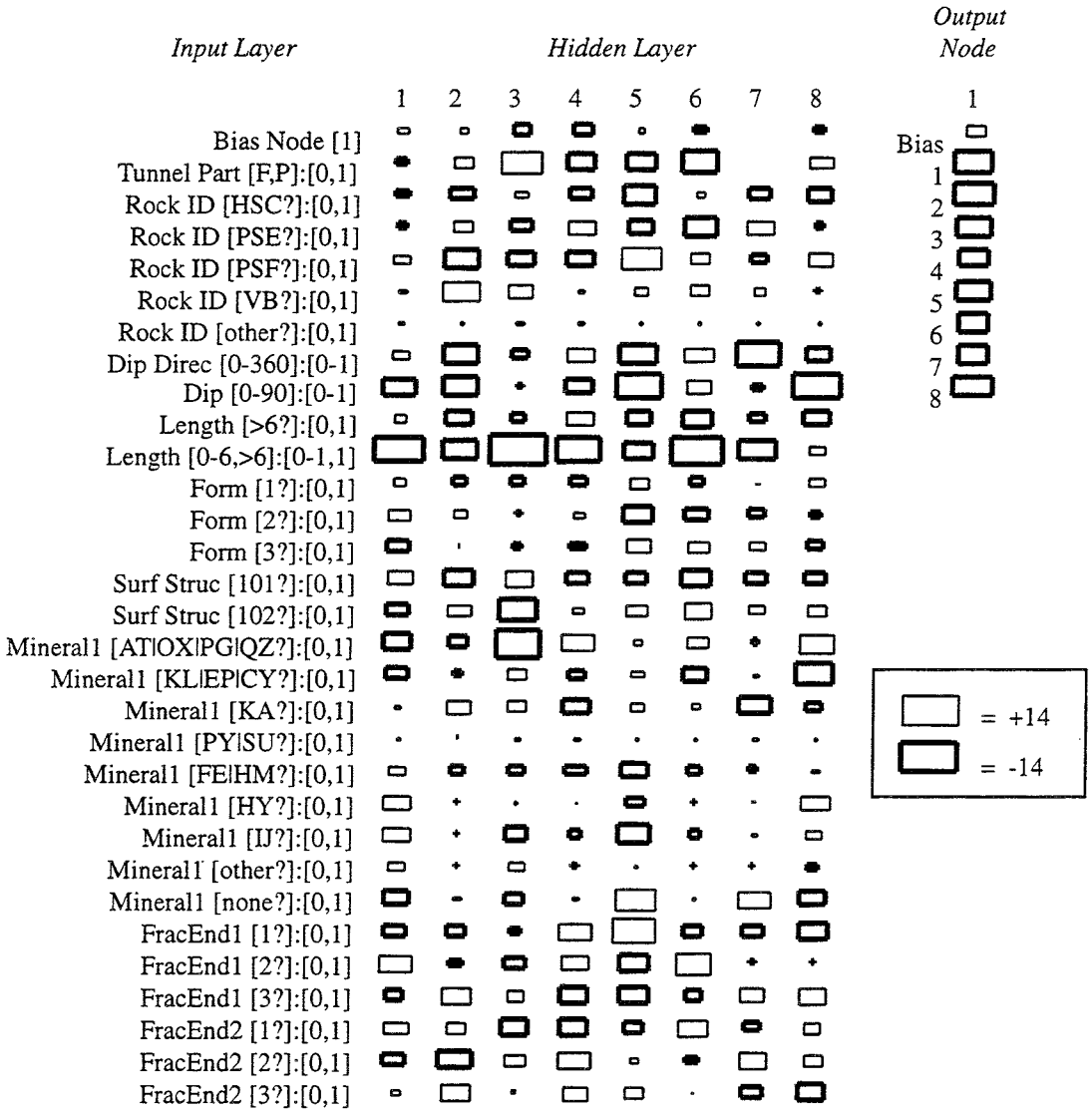

FIGURE **A-5**

SYNAPTIC WEIGHTS – TRAINING SET T2
2000 TRAINING EPOCHS
SKB/ÄSPÖ-DFN/SWEDEN

- *Impact on Äspö DFN models:* The neural network correctly identified rock type HSC as having a positive correlation to fracture network. Two-way frequency table analysis indicated that rock type HSC (aplite or fine-grained granite) contained a greater proportion of conductive fractures than the other Äspö rock types. However, the conditioning of conductive fracture intensity to rock type HSC would probably be of little utility to DFN models of the Äspö site for the following reasons: (1) the correlation itself is modest, (2) the aplite comprises a small portion of the Äspö rock mass, and (3) surface and subsurface data places only limited constraints on the distribution of HSC across the Äspö site.

APPENDIX B

FREQUENCY AND CUMULATIVE PROBABILITY HISTOGRAMS FOR BLOCK-SCALE FLOW CALCULATIONS

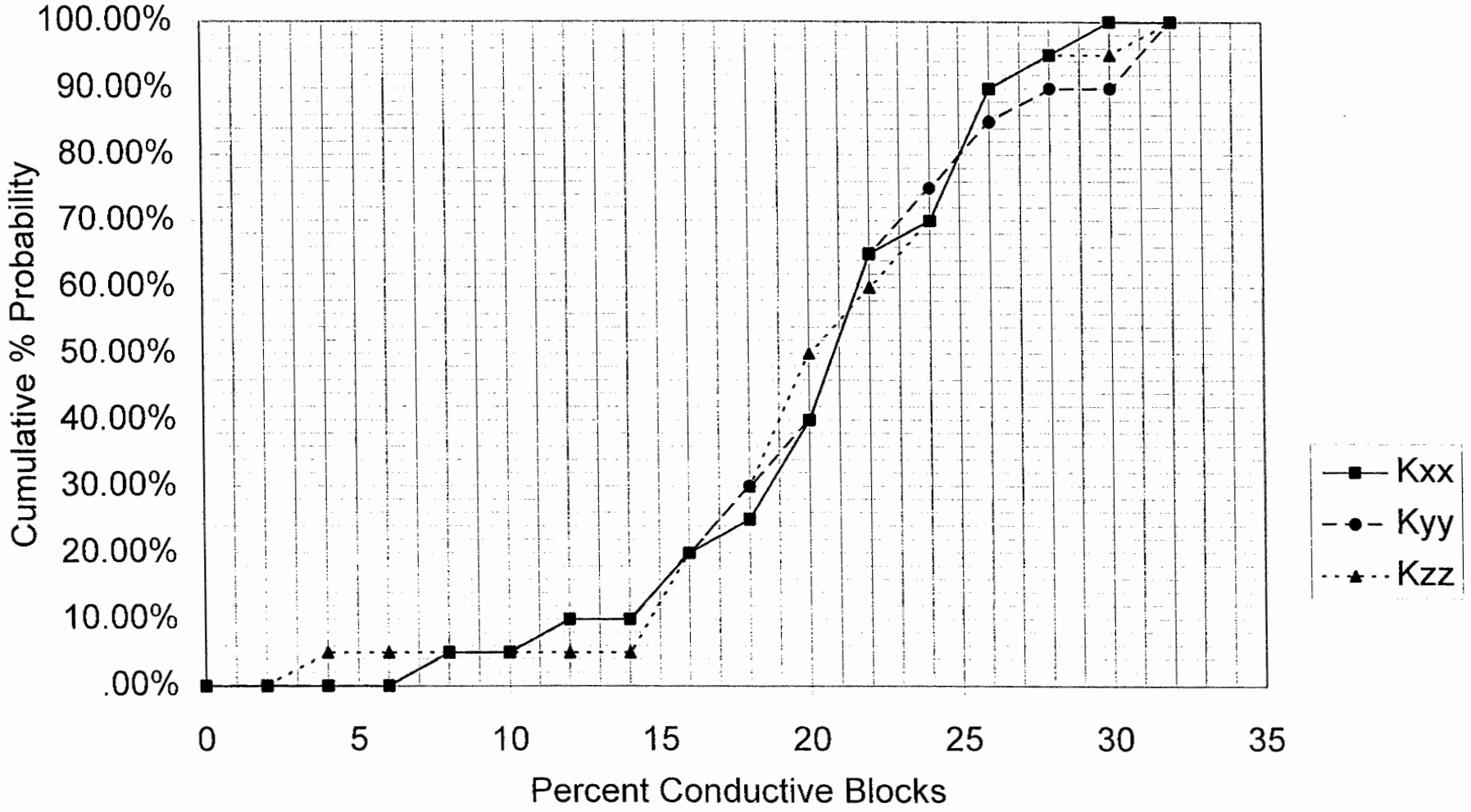

FIGURE **B-1a**
CONDUCTIVE BLOCK PERCENTAGE, 10M BLOCKS, MEAN FRACTURE RADIUS = 6.0M
SKB/BLOCK K/SWEDEN

PROJECT NO. IC3 1161.003 DRAWING NO. 63003 DATE 9/8/94 DRAWN BY EA

Golder Associates

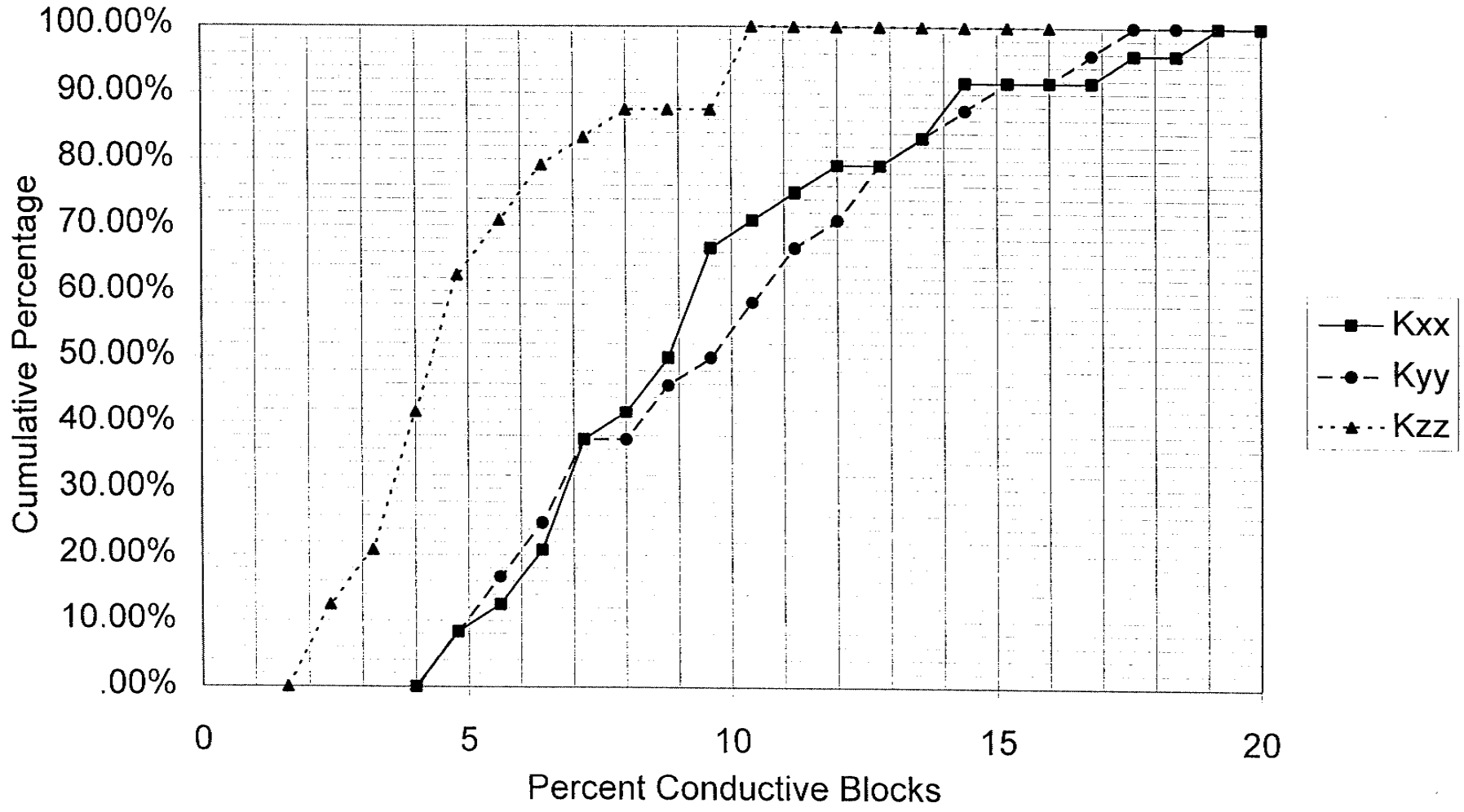

FIGURE **B-1b**
CONDUCTIVE BLOCK PERCENTAGE, 10M BLOCKS, MEAN FRACTURE RADIUS = 13.7M
SKB/BLOCK K/SWEDEN

PROJECT NO. IC3 1161.003 DRAWING NO. 63004 DATE 9/8/94 DRAWN BY EA

Golder Associates

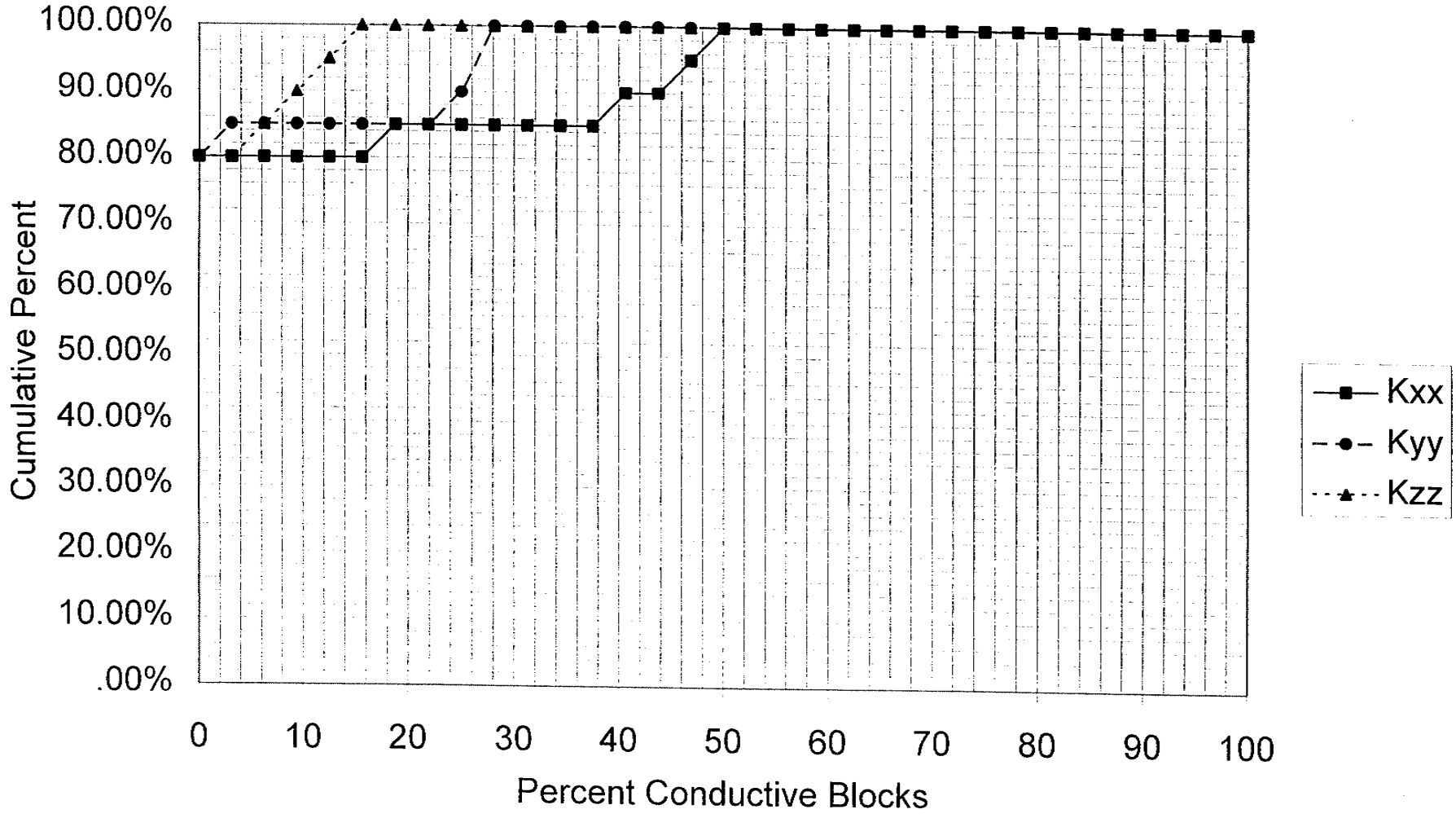

FIGURE **B-2a**
CONDUCTIVE BLOCK PERCENTAGE, 20M BLOCKS, MEAN FRACTURE RADIUS = 6.0M
SKB/BLOCK K/SWEDEN

PROJECT NO. IC3 1161.003 DRAWING NO. 63005 DATE 9/8/94 DRAWN BY EA

Golder Associates

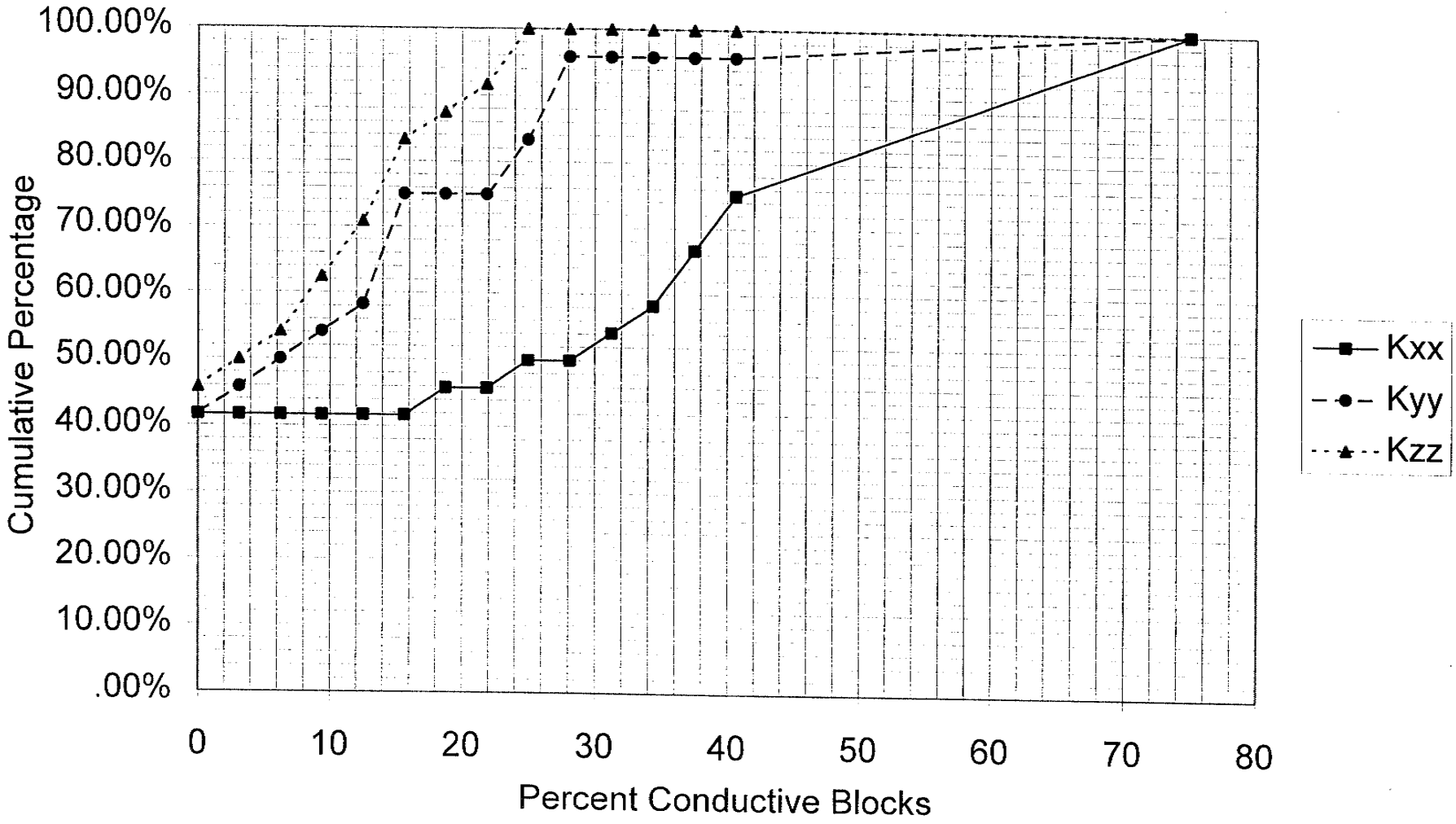

FIGURE **B-2b**

CONDUCTIVE BLOCK PERCENTAGE, 20M BLOCKS, MEAN FRACTURE RADIUS = 13.7M

SKB/BLOCK K/SWEDEN

PROJECT NO. IC3 1161.003 DRAWING NO. 63006 DATE 9/8/94 DRAWN BY EA

Golder Associates

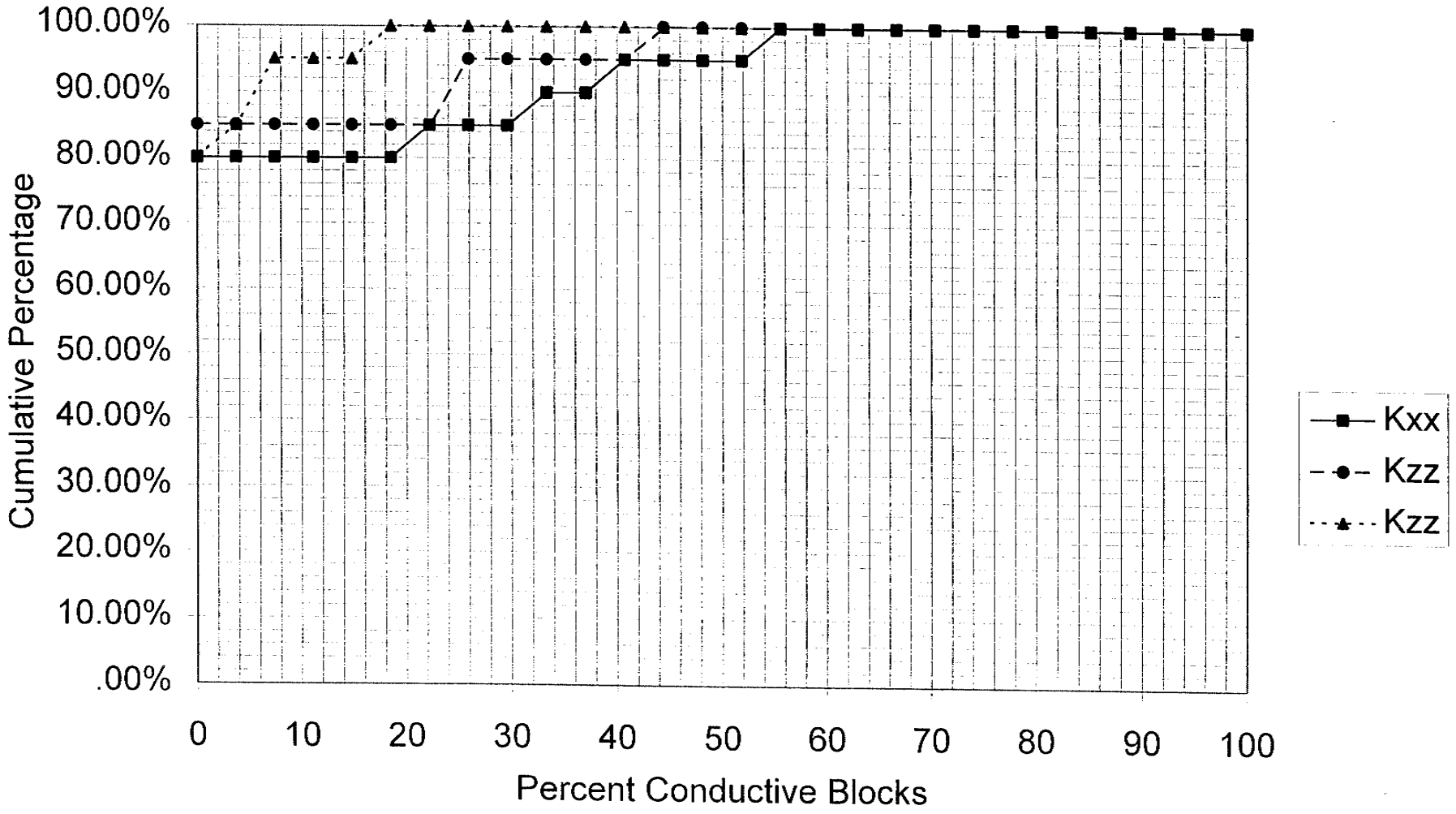

FIGURE **B-3a**
CONDUCTIVE BLOCK PERCENTAGE, 30M BLOCKS, MEAN FRACTURE RADIUS = 6.0M
SKB/BLOCK K/SWEDEN

PROJECT NO. IC3 1161.003 DRAWING NO. 63007 DATE 9/8/94 DRAWN BY EA

Golder Associates

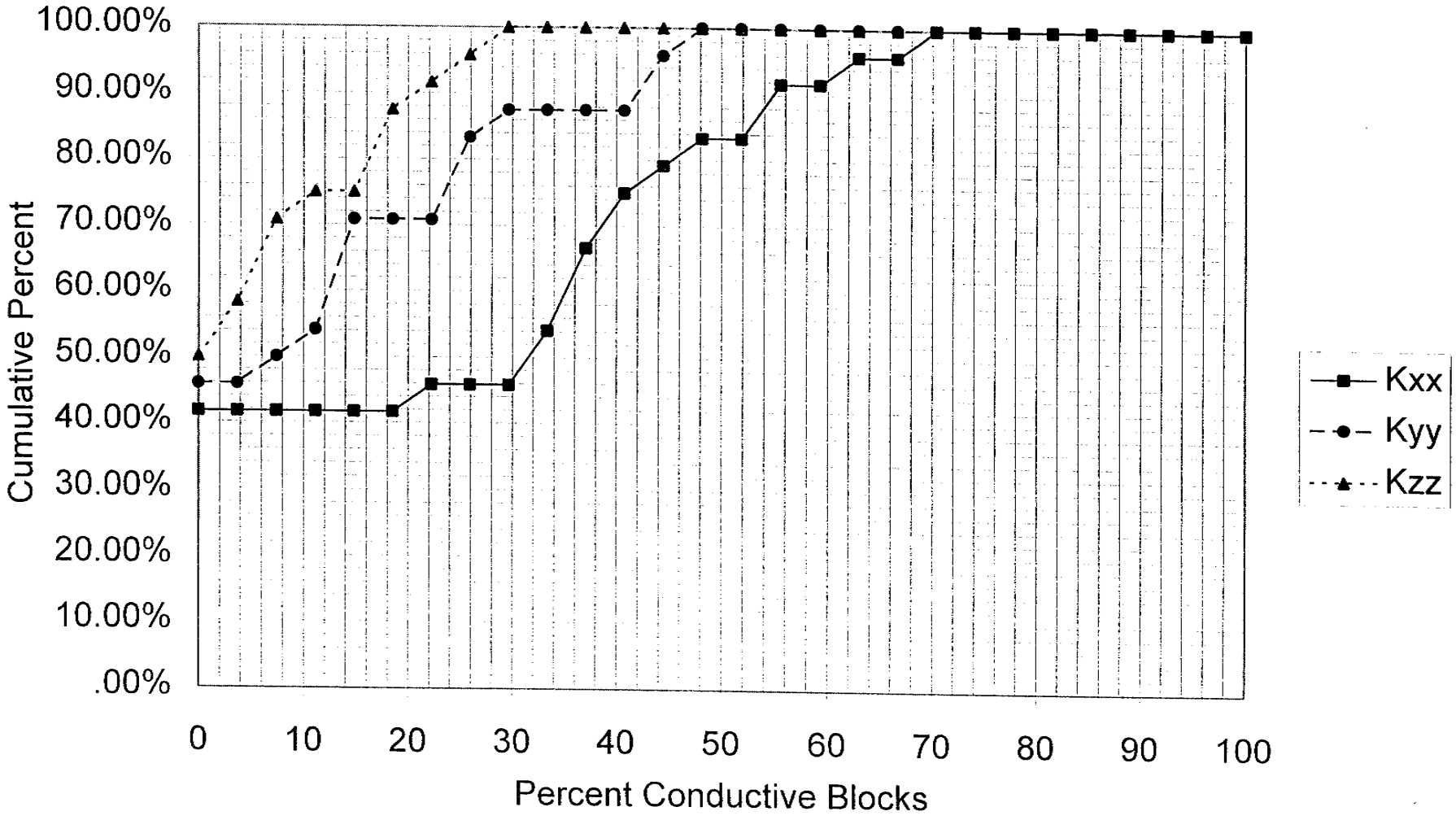

FIGURE **B-3b**
CONDUCTIVE BLOCK PERCENTAGE, 30M BLOCKS, MEAN FRACTURE RADIUS = 13.7M
SKB/BLOCK K/SWEDEN

PROJECT NO. IC3 1161.003 DRAWING NO. 63008 DATE 9/8/94 DRAWN BY EA

Golder Associates

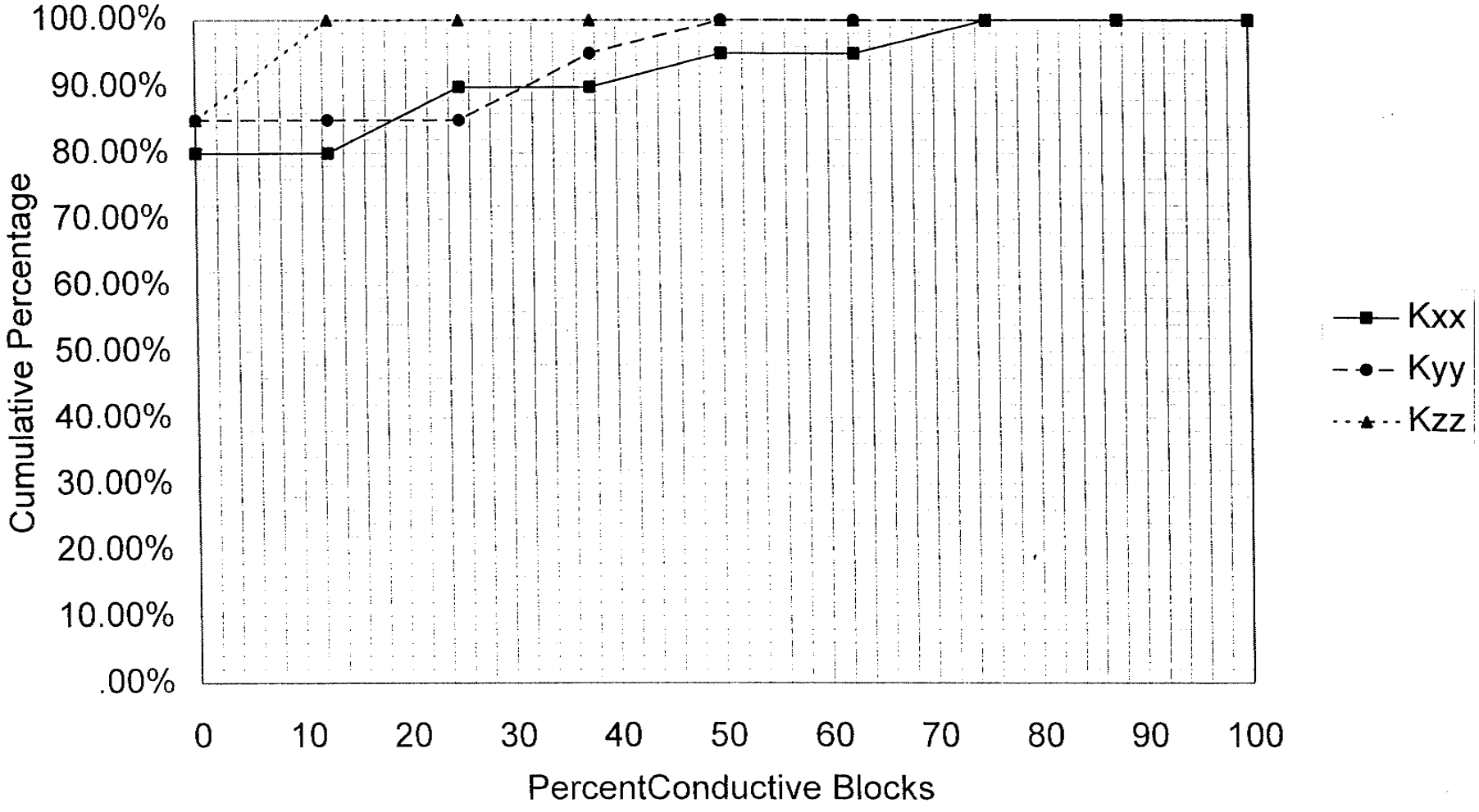

FIGURE **B-4a**
CONDUCTIVE BLOCK PERCENTAGE, 40M BLOCKS, MEAN FRACTURE RADIUS = 6.0M
SKB/BLOCK K/SWEDEN

PROJECT NO. IC3 1161.003 DRAWING NO. 63009 DATE 9/8/94 DRAWN BY EA

Golder Associates

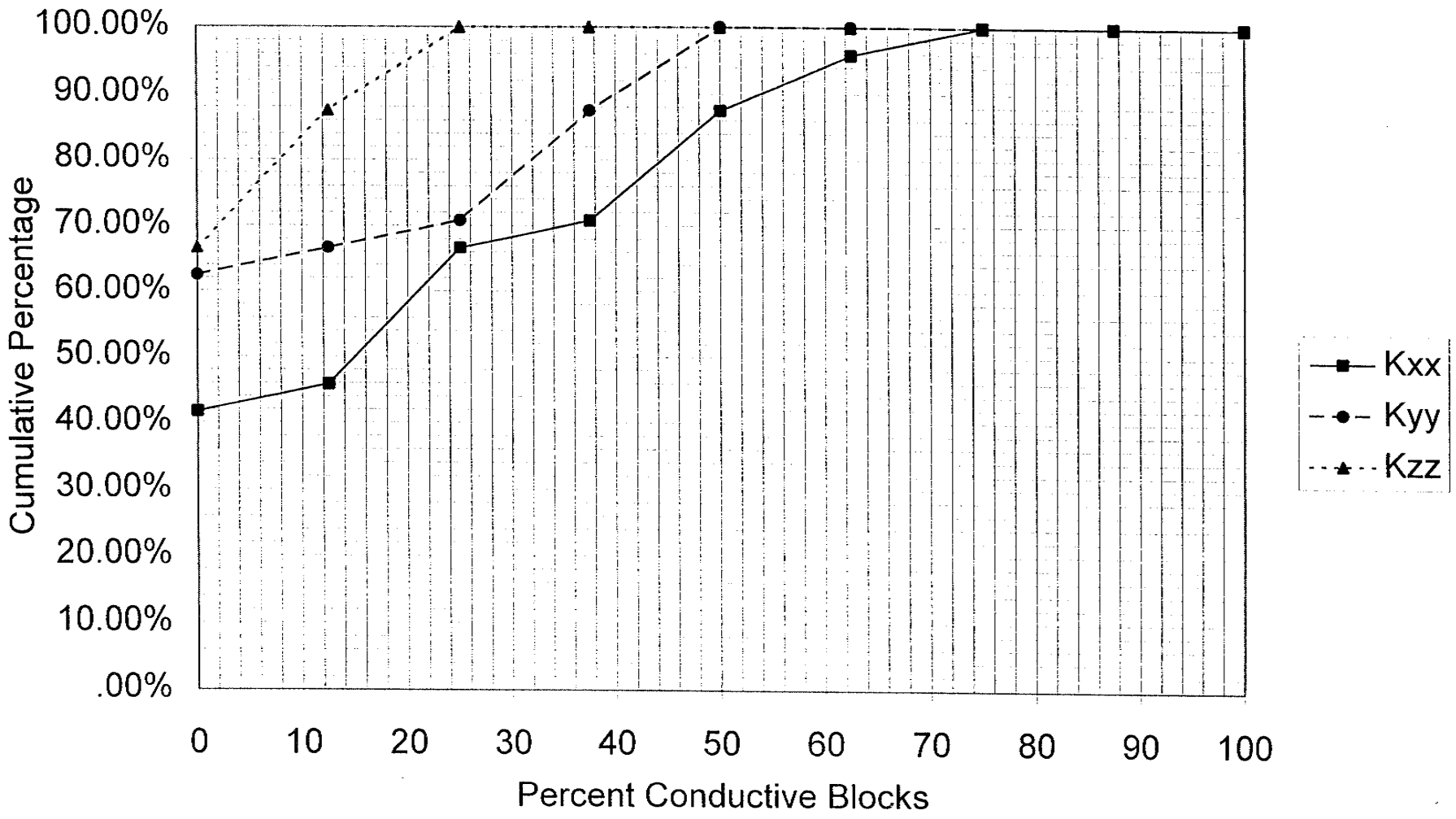

FIGURE **B-4b**
CONDUCTIVE BLOCK PERCENTAGE, 40M BLOCKS, MEAN FRACTURE RADIUS = 13.7M
SKB/BLOCK K/SWEDEN

PROJECT NO. IC3 1161.003 DRAWING NO. 63010 DATE 9/8/94 DRAWN BY EA

Golder Associates

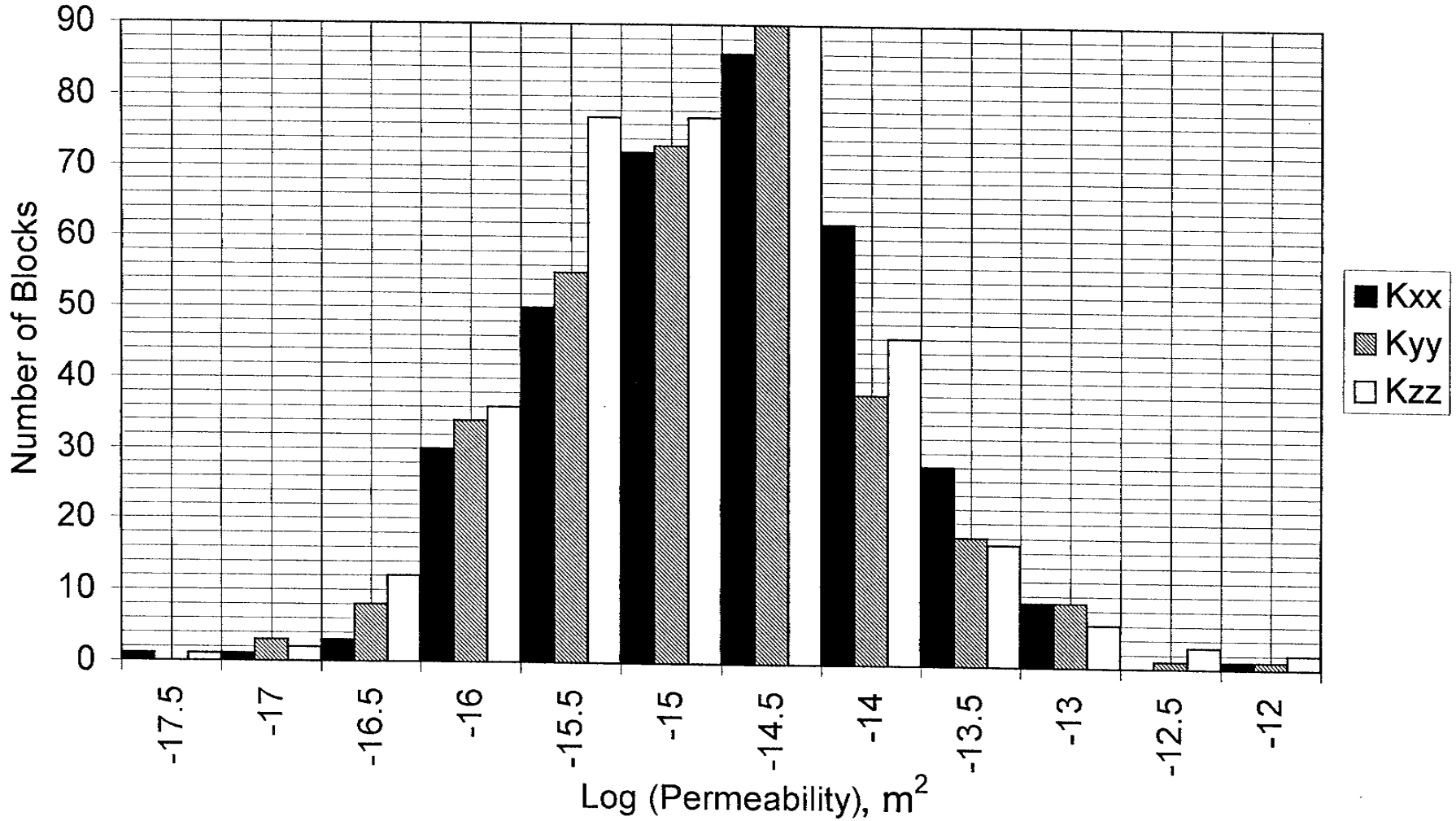

FIGURE **B-5a**
FREQUENCY HISTOGRAM FOR 10M BLOCKS, MEAN FRACTURE RADIUS = 6.0M
SKB/BLOCK K/SWEDEN

PROJECT NO. IC3 1161.003 DRAWING NO. 60816 DATE 9/8/95 DRAWN BY EA

Golder Associates

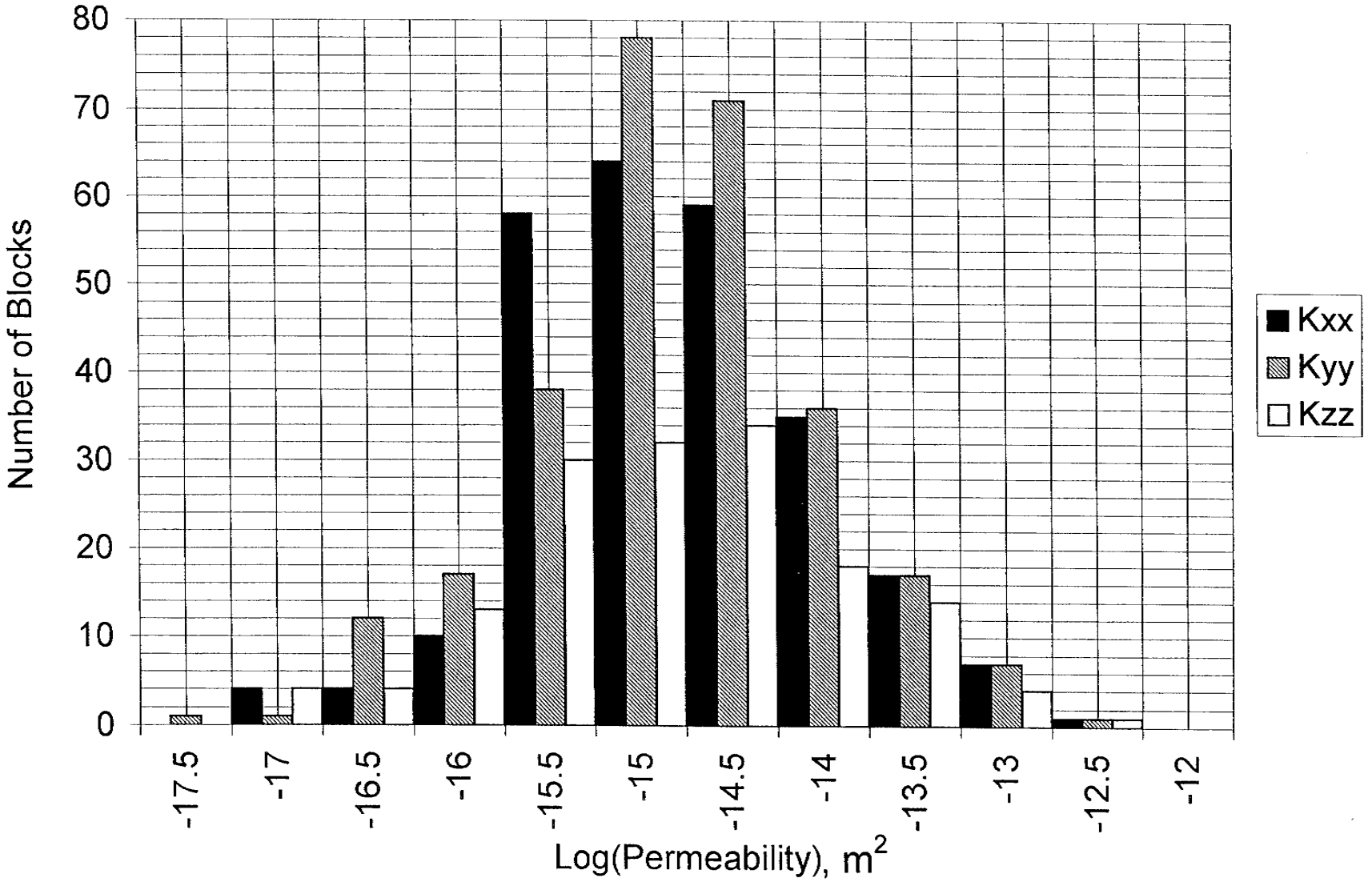

FIGURE **B-5b**
FREQUENCY HISTOGRAM FOR 10M BLOCKS, MEAN FRACTURE RADIUS = 13.7M
SKB/BLOCK K/SWEDEN

PROJECT NO. IC3 1161.003 DRAWING NO. 60817 DATE 9/8/95 DRAWN BY EA

Golder Associates

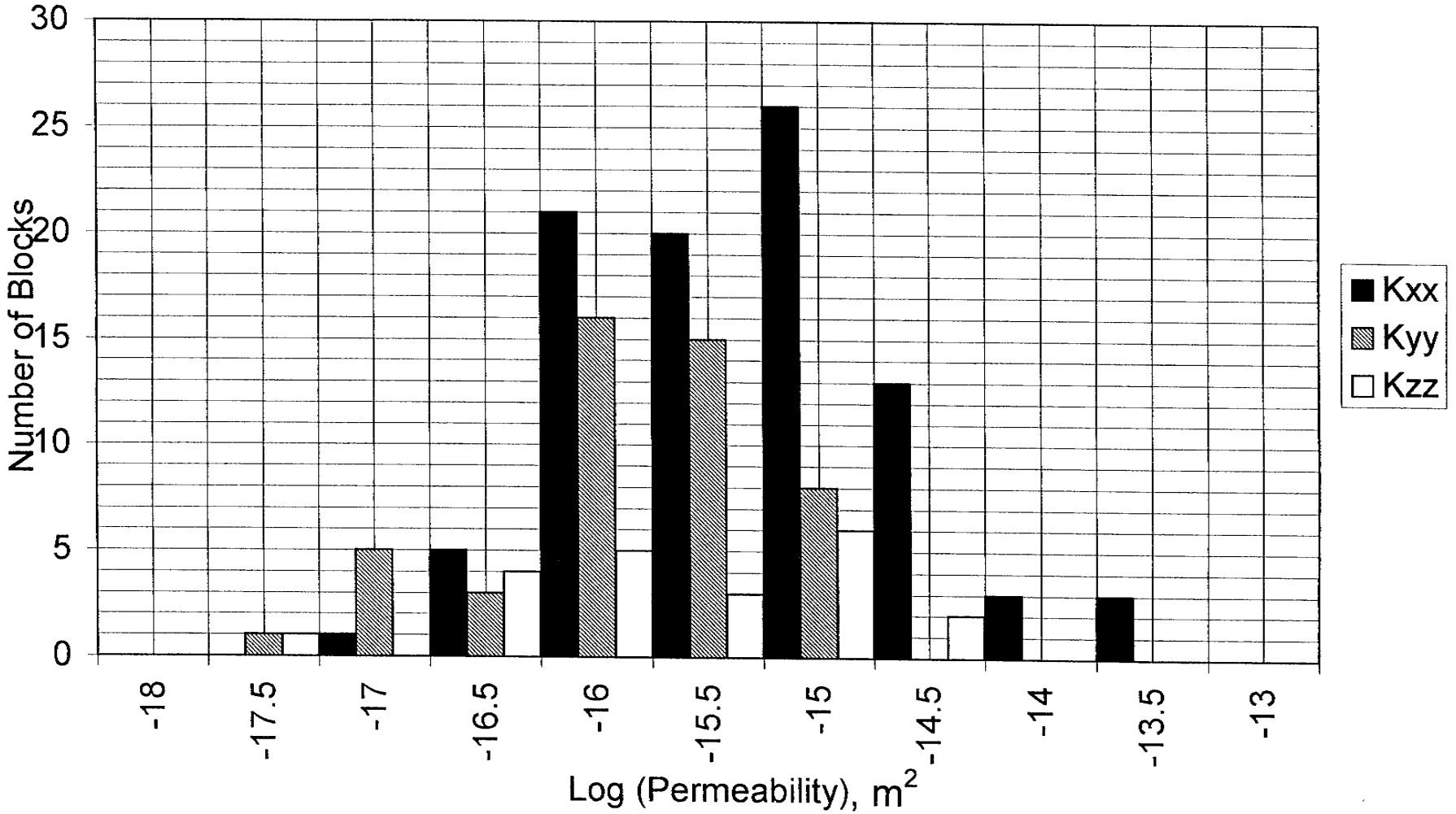

FIGURE **B-6a**
FREQUENCY HISTOGRAM FOR 20M BLOCKS, MEAN FRACTURE RADIUS = 6.0M
SKB/BLOCK K/SWEDEN

PROJECT NO. IC3 1161.003 DRAWING NO. 60818 DATE 9/8/95 DRAWN BY EA

Golder Associates

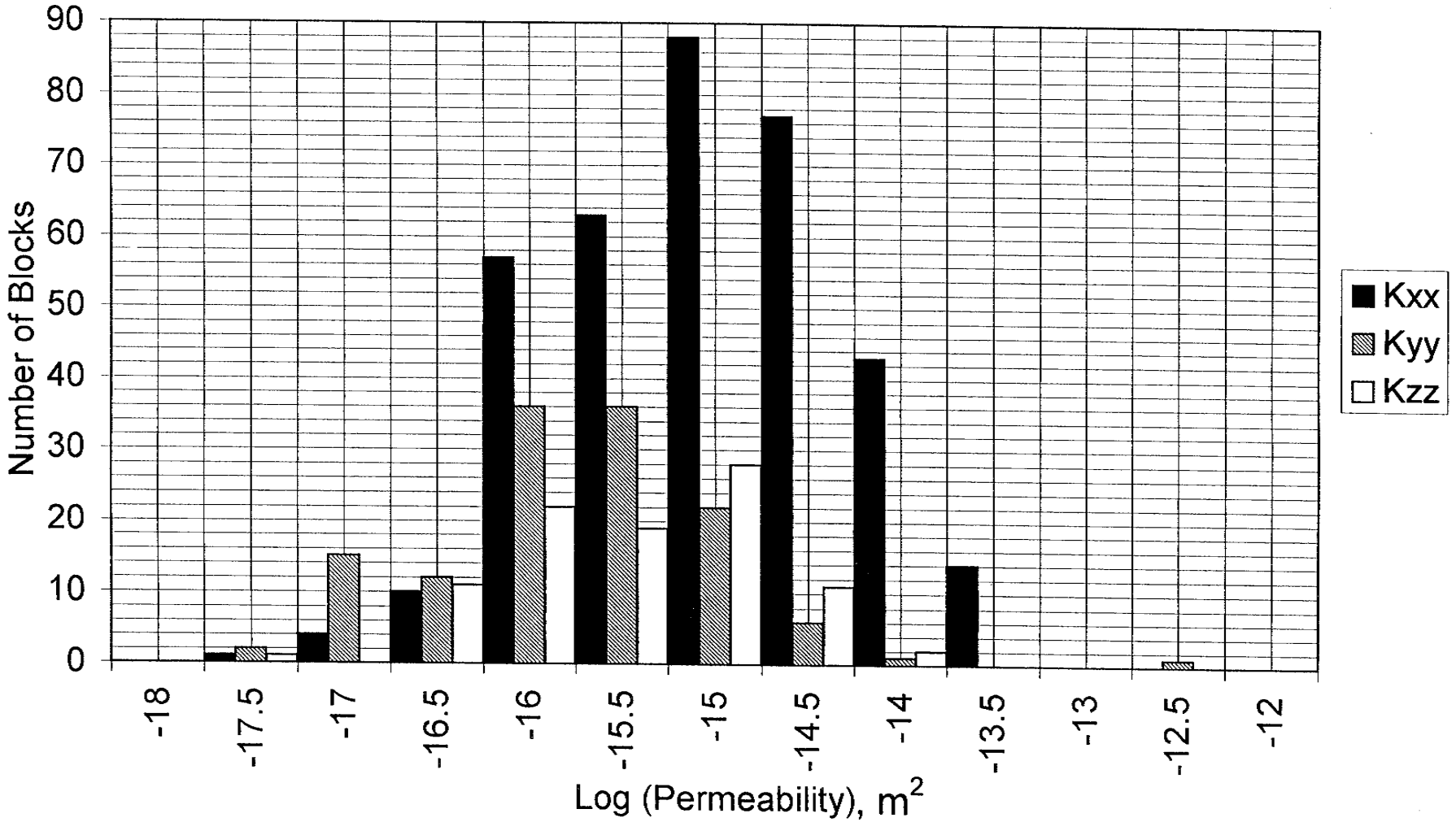

FIGURE **B-6b**
FREQUENCY HISTOGRAM FOR 20M BLOCKS, MEAN FRACTURE RADIUS = 13.7M
SKB/BLOCK K/SWEDEN

PROJECT NO. IC3 1161.003 DRAWING NO. 60819 DATE 9/8/95 DRAWN BY EA

Golder Associates

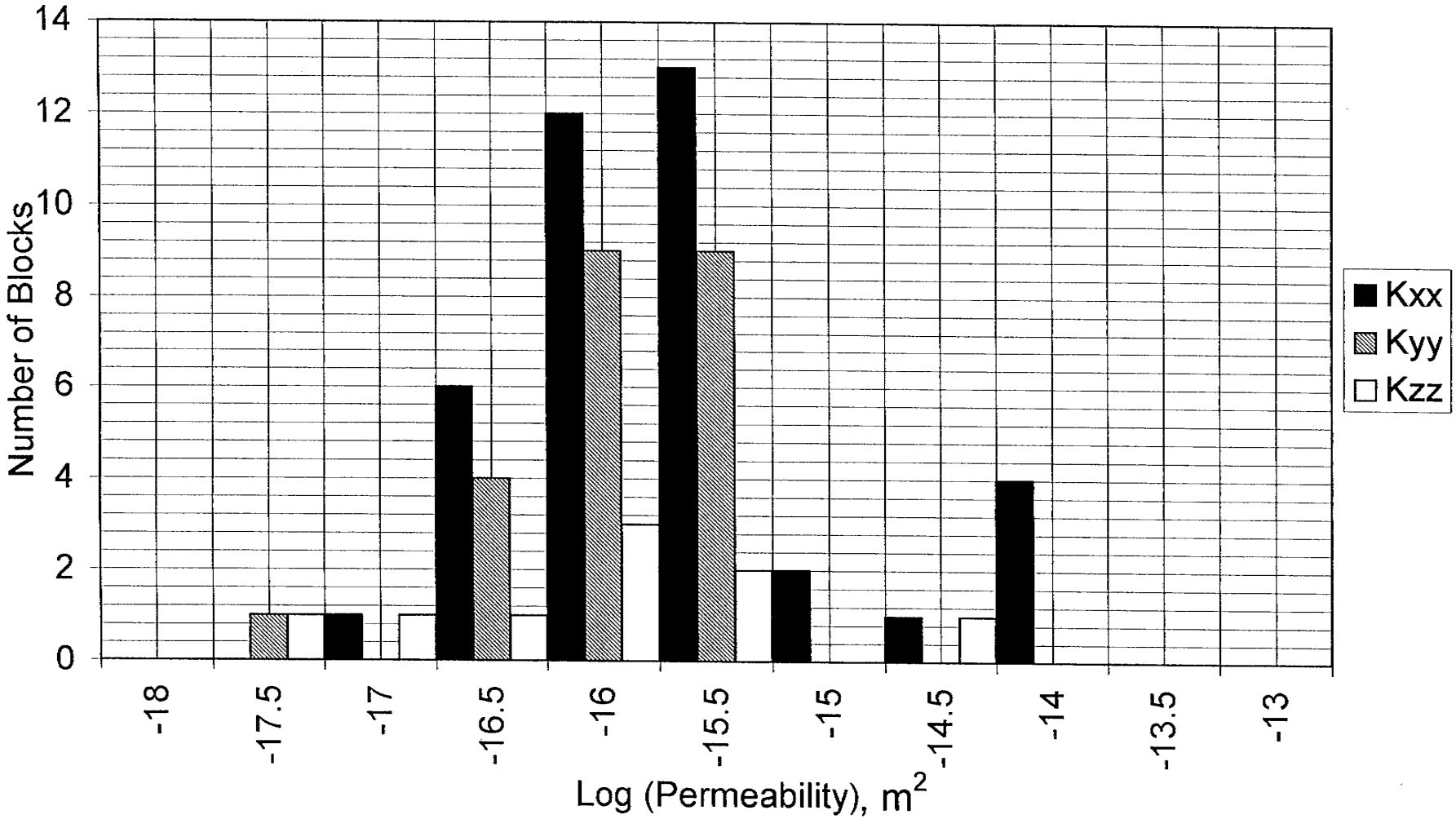

FIGURE **B-7a**
FREQUENCY HISTOGRAM FOR 30M BLOCKS, MEAN FRACTURE RADIUS = 6.0M
SKB/BLOCK K/SWEDEN

PROJECT NO. tC3 1161.003 DRAWING NO. 60820 DATE 9/8/95 DRAWN BY EA

Golder Associates

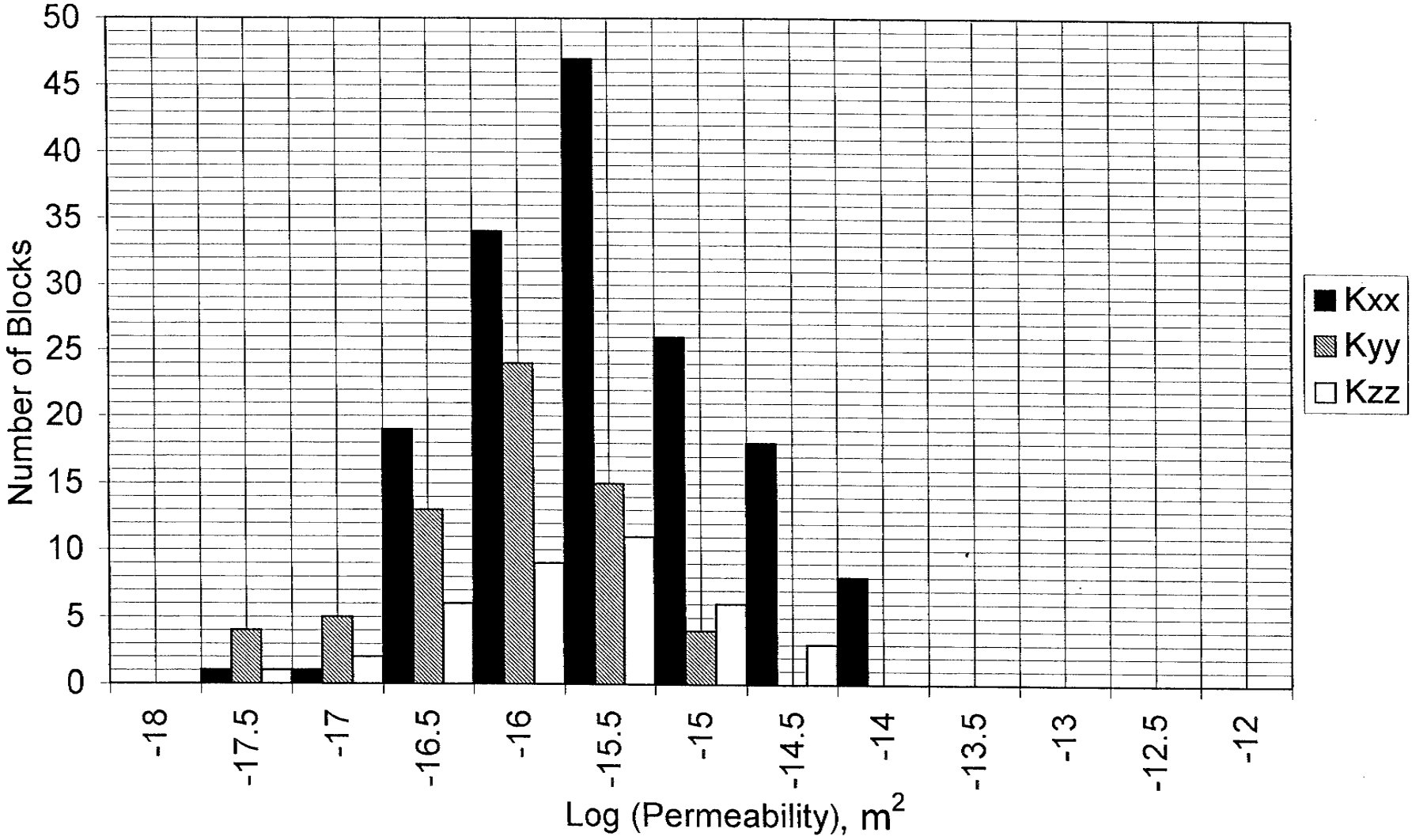

FIGURE **B-7b**
FREQUENCY HISTOGRAM FOR 30M BLOCKS, MEAN FRACTURE RADIUS = 13.7M
SKB/BLOCK K/SWEDEN

PROJECT NO. IC3 1161.003 DRAWING NO. 60821 DATE 9/8/95 DRAWN BY EA

Golder Associates

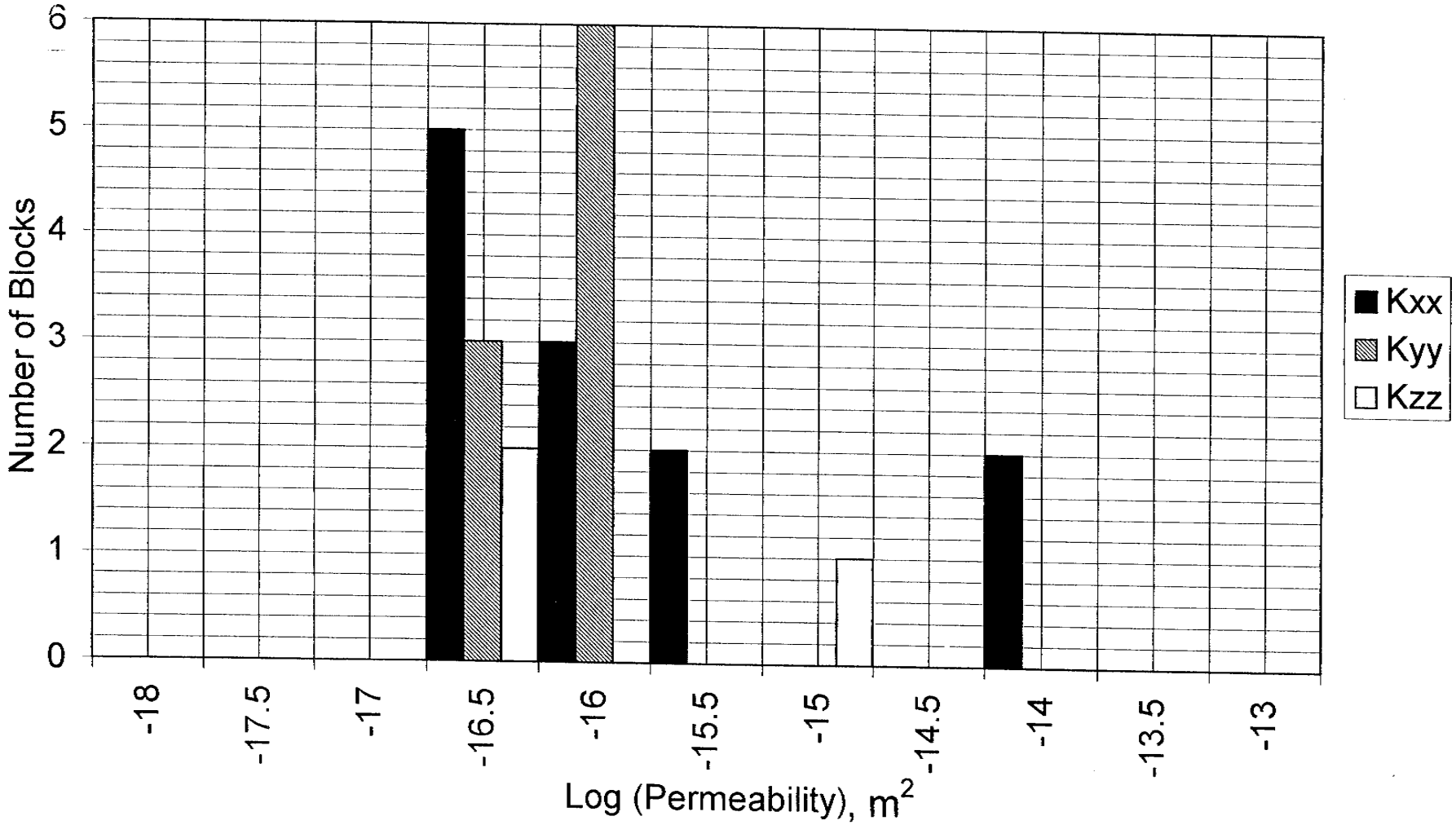

FIGURE **B-8a**
FREQUENCY HISTOGRAM FOR 40M BLOCKS, MEAN FRACTURE RADIUS = 6.0M
SKB/BLOCK K/SWEDEN

PROJECT NO. IC3 1161.003 DRAWING NO. 60822 DATE 9/8/95 DRAWN BY EA

Golder Associates

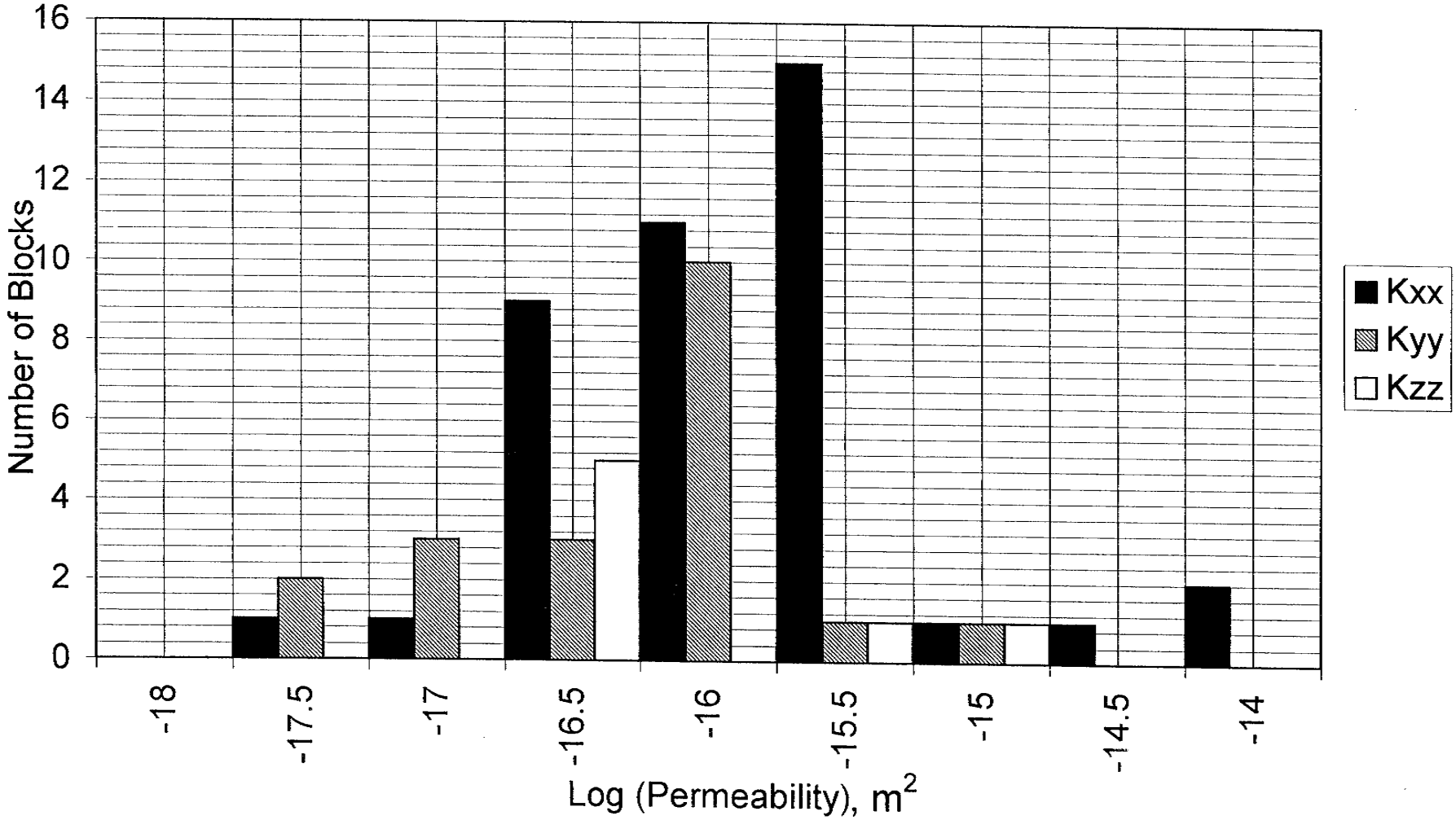

FIGURE **B-8b**
FREQUENCY HISTOGRAM FOR 40M BLOCKS, MEAN FRACTURE RADIUS = 13.7M
SKB/BLOCK K/SWEDEN

PROJECT NO. IC3 1161.003 DRAWING NO. 60823 DATE 9/8/95 DRAWN BY EA

Golder Associates

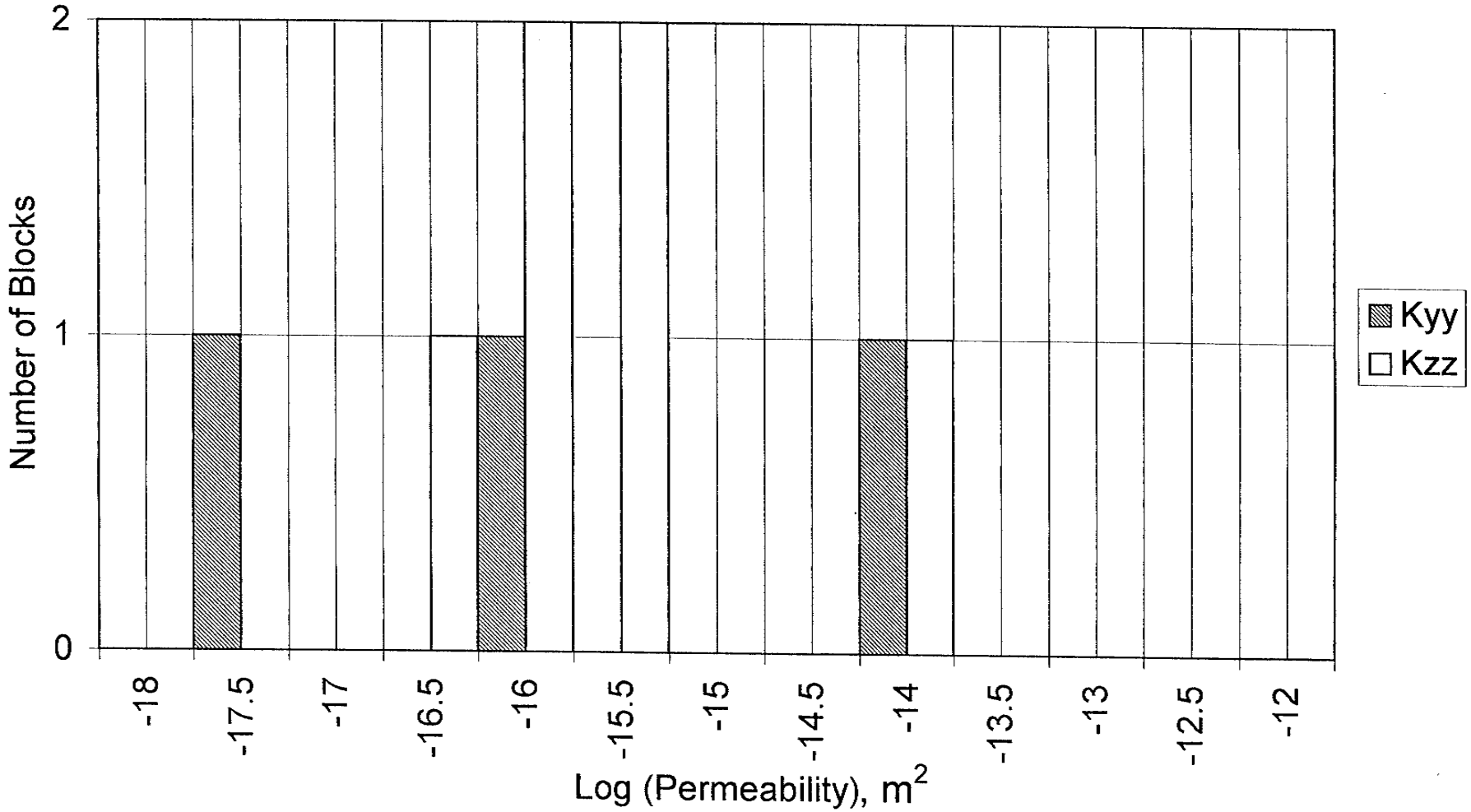

FIGURE **B-9a**
FREQUENCY HISTOGRAM FOR 50M BLOCKS, MEAN FRACTURE RADIUS = 6.0M
SKB/BLOCK K/SWEDEN

PROJECT NO. IC3 1161.003 DRAWING NO. 60824 DATE 9/8/95 DRAWN BY EA

Golder Associates

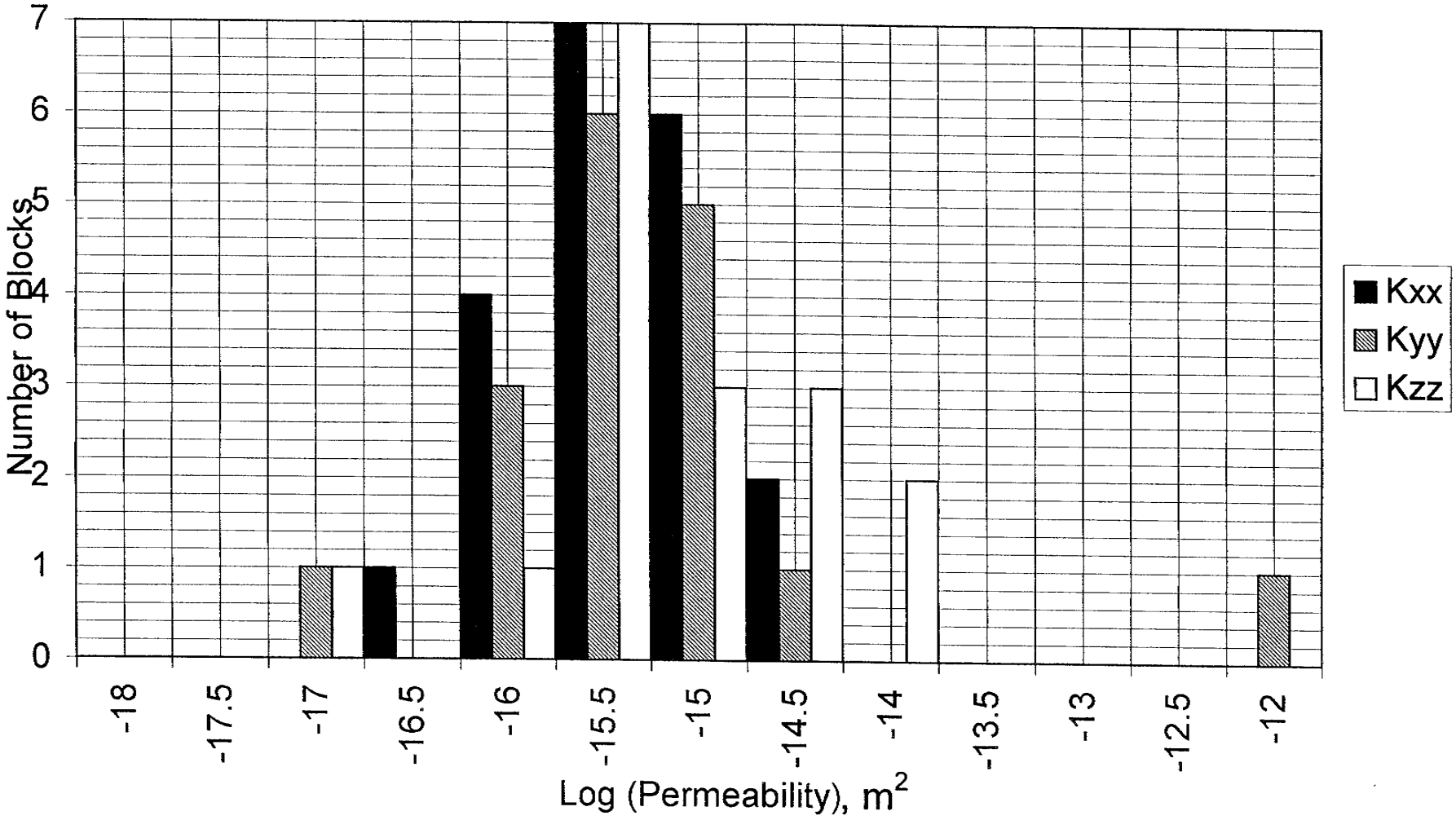

FIGURE **B-9b**
FREQUENCY HISTOGRAM FOR 50M BLOCKS, MEAN FRACTURE RADIUS = 13.7M
SKB/BLOCK K/SWEDEN

PROJECT NO. IC3 1161.003 DRAWING NO. 60825 DATE 9/8/95 DRAWN BY EA

Golder Associates

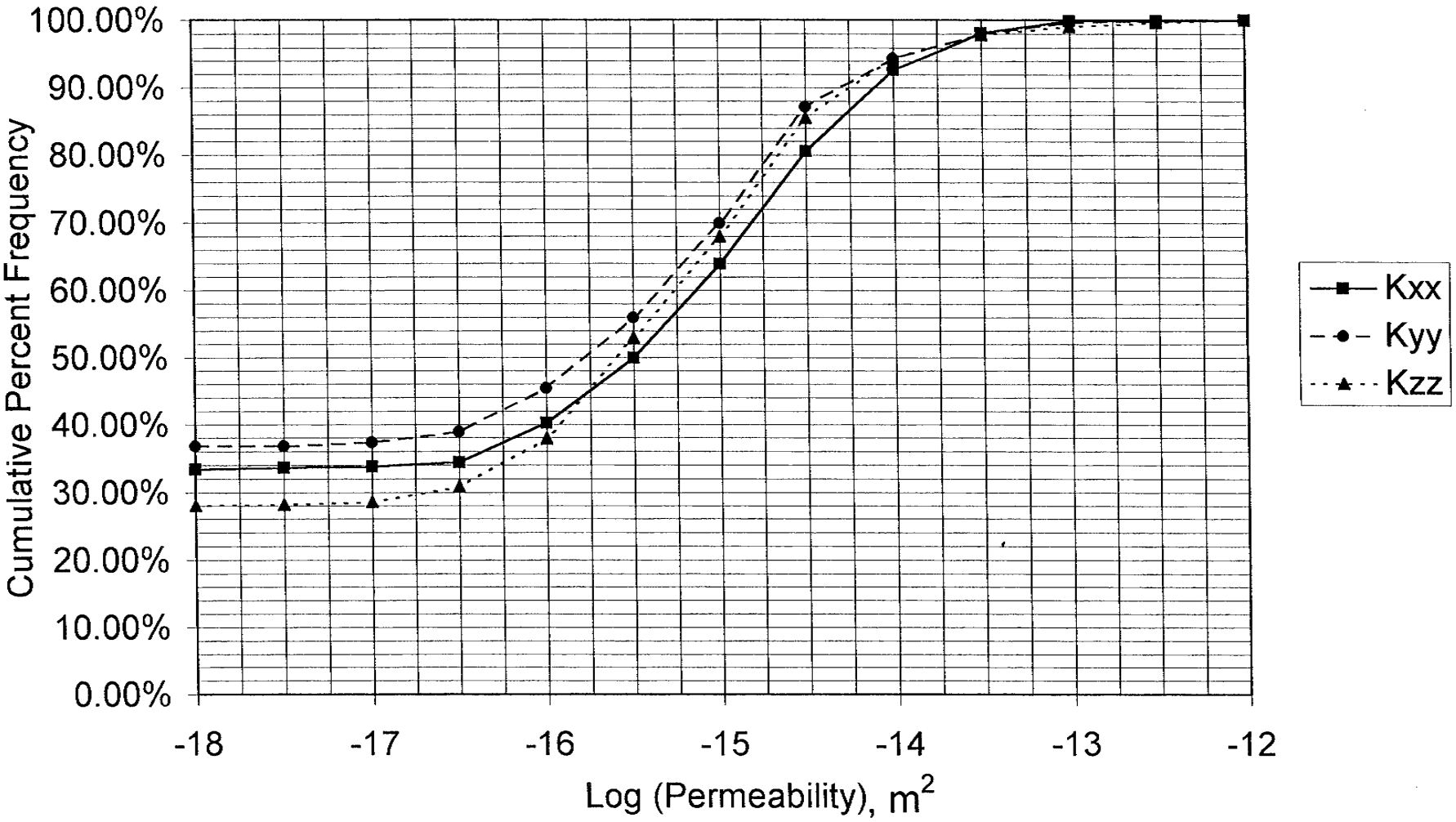

FIGURE **B-10a**
CUMULATIVE FREQUENCY HISTOGRAM FOR 10M BLOCKS, MEAN FRACTURE RADIUS = 6.0M
SKB/BLOCK K/SWEDEN

PROJECT NO. IC3 1161.003 DRAWING NO. 60826 DATE 9/8/95 DRAWN BY EA

Golder Associates

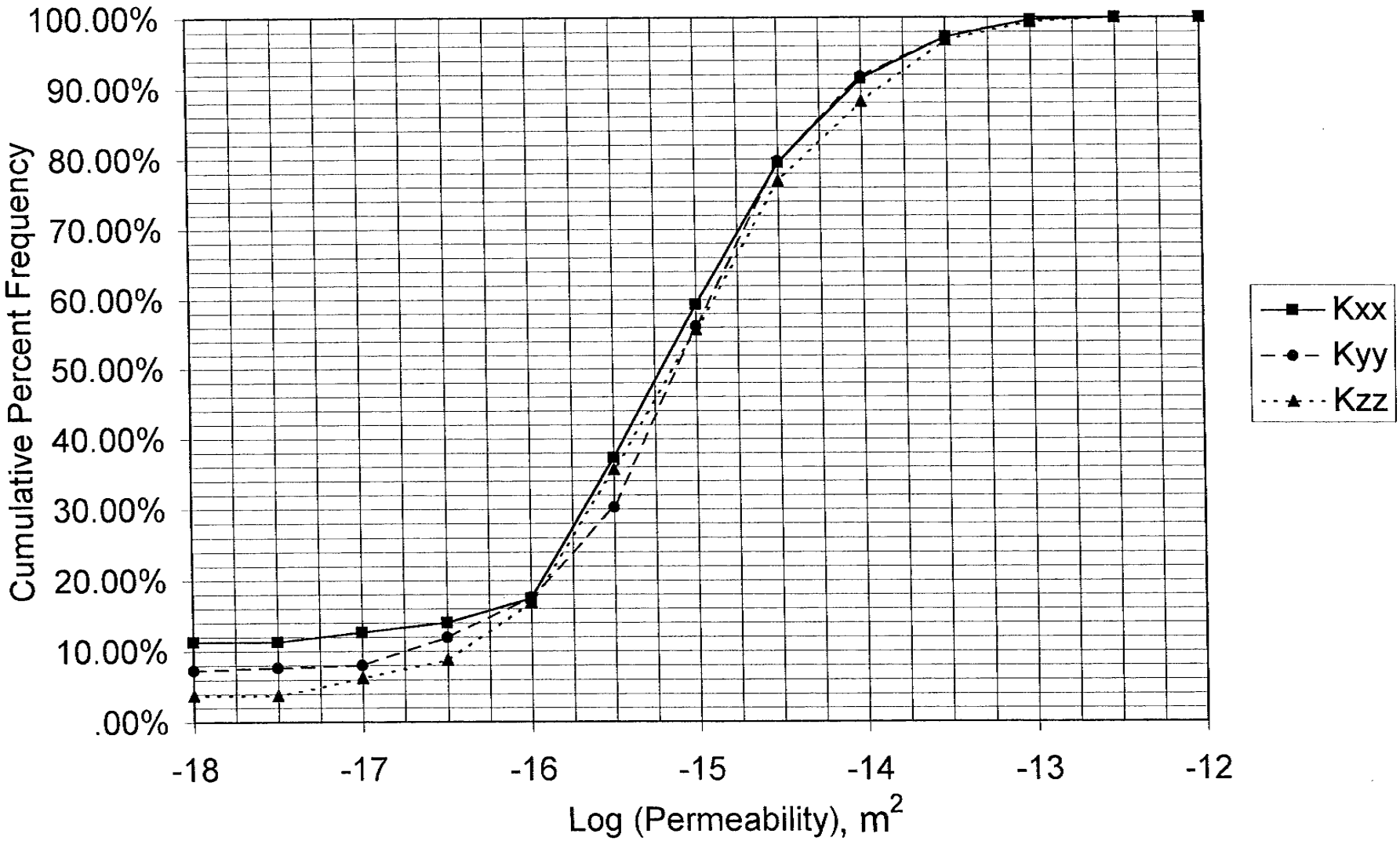

FIGURE **B-10b**
CUMULATIVE FREQUENCY HISTOGRAM FOR 10M BLOCKS, MEAN FRACTURE RADIUS = 13.7M
SKB/BLOCK K/SWEDEN

PROJECT NO. IC3 1161.003 DRAWING NO. 60827 DATE 9/8/95 DRAWN BY EA

Golder Associates

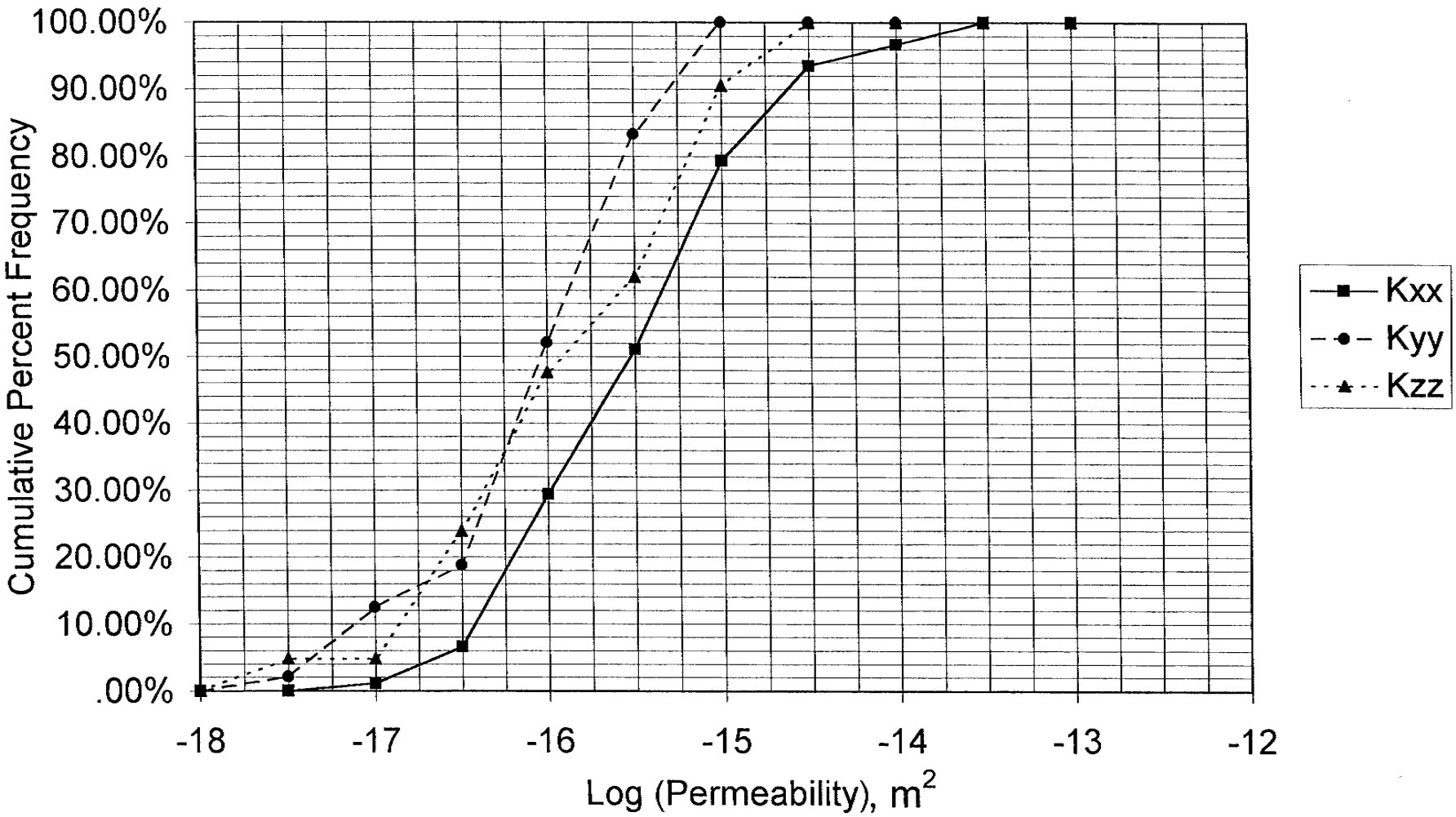

FIGURE **B-11a**
CUMULATIVE FREQUENCY HISTOGRAM FOR 20M BLOCKS, MEAN FRACTURE RADIUS = 6.0M
SKB/BLOCK K/SWEDEN

PROJECT NO. IC3 1161.003 DRAWING NO. 60828 DATE 9/8/95 DRAWN BY EA

Golder Associates

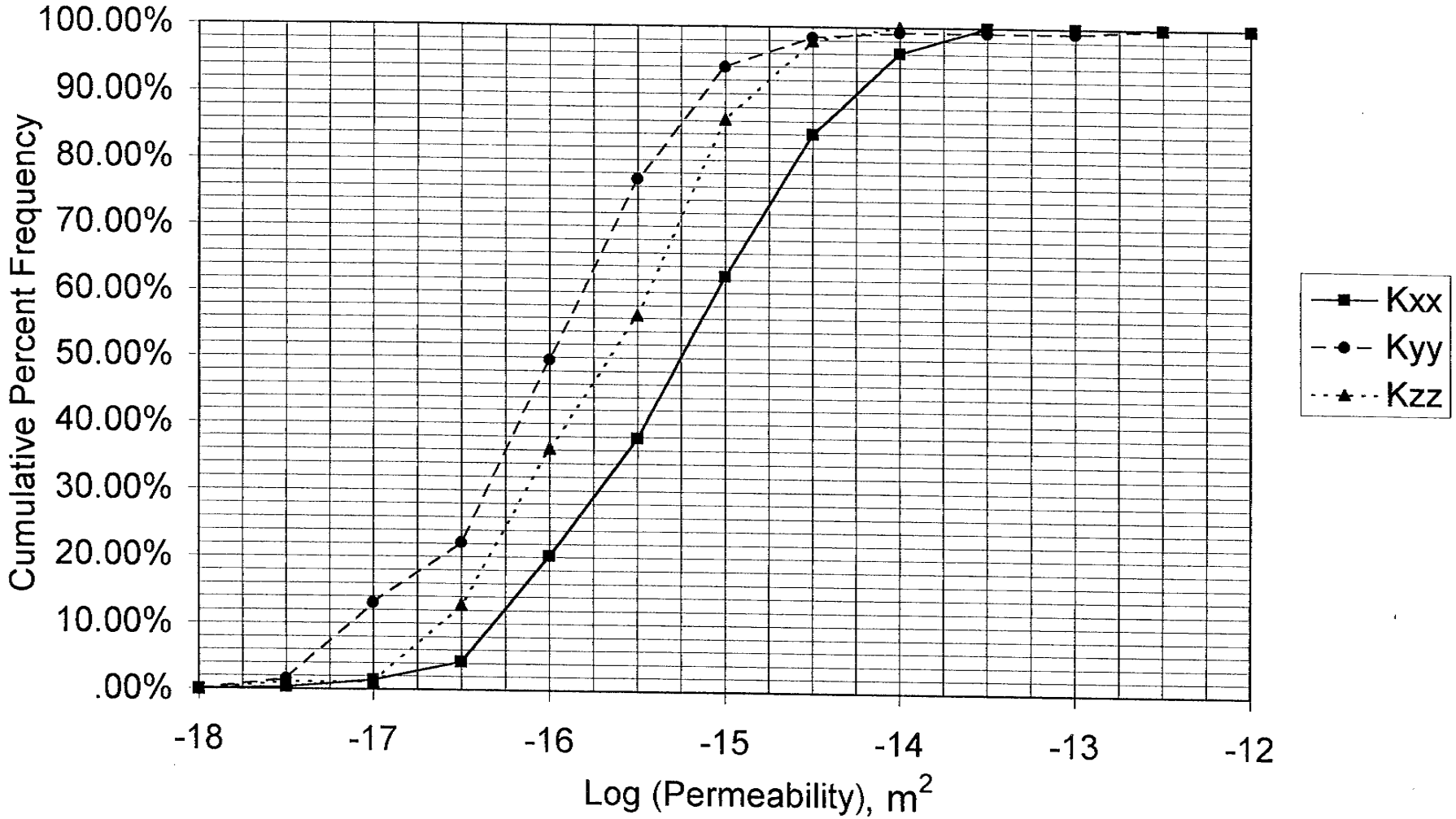

FIGURE **B-11b**
CUMULATIVE FREQUENCY HISTOGRAM FOR 20M BLOCKS, MEAN FRACTURE RADIUS = 13.7M
SKB/BLOCK K/SWEDEN

PROJECT NO. IC3 1161.003 DRAWING NO. 60829 DATE 9/8/95 DRAWN BY EA

Golder Associates

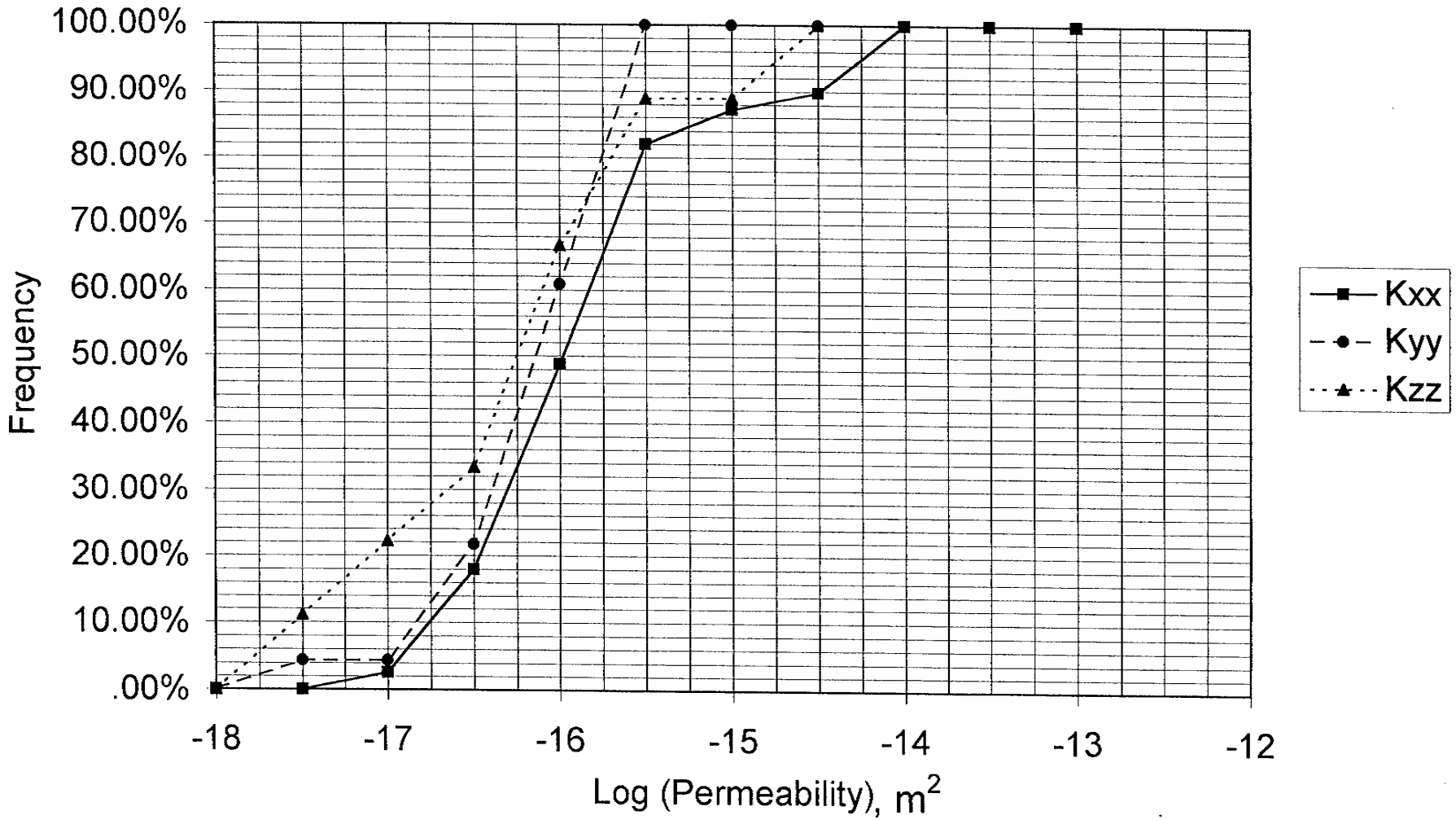

FIGURE **B-12a**
CUMULATIVE FREQUENCY HISTOGRAM FOR 30M BLOCKS, MEAN FRACTURE RADIUS = 6.0M
SKB/BLOCK K/SWEDEN

PROJECT NO. IC3 1161.003 DRAWING NO. 60830 DATE 9/8/95 DRAWN BY EA

Golder Associates

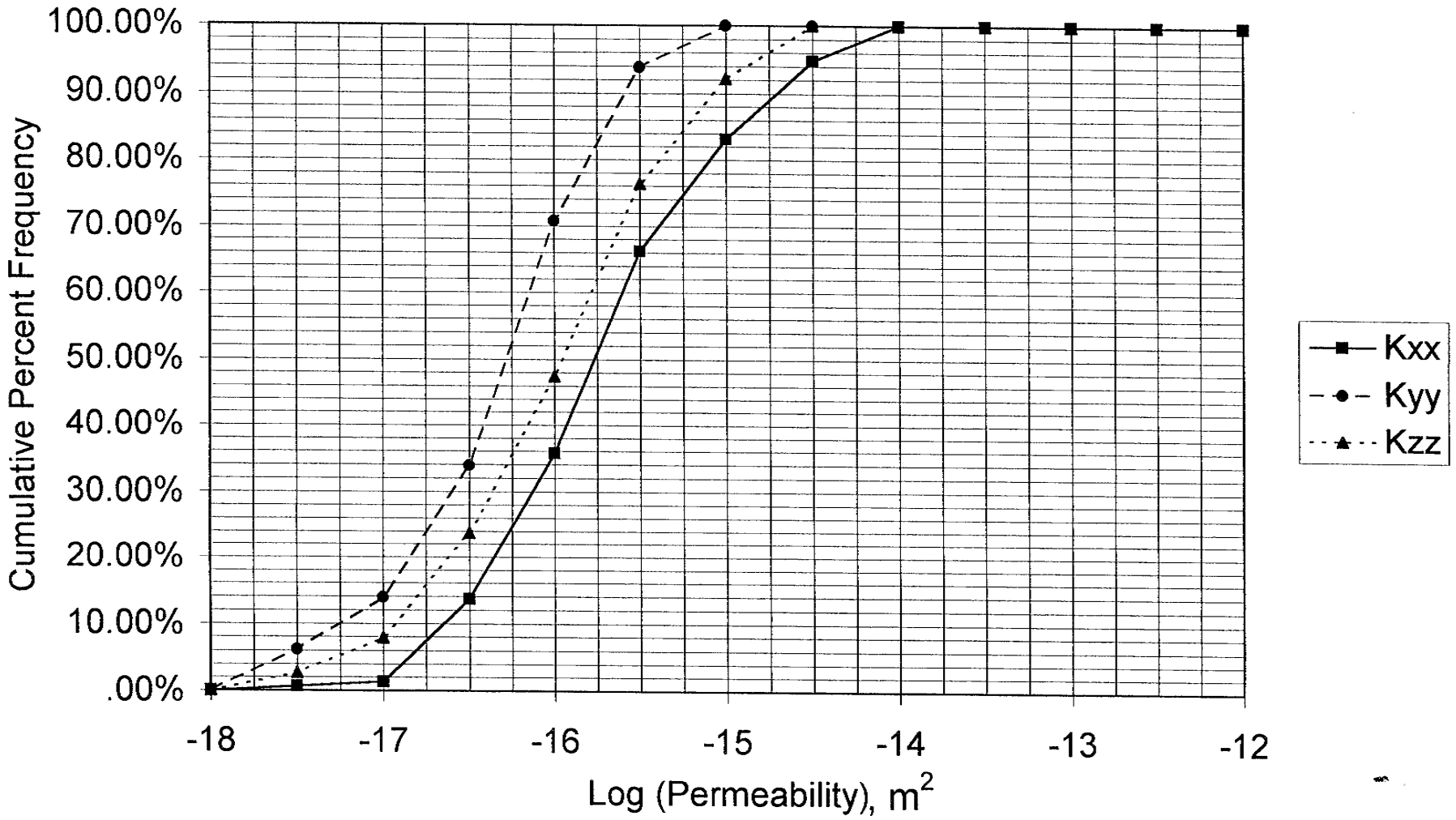

FIGURE **B-12b**
CUMULATIVE FREQUENCY HISTOGRAM FOR 30M BLOCKS, MEAN FRACTURE RADIUS = 13.7M
SKB/BLOCK K/SWEDEN

PROJECT NO. IC3 1161.003 DRAWING NO. 60831 DATE 9/8/95 DRAWN BY EA

Golder Associates

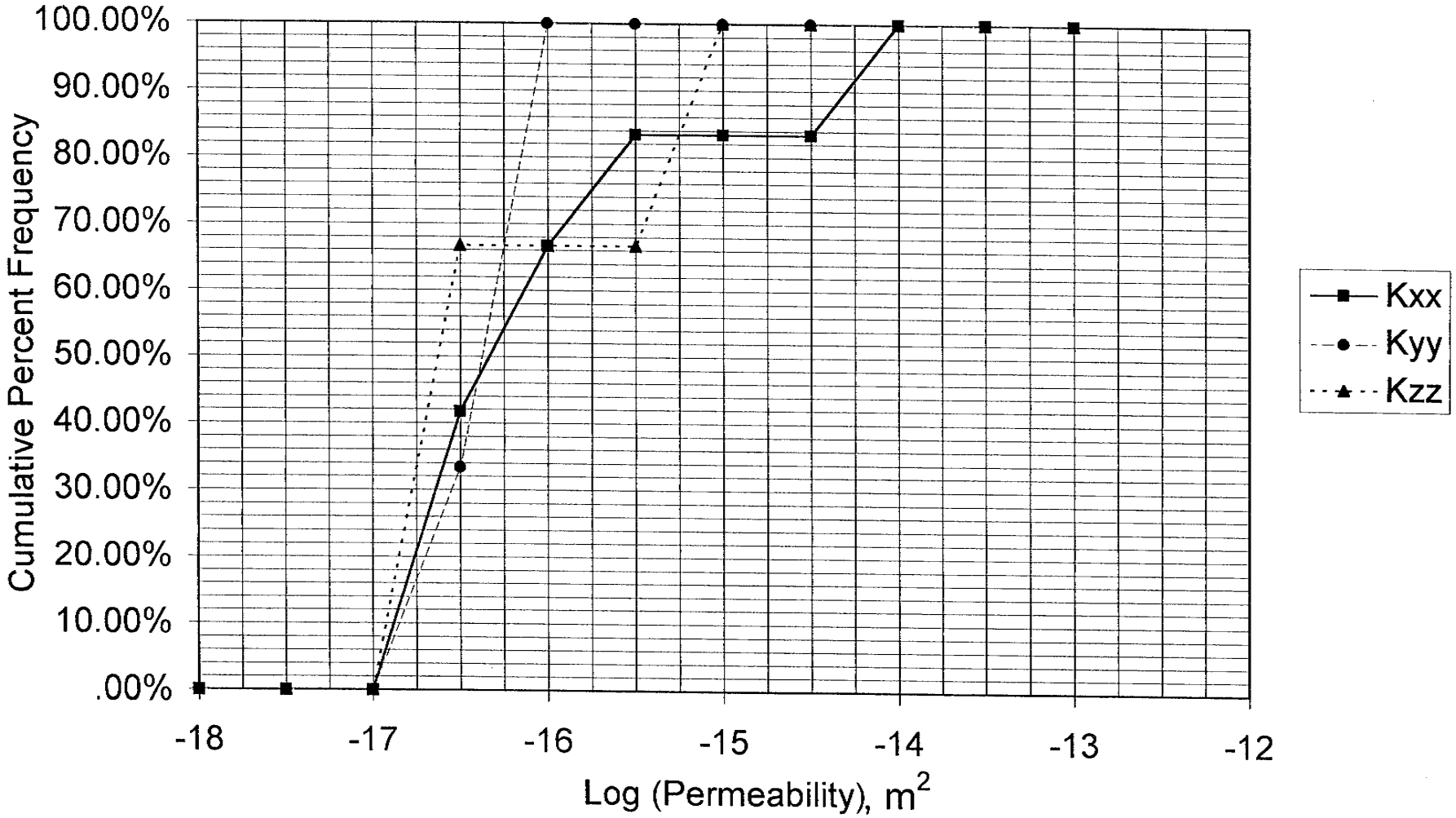

FIGURE **B-13a**
CUMULATIVE FREQUENCY HISTOGRAM FOR 40M BLOCKS, MEAN FRACTURE RADIUS = 6.0M
SKB/BLOCK K/SWEDEN

PROJECT NO. IC3 1161.003 DRAWING NO. 60832 DATE 9/8/95 DRAWN BY EA

Golder Associates

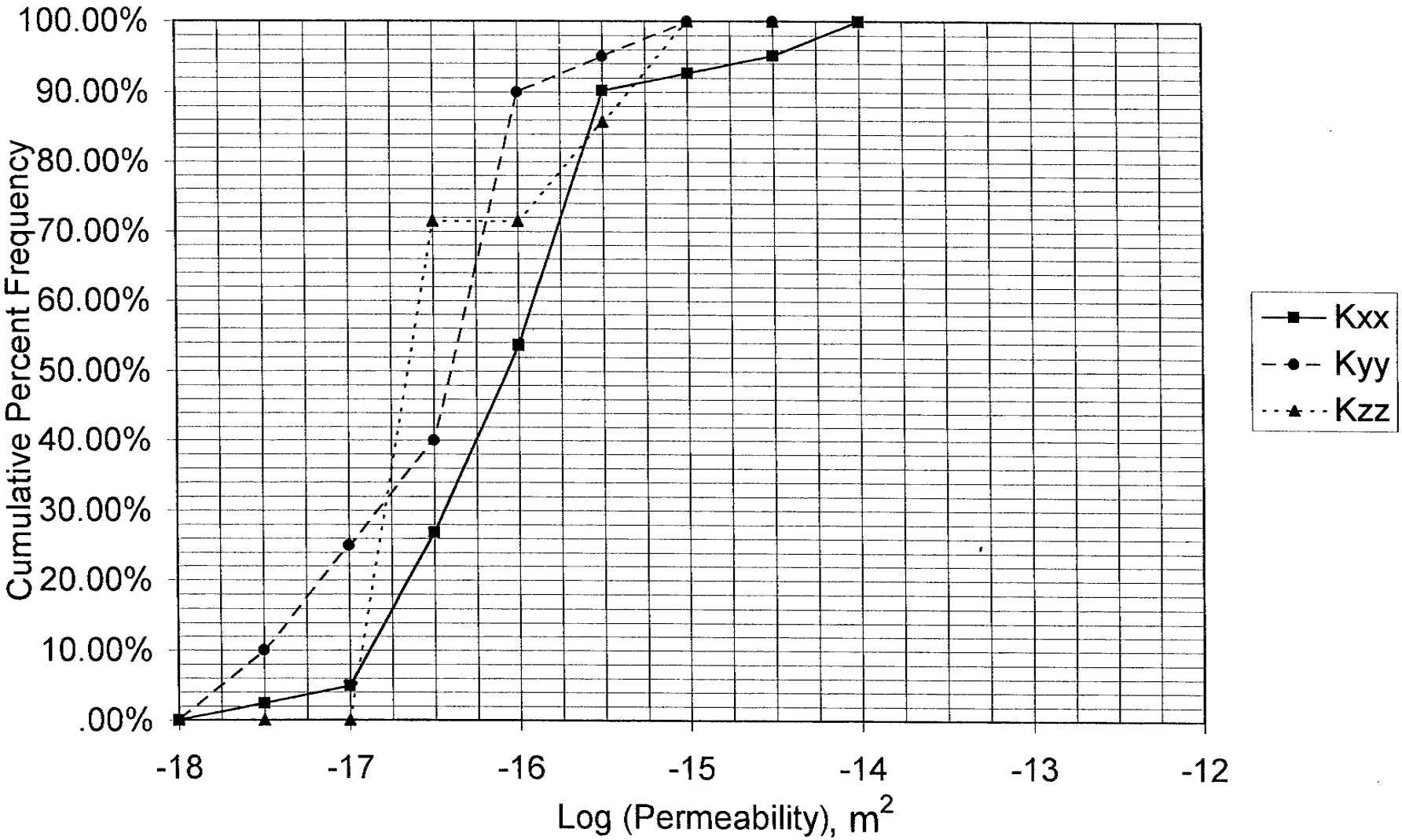

FIGURE **B-13b**
CUMULATIVE FREQUENCY HISTOGRAM FOR 40M BLOCKS, MEAN FRACTURE RADIUS = 13.7M
SKB/BLOCK K/SWEDEN

PROJECT NO. IC3 1161.003 DRAWING NO. 60833 DATE 9/8/95 DRAWN BY EA

Golder Associates

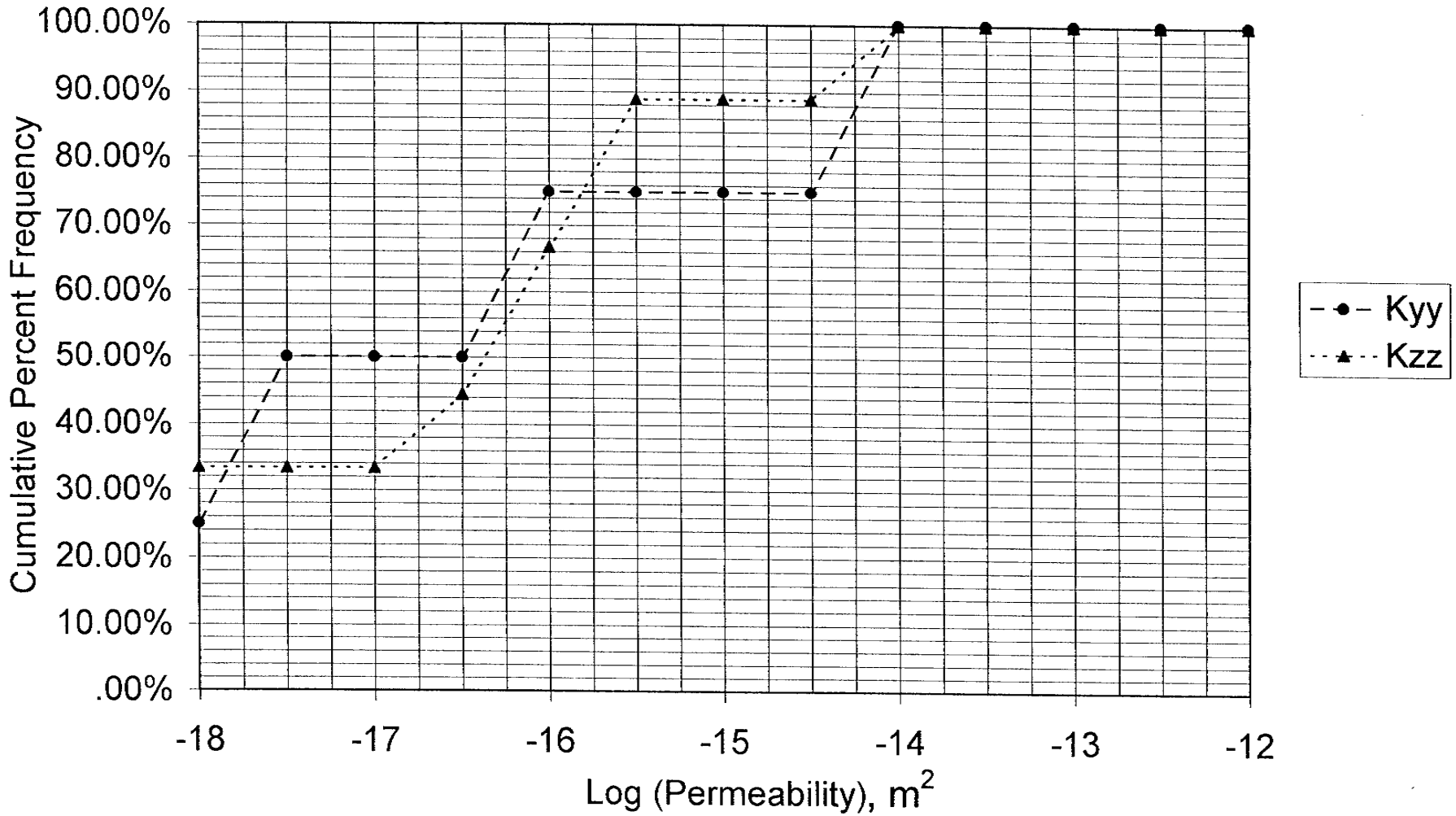

FIGURE **B-14a**
CUMULATIVE FREQUENCY HISTOGRAM FOR 50M BLOCKS, MEAN FRACTURE RADIUS = 6.0M
SKB/BLOCK K/SWEDEN

PROJECT NO. IC3 1161.003 DRAWING NO. 60834 DATE 9/8/95 DRAWN BY EA

Golder Associates

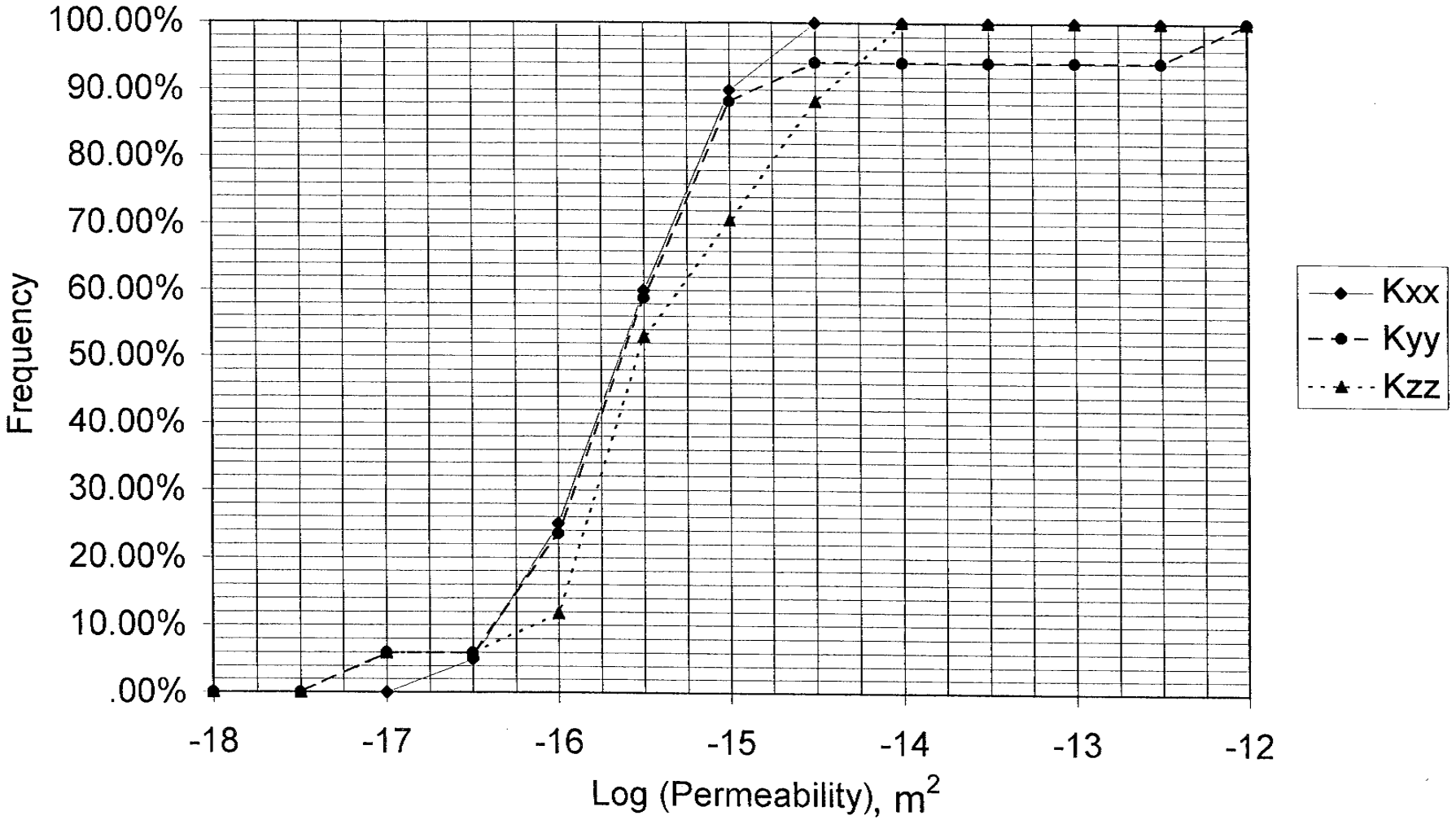

FIGURE **B-14b**
CUMULATIVE FREQUENCY HISTOGRAM FOR 50M BLOCKS, MEAN FRACTURE RADIUS = 13.7M
SKB/BLOCK K/SWEDEN

PROJECT NO. IC3 1161.003 DRAWING NO. 60835 DATE 9/8/95 DRAWN BY EA

Golder Associates

List of SKB reports

Annual Reports

1977-78
TR 121
KBS Technical Reports 1 – 120
Summaries
Stockholm, May 1979

1979
TR 79-28
The KBS Annual Report 1979
KBS Technical Reports 79-01 – 79-27
Summaries
Stockholm, March 1980

1980
TR 80-26
The KBS Annual Report 1980
KBS Technical Reports 80-01 – 80-25
Summaries
Stockholm, March 1981

1981
TR 81-17
The KBS Annual Report 1981
KBS Technical Reports 81-01 – 81-16
Summaries
Stockholm, April 1982

1982
TR 82-28
The KBS Annual Report 1982
KBS Technical Reports 82-01 – 82-27
Summaries
Stockholm, July 1983

1983
TR 83-77
The KBS Annual Report 1983
KBS Technical Reports 83-01 – 83-76
Summaries
Stockholm, June 1984

1984
TR 85-01
Annual Research and Development Report 1984
Including Summaries of Technical Reports Issued during 1984. (Technical Reports 84-01 – 84-19)
Stockholm, June 1985

1985
TR 85-20
Annual Research and Development Report 1985
Including Summaries of Technical Reports Issued during 1985. (Technical Reports 85-01 – 85-19)
Stockholm, May 1986

1986
TR 86-31
SKB Annual Report 1986
Including Summaries of Technical Reports Issued during 1986
Stockholm, May 1987

1987
TR 87-33
SKB Annual Report 1987
Including Summaries of Technical Reports Issued during 1987
Stockholm, May 1988

1988
TR 88-32
SKB Annual Report 1988
Including Summaries of Technical Reports Issued during 1988
Stockholm, May 1989

1989
TR 89-40
SKB Annual Report 1989
Including Summaries of Technical Reports Issued during 1989
Stockholm, May 1990

1990
TR 90-46
SKB Annual Report 1990
Including Summaries of Technical Reports Issued during 1990
Stockholm, May 1991

1991
TR 91-64
SKB Annual Report 1991
Including Summaries of Technical Reports Issued during 1991
Stockholm, April 1992

1992
TR 92-46
SKB Annual Report 1992
Including Summaries of Technical Reports Issued during 1992
Stockholm, May 1993

1993
TR 93-34
SKB Annual Report 1993
Including Summaries of Technical Reports Issued during 1993
Stockholm, May 1994

1994

TR 94-33

SKB Annual Report 1994

Including Summaries of Technical Reports Issued during 1994.
Stockholm, May 1995

List of SKB Technical Reports 1995

TR 95-01

Biotite and chlorite weathering at 25°C. The dependence of pH and (bi) carbonate on weathering kinetics, dissolution stoichiometry, and solubility; and the relation to redox conditions in granitic aquifers

Maria Malmström[1], Steven Banwart[1], Lara Duro[2], Paul Wersin[3], Jordi Bruno[3]
[1] Royal Institute of Technology, Department of Inorganic Chemistry, Stockholm, Sweden
[2] Universidad Politécnica de Cataluña, Departmento de Inginería Química, Barcelona, Spain
[3] MBT Tecnología Ambiental, Cerdanyola, Spain
January 1995

TR 95-02

Copper canister with cast inner component. Amendment to project on Alternative Systems Study (PASS), SKB TR 93-04

Lars Werme, Joachim Eriksson
Swedish Nuclear Fuel and Waste Management Co, Stockholm, Sweden
March 1995

TR 95-03

Prestudy of final disposal of long-lived low and intermediate level waste

Marie Wiborgh (ed.)
Kemakta Konsult AB, Stockholm, Sweden
January 1995

TR 95-04

Spent nuclear fuel corrosion: The application of ICP-MS to direct actinide analysis

R S Forsyth[1], U-B Eklund[2]
[1] Caledon-Consult AB, Nyköping, Sweden
[2] Studsvik Nuclear AB, Nyköping, Sweden
March 1995

TR 95-06

Palaeohydrological implications in the Baltic area and its relation to the groundwater at Äspö, south-eastern Sweden – A literature study

Bill Wallin
Geokema AB, Lidingö, Sweden
March, 1995

TR 95-07

Äspö Hard Rock Laboratory Annual Report 1994

SKB
April 1995

TR 95-08

Feasibility study for siting of a deep repository within the Storuman municipality

Swedish Nuclear Fuel and Waste Management Co., Stockholm
January 1995

TR 95-09

A thermodynamic data base for Tc to calculate equilibrium solubilities at temperatures up to 300°C

Ignasi Puigdomènech[1], Jordi Bruno[2]
[1] Studsvik AB, Nyköping, Sweden
[2] Intera Information Technologies SL, Cerdanyola, Spain
April 1995

TR 95-10

Investigations of subterranean microorganisms. Their importance for performance assessment of radioactive waste disposal

Karsten Pedersen[1], Fred Karlsson[2]
[1] Göteborg University, General and Marine Microbiology, The Lundberg Institute, Göteborg, Sweden
[2] Swedish Nuclear Fuel and Waste Management Co., Stockholm, Sweden
June 1995

TR 95-11

Solute transport in fractured media – The important mechanisms for performance assessment

Luis Moreno, Björn Gylling, Ivars Neretnieks
Department of Chemical Engineering and Technology, Royal Institute of Technology, Stockholm, Sweden
June 1995

TR 95-12

Literature survey of matrix diffusion theory and of experiments and data including natural analogues

Yvonne Ohlsson, Ivars Neretnieks
Department of Chemical Engineering and Technology, Royal Institute of Technology, Stockholm, Sweden
August 1995

TR 95-13

Interactions of trace elements with fracture filling minerals from the Äspö Hard Rock Laboratory

Ove Landström[1], Eva-Lena Tullborg[2]
[1] Studsvik Eco & Safety AB
[2] Terralogica AB
June 1995

TR 95-14

Consequences of using crushed crystalline rock as ballast in KBS-3 tunnels instead of rounded quartz particles

Roland Pusch
Clay Technology AB
February 1995